LOCKHEED MARTIN ENERGY RESEARCH LIBRARIES

3 4456 0515547 1

CENTRAL RESEARCH LIBRARY

2

ORNL-4400
UC-4 -- Chemistry

REACTOR CHEMISTRY DIVISION

ANNUAL PROGRESS REPORT

FOR PERIOD ENDING DECEMBER 31, 1968

OAK RIDGE NATIONAL LABORATORY
operated by
UNION CARBIDE CORPORATION
for the
U.S. ATOMIC ENERGY COMMISSION

OAK RIDGE NATIONAL LABORATORY
CENTRAL RESEARCH LIBRARY
DOCUMENT COLLECTION
LIBRARY LOAN COPY
DO NOT TRANSFER TO ANOTHER PERSON
If you wish someone else to see this document, send in name with document and the library will arrange a loan.

Printed in the United States of America. Available from Clearinghouse for Federal Scientific and Technical Information, National Bureau of Standards, U.S. Department of Commerce, Springfield, Virginia 22151
Price: Printed Copy $3.00; Microfiche $0.65

LEGAL NOTICE

This report was prepared as an account of Government sponsored work. Neither the United States, nor the Commission, nor any person acting on behalf of the Commission:

A. Makes any warranty or representation, expressed or implied, with respect to the accuracy, completeness, or usefulness of the information contained in this report, or that the use of any information, apparatus, method, or process disclosed in this report may not infringe privately owned rights; or

B. Assumes any liabilities with respect to the use of, or for damages resulting from the use of any information, apparatus, method, or process disclosed in this report.

As used in the above, "person acting on behalf of the Commission" includes any employee or contractor of the Commission, or employee of such contractor, to the extent that such employee or contractor of the Commission, or employee of such contractor prepares, disseminates, or provides access to, any information pursuant to his employment or contract with the Commission, or his employment with such contractor.

ORNL-4400
UC-4 – Chemistry

Contract No. W-7405-eng-26

REACTOR CHEMISTRY DIVISION
ANNUAL PROGRESS REPORT
For Period Ending December 31, 1968

Director
W. R. Grimes

Associate Directors
E. G. Bohlmann
H. F. McDuffie
G. M. Watson

Senior Scientific Advisor
F. F. Blankenship

FEBRUARY 1970

OAK RIDGE NATIONAL LABORATORY
Oak Ridge, Tennessee
operated by
UNION CARBIDE CORPORATION
for the
U. S. ATOMIC ENERGY COMMISSION

LOCKHEED MARTIN ENERGY RESEARCH LIBRARIES
3 4456 0515547 1

Reports previously issued in this series are as follows:

ORNL-2931	Period Ending January 31, 1960
ORNL-3127	Period Ending January 31, 1961
ORNL-3262	Period Ending January 31, 1962
ORNL-3417	Period Ending January 31, 1963
ORNL-3591	Period Ending January 31, 1964
ORNL-3789	Period Ending January 31, 1965
ORNL-3913	Period Ending December 31, 1965
ORNL-4076	Period Ending December 31, 1966
ORNL-4229	Period Ending December 31, 1967

Contents

PART I. MOLTEN-SALT CHEMISTRY

1. Chemical Studies of Molten-Salt Systems

A POLYMER MODEL FOR LiF-BeF_2 MELTS

C. F. Baes, Jr. 1

A model which considers the formation of all possible anionic polymeric species $Be_aF_b^{(b-2a)-}$ in which Be^{2+} is coordinated by four F^- ions can account for the nonideal behavior of this system.

VISCOSITY AND DENSITY OF MOLTEN BeF_2-LiF SOLUTIONS

Stanley Cantor, W. T. Ward, and C. T. Moynihan 4

The previously reported measurements of these properties have, upon careful reexamination, been successfully correlated by relatively simple equations.

OXIDE-FLUORIDE EQUILIBRIA

C. F. Baes, Jr. 5

The Chemistry of Silica in Molten Fluorides: The Reactions of Be_2SiO_4 with 2LiF-BeF_2

C. E. Bamberger 5

The partial pressure of SiF_4 generated by equilibration of Be_2SiO_4 and BeO with this molten fluoride agree well with predicted values above 700°C but show an unexplained discrepancy below this temperature.

A Stirred Reaction Vessel for Molten Fluorides

C. E. Bamberger, T. J. Golson, and J. Nicholson 6

This apparatus permits continuous, vigorous agitation of reaction mixtures while remaining gastight.

The Distribution of U^{4+} Between Molten LiF-BeF_2-ThF_4-UF_4 and a (U-Th)O_2 Solid Solution

C. E. Bamberger and A. L. Johnson 8

The distribution of U^{4+} and Th^{4+} between molten LiF-BeF_2-ThF_4 (72-16-12) and a (U-Th)O_2 solid solution phase strongly favors the extraction of U^{4+} by the oxide phase. The equilibrium quotient shows a strong dependence on the oxide-phase composition and the temperature.

AN Ni, NiO, BeO ELECTRODE OF THE THIRD KIND AS A REFERENCE ELECTRODE IN MOLTEN FLUORIDES

B. F. Hitch and C. F. Baes, Jr. 9

This electrode, which produces a stable potential when contained in silica, offers advantages over the $Be^{2+}|Be^0$ and $HF,H_2|F^-$ reference electrodes.

IONIC TRANSPORT PROPERTIES IN MOLTEN FLUORIDES

K. A. Romberger and J. Braunstein 11

The emf has been measured for concentration cells with transference in the system BeF_2-LiF at 500°C with beryllium electrodes. The transference number of lithium ion at mole fractions of BeF_2 between 0.33 and 0.51 is $\bar{t}_{Li} = 1 - \bar{t}_{Be} = 1 \pm 0.05$ relative to fluoride ion.

ELECTRICAL CONDUCTANCE MEASUREMENTS IN MOLTEN SALTS

A Review of Electrical Conductance Measurements in Fused Fluorides

G. D. Robbins 12

A review of electrical conductance measurements of 16 groups of investigators for 56 molten-fluoride systems, covering the period 1927 to 1967, has been completed. Particular emphasis is placed on cell and electrode material and design, on measuring bridges, and on the frequency dispersion of the measured resistance.

Specific Electrical Conductance of Molten KNO_3

G. D. Robbins and J. Braunstein 15

A careful determination of the specific conductance vs temperature characteristics of a suitable molten salt for use as a reference standard in determining cell constants, molten potassium nitrate, has been performed. The results resolve conflicting published data for this material.

Electrical Conductivity of Molten LiF-BeF_2 Mixtures
G. D. Robbins and J. Braunstein 17
Electrical conductivities and their temperature dependence have been studied in the molten LiF-BeF_2 system for compositions ranging from 38 to 52 mole % beryllium fluoride. The temperature dependence of the eutectic mixture (52 mole % BeF_2) has been analyzed in terms of the zero mobility temperature concept, and a theoretical glass transition temperature of 350 (±25)°K is suggested.

Electrical Conductances of Molten Salts at High Pressures
A. S. Quist 21
In collaboration with scientists at the University of Karlsruhe, West Germany, an apparatus has been designed, constructed, and tested for measuring the electrical conductances of molten salts to 850°C and 8000 bars.

APPARATUS AND TECHNIQUES FOR SPECTROSCOPIC MEASUREMENTS IN FLUORIDE MEDIA
L. M. Toth, J. P. Young, and G. P. Smith 22
The establishment of a molten-fluoride visible-ultraviolet absorption spectroscopy program has been essentially completed through the assistance of groups in the Metals and Ceramics Division and the Analytical Chemistry Division. It includes the development of a diamond-windowed spectrophotometric cell which is unreactive to molten fluorides and the production of fluoride solvents and solutes of the quality required for spectroscopy.

CRYSTAL STRUCTURES OF COMPLEX FLUORIDES
G. D. Brunton 24
Crystal structures have been determined or refined for $NaBF_4$, $(Na,Li)_7Th_6F_{31}$, Na_3CrF_6, $Cs_4Mg_3F_{10}$, and K_3MoF_6.

2. Direct Support for the Molten Salt Reactor Experiment 30
These studies will be reported in the Reactor Chemistry Division Annual Progress Report for Period Ending December 31, 1969.

3. Behavior of Fission Products and Protactinium in Molten Fluorides

STUDIES OF PARTICLES IN AND ABOVE MOLTEN SALTS

Radioaerosol Formation over Molten Salts
H. W. Kohn, S. S. Kirslis, and F. F. Blankenship 31
Small amounts of ^{95}Nb and ^{95}Zr escape from tagged fuel salt regardless of the reduction potential of the melt.

Bubbles, Drops, and Entrainment in Molten Salts
H. W. Kohn 31
The behavior of bubbles and fine drops is reviewed, and their role in entrainment is evaluated.

Metallic Colloids in Molten Salts
H. W. Kohn and F. F. Blankenship 33
Several methods of preparing metal sols in Li_2BeF_4 and in molten nitrates are described.

SYNTHESIS OF NOBLE METAL FLUORIDES AND IDENTIFICATION OF SPECIES IN AND ABOVE MOLTEN FLUORIDES

Synthesis of MoF_4 and RuF_3; Kinetic and Mass Spectrophotometric Studies
C. F. Weaver 33
MoF_4 and RuF_3 were synthesized and characterized. Earlier work is briefly reviewed.

Kinetic Behavior of Trivalent Molybdenum in Molten 2LiF·BeF_2
H. A. Friedman, J. W. Gooch, Jr., and D. N. Hess 34
The stability of Mo^{3+} in molten 2LiF·BeF_2 with respect to container materials, pretreatment of container, helium flow rates, and temperature was investigated.

Mass Spectrometric Studies of Fluorides
J. D. Redman 36
Mass spectrometric studies of the vapor phase over MoF_3 dissolved in 2LiF·BeF_2, pure RuF_3, pure NbF_5, and a solution of LiF-BeF_2-ThF_4-AlF_3-PrF_3 are described.

Spectrophotometric Examination of Molybdenum Fluorides in Molten LiF-BeF_2 Mixtures

MoF_3 Fluoride Solution Spectra
L. M. Toth, J. P. Young, and G. P. Smith 39
Solutions of MoF_3 in LiF-BeF_2 (66-34 mole %) exhibit peaks at 472 and 353 mμ, and the MoF_3 was found to be present as Mo^{3+} ions which are octahedrally coordinated to fluoride ions to form MoF_6^{3-}.

K_3MoF_6 Synthesis and Spectrum
L. M. Toth and G. P. Smith 40

A comparison of the spectrum of K_3MoF_6 crystals, formed by fusing KF and MoF_3 in a platinum tube at 880°C, with that of MoF_3 dissolved in $LiF-BeF_2$ (66-34 mole %) gave conclusive evidence that the species present in the molten fluoride mixture is MoF_6^{3-}.

Vapor-Phase Studies over MoF_3 Solutions
L. M. Toth, J. P. Young, and G. P. Smith 41
Spectrophotometric examination of the vapor phase over solutions of MoF_3 in $LiF-BeF_2$ (66-34 mole %) at 700°C showed that the partial pressure of MoF_6 was below the detectable limit of 0.020 torr.

REPROCESSING STUDIES FOR MOLTEN-SALT BREEDER REACTORS

Reductive Extraction of ^{233}Pa, Uranium, and Zirconium from Molten $LiF-BeF_2-ThF_4$ Mixtures into Bismuth
D. M. Moulton, W. Jennings, Jr., W. R. Grimes, and J. H. Shaffer 41
The distribution of uranium and protactinium between bismuth and $LiF-BeF_2-ThF_4$ (72-16-12 mole % and 68-20-12 mole %) has been measured at 600 and 700°C. The distribution of zirconium between bismuth and the latter salt has also been found.

Protactinium Studies in the High-Alpha Laboratory
C. J. Barton, H. H. Stone, J. C. Mailen, and R. G. Ross 43
Our studies showed that reductive extraction of protactinium and uranium using a Bi-Th alloy as the metal phase is feasible for both two-region blanket and single-fluid $LiF-BeF_2-ThF_4$ compositions.

Further Studies of the Reductive Extraction of Protactinium from Single-Fluid MSBR Fuel Salt by Thorium in Molten Bismuth
R. G. Ross, C. E. Bamberger, and C. F. Baes, Jr. 45
Equilibrium protactinium extraction results show no effect of the uranium level in the bismuth.

Reductive Extraction of Rare Earths from Molten Fluorides into Molten Metals
D. M. Moulton, W. P. Teichert, W. K. R. Finnell, W. Jennings, Jr., W. R. Grimes, and J. H. Shaffer 47
Data on the distribution of cerium between various compositions of $LiF-BeF_2-ThF_4$ mixtures and bismuth were obtained. Cerium extractions into other metal mixtures were also performed in an exploratory program.

The Behavior of Metals with Two Oxidation States upon Reduction from Molten Salts into Liquid Metals
D. M. Moulton 51
It has been shown that there is a tendency for the lower oxidation states of metal ions to be destabilized in reductive extraction systems. For europium, samarium, and cerium the lower states are stable enough to appear anyway, but the anomalously low valence states sometimes reported for these and other metals are probably wrong. Uranium is an intermediate case where the ion is mostly but not completely reduced to the trivalent condition.

Separation of Cerium from Thorium in Bismuth by Cold-Zone Deposition of Thorium Bismuthide
D. M. Richardson, W. K. R. Finnell, W. R. Grimes, and J. H. Shaffer 53
A simple pump loop experiment is in progress to examine the precipitation of thorium from bismuth containing cerium in a manner that may be applied to the reprocessing requirements of the MSBR. Fabrication of the system is complete, and preparatory operations are in progress.

Zone Melting of Fluoride Salts
E. L. Compere and Terry Dorsett 54
Zone melting tests of $LiF-BeF_2-ThF_4CeF_3$ mixtures (72-16-12-0.3 or 0.03) indicated that no appreciable separation resulted for cerium or thorium as a result of zone passage. Crystallization consistent with tie-line and solubility data permits high-density phases enriched in thorium to settle.

Removal of Thorium from Single-Fluid Fuel Compositions by Fractional Crystallization
C. J. Barton 55
An experiment on removal of ThF_4 from the mixture $LiF-BeF_2-ThF_4$ (58-30-12 mole %) by fractional crystallization showed that more than half the ThF_4 precipitated before loss of CeF_3, present initially at a concentration of 100 ppm, from the melt occurred.

PART II. AQUEOUS REACTORS AND DESALINATION

4. Corrosion and Chemical Behavior in Reactor and Desalination Environments

ASSESSMENT OF WATER TECHNOLOGY IN BOILING- AND PRESSURIZED-WATER REACTORS
G. H. Jenks 57
Review and assessment of water technology in pressurized- and boiling-water reactors is continuing as part of U.S. Army-supported work at this Laboratory.

WATER CHEMISTRY IN A SMALL STATE-OF-THE-ART PRESSURIZED-WATER REACTOR
G. H. Jenks 57
A reference design and technology assessment of a 1500-kw (electrical) state-of-the-art pressurized-water reactor was made by ORNL, and we provided recommendations in areas related to water technology in the primary system.

RDT STANDARDS FOR PRIMARY COOLANT SYSTEMS OF WATER REACTORS
H. C. Savage, P. D. Neumann, and G. H. Jenks 60
We are preparing RDT standards which will establish requirements for the coolant chemistry for the primary coolant systems of pressurized-water, boiling-water, and research or test reactors.

CORROSION OF ELECTROLESS PLATED NICKEL ON ALUMINUM AT HIGH HEAT FLUXES
J. C. Griess, R. D. Cheverton, and J. R. McGuffey 61
As-plated electroless nickel on aluminum showed no tendency to peel from the surface with heat fluxes as high as 1.5×10^6 Btu hr^{-1} ft^{-2} across a water-cooled interface during a 527-hr test, although some cracks developed in the plate.

CORROSION OF MATERIALS IN IODINE-ABSORBING REACTOR CONTAINMENT SPRAY SOLUTIONS
J. C. Griess and A. L. Bacarella 62
The corrosion resistance of a number of materials in iodine-absorbing spray solutions is being determined.

CORROSION OF COPPER ALLOYS IN SODIUM CHLORIDE SOLUTIONS
J. C. Griess and E. G. Bohlmann 64
The effect of low concentrations of sulfide and cystine in 1 *m* NaCl on the corrosion of four copper alloys was determined at 125°C.

CARBON DIOXIDE SCALE SUPPRESSION STUDIES
S. A. Reed, D. M. Eissenberg, and C. C. Littlefield 66
The feasibility of controlling alkaline scale formation in seawater distillation equipment by a self-sustaining feed treatment cycle utilizing only the carbon dioxide which occurs naturally in seawater has been demonstrated. Current investigations are directed toward optimizing the process flowsheet and determining engineering scaling parameters for the design of a 30-gpm pilot plant.

OSW MATERIALS INFORMATION CENTER
J. L. English and S. A. Reed 67
The Office of Saline Water has established a computerized Materials Information Center at Oak Ridge National Laboratory for the purpose of developing procedures for the organization, evaluation, and dissemination of information relating to the corrosion and performance of materials for construction used in saline-water conversion processes. The Center will be in full operation by the end of fiscal year 1969, with the first indexed bibliographic report to be issued early in 1969.

5. Electrical Conductance of Aqueous Electrolytes to 800°C and 4000 Bars

ELECTRICAL CONDUCTANCES OF AQUEOUS SODIUM IODIDE AND THE COMPARATIVE THERMODYNAMIC BEHAVIOR OF AQUEOUS SODIUM HALIDE SOLUTIONS TO 800°C AND 4000 BARS
L. A. Dunn and W. L. Marshall 69
Electrical conductance measurements of aqueous sodium iodide solutions to 800°C and 4000 bars show comparatively similar ionization behavior with sodium chloride and sodium bromide. Evaluation shows that the complete thermodynamic behavior of each electrolyte is described in the range of 400 to 800°C with only three constants, ΔH°, ΔS°, and k, the net change in waters of solvation. These constants are also independent of pressure.

THE ELECTRICAL CONDUCTANCES OF SOME ALKALI-METAL HALIDES IN AQUEOUS SOLUTIONS FROM 0 TO 800°C AND AT PRESSURES TO 4000 BARS
A. S. Quist, W. Jennings, Jr., and W. L. Marshall 71
Electrical conductances of 14 alkali-metal halides are compared over the temperature range 0 to 800°C and at pressures to 4000 bars. Relative differences in conductance behavior are explained chiefly in terms of their effects on the structure of water.

ION PRODUCT OF WATER TO 800°C FROM ELECTRICAL CONDUCTANCE BEHAVIOR OF AMMONIUM BROMIDE SOLUTIONS AND RELATED ELECTROLYTES
A. S. Quist, W. Jennings, Jr., and W. L. Marshall 74
Measurements of the electrical conductance of ammonium bromide to 800°C and 4000 bars show that this salt behaves similarly to alkali-metal halides to 400°C, but at higher temperatures hydrolyzes to produce NH_4OH and HBr. By using also the conductances of NaBr, HBr, and NH_4OH, calculations of the ion product of water as a function of density at the high temperatures have been performed.

ELECTRICAL CONDUCTANCES OF 0.01 *m* KNO_3 SOLUTIONS TO 800°C AND 4000 BARS
A. S. Quist, W. Jennings, Jr., and W. L. Marshall 75
Electrical conductances of KNO_3 solutions to 800°C and 4000 bars do not indicate unusual behavior such as hydrolysis or decomposition of nitrate. The behavior is qualitatively similar to that of the alkali halides.

ELECTRICAL CONDUCTANCES OF 0.01 *m* AQUEOUS $(CH_3)_4NBr$ SOLUTIONS TO 800°C AND 4000 BARS
A. S. Quist and W. Jennings, Jr. 76
The electrical conductances of tetramethylammonium bromide solutions are considerably less than comparable solutions of ammonium bromide to 300°C, probably because of the larger size of the tetramethylammonium ion. At higher temperatures (400 to 600°C), extensive hydrolysis or decomposition of the $(CH_3)_4N^+$ ion is indicated. Probably this ion forms four molecules of CH_3OH and the NH_4^+ ion; the conductance then becomes comparable with that of NH_4Br.

6. Physical Chemistry of High-Temperature Aqueous Solutions

EQUILIBRIUM QUOTIENTS AT 25°C FOR $CaSO_4$ IN SEVERAL AQUEOUS MIXED-ELECTROLYTE SOLUTIONS
L. B. Yeatts and W. L. Marshall 77
Comparisons of the solubility and ionization equilibrium quotients of $CaSO_4$ at 25°C in the four mixed-electrolyte systems Na_2SO_4-$NaNO_3$-H_2O, Na_2SO_4-NaCl-H_2O, Li_2SO_4-$LiNO_3$-H_2O, and Li_2SO_4-LiCl-H_2O show good agreement at an ionic strength of 0.5. However, at the higher ionic strengths of 2 and 6, large differences in the quotients among the systems become apparent.

SOLUBILITY OF Fe_3O_4 AT ELEVATED TEMPERATURES
F. H. Sweeton, R. W. Ray, and C. F. Baes, Jr. 79
Solubility behavior in acid and basic solutions up to 300°C is interpreted in terms of the formation of Fe^{2+}, $FeOH^+$, $Fe(OH)_2$, and $Fe(OH)_3^-$ in solution.

FLUORIDE COMPLEXES OF BERYLLIUM(II) IN AQUEOUS MEDIA
R. E. Mesmer and C. F. Baes, Jr. 82
The thermodynamic parameters for the formation of beryllium(II) fluoride complexes $BeF_n^{(2-n)+}$ have been determined potentiometrically in 1 *m* (Na)Cl using the lanthanum fluoride electrode along with H_2 electrodes. The reactions are slightly exothermic, with positive entropy changes contributing to their stability.

CORRELATION OF ΔH AND ΔS FOR THE ASSOCIATION OF THE RARE-EARTH(III) IONS WITH FLUORIDE
R. E. Mesmer and C. F. Baes, Jr. 84
An excellent correlation of the ΔH and ΔS for the association of rare-earth(III) ions with fluoride (1:1) has been found. The trends in these quantities with atomic number of the rare-earth ion are discussed.

EMPIRICAL RELATIONSHIPS FOR STABILITY OF INORGANIC FLUORIDE COMPLEXES
R. E. Mesmer and C. F. Baes, Jr. 85
Empirical relationships have been found which relate the stabilities of the inorganic fluoride complexes to the charge and radius of the cation. Such relationships should be of value in predicting the stability of complexes with useful accuracy.

APPARATUS FOR EMF TITRATIONS AT ELEVATED TEMPERATURES
R. E. Mesmer, F. H. Sweeton, and C. F. Baes, Jr. 86
A newly constructed high-temperature apparatus for emf titration measurements was tested by measuring Q_w, the ion product for water, from 50 to 292°C. The high precision of the data indicates the suitability of the apparatus for studying hydrolysis and other protolytic equilibria up to 250–300°C.

A FLOWING EMF CELL FOR MEASUREMENTS AT ELEVATED TEMPERATURES
F. H. Sweeton, R. E. Mesmer, R. W. Ray, and C. F. Baes, Jr. 88
An emf cell and the associated equipment for measuring the dissociation of water at temperatures up to 300°C have been assembled and are essentially ready for use.

EFFECT OF SOLVENT ON THE ELECTROCHEMISTRY OF IRON
A. L. Bacarella and A. L. Sutton 89
The kinetics of the anodic dissolution of iron in ethanol–water–sulfuric acid solutions is being studied to determine the corrosion mechanism in the presence of ethanol and to test the applicability of "an absolute acidity scale."

AN IMPROVED HIGH-TEMPERATURE ISOPIESTIC UNIT
H. F. McDuffie, P. B. Bien, R. W. Ray, and J. Braunstein 92
Installation of an improved electromagnetic balance in the assembly for isopiestic studies up to 200°C and 15.6 bars is complete. The system is under test with standard solutions.

PART III. CHEMICAL SUPPORT FOR HIGH-TEMPERATURE SOLID FUELED REACTORS

7. Diffusion Processes

DIFFUSION STUDIES IN NOBLE-GAS SYSTEMS
M. D. Silverman and A. P. Malinauskas 93
Experimental investigations of the diffusion characteristics of all of the possible binary combinations among the noble gases have been completed.

THERMAL TRANSPIRATION
B. K. Annis, J. W. Gooch, R. E. Fuson, and A. P. Malinauskas 94
Several aspects of the phenomenon had been investigated. These include studies of deviations from the theoretical low-pressure limit, the determination of rotational collision numbers, and the extension to binary systems.

DETERMINATION OF THE VISCOSITY COEFFICIENTS OF GASES
S. J. Whisenhunt, Jr., J. Q. Searcy, and A. P. Malinauskas 96
A simple, inexpensive apparatus has been developed for the determination of the viscosity coefficients of gases at room temperature. The experimental data yield results of about 2% accuracy; helium, however, displayed a surprisingly anomalous behavior whose nature remains unexplained.

SELF-DIFFUSION OF ^{14}C IN PYROCARBON STRUCTURES
R. B. Evans III, L. D. Love, and E. H. Kobisk 97
Techniques developed to perform the experimental measurements are reviewed, with particular emphasis on the ^{14}C labeling of diffusion specimens. Initial results for pyrocarbons are reported on a tentative basis since they indicate fair agreement with the limited amount of self-diffusion data currently available.

GAS TRANSPORT IN VENTED FUEL ELEMENTS AND CONTROL RODS
R. B. Evans III, D. E. Bruins, and E. A. Mason 100
This work involves the design of a venting system that allows pressure equilization without release of too much activity. A generalized treatment resulted without resort to the heavy mathematical artillery of the Chapman-Enskog theory of gases.

SIMPLIFIED COUNTERDIFFUSION APPARATUS FOR CHARACTERIZING VENTS AND VENT COMPONENTS
R. B. Evans III and E. A. Mason 101
A simple technique for characterizing fuel element vents has been perfected. The distinguishing features of this technique over other types of apparatus are simplicity and accuracy.

8. Irradiation Behavior of High-Temperature Fuel Materials

O. Sisman

IN-PILE TESTS OF COATED FUEL PARTICLES
P. E. Reagan, E. L. Long, Jr., J. G. Morgan, and T. W. Fulton 103
Buffer-isotropic pyrolytic-carbon-coated uranium oxide particles performed well during irradiation at 900°C, and similar coatings applied to thorium-uranium oxide particles in TURF performed well at 1250°C, but thin isotropic pyrolytic carbon coatings, in the 20-μ range, did not retain fission gases sufficiently well to meet the High-Temperature Gas-Cooled Reactor design criteria.

IN-PILE TESTS OF BONDED BEDS OF COATED FUEL PARTICLES
P. E. Reagan, E. L. Long, Jr., J. G. Morgan, and T. W. Fulton 104
Bonded beds of coated fuel particles performed well up to 35% heavy metal burnup at 1250 to 1350°C, but temperature excursions caused coating failure at about 1600°C, and after 160 hr at 1700°C, an estimated 1% of the coatings had failed.

FISSION PRODUCT RELEASE BY POSTIRRADIATION ANNEALING OF COATED FUEL PARTICLES
M. T. Morgan, J. G. Morgan, and R. L. Towns 106
In contrast with an earlier experiment, recent experiments have shown that ^{137}Cs is retained along with other important fission products by SiC barrier layers in irradiated coated fuel particles during high-temperature anneals, but a significant fraction of ^{99}Mo was released at 2000°C during a 19-hr anneal.

MECHANISM OF FISSION GAS RELEASE FROM FUELED PYROCARBON-COATED MICROSPHERES
C. D. Baumann and P. E. Reagan 106
The release of fission gas from coated fuel particles is shown to be by diffusion from fuel contamination in the coating below about 1600°C and by diffusion through the coating from the fuel core above this temperature.

RELEASE OF IODINE FROM BROKEN COATED PARTICLES
M. T. Morgan, J. G. Morgan, and R. L. Towns 108
Results from postirradiation annealing experiments on cracked coated fuel particles indicated: (1) that a large fraction of the iodine released comes from the coatings, (2) that the fraction of iodine contained in the coatings of irradiated particles is a function of irradiation time and temperature, and (3) that iodine release from cracked coated UO_2 particles is a factor of 10 to 17 times that from cracked coated UC_2 particles.

POSTIRRADIATION STUDIES OF HIGH-BURNUP COATED PARTICLES
D. R. Cuneo, J. A. Conlin, J. H. Coobs, E. L. Long, Jr., and H. E. Robertson 109
The OR-1010-SB pyrolytic-carbon-coated UO_2 particles contained in bonded beds in high-burnup experiment No. 3 operated at 1150–1300°C to 35–38% burnup with 5–10% coating failure and to 39–41% burnup with 15–25% coating failure.

EXPERIMENTAL TEST OF THE FREVAP-8 CODE FOR CALCULATING METAL FISSION PRODUCT RELEASE FROM HTGR FUEL ELEMENTS
H. J. deNordwall, V. H. Pierce, and L. R. Zumwalt 111
The validity of calculations of the release of fission product metals from HTGR fuel elements is being tested by comparison of experimental results with those calculated by the FREVAP-8 and FIPER codes.

FISSION GAS RELEASE AND PHYSICAL PROPERTIES DURING IRRADIATION

Fission Gas Release During Fissioning of UO_2
R. M. Carroll, R. B. Perez, and O. Sisman 115
At low fission density the fission-created defects have little effect on fission gas release, but in the 10^{12} range the defect traps become dominating, and at about 10^{14} fissions cm^{-3} sec^{-1} the fission-created defects are so dense that they react with each other to accelerate the gas release.

Fission Gas Release During Fissioning of UN and $(Pu,U)O_2$
R. M. Carroll, R. B. Perez, and O. Sisman 116
The fission gas release from both UN and $(Pu,U)O_2$ was observed to be coming from very small cracks, which may be a characteristic of the material studied.

In-Pile Thermal Conductivity of Fuel Materials
R. M. Carroll, R. B. Perez, and J. G. Morgan 117
Some problems have been encountered in the in-pile thermal conductivity studies: the nonfission heating was larger than expected, and the fuel appears to be releasing stored energy during a step increase in temperature.

PART IV. NUCLEAR SAFETY

9. Nuclear Safety Tests in Major Facilities

AGING BEHAVIOR OF FISSION PRODUCTS RELEASED BY IN-PILE MELTING OF UO_2
B. F. Roberts, S. H. Freid, O. W. Thomas, W. H. Montgomery, and O. Sisman 118
The time-dependent behavior of fission-product aerosols generated in the ORR In-Pile Nuclear Safety Installation was studied in a condensing steam atmosphere with air present and compared with results of similar experiments conducted earlier in which air only was present.

IN-PILE BEHAVIOR OF HTGR FUEL ELEMENTS IN MIXTURES OF STEAM AND HELIUM
S. H. Freid, H. J. deNordwall, B. F. Roberts, O. Sisman, and W. H. Montgomery 120
Apparatus has been designed to demonstrate that rates of removal of carbon from HTGR fuel elements measured in the laboratory are applicable to in-pile conditions.

TREAT FUEL ROD FAILURE LOSS-OF-COOLANT EXPERIMENT
G. W. Parker and R. A. Lorenz 121
Fuel rod failure characteristics and fission-product release will be determined with seven-rod bundles of Zircaloy-clad UO_2 rods under loss-of-coolant accident conditions in the TREAT reactor.

PROMPT CLAD FAILURE RELEASE OF FISSION PRODUCTS FROM REACTOR FUEL ELEMENTS (OUT OF PILE)
G. W. Parker and M. F. Osborne 123
Fission product release data from high-temperature rupture tests of irradiated Zircaloy fuel capsules agree reasonably well with predictions; test conditions will be extended to more rapid temperature transients and to fuel irradiated at higher temperature.

EFFECT OF EMERGENCY CORE COOLANT ON FISSION PRODUCT PROMPT FAILURE RELEASE AND CONTAINMENT BEHAVIOR
G. W. Parker, R. A. Lorenz, and H. Feuerstein 125
An experimental program to define the chemical reactions of fission-product halogens and cesium on zircaloy fuel rod cladding and the effect on accidental release under emergency core coolant safeguarded conditions has given some insight into the radioiodine-zirconium retention process which suggests that the prompt release may be limited to 20% or less.

10. AEROSOL BEHAVIOR

FISSION PRODUCT DEPOSITION CHARACTERISTICS IN THERMAL GRADIENT TUBES
C. M. Blood and A. P. Malinauskas 127
Preliminary assessment of experimental data on the deposition profile of ^{110}Ag in a linear thermal gradient tube indicates that the device offers a promising means of obtaining thermodynamic and transport property data on gas-borne fission products. These data, in turn, can aid in the identification of the species involved with respect to chemical form.

FILTRATION OF AEROSOLS
R. E. Adams, R. J. Davis, J. S. Gill, and J. Truitt 128
The performance of commercially available filter media with aerosols similar to those expected under accident conditions is being studied.

BEHAVIOR OF AEROSOLS IN A REACTOR CONTAINMENT VESSEL
R. E. Adams, R. J. Davis, J. S. Gill, and J. Truitt 129
This program has the purpose of providing a means of predicting aerosol concentration in a reactor containment vessel as a function of time after an accident.

EFFECT OF AEROSOL MASS CONCENTRATION ON THE NATURAL REMOVAL RATE IN A REACTOR CONTAINMENT VESSEL
G. W. Parker, R. A. Lorenz, W. J. Martin, and G. E. Creek 131
An empirical method for estimating the natural settling rate of dense particulate clouds has been developed based on direct observation of the change in rate of settling of U_3O_8 particles and of change in particle size distribution with time.

11. Behavior of Elemental and Combined Iodine

SAMPLERS FOR CHARACTERIZATION OF IODINE
R. E. Adams, R. L. Bennett, and W. H. Hinds 134
Analytical samplers developed to distinguish and measure particulate, elemental, and less reactive iodine forms by means of a silver honeycomb, filters, and charcoal have been tested under a wide range of operating conditions.

REMOVAL OF MOLECULAR FORMS OF RADIOIODINE FROM MOIST-AIR SYSTEMS
R. E. Adams, R. D. Ackley, and Zell Combs 135
In the removal of radioiodine, either as I_2 or CH_3I, from flowing air by iodized charcoal, the effect of high relative humidity has been observed to be a critical parameter.

RADIOIODINE TRAPPING IN OFF-GAS SYSTEMS OF FUEL REPROCESSING PLANTS
R. E. Adams, R. D. Ackley, and Zell Combs 136
Radioiodine trapping from fuel reprocessing plants is being investigated to (1) determine the effects of airborne reagent vapors on the radioiodine trapping capability of iodized charcoal and (2) investigate the application of Hopcalite, an oxidizing catalyst, for decomposing the vapors of organic solvents (used in processing operations) prior to their adsorption by the charcoal.

REACTIONS OF IODINE VAPOR IN CONTAINMENT SYSTEMS
R. E. Adams, R. L. Bennett, and Ruth Slusher 137
The formation of alkyl halides by reaction of iodine with organic paints as well as the thermal and radiation-induced reactions of iodine with methane have been examined.

REACTIONS OF METHYL IODIDE WITH CHEMICAL SPRAY SOLUTIONS
R. E. Adams, R. L. Bennett, and Ruth Slusher 138
The reaction rate of CH_3I in solution with two containment spray solutions being considered for use after a reactor accident, base-borate and base-borate-thiosulfate, was measured over the temperature range 30 to 70°C.

UPTAKE OF CH_3I BY WATER SOLUTIONS AND DROPS
B. A. Soldano and W. T. Ward 140
Wind tunnel studies augmented with bubbler flow tests show that the addition of an iminic surfactant (Dow PEI 1000) and a reducing agent ($Na_2S_2O_3$ or formaldehyde) to a basic (pH 9.1) solution containing borates materially improves the adsorption of CH_3I.

12. Special Nuclear Safety Studies

IGNITION OF CHARCOAL ADSORBERS BY FISSION PRODUCT DECAY HEAT
R. E. Adams and R. P. Shields 142
Ignition of charcoal is being studied in the laboratory and in-pile to determine the influence of fission products and irradiation; a model is being developed to describe temperature profiles in operating adsorbers.

KINETICS OF THE STEAM-GRAPHITE REACTION
C. M. Blood, J. W. Gooch, B. K. Annis, and A. P. Malinauskas 143
Experimental evidence suggests that greater emphasis should be placed upon transient effects in order that the data on oxidation of graphite by steam be applicable to reactor safety analyses.

EFFECT OF WATER VAPOR ON THE VOLATILITY OF FISSION PRODUCT OXIDES
J. W. Gooch, J. D. Redman, and A. P. Malinauskas 144
Experimental studies of the vapor pressure enhancement of TeO_2 due to water vapor support the proposal that the phenomenon arises through the formation of gaseous $TeO(OH)_2$. The characteristic heat of the associated reaction is only about half as large as the heat of sublimation of TeO_2. However, mass spectrometric studies failed to establish the existence of $TeO(OH)_2$.

PART V. SPECIAL RESEARCHES

13. Effects of Neutron Irradiation on Refractory Materials

BEHAVIOR OF REFRACTORY METAL MONOCARBIDES
G. W. Keilholtz, R. E. Moore, and H. E. Robertson 147
Refractory metal monocarbides made by three different processes underwent very little or no change in microstructure, gross dimensions, or lattice parameters during exposure to large doses of fast neutrons at 1000 to 1100°C.

BEHAVIOR OF ALUMINA
G. W. Keilholtz, R. E. Moore, H. E. Robertson, and D. A. Dyslin 148
Fast neutrons cause more damage to alumina at temperatures in the range 600 to 900°C than at lower temperatures, but damage may be minimized by maintaining it at very high temperatures (1000°C or higher) and by using alumina of small grain size and high purity.

14. Effects of Radiation on Organic Materials

O. Sisman

TRAPPED ELECTRONS IN GAMMA-IRRADIATED POLYMERS
R. M. Keyser, W. W. Parkinson, and F. Williams 151
Trapped electrons have been sutdied at 77°K in several gamma-irradiated polymers by means of electron spin resonance spectroscopy.

RADIATION-INDUCED REACTIONS OF HYDROCARBONS
W. W. Parkinson, W. K. Kirkland, and R. M. Keyser 152
Vacuum fractionation of the products of irradiating solutions of naphthalene in hexane has revealed that a major portion have molecular weights greater than hexylnaphthalene, with yields of about $G = 0.9$.

ADDITION REACTIONS OF FURAN DERIVATIVES
J. J. J. Myron and W. W. Parkinson 153
Radiation-induced addition reactions of furan derivatives have been investigated, but the observed yields were inadequate for commercial utility.

DEVELOPMENT OF RADIATION-RESISTANT INSULATORS
M. J. Kelley, W. W. Parkinson, and B. J. Sturm 155
Postirradiation electrical property measurements on otherwise suitable dosimeter insulating materials have shown that desirable postirradiation decay properties are supplied by emulsion polymerization using persulfate catalysts or by deliberate additions of polymeric phosphites.

THE RADIATION CHEMISTRY OF THE REGISTRATION OF PARTICLE TRACKS IN PLASTICS
D. R. Sears, C. D. Bopp, and W. W. Parkinson 156
The gaseous radiation products from the two most common and most sensitive track-registering plastics, cellulose nitrate and acetate, have been measured, and track registration by recrystallization of fluorocarbons was explored.

15. Surface Chemistry

HEATS OF IMMERSION IN THE ZIRCONIUM OXIDE–WATER SYSTEM
H. F. Holmes, E. L. Fuller, Jr., and R. B. Gammage 158
The magnitude and variation of the heat of immersion of zirconium oxide in water are markedly dependent on the thermal history of the sample.

ADSORPTION OF WATER VAPOR ON THORIUM OXIDE BETWEEN 25 AND 500°C
R. B. Gammage, E. L. Fuller, Jr., and H. F. Holmes 159
The irreversible binding of molecular water below 300°C is a complicating factor in the adsorption of water on thorium oxide.

THORIUM OXIDE: THE INFLUENCE OF SURFACE WATER ON THE ADSORPTION OF NITROGEN AND THE *t* METHOD
R. B. Gammage, E. L. Fuller, Jr., and H. F. Holmes 160
Irreversibly bound molecular water coupled with the heterogeneity of the substrate has a marked effect in the adsorption of nitrogen on thorium oxide.

INFRARED SPECTRA OF THORIUM OXIDE SURFACES AND ADSORBED WATER
E. L. Fuller, Jr., H. F. Holmes, and R. B. Gammage 161
The spectra demonstrate the existence of four different hydroxyl groups and, in addition, numerous vibrations in the 200 to 2000 cm^{-1} region which may be inherent in the substrate.

PUBLICATIONS 164

PAPERS PRESENTED AT SCIENTIFIC AND TECHNICAL MEETINGS 169

Part I. Molten-Salt Chemistry

1. Chemical Studies of Molten-Salt Systems

A POLYMER MODEL FOR LiF-BeF_2 MELTS

C. F. Baes, Jr.

The structure of crystalline BeF_2, analogous to that of SiO_2, consists of BeF_4^{2-} tetrahedra which share corners to form a three-dimensional network. Liquid BeF_2, highly viscous and poorly conducting, obviously retains much of this polymeric character. When a basic fluoride such as LiF is added to BeF_2, the viscosity drops sharply, presumably because bridging fluoride linkages are broken in the melt.

$$-\overset{|}{\underset{|}{\mathrm{Be}}}-\mathrm{F}-\overset{|}{\underset{|}{\mathrm{Be}}}- + \mathrm{F}^- \rightleftharpoons -\overset{|}{\underset{|}{\mathrm{Be}}}-\mathrm{F}^{-1/2} + {}^{-1/2}\mathrm{F}-\overset{|}{\underset{|}{\mathrm{Be}}}- \qquad (1)$$

A model, presented previously in preliminary form,[1] has been developed to describe the mixture of polymeric species $Be_aF_b^{(b-2a)-}$ which one might expect in such LiF-BeF_2 melts on the basis of the deviations from ideality which are exhibited by this system.[2]

In this model it is assumed that all the possible polymeric species Be_aF_b which can be constructed of BeF_4 tetrahedra by sharing corners or edges will be formed. These structures extend from (1) linear polymers (Be_aF_{3a+1}) in which only corners are shared, to (2) increasingly cross-linked structures (Be_aF_{3a+1-c}, where c denotes the number of cross links), to (3) the most fully cross-linked structure (Be_aF_{2a+2}), in which all the tetrahedra share edges to form a chain.

The relative stability of each of the numerous complexes, and hence their abundance, is defined by the polymerization equilibrium

$$a\mathrm{BeF_4}^{2-} \rightleftharpoons \mathrm{Be}_a\mathrm{F}_b^{(b-2a)-} + (4a-b)\mathrm{F}^- , \qquad (2)$$

for which the equilibrium constant

$$K_{a,b} = \frac{a_{\mathrm{Be}_a\mathrm{F}_b}\, a_{\mathrm{F}}^{4a-b}}{a^a_{\mathrm{BeF_4}}} \qquad (3)$$

is given by

$$\log K_{a,b} = \frac{(4a-b)G}{RT} - \frac{(d)G_r}{RT} . \qquad (4)$$

The first term on the right in Eq. (4) is derived from the condition that in terms of the number of bridging fluorides (–F–) and free fluorides (F^-) produced and the number of terminal fluorides (–F) consumed, equilibrium (2) is equivalent to the reverse of (1), taken $4a - b$ times. G is the free energy associated with reaction (1). The second term on the right is a correction which allows for possible instability of species which are too highly cross linked. G_r, like G, is an adjustable free energy parameter, and d is an integer which reflects the degree of overcondensation. More specifically,

$$d = a(\mathrm{min}) - a , \qquad (5)$$

where a(min) is the minimum number of beryllium atoms for a given number of cross links (c) which are sufficient to construct a complex in which all rings contain six BeF_4 tetrahedra as in crystalline BeF_2.

[1] C. F. Baes, Jr., *Reactor Chem. Div. Ann. Progr. Rept. Dec. 31, 1966*, ORNL-4076, p. 15.

[2] B. F. Hitch and C. F. Baes, Jr., *An EMF Study of LiF-BeF_2 Solutions*, ORNL-4257 (July 1968).

When a exceeds a(min), d is defined as zero. As a falls below this value, smaller rings must be formed, and d takes on positive values. The values of a(min) have been calculated by considering crystallites of BeF_2 of various sizes.

Expressions for the activities of the various species were derived on the assumption that, as in mixtures of linear polymers, the entropy of mixing may be approximated in terms of volume fractions ϕ:

$$\Delta S_m = R\Sigma n_{a,b} \ln \phi_{a,b} \,. \tag{6}$$

(Since F^- ions are large compared with Be^{2+} and should determine the volume of the species, the volume fraction is approximated as the ratio of fluoride present in the species Be_aF_b to the total fluoride.) The heat of mixing is defined:

$$\Delta H_m = H\phi_F \Sigma(2b - 4a)n_{a,b} \,. \tag{7}$$

Here the term $2b - 4a$ is the number of terminal fluorides in each species. The summation then is the total of same, and the product of that and the fraction of all fluorides which are free (ϕ_F) is assumed to be proportional to the heat of mixing. Finally, the activity of a given species is obtained from

$$RT \ln a_{Be_aF_b} = \frac{\partial(\Delta H_m - T\,\Delta S_m)}{\partial n_{a,b}} \,. \tag{8}$$

Introduction of the resulting expressions into the equation (4) for $K_{a,b}$ produces the following expression for the volume fraction of a given species:

$$\phi_{a,b} = \frac{(e\phi_{1,4})^a}{e\,C^d}\left[\frac{AB\left(\phi_F - 0.5 + \frac{X_2}{1+X_2}\right)}{e\phi_F}\right]^{(4a-b)} , \tag{9}$$

wherein

$$A = e^{G/RT} \,,\quad B = e^{4H/RT} \,,\quad C = e^{G_r/RT} \,,$$

and X_2 is the mole fraction of BeF_2. To solve this equation at a given composition, with G, G_r, and H specified, it is necessary first to determine the values of ϕ_F and $\phi_{1,4}$ (the volume fraction of BeF_4) which satisfy the material balance relations

$$\Sigma\phi_{a,b} = 1 \,;\; \Sigma(a\phi_{a,b}/b) = \frac{X_2}{1+X_2} \,. \tag{10}$$

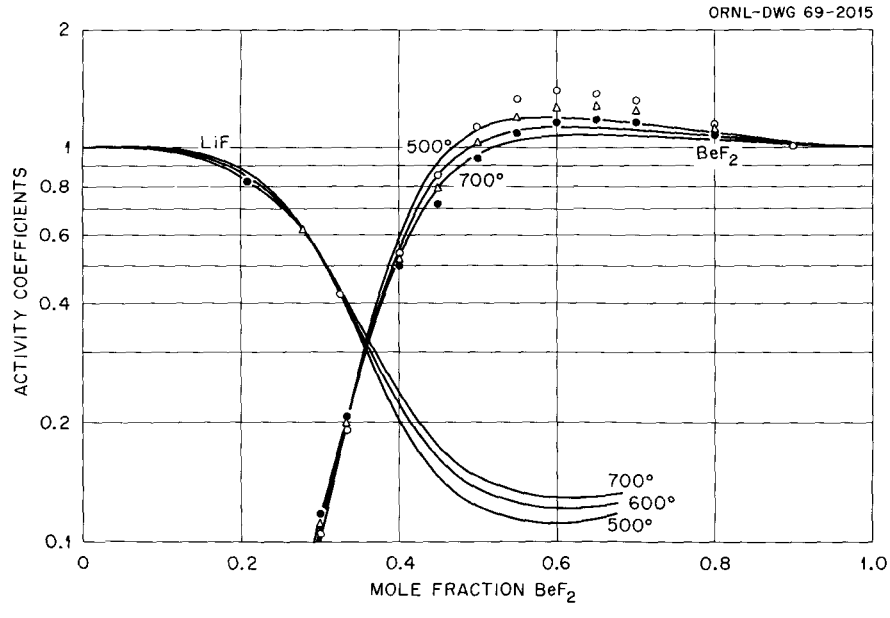

Fig. 1.1. Comparison of γ_{BeF_2} Calculated from the Polymer Model (Solid Curves) with Experimental Values. The curves for LiF calculated from the model agree well with γ_{LiF} values derived from the LiF liquidus.[3]

This is done by substitution of (9) into the summations of Eqs. (10) and then determining by successive approximation the values of ϕ_F and $\phi_{1,4}$ which satisfy the material balance equations.

The activity of the components may then be derived as follows: The activity of LiF is assumed equal to the activity of free F^- ion since in this model Li^+ is the only cation and is assumed to have a unit activity. From Eq. (8),

$$\ln a_{LiF} = \ln a_{F^-} = \ln \phi_F + (1 - \phi_F) \left\{ 1 - \frac{1}{\bar{b}} + \frac{H}{RT}\left[2(1 - \phi_F) - \frac{4X_2}{1 + X_2} \right] \right\} . \quad (11)$$

The activity of BeF_2 can be deduced from the porportionality

$$a_{BeF_2} \propto a_{BeF_4}/a^2_{F^-} , \quad (12)$$

with the expression for a_{BeF_4} (as for a_{F^-} above) obtained from Eq. (8). These expressions for the activity involve the average degree of polymerization $\bar{b}$, defined as

$$\bar{b} = \Sigma \phi_{a,b} / \Sigma(\phi_{a,b}/b) . \quad (13)$$

Thus, application of this model to the calculation of the abundance of polymeric species and the component activities in a given melt requires the repeated evaluation of the three summations $\Sigma\phi_{a,b}$, $\Sigma(\phi_{a,b}/b)$, and $\Sigma(a\phi_{a,b}/b)$, which often converge slowly. Hence a computer must be used.

This model has been compared with observed activities derived from emf measurements[2] and from the LiF liquidus data[3] in the LiF-BeF_2 system by a least-squares procedure in which the parameters H, G, and G_r were optimized. The calculated and observed activity coefficients for BeF_2 are compared in Fig. 1.1. The agreement, on the average, is within two standard deviations of the experimental values and is considered quite good in view of the small number of adjustable parameters in the model. Using these parameters (Table 1.1), the distribution of representative polymeric species has been calculated as a function of composition in LiF-BeF_2 melts (Fig. 1.2).

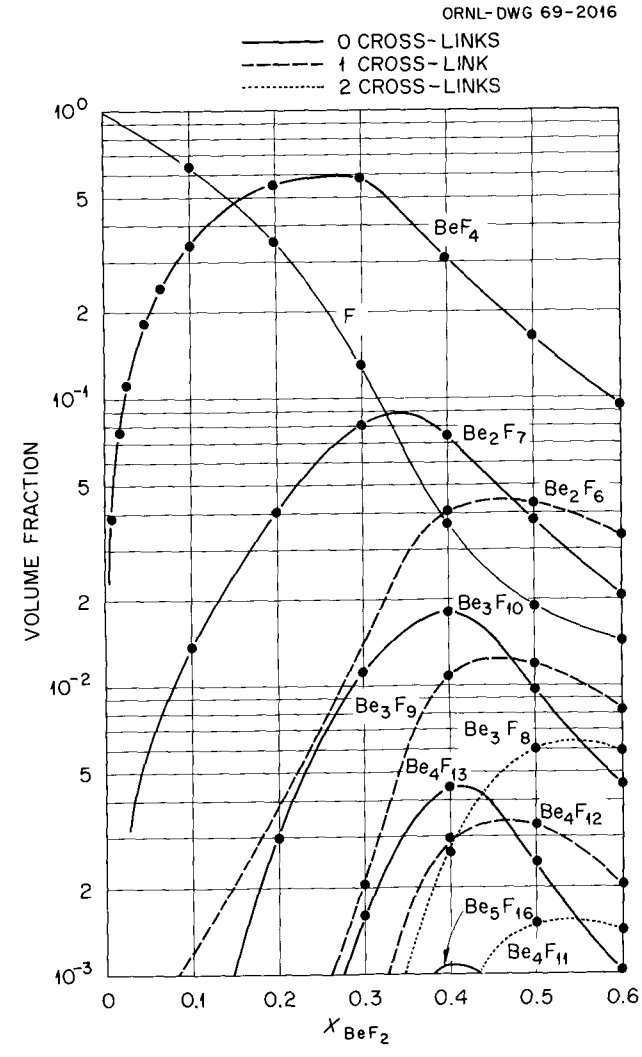

Fig. 1.2. Calculated Volume Fraction of Various Polymeric Anionic Species in LiF-BeF_2 Melts at 600°C.

Table 1.1. Parameter Values for LiF-BeF_2 Determined by a Least-Squares Fit of Polymer Model for EMF Data[2]

Parameter	Value of Parameter (cal) at –			
	500°C	600°C	700°C	800°C
G	−3674	−4016	−4359	−4701
H	−748	−748	−748	−748
G_r	−148	−39	48	118

[3]R. F. Thoma *et al.*, *J. Nucl. Mater.* 27, 166 (1968).

VISCOSITY AND DENSITY OF MOLTEN BeF_2-LiF SOLUTIONS

Stanley Cantor W. T. Ward
C. T. Moynihan[4]

Experimental measurements of these properties and preliminary interpretation of the data have been reported previously.[5,6] In this report we give a summary of further interpretation of the data from this system.

The LiF-BeF_2 system shows a very great decrease in viscosity as small quantities of LiF are added to BeF_2. This behavior is similar to the drastic viscosity reduction observed in melts of SiO_2[7] and of GeO_2[8] as either alkaline or alkaline-earth oxide is added. As single-component melts, BeF_2, SiO_2, and GeO_2 may be characterized as network liquids in which tetrahedral molecular units are bridged at corners. The dissolution of LiF in BeF_2 is believed to weaken the network structure by severing the fluoride bridges. The breakup should be correlated with a positive partial excess entropy of solution of BeF_2 ($\bar{S}^E_{BeF_2}$). This indeed is the case; Holm and Kleppa,[9] in combining free energy data with their measured enthalpies, showed that $\bar{S}^E_{BeF_2}$ rises rapidly with LiF concentration up to about 50 mole % LiF; at higher concentrations of LiF, the rise in $\bar{S}^E_{BeF_2}$ is less steep.

Besides breaking up the network of linkages between beryllium and fluorine, the introduction of LiF into a BeF_2 melt has another effect – an increase in the volume expansivity. The free volume[10] and the configuration entropy theories of liquid transport suggest a correlation between expansivity and E_η, the energy of activation for viscous flow, based on the hypothesis that increasing the expansivity will increase the temperature dependence of liquid free volume or configurational entropy and, correspondingly, decrease E_η. An apparent relationship between the reciprocal of expansivity ($1/\alpha$) and E_η is shown in Fig. 1.3. From

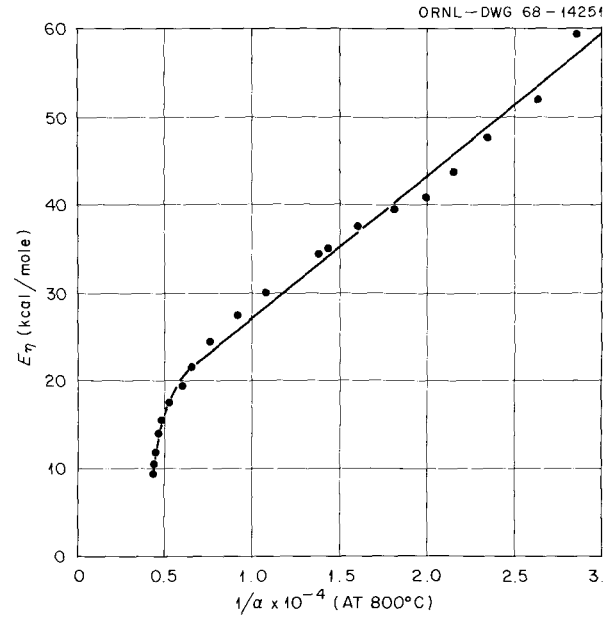

Fig. 1.3. Energy of Activation for Viscous Flow vs Reciprocal of Expansivity for the BeF_2-LiF System at 800°C.

59.5 to 21.5 kcal/mole, E_η is essentially linear with $1/\alpha$. The linear portion of Fig. 1.3 corresponds to the composition range 100–70 mole % BeF_2, where the melts are predominantly network liquids. For $E_\eta < 20$ kcal, representing BeF_2 contents < 65 mole %, the linear relationship between E_η and $1/\alpha$ changes drastically, possibly because the melt has lost its network character.

For all compositions studied the temperature dependence of viscosities in the BeF_2-LiF system can be represented within experimental error by a two-parameter Arrhenius equation

$$\eta = A \exp(E_\eta/RT) , \tag{14}$$

in which E_η, the activation energy for viscous flow, is apparently independent of temperature. Angell[11] has noted that non-Arrhenius behavior implicit in free volume[10] or configurational entropy treatments of liquid transport[12] appears only below $2T_0$, where T_0 is taken to be an ideal glass transition or "zero mobility" temperature. Although we cannot be certain, it seems probable that T_0, which is composition dependent,

[4]Chemistry Dept., California State College at Los Angeles; summer participant, 1966.

[5]S. Cantor and W. T. Ward, *Reactor Chem. Div. Ann. Progr. Rept. Dec. 31, 1965,* ORNL-3913, pp. 27–28.

[6]C. T. Moynihan and S. Cantor, *Reactor Chem. Div. Ann. Progr. Rept. Dec. 31, 1966,* ORNL-4076, pp. 25–28.

[7]J. O'M. Bockris, J. D. MacKenzie, and J. A. Kitchener, *Trans. Faraday Soc.* 51, 1734 (1955).

[8]E. F. Riebling, *J. Chem. Phys.* 36, 1889 (1963).

[9]J. L. Holm and O. J. Kleppa, *Inorg. Chem.*, in press (1969).

[10]M. H. Cohen and D. Turnbull, *J. Chem. Phys.* 31, 1164 (1959).

[11]C. A. Angell, *J. Am. Ceram. Soc.* 51, 123 (1968).

[12]C. A. Angell, *J. Phys. Chem.* 70, 2793 (1966).

decreases with increasing LiF concentration; even for compositions measured at relatively low temperatures, the values of T_0 were probably sufficiently low to preclude the observation of non-Arrhenius behavior.

The experimental results and their interpretation constitute a paper accepted for publication in the *Journal of Chemical Physics.*

OXIDE-FLUORIDE EQUILIBRIA

C. F. Baes, Jr.

The Chemistry of Silica in Molten Fluorides: The Reactions of Be_2SiO_4 with $2LiF\text{-}BeF_2$

C. E. Bamberger

As reported previously,[13–15] silica has been found in a number of applications to be a satisfactory container material for melts in which $2LiF\text{-}BeF_2$ is the solvent salt. The partial pressures of SiF_4 generated by the reaction

$$SiO_2(c) + 4F^- \rightleftharpoons 2O^{2-} + SiF_4(g) \qquad (15)$$

generally are low, and the oxide ion produced can easily be held to low levels if the SiF_4 is not swept away or, better, if SiF_4 is introduced with the cover gas. If the above reaction is allowed to proceed to the right by sweeping away the SiF_4 produced, the oxide ion concentration will increase until a new oxide-containing phase is precipitated. Beryllium oxide is normally the least soluble oxide in $2LiF\text{-}BeF_2$, but, in the presence of SiO_2, phenacite (Be_2SiO_4) should be the first to appear under equilibrium conditions since

$$SiO_2 + 2BeO \rightarrow Be_2SiO_4 \ . \qquad (16)$$

Accordingly, SiO_2 and Be_2SiO_4 together with $2LiF\text{-}BeF_2$ determine an equilibrium partial pressure of SiF_4 by the reaction

$$2SiO_2(c) + 2BeF_2(d) \rightleftharpoons Be_2SiO_4(c) + SiF_4(g) \ , \qquad (17)$$

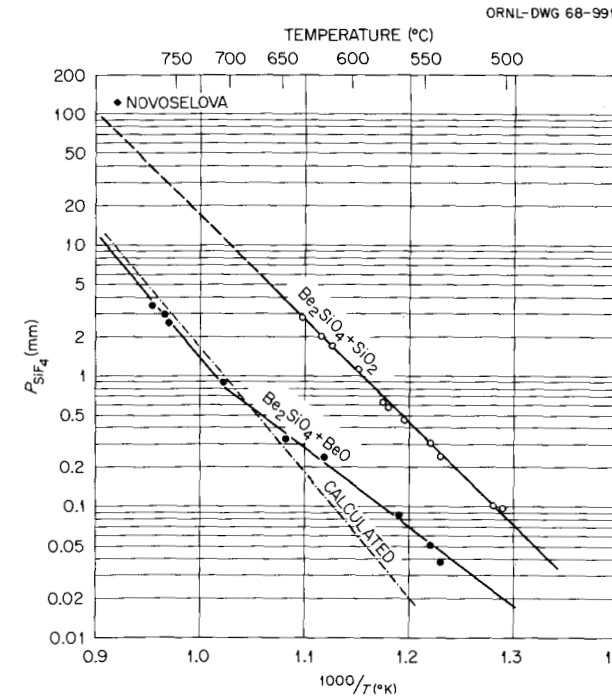

Fig. 1.4. Partial Pressures of SiF_4 Produced by Equilibration of Molten Li_2BeF_4 with Be_2SiO_4 + SiO_2 (Upper Curve) and with Be_2SiO_4 + BeO (Lower Curve). The dashed line is calculated from the upper curve and the reported heat and temperature of decomposition of Be_2SiO_4 into BeO and SiO_2.

for which we have reported[16]

$$\log P_{SiF_4} = 5.864 - 7576/T \ (\text{atm}) \ . \qquad (18)$$

In continuing these studies we have determined the lower partial pressures of SiF_4 generated when, in effect, all the SiO_2 has been consumed by the above reaction and, now, BeO appears as a solid phase. The reaction which is then expected is

$$Be_2SiO_4(c) + 2BeF_2(d) \rightleftharpoons 4BeO(c) + SiF_4(g) \ . \qquad (19)$$

The lower partial pressures observed for this equilibrium are compared with those found previously for (17) in Fig. 1.4. The lower dashed line represents the pressures which may be predicted by combining the previous results (Eq. 18) with Holm and Kleppa's

[13] C. E. Bamberger, R. B. Allen, and C. F. Baes, Jr., *Reactor Chem. Div. Ann. Progr. Rept. Dec. 31, 1967,* ORNL-4229, p. 60.

[14] C. E. Bamberger, C. F. Baes, Jr., and J. P. Young, *J. Inorg. Nucl. Chem.* 30, 1979 (1968).

[15] C. E. Bamberger *et al., Reactor Chem. Div. Ann. Progr. Rept. Dec. 31, 1967,* ORNL-4229, p. 20.

[16] C. E. Bamberger and C. F. Baes, Jr., *MSR Program Semiann. Progr. Rept. Feb. 29, 1968,* ORNL-4254, p. 146.

recently reported value[17] for the enthalpy of reaction (16),

$$\Delta H(16) = -4.7 \text{ kcal} .$$

Thus, since

$$\Delta H(17) - \Delta H(19) = 2\Delta H(16) ,$$

the difference in slopes of the upper line and the lower, dashed line in the figure is determined by $\Delta H(16)$. With the further requirement that the two lines must intersect at the temperature of decomposition of phenacite into BeO and SiO_2 – reported by Morgan and Hummel[18] as 1560°C – the dashed line is determined, giving

$$\log P_{SiF_4} = 6.786 - 9526/T \text{(atm)} . \qquad (20)$$

The data actually obtained above 700°C are seen to agree quite well with the predicted behavior. Below this temperature, however, the measured pressures are increasingly higher than the predicted values. One explanation for this effect would be the appearance of a new solid phase below 700°C, one in which the BeO/SiO_2 ratio is greater than 2 and which perhaps contains fluoride. Such silicates of Ca, Ba, and Sr are known in which the MO/SiO_2 ratio is 3, but are not known for Mg or Be. Furthermore, we have been unable to produce readily detectable amounts of such a new compound in mixtures of SiO_2, Be_2SiO_4, and BeO equilibrated with Li_2BeF_4 at 625 to 650°C for as much as 30 days.

Another possible explanation is the existence of a previously unsuspected solid-state transition in BeO occurring at or below 700°C with a transition heat of ~4 kcal/mole. To our knowledge, however, no other evidence of such a transition exists. In fact, in our measurements, the same x-ray powder pattern has been found for all BeO samples, whether equilibrated above or below 700°C, and this pattern agrees with that reported in the literature. Hence the possibility of a transition in BeO seems unlikely.

Whatever the explanation of this somewhat high value of P_{SiF_4} below 700°C in the latest measurements, the chemistry of silica in $2LiF\text{-}BeF_2$ melts is now fairly well defined. In future measurements we plan to explore possible ion exchange properties of Be_2SiO_4 (which has an open structure[19]) and any rare-earth-containing silicates which might be produced by equilibration of Be_2SiO_4 with $LiF\text{-}BeF_2$ melts containing rare-earth trifluorides.

[17] J. L. Holm and O. J. Kleppa, *Acta Chem. Scand.* 20, 2568 (1966).

[18] R. A. Morgan and F. A. Hummel, *J. Am. Ceram. Soc.* 32, 250 (1949).

A Stirred Reaction Vessel for Molten Fluorides

C. E. Bamberger T. J. Golson[20]
J. Nicholson[20]

In our previous studies of heterogeneous equilibria involving molten fluorides, we have usually provided agitation by bubbling a stream of gas – either an inert gas or a gas mixture containing reactants – through the molten salt. Occasionally, when stronger agitation seemed necessary, we have used rocking furnaces[21] or a stirred vessel.[22] More recently, in order to study ion exchange equilibria between a dense oxide phase and a molten fluoride phase (cf. following section) we designed a reaction vessel which can provide quite vigorous agitation for long periods while remaining essentially gastight. This stirred vessel includes the following features (Fig. 1.5):

1. The shaft seal is provided by an oil-lubricated Quad-X ring,[23] a ring of soft silicone rubber with a roughly square cross section. When in place, it is compressed sufficiently to make a gastight seal at two points on the shaft. Since it is not compressed by a packing nut, it is easily removed for replacement.
2. The upper (cooled) bearing for the shaft is a sleeve of Teflon or of oil-impregnated metal. The lower (hot) bearing is a sleeve of graphite which is easily replaceable.
3. The stirrer is driven by a flexible cable connected to a variable-speed dc motor, the speed of which may be varied continuously from 60 to 1760 rpm.
4. The shaft and stirrer blade (of Hastelloy N) can easily be removed and replaced. The vessel, flanged to the stirrer assembly, is cheap to fabricate and is easily replaced.

[19] W. L. Bragg and W. H. Zachariasen, *Z. Krist.* 72, 518 (1930).

[20] General Engineering Division.

[21] K. A. Romberger, C. F. Baes, Jr., and H. H. Stone, *J. Inorg. Nucl. Chem.* 29, 1619 (1967).

[22] J. E. Eorgan *et al., Reactor Chem. Div. Ann. Progr. Rept. Dec. 31, 1964,* ORNL-3591, p. 45.

[23] Manufactured by Minnesota Rubber Co., Minneapolis, Minn.

ORNL-DWG 68-3432RA

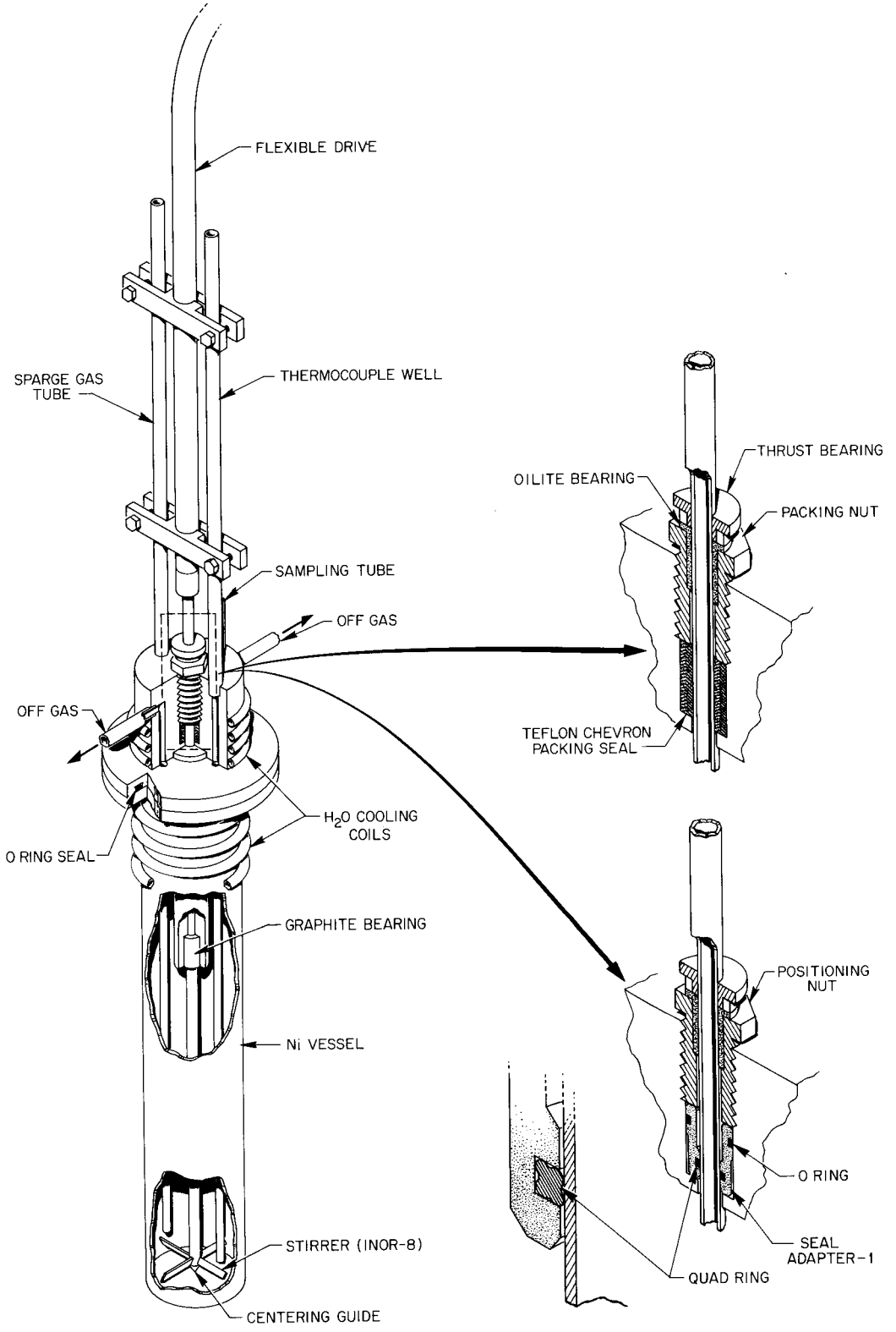

Fig. 1.5. Stirred Reaction Vessel for Molten Fluorides.

This assembly has been operated continuously for as long as 14 days at 500 rpm with a positive internal gas pressure of 50 cm before an appreciable leakage rate developed as a result of wear of the Quad-X ring. At such times the ring may quickly be replaced, with the vessel at temperature, and operation resumed.

In the original version of the apparatus,[24] the seal was provided by several Teflon chevron rings[25] stacked on the shaft and compressed with a packing nut (Fig. 1.5). These were found to wear so rapidly at 150 rpm, even when lubricated with oil, that daily tightening of the packing nut was necessary to provide leak tightness. Replacement – a more difficult operation – was necessary every seven days or so.

This stirred vessel has greatly facilitated the equilibration of $(U\text{-}Th)O_2$ solid solutions with molten fluorides, the results of which are described in the following section. No doubt it will prove similarly useful in a number of future studies of heterogeneous equilibria involving molten fluorides.

The Distribution of U^{4+} Between Molten $LiF\text{-}BeF_2\text{-}ThF_4\text{-}UF_4$ and a $(U\text{-}Th)O_2$ Solid Solution

C. E. Bamberger A. L. Johnson

A preliminary study[26] of U^{4+} distribution between molten $2LiF\text{-}BeF_2$ containing Th^{4+} and a $(U\text{-}Th)O_2$ solid solution by the ion exchange reaction

$$U^{4+}(F) + Th^{4+}(O) \rightleftharpoons U^{4+}(O) + Th^{4+}(F) \qquad (21)$$

indicated that the distribution quotient,

$$Q = \frac{X_{UO_2} X_{ThF_4}}{X_{UF_4} X_{ThO_2}}, \qquad (22)$$

has a value between 1000 and 2000 at 600°C. This two-phase system, which may be viewed as a solvent extraction system in which one of the phases is the oxide solid solution, is being studied further because of its obvious relevance to the oxide chemistry of a single-fluid MSBR fuel and because of its potential value as a reprocessing method.[27]

In the present measurements the rocking furnace used previously has been replaced by a stirred, gastight vessel (see preceding section, this report) wherein the phases to be equilibrated can be agitated vigorously under argon, and in which samples can be taken or additions made conveniently. The composition of the oxide phases has been changed readily by additions of UO_2, ThO_2, or UF_4 mixed with LiF, BeF_2, and ThF_4 such that the composition of the fluoride phase is held near $LiF\text{-}BeF_2\text{-}ThF_4$ (72-16-12). The fluoride phase has been sampled frequently by means of copper filter sticks, and uranium analysis of these samples obtained to follow the $U^{4+}\text{-}Th^{4+}$ exchange. Material balances have been used to determine the concentrations of the other major components of the fluoride phase and the composition of the oxide phase. The oxide phase, sampled less frequently, has been analyzed by x-ray diffraction.[28] This has served to show, as expected, that a homogeneous $(U\text{-}Th)O_2$ solid solution is always the equilibrium oxide phase. Its composition, based on a determination of the lattice constant, has been within 3% of the material balance value.

In the first run made with the stirred vessel, it was found that with the relatively large amounts of oxide employed (550 g of oxide phase to 600 g of fluoride phase), a stirring rate of 150 rpm was insufficient even to homogenize the heavy oxides after many hours of stirring. In subsequent runs, the amount of the oxide phase was reduced (e.g., 140 g of oxide to 600 g of fluoride), and, with improvements in the design of the stirrer seal (see preceding section), the stirring rate was increased to 500 rpm.

Under these conditions, complete mixing evidently was obtained since successive samples of the fluoride phase indicated that equilibrium was reached in less than 70 hr (Fig. 1.6) whether the previously equilibrated system had been disturbed by the addition of UO_2, ThO_2, or UF_4, or just by changing the temperature. The path followed by the UF_4 concentration of the fluoride phase was unexpectedly complex when UO_2 or ThO_2 was added, showing both a maximum above and a minimum below the final equilibrium value. While considerably more information is needed concerning the effects of a number of variables – such as the stirring rate, the quantities of each phase, and the

[24] C. E. Bamberger, C. F. Baes, Jr., T. J. Golson, and J. Nicholson, *MSR Program Semiann. Progr. Rept. Feb. 29, 1968*, ORNL-4254, p. 146.

[25] Manufactured by Crane Packing Co., Morton Grove, Ill.

[26] B. F. Hitch, C. E. Bamberger, and C. F. Baes, Jr., *Reactor Chem. Div. Ann. Progr. Rept. Dec. 31, 1966*, ORNL-4076, p. 18.

[27] C. E. Bamberger and C. F. Baes, Jr., *MSR Program Semiann. Progr. Rept. Aug. 31, 1968*, ORNL-4344, in press.

[28] Performed by R. L. Sherman, Analytical Chemistry Division.

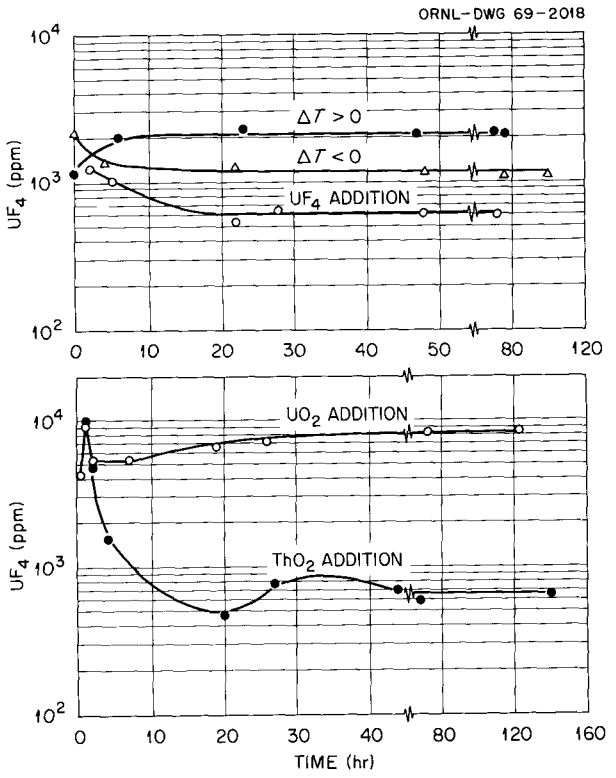

Fig. 1.6. Approach to Equilibrium in the Exchange of U^{4+} and Th^{4+} Between Molten Fluoride and Solid Oxide Solutions.

amounts of material to be exchanged – before the rate of approach to equilibrium can be predicted or perhaps significantly increased, it seems clear from the present results that the exchange process is as rapid and reversible as could be expected in view of the fact that each time the system is disturbed the return to equilibrium requires that the composition of the entire oxide phase must be changed by repeated recrystallization.

The equilibrium results obtained thus far (Fig. 1.7) show that the exchange quotient Q increases with the uranium content of the oxide phase and, furthermore, that Q decreases rapidly with increasing temperature; thus, at $X_{UO_2} = 0.65$,

$$\log Q = -0.1206 + 2574(1/T) . \qquad (23)$$

Since the exchange reaction [Eq. (21)] involves two ions of the same charge and nearly the same size, Q might have been expected to be near unity. Actually, however, it has been known for some time that UO_2 is much less soluble than ThO_2 in molten fluorides[29] and, hence, Q indeed should be considerably above unity. The dependency of Q on composition of the oxide

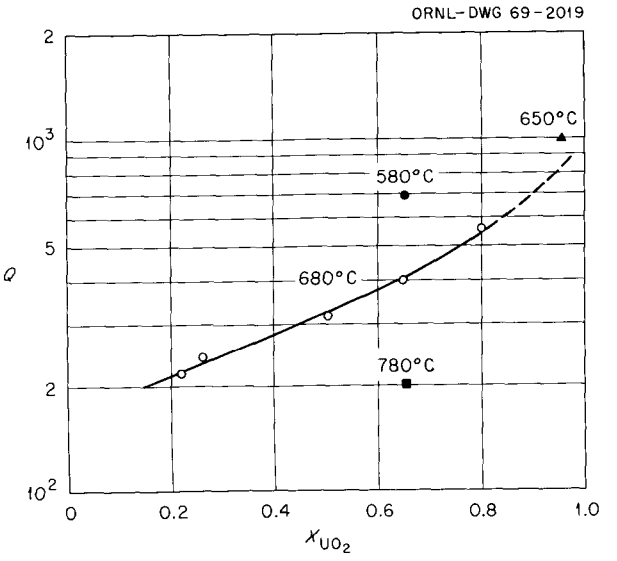

Fig. 1.7. Variation of the Quotient for Reaction (21) with Composition of the Oxide Phase and with Temperature.

phase suggests that this phase is fairly nonideal. The small value of the intercept in Eq. (23) indicates that the entropy of exchange is essentially zero, and hence that this nonideal behavior is caused primarily by an excess heat of mixing in the solid solution.

In future measurements, the effect on Q of variation in the salt-phase composition will be determined, the distribution of Pa^{4+} in the presence of both U^{4+} and Th^{4+} will be examined, and finally the concentration of oxide ion in the fluoride phase will be determined at phase compositions which are expected to be typical of an MSBR.

AN Ni, NiO, BeO ELECTRODE OF THE THIRD KIND AS A REFERENCE ELECTRODE IN MOLTEN FLUORIDES

B. F. Hitch C. F. Baes, Jr.

As reported previously,[30,31] the $Be^{2+}|Be$ and the $HF,H_2|F^-$ electrodes are stable reference electrodes for use in $LiF\text{-}BeF_2$ mixtures. However, both electrodes have disadvantages. Because of the strong reducing

[29] J. H. Shaffer, G. M. Watson, and W. R. Grimes, *Reactor Chem. Div. Ann. Progr. Rept. Jan. 31, 1960,* ORNL-2931, p. 90.

[30] G. Dirian, K. A. Romberger, and C. F. Baes, Jr., *Reactor Chem. Div. Ann. Progr. Rept. Jan. 31, 1965,* ORNL-3789, p. 76.

[31] B. F. Hitch and C. F. Baes, Jr., *An EMF Study of $LiF\text{-}BeF_2$ Solutions,* ORNL-4257 (July 1968).

power of the $Be^{2+}|Be$ electrode, it is easily poisoned by impurities or solutes which are reduced and deposited as metals on the electrode surface. Hence it is necessary to maintain the melt in the vicinity of this electrode quite free of such reducible substances. This electrode can develop dendritic crystals of beryllium metal on its surface as a result of mass transfer, and these can short the electrode to the cell wall if adequate clearance has not been provided. The $HF,H_2|F^-$ electrode is somewhat inconvenient to use because it requires an $HF\text{-}H_2$ gas mixture of known composition. A more serious disadvantage of this electrode is that hydrogen is a reactive, rapidly diffusing gas which is hard to confine to the vicinity of the electrode.

In continuing our efforts to develop reference electrodes for use in molten fluorides we have investigated the electrode

$$Ni^0|BeO(c)\ ,\ NiO(c)|LiF\text{-}BeF_2(66\text{-}34)| \qquad (24)$$

vs the $Be^{2+}|Be^0$ electrode.[31,32] If the melt in contact with the nickel electrode is saturated with both NiO and BeO, then the dissolved oxide concentration is fixed by the solubility equilibrium of BeO:

$$BeO(c) \rightleftharpoons Be^{2+} + O^{2-} \qquad (25)$$

(e.g., $[O^{2-}] \cong 0.01$ mole/kg at 600°C[32]), and hence the nickel ion concentration is fixed by the solubility equilibrium of NiO:

$$NiO(c) \rightleftharpoons Ni^{2+} + O^{2-} \qquad (26)$$

($[Ni^{2+}] \sim 0.001$ mole/kg at 600°C).[33] This should establish a potential at the nickel electrode which depends only on the temperature and the composition of the $LiF\text{-}BeF_2$ salt mixture used. The low concentration of Ni^{2+} produced by this oxide mixture renders this electrode – an electrode of the third kind – considerably less oxidizing than a saturated $NiF_2|Ni$ electrode. When this electrode is measured against the $Be^{2+}|Be^0$ electrode, the assumed cell reaction is

$$Be^0 + NiO(c) \rightleftharpoons BeO(c) + Ni^0\ . \qquad (27)$$

Since all the reactants and products are at fixed activities, the measured cell potential should be the standard potential E°, and a function only of temperature. X-ray analysis has confirmed that NiO, BeO, and $LiF\text{-}BeF_2$ (66-34) are indeed the only constituents in the $Ni^{2+}|Ni$ electrode compartment.

The reaction vessel used for our experiments was constructed of 2½-in. nickel pipe separated into two compartments by a 1/16-in. nickel sheet welded down through the center. Melt contact between the two compartments was provided by a ½-in.-diam sintered nickel (0.0015 in. porosity) frit. Each compartment of the reaction vessel was fitted with an entry port for an electrode, a gas sparging line, and a thermocouple well. The $Ni^{2+}|Ni$ electrode was further compartmented to contain the oxides and the dissolved NiF_2. The beryllium electrode was used without any compartmentation.

In our early potentiometric measurements of the above cell, the compartment for the nickel electrode was constructed of copper tubing with a copper frit (25 to 40 μ porosity) welded onto the lower end. Excess BeO and NiO were added to this compartment and the $LiF\text{-}BeF_2$ solution was then forced through the copper frit into the compartment by a small gas pressure. A nickel tube served as the nickel electrode and also permitted gas sparging. Cell potentials were erratic, but on various occasions we were able to achieve stable potentials for as long as 24 hr. The major difficulty encountered was that the cell potential would reach a maximum value, then begin drifting toward a lesser value. In an attempt to improve the performance of the Ni electrode, we modified the compartment described above by using a more dense copper frit (<10 μ pore size), and in another version we used nickel tubing clad in copper. Neither modification resulted in any significant improvement in the behavior of the cell potential.

Since the possibility of electrical shorts between the $Ni^{2+}|Ni$ electrode and the metal electrode compartments could have been responsible for some of the difficulties described above, we fabricated a compartment using silica tubing and a silica frit. The silica served as an electrical insulator for the Ni electrode and contained the oxide-saturated $2LiF\text{-}BeF_2$ mixture.[34] An improved Ni electrode was also used in the silica compartments. This electrode was fabricated by welding a small (3/16 × 3/8 in.) rectangle of sintered metal to 1/8-in. nickel rod. The sintered nickel was then "painted" with an aqueous slurry of $Ni(OH)_2$ and fired

[32] B. F. Hitch and C. F. Baes, Jr., *MSR Program Semiann. Progr. Rept. Feb. 28, 1967*, ORNL-4119, p. 144.

[33] C. F. Baes, Jr., "The Chemistry and Thermodynamics of Molten-Salt Reactor Fluoride Solutions," p. 409 in *Thermodynamics*, vol. 1, IAEA, Vienna, 1966.

[34] C. E. Bamberger, C. F. Baes, Jr., and J. P. Young, *J. Inorg. Nucl. Chem.* 30, 1979 (1968).

at 1000°C. This provided a larger surface area for the electrode reaction as well as a source of NiO.

Using a silica compartment and the improved Ni electrode we obtained standard cell potentials (E°) over a temperature range of 525–715°C, as shown in Fig. 1.8. Potential measurements were made over a period of one week, and although the silica was attacked by the fluoride melt, it did not rupture, nor did the electrode potential show any appreciable variation during this period. The standard cell potential compares well with values calculated using the formation free energies of BeO and NiO.

The $Ni^{2+}|Ni$ electrode described above shows promise for use as a reference electrode in molten fluorides. We are presently trying to improve the compartment assembly for this electrode. In one version now in use, the silica is clad with nickel tubing to prevent direct contact of the melt outside of the compartment with the silica. This electrode assembly is being used to measure the redox potential of the U^{4+}/U^{3+} couple. Results obtained so far are not in agreement with cell potentials calculated from available thermochemical data.[33] However, zirconium metal is being used as a reductant in this experiment to reduce U^{4+} to U^{3+}, and it is possible that the inconsistency is due to the reduction of impurities in the melt or possibly the alloying of Zr^0 with the nickel vessel. Another compartment presently being investigated uses BeO tubing for the inner compartment instead of silica to provide electrical insulation for the electrode and to contain the oxide-saturated melt.

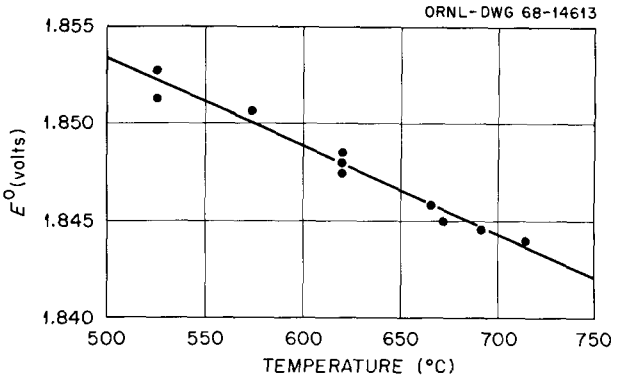

Fig. 1.8. Standard Cell Potentials (E°) of the Cell $Be^0|LiF\text{-}BeF_2$ (66-34)$|NiO(c),BeO(c)|Ni^0$ as a Function of Temperature.

IONIC TRANSPORT PROPERTIES IN MOLTEN FLUORIDES

K. A. Romberger J. Braunstein

A program has been started which has as its objective the systematic investigation and interpretation of the ionic transport properties in molten fluorides. $LiF\text{-}BeF_2$ mixtures are being used as the model solvent system. The initial studies in this program have been to develop reference electrodes for voltammetry and potentiometry in order to investigate electrical and diffusional mobilities of the ions in these melts.

Hitch and Baes[35] have demonstrated the applicability of beryllium and hydrogen–hydrogen fluoride electrodes to measurements of activities in molten mixtures of lithium fluoride and beryllium fluoride. We here demonstrate the application of concentration cells with beryllium electrodes to the evaluation of the (Hittorf or internal) transference numbers in these mixtures.

The emf of the concentration cell with transference

$$\text{Be} \left| \begin{array}{c} \text{LiF} \\ \text{BeF}_2 \\ \text{I} \end{array} \right| \begin{array}{c} \text{LiF} \\ \text{BeF}_2 \\ \text{II} \end{array} \left| \text{Be} \right.$$

may be written,[36] by consideration of the electrode and transport processes and the Gibbs-Duhem equation, as

$$E_t = \int_{\text{I}}^{\text{II}} t_{\text{Li}} \left(\frac{1+x}{1-x} \right) dE_w \,, \tag{28}$$

where E_t is the emf of the concentration cell with transference, t_{Li} is the internal transference number of lithium ion (taking fluoride as the reference ion), x is the mole fraction of BeF_2, and E_w is the emf of a concentration cell without transference; I and II represent the compositions of the $LiF\text{-}BeF_2$ mixtures in the two electrode compartments. Thus the transference number of lithium ion ($t_{\text{Li}} = 1 - t_{\text{Be}}$) can be obtained as a function of composition from Eq. (28) as

$$t_{\text{Li}} = \left(\frac{1-x}{1+x} \right) \frac{dE_t}{dE_w} \,, \tag{29}$$

or, by averaging over composition ranges where the transference number does not vary rapidly, as

[35] B. F. Hitch and C. F. Baes, Jr., *Reactor Chem. Div. Ann. Progr. Rept. Dec. 31, 1967*, ORNL-4229, p. 52.

[36] C. Wagner, p. 11 in *Electrochemistry and Electrochemical Engineering*, ed. by P. Delahay, Interscience, New York, 1966.

$$\bar{t}_{Li} = \frac{\Delta E_t}{\int_{I}^{II} \left(\frac{1+x}{1-x} \right) dE_w} . \qquad (30)$$

Emf measurements were made in a silica apparatus, described previously,[37] with a coarse fritted silica disk separating the mixtures of differing composition. The porosity was high enough to ensure conduction through the melt rather than through a silica membrane,[38] but proper positioning prevented leakage during the time of the measurements. The temperature was maintained at 500°C, and the compositions varied between 0.33 and 0.51 mole fraction BeF_2. The emf measurements, E_t, were stable to ±0.1 mv and reproducible within ±2 mv, as determined by measurements with two different reference half-cells and by cycling the composition from 0.34 to 0.51 and back to 0.33 mole fraction BeF_2. The deviations from a smooth curve of E_w, obtained from the data of Hitch and Baes,[35] also were ±2 mv.

Figure 1.9 is a plot of E_t and E_w vs composition, both relative to a reference half-cell containing 0.34 mole fraction BeF_2. The difference between these curves is an apparent liquid junction potential, which is 100 mv for the junction of 35 and 51 mole % BeF_2.

Graphical integration of Eq. (30) over the range 0.33–0.51 mole fraction BeF_2 yielded a mean value of t_{Li} = 1.0 ± 0.05 (hence t_{Be} = 0 ∓ 0.05). The uncertainty in the transference numbers corresponds to the emf error of ±2 mv. Estimates of t_{Li} over smaller intervals of composition showed some scatter but led to values of t_{Li} >0.9. In view of the extremely high electrostatic interactions between beryllium and fluoride ions, it is not surprising that the mobility of beryllium ion relative to fluoride ion is virtually zero and that lithium ions are the principal current carriers.

If beryllium electrodes are used in the same cell with electrodes reversible to lithium ions, a concentration cell without transference can be formed. The emf's of such a cell yield values of E_w directly, so that transference numbers can be obtained without recourse to outside data. Attempts are continuing to develop lithium in bismuth alloy electrodes and to test their reversibility and stability in these fluoride systems. Such electrodes will be useful not only for transference number studies but also as reference electrodes for voltammetry.

[37]K. A. Romberger, *MSR Program Semiann. Progr. Rept. Feb. 29, 1968,* ORNL-4254, p. 149.

[38]W. K. Behl and J. Egan, *J. Phys. Chem.* 71, 1765 (1967).

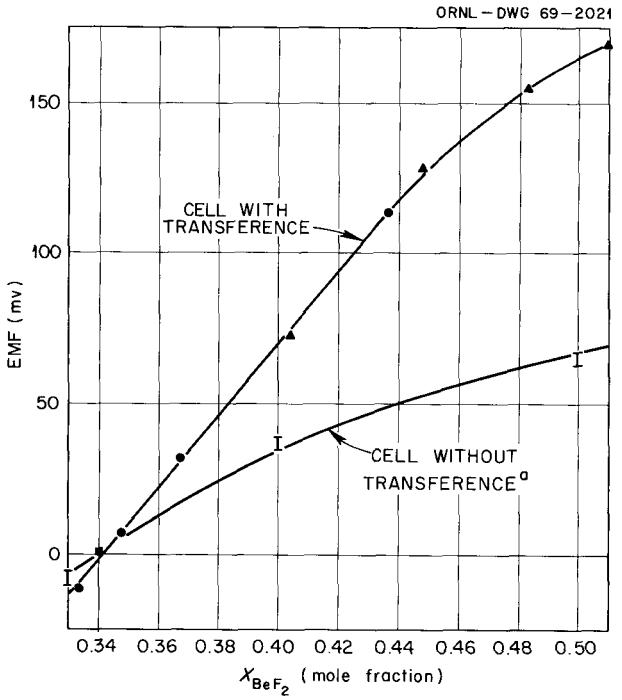

Fig. 1.9. Measured EMF of the Concentration Cell with Transference (E_t) and Calculated EMF of the Concentration Cell Without Transference (E_w) vs Composition in the System BeF_2-LiF at 500°C.

ELECTRICAL CONDUCTANCE MEASUREMENTS IN MOLTEN SALTS

A Review of Electrical Conductance Measurements in Fused Fluorides

G. D. Robbins

A review of electrical conductance measurements in molten fluorides has been completed[39] which covers the period 1927 to 1967 and includes some 56 fused fluoride systems. Table 1.2 represents the results, which may be summarized as follows:

I. Because of the high specific conductance of most molten salts (1 to 6 ohm^{-1} cm^{-1}),[40] experimental approaches have tended to fall into two groups:[41] (*a*) use of capillary-containing cells, which results in a

[39]G. D. Robbins, *Electrical Conductivity of Molten Fluorides. A Review,* ORNL-TM-2180 (Mar. 26, 1968).

[40]I. S. Yaffe and E. R. Van Artsdalen, *J. Phys. Chem.* 60, 1125 (1956).

[41]G. J. Janz, C. Solomons, and H. J. Gardner, *Chem. Rev.* 58, 461 (1958).

Table 1.2. Electrical Conductance Investigations of Molten-Fluoride Systems

No.	System	Ref.	Cell, [R] or (ℓ/a)	Electrodes	Bridge (Detector)	f (kHz) of Measurement	R vs. f	Vpp (v)
1	LiF	a	Pt crucible [R] ≃ 0.1 Ω	Pt crucible and platinized Pt foil (3 x 4 mm)	Wheatstone (telephone)	6	N.S. = Not stated	N. S.
2	LiF	b	Two Pt(80%)-Rh hemispheres (d ≈ 3/4" and 2"). These are also current electrodes.	Two Pt(80%)-Rh rods (d = 0.01"). These are potential-measuring electrodes.	Specially developed by E. Fairstein(c) f range = .2-6 kHz; R range = 0.01-10 Ω (oscilloscope)	N.S.	N.S.	N. S.
3	LiF	d e	Hot-pressed BN cylinder (id ≈ 3/16" surrounded by graphite, [R] ≃ [illegible] Ω. (ℓ/a) = 17-39 cm⁻¹	Inconel rod and Inconel plate across ends of BN cylinder.	Wheatstone, no capacitors (oscilloscope)	2	"Did not vary appreciably between 1 and 20 kHz."	N.S.
4	LiF	f g	Pt crucible (vol. = 39 cm³), (ℓ/a) ≃ 0.28 cm⁻¹	Two platinized Pt foils (10 x 10 mm)	Thomson-type (oscilloscope)	50	r-dependency at lower f, independent at 50 kHz	~ 0.05
5	LiF	h	Graphite crucible (id = 3.5", 5" deep) containing 2 BN cylinders (id = 3/16") encased in graphite and enlarged at top to accommodate electrodes, (ℓ/a) ~ 100 cm⁻¹	Two 1/4" Mo tubes fitting into upper portions of BN cylinders	Jones (null detector)	10	f independent 1-20 kHz	N. S.
6	NaF	i j	Pt crucible (400 ml), (ℓ/a) = 0.0835 cm⁻¹	Hemispherical Pt electrodes, platinized originally.	Kelvin	0.6 to 4	r ∝ f^-1/2 extrapolated to f = ∞	10
7	NaF	k	Pt crucible (0.2 mm wall), [R] = 0.02 Ω	Crucible and a Pt cylinder (area = 2 cm²), both platinized	N. S.	0.15 to 8	N. S.	N. S.
8	NaF	d e	Same as No. 3	No. 3	No. 3	No. 3	No. 3	No. 3
9	NaF	f g	Same as No. 4	No. 4	No. 4	No. 4	No. 4	No. 4
10	NaF	h	Same as No. 5	No. 5	No. 5	No. 5	No. 5	No. 5
11	KF	a	Same as No. 1	No. 1	No. 1	No. 1	No. 1	No. 1
12	KF	b	Same as No. 2	No. 2	No. 2	No. 2	No. 2	No. 2
13	KF	d e	Same as No. 3	No. 3	No. 3	No. 3	No. 3	No. 3
14	KF	f g	Same as No. 4	No. 4	No. 4	No. 4	No. 4	No. 4
15	KF	l m n	MgO, single crystal, dip cell; Pt container	Container and Pt electrode	Jones	0.5 to 10	Varied < 0.3% over f range	N. S.
16	CsF	b	Same as No. 2	No. 2	No. 2	No. 2	No. 2	No. 2
17	CsF	m n	Same as No. 15	No. 15	No. 15	No. 15	No. 15	No. 15
18	AgF	f g	Same as No. 4	No. 4	No. 4	No. 4	No. 4	No. 4
19	BeF_2	o p	Pt-Rh(20%) crucible (id = 2", ht. = 2-1/2")(ℓ/a) = 0.11 or 0.28 cm⁻¹	Crucible and Pt-Rh (20%) bob	"Wheatstone R-C Bridge" (scope or VTVM)	2-10	f independent 2-10 kHz	N. S.
20	CaF_2	q	Carbon crucible	Mo electrodes	N.S.	N.S.	N.S.	N.S.
21	MnF_2, CuF_2, ZnF_2, PbF_2, KBF_4, Na_2TaF_7, K_2TiF_6, K_2TaF_7	f g	Same as No. 4	No. 4	No. 4	No. 4	No. 4	No. 4
22	Li_3AlF_6	d e	Same as No. 3	No. 3	No. 3	No. 3	No. 3	No. 3
23	Na_3AlF_6	r	Fused MgO tube (d = 0.99, ℓ = 10.3 cm) (ℓ/a) = 0.0752 cm⁻¹	Graphite plates across ends of tube	Wheatstone R and R in parallel(telephone)	Two f's	N.S.	N.S.
24	Na_3AlF_6	j	Same as No. 6	No. 6	No. 6	No. 6	No. 6	No. 6
25	Na_3AlF_6	k	Same as No. 7	No. 7	No. 7	No. 7	No. 7	No. 7
26	Na_3AlF_6	d e	Same as No. 3	No. 3	No. 3	No. 3	No. 3	No. 3
27	Na_3AlF_6	f g	Same as No. 4	No. 4	No. 4	No. 4	No. 4	No. 4
28	Na_3AlF_6	s	Pt hemisphere (od = 4 cm), (ℓ/a) = 0.386 cm⁻¹	Container and Pt rod (d = 3 mm)	Thomson plus phase indicator	5	N.S.	N.S.
29	K_3AlF_6	d e	Same as No. 3	No. 3	No. 3	No. 3	No. 3	No. 3
30	LiF + ThF_4	h	Same as No. 5	No. 5	No. 5	No. 5	No. 5	No. 5
31	LiF + UF_4	h	Same as No. 5	No. 5	No. 5	No. 5	No. 5	No. 5
32	NaF + CaF_2 (67 w %)	t	Pt crucible [R] ≃ 0.1 Ω	Crucible and Pt rod, both platinized originally.	Carey-Foster	1	N.S.	N.S.
33	NaF + SrF_2 (67 w %)	t	Same as No. 32	No. 32	No. 32	No. 32	No. 32	No. 32
34	NaF + BaF_2 (67 w %)	t	Same as No. 32	No. 32	No. 32	No. 32	No. 32	No. 32
35	NaF + ZrF_4	u	Hot-pressed BeO tube in a cylindrical Pt crucible (ℓ/a) = 24 cm⁻¹	Pt crucible across bottom of the tube and Pt rod at top	Wheatstone, R and R in parallel (oscilloscope)	1	N. S.	N. S.
36	NaF + ThF_4	h	Same as No. 5	No. 5	No. 5	No. 5	No. 5	No. 5
37	NaF + UF_4	h	Same as No. 5	No. 5	No. 5	No. 5	No. 5	No. 5
38	NaF + $NaBF_4$	v	Described in Ref. w, not readily available	Pt electrodes	Wheatstone, with balancing R (oscilloscope)	5	N. S.	N. S.
39	NaF + Na_3AlF_6	i j	Same as No. 6	No. 6	No. 6	No. 6	No. 6	No. 6
40	KF + KBF_4	v	Same as No. 38	No. 38	No. 38	No. 38	No. 38	No. 38
41	MgF_2 + Na_3AlF_6	x	Pt cell	N.S.	Wheatstone, R and R in parallel (oscilloscope)	N.S.	N. S.	N. S.
42	CaF_2 + Na_3AlF_6	y r	Graphite crucible [R] ≃ 0.5 Ω	Carbon anode and molten Al cathode	Wheatstone, R and R in parallel (telephone)	Two f's	N. S.	N. S.
43	CaF_2+ Na_3AlF_6	i j	Same as No. 6	No. 6	No. 6	No. 6	No. 6	No. 6
44	CaF- Na_3AlF_6 (81 m%)	d e	Same as No. 3	No. 3	No. 3	No. 3	No. 3	No. 3
45	AlF_3- Na_3AlF_6	x	Same as No. 41	No. 41	No. 41	No. 41	No. 41	No. 41
46	AlF_3 + Na_3AlF_6	i j	Same as No. 6	No. 6	No. 6	No. 6	No. 6	No. 6
47	Li_3AlF_6 + Na_3AlF_6 (40 w %)	d e	Same as No. 3	No. 3	No. 3	No. 3	No. 3	No. 3
48	LiF-NaF-KF(46.5-11.5-42 m%)	u	Hemispherical Pt crucible (ℓ/a) = 0.162	Current electrodes: crucible and Pt sphere: potential electrodes: crucible and Pt cylinder surrounding sphere	No bridge; VTVM and ammeter	0.5	N. S.	N. S.
49	NaF + ZrF_4 + UF_4	u	Same as No. 48	No. 48	No. 48	No. 48	No. 48	No. 48

Table 1.2 (continued)

[a]E. Ryschkewitsch, *Z. Elektrochem.* **39**, 531 (1933).

[b]I. S. Yaffe and E. R. Van Artsdalen, *Chem. Div. Semiann. Progr. Rept. June 20, 1956,* ORNL-2159, p. 77.

[c]E. Fairstein, *Instrumentation and Controls Div. Semiann. Progr. Rept. July 31, 1955,* ORNL-1997, p. 9.

[d]E. W. Yim and M. Feinleib, *J. Electrochem. Soc.* **104**, 622 (1957).

[e]*Ibid.*, 626 (1957).

[f]H. Winterhager and L. Werner, *Forschungsber. Wirtsch. Verkehrsministeriums Nordrhein-Westfalen,* No. 438 (1957).

[g]*Ibid.*, No. 341 (1956).

[h]E. A. Brown and B. Porter, U.S. Department of Interior, Bureau of Mines, I28.23:6500 (1964).

[i]J. D. Edwards *et al.*, *J. Electrochem. Soc.* **100**, 508 (1953).

[j]J. D. Edwards *et al.*, *J. Electrochem. Soc.* **99**, 527 (1952).

[k]G. J. Landon and A. R. Ubbelohde, *Proc. Roy. Soc.* **A240**, 160 (1957).

[l]H. R. Bronstein and M. A. Bredig, *Chem. Div. Ann. Progr. Rept. June 20, 1959,* ORNL-2782, p. 59.

[m]H. R. Bronstein and M. A. Bredig, *J. Am. Chem. Soc.* **80**, 2077 (1958).

[n]H. R. Bronstein, A. S. Dworkin, and M. A. Bredig, *Chem. Div. Ann. Progr. Rept. June 20, 1960,* ORNL-2983, p. 65.

[o]J. D. Mackenzie, *J. Chem. Phys.* **32**, 1150 (1960).

[p]J. D. Mackenzie, *Rev. Sci. Instr.* **27**, 297 (1956).

[q]T. Bååk, *Acta Chem. Scand.* **8**, 1727 (1954).

[r]J. W. Cuthbertson and J. Waddington, *Trans. Faraday Soc.* **32**, 745 (1936).

[s]J. Bajcsy, M. Malinovsky, and K. Matiasovsky, *Electrochim. Acta* **7**, 543 (1962).

[t]M. deK. Thompson and A. L. Kaye, *Trans. Electrochem. Soc.* **67**, 169 (1935).

[u]N. D. Greene, ORNL-CF-54-8-64 (1954).

[v]V. G. Selivanov and V. V. Stender, *Russ. J. Inorg. Chem.* **4**, 934 (1959).

[w]G. A. Meerson and M. P. Smirnov, *Khim. Redkikh Elementov, Akad. Nauk SSSR* **2**, 133 (1955).

[x]E. Batslavik and A. I. Belyayev, *Russ. J. Inorg. Chem.* **3**(4), 324 (1958).

[y]T. G. Pearson and J. Waddington, *Discussions Faraday Soc.* **1**, 307 (1947).

cell constant of several hundred reciprocal centimeters, the capillaries being constructed from electrically insulating materials; or, (*b*) use of metallic cells in which the container is usually one electrode, with a second electrode positioned in the melt. The latter type of cell has cell constants of the order of a few tenths of a reciprocal centimeter, requiring quite accurate measuring bridges and determination of lead resistances. Since the value of measured resistance in such cells is less than 1 ohm, cells of type *a* are clearly desirable for use in molten salts. Boron nitride and single-crystal magnesium oxide have been employed in capillary construction in cells of type *a*, while platinum, platinum-rhodium (20%), Inconel, molybdenum, hot-pressed BeO, fused MgO, and graphite have been used for container and electrode materials.

II. The common practice of measuring resistance with a Wheatstone-type bridge having a parallel resistance and capacitance in the balancing arm can result in considerable error if the relation for resistive and phase balance,

$$R_p = R_s[1 + R_p^2 C_p^2 (2\pi f)^2] \ , \qquad (31)$$

is not employed in determining the solution resistance. In this expression R_p and C_p are the parallel balancing resistance and capacitance; R_s, the solution resistance; and f, the measuring frequency. Use of this correction can be avoided by employing a bridge with the balancing resistance and capacitance in series.[42]

[42]G. D. Robbins and J. Braunstein, *Reactor Chem. Div. Ann. Progr. Rept. Dec. 31, 1967,* ORNL-4229, p. 57.

III. The frequency dependence of measured resistance and the practice of measuring resistance at a series of frequencies and extrapolating to infinite frequency as a function of $f^{-1/2}$ is examined in terms of electrode process concepts. One group of investigators followed this procedure, while three others found no appreciable variation of resistance with frequency. Unfortunately, the majority of investigators did not address themselves to this question. Recommendations have been made for reducing errors in conductance measurements.[43]

Specific Electrical Conductance of Molten KNO_3

G. D. Robbins J. Braunstein

Investigations of electrical conductivity in molten salts are essential to the understanding of transport processes in these materials. In particular, the testing of theories, such as the zero mobility concept of Angell,[44,45] requires accurate and precise determination of the temperature variation of specific conductance. The determination of electrical conductivities of molten fluorides is a continuing program at this Laboratory.

As is well known, specific conductances, K, are obtained from measured resistance, R, by employing the relation

$$K = (1/R)\,(l/a)\,, \tag{32}$$

where l/a is the cell constant. The value of l/a usually is obtained by measuring the resistance of a material of known specific conductance, preferably one having similar properties to the system to be investigated. Based on ease of handling, availability, stability to atmospheric conditions, and compatibility with container materials, especially silica, molten potassium nitrate would seem the most reasonable choice among molten salts for such a reference material. However, as Fig. 1.10 demonstrates, the results of several reported investigations in this system at temperatures up to 100°C above the melting point differ by amounts considerably larger than the claimed experimental uncertainty.

In a recent review of electrical conductance measurements in molten fluorides[39] errors arising from the use of a Wheatstone-type (or Jones) conductance bridge were discussed. Some possible origins of frequency variation of the measured resistance were also presented.

The object of this work was a careful measurement of specific conductance as a function of temperature for molten potassium nitrate to provide reliable values for use in cell constant determination in our molten-fluoride program. Because of the frequent use of potassium nitrate as a reference point in studies of transport properties of molten salts,[44–47] accurate values of its specific conductance and temperature dependence are important quantities in their own right to the physical chemistry of molten salts.

Figure 1.11 shows the type of silica conductance cell employed in these determinations. As discussed previously,[39] errors can arise in determining molten-salt conductivities from the use of measuring bridges with a balancing arm having a parallel resistance and capacitance. Accordingly, a specially constructed bridge[48] with series components in the balancing arm was employed in measuring resistances in the molten nitrate. For the determination of the cell constant a 0.1 demal aqueous potassium chloride solution (prepared from single-crystal KCl) was used, for which the specific conductance is well established.[49,50] The resistance of the aqueous electrolyte was determined in a controlled-temperature bath at 25°C employing the Jones bridge because of the large resistances involved. Specific experimental details may be found in ref. 51.

Table 1.3 shows specific conductance vs temperature data for molten potassium nitrate as determined with the series-component bridge. To check for errors in conductance due to nitrite formation, the following

[43] G. D. Robbins and J. Braunstein, *Proc. Symp. on Characterization and Analysis in Molten Salts, 156th National ACS Meeting, Sept. 8–13, 1968, Atlantic City, N.J.*, ed. by G. Mamantov, Marcel Dekker, New York, in press.

[44] C. A. Angell, *J. Phys. Chem.* 68, 1917 (1964).

[45] C. A. Angell, *J. Phys. Chem.* 70, 2793 (1966).

[46] B. DeNooijer, *The Electrical Conductivity of Molten Nitrates and Binary Nitrates*, thesis, University of Amsterdam, Netherlands, 1965.

[47] J. C. T. Kwak, *Diffusional and Electrical Mobilities of Tracer Ions in Ionic Liquids*, thesis, University of Amsterdam, Netherlands, 1967.

[48] G. D. Robbins and J. Braunstein, *Reactor Chem. Div. Ann. Progr. Rept. Dec. 31, 1967*, ORNL-4229, p. 57.

[49] R. A. Robinson and R. H. Stokes, *Electrolyte Solutions*, p. 462, 2d ed., Butterworths, London, 1959.

[50] G. Jones and B. C. Bradshaw, *J. Am. Chem. Soc.* 55, 1780 (1933).

[51] G. D. Robbins and J. Braunstein, *The Specific Conductance of Potassium Nitrate*, ORNL-4375 (December 1968).

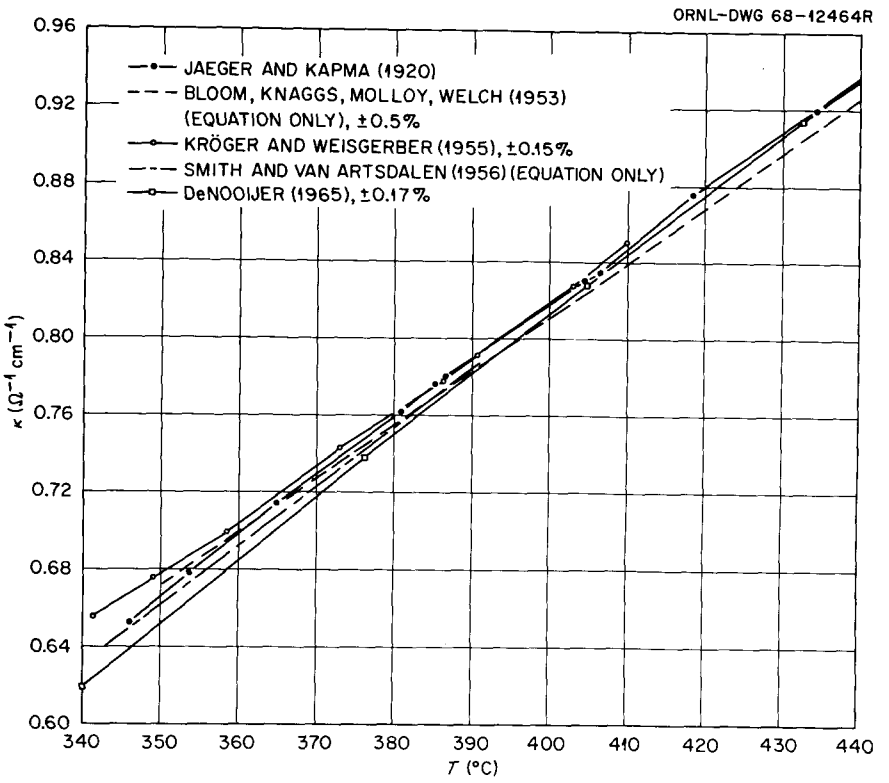

Fig. 1.10. Published Specific Conductance vs Temperature Values for Molten KNO_3. Data from refs. 48 and 54 and the following: F. M. Jaeger and B. Kapma, *Z. Anorg. Chem.* 113, 27(1920); H. Bloom, L. W. Knaggs, J. J. Molloy, and D. Welch, *Trans. Faraday Soc.* 49, 1458(1953); K. Kröger and P. Weisgerber, *Z. Phys. Chem. (Frankfurt)* 5, 192(1955).

procedure was adopted: Between each resistance determination at successively higher temperatures the resistance was measured near the melting point (see Fig. 1.12). It was planned to discard the last datum at the elevated temperature when a low-temperature value failed to duplicate the previously determined values. However, no discrepancy appeared up to 541°C, the temperature limit of the furnace. From this one might conclude either that sufficiently little nitrite had formed to be detected, or that the specific conductances of KNO_3 and KNO_2 were identical within the limits of measurements – in which case the results remained valid. However, the possibility exists for identical conductivities near 350°C with divergent values appearing at increased temperatures. Accordingly, an addition of 5 mole % KNO_2 was made, which resulted in the datum represented by the triangle (see Fig. 1.12) at 359°C, well outside the data scatter.

To recheck the KNO_3 specific conductance results, a completely new dip cell was constructed and its cell constant (141.4 cm^{-1}) determined in 0.1 demal KCl as before. A newly calibrated Pt vs Pt-Rh (10%) thermocouple measured temperature. The squares at 370 and 422°C show these results.

The curve shown in Fig. 1.12 represents the computer-fitted least-squares equation ($\sigma = 0.0008$)

$$\kappa = -0.7098 + 4.6203 \times 10^{-3} t(^\circ\mathrm{C}) - 2.0221 \times 10^{-6} t^2 , \quad (33)$$

based on the 24 data in Table 1.3. Figure 1.13 shows the super position of Figs. 1.10 and 1.12, where it is evident that only the limited temperature range equation of Smith and Van Artsdalen[52] agrees well with the results reported here. We consider these results to have an accuracy of better than ±0.5% and to demonstrate the potential of KNO_3 as a molten-salt conductance standard.

[52] D. F. Smith and E. R. Van Artsdalen, *Chem. Div. Ann. Progr. Rept. June 20, 1956*, ORNL-2159, p. 80.

ORNL-DWG 68-7818

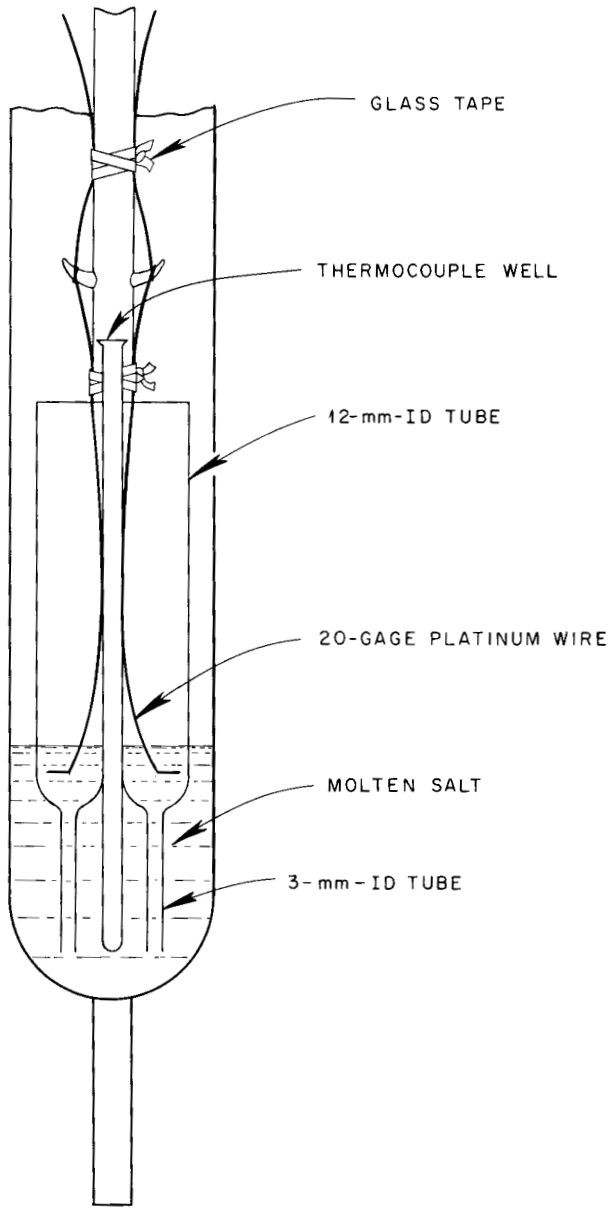

Fig. 1.11. Silica Conductance Cell.

Table 1.3. Specific Conductance of KNO_3 vs Temperature

T(°C)	κ (ohm^{-1} cm^{-1})
345.4	0.645_9
349.9	0.659_9
351.6	0.664_7
353.5	0.670_5
353.5	0.669_6
354.9	0.675_8
355.4	0.676_4
357.5	0.683_4
358.5	0.686_7
360.6	0.692_1
360.8	0.693_4
363.7	0.704_2
376.6	0.744_4
380.0	0.753_6
386.6	0.774_0
392.0	0.790_8
419.9	0.873_1
445.2	0.946_2
464.4	1.001_4
485.2	1.056_5
485.7	1.055_7
499.5	1.093_7
520.5	1.147_0
541.3	1.198_8

Electrical Conductivity of Molten LiF-BeF_2 Mixtures

G. D. Robbins J. Braunstein

The electrical conductivity vs temperature characteristics of molten LiF-BeF_2 mixtures[53] ranging in composition from 38 to 52 mole % BeF_2 have been determined in the silica cell shown in the previous section. The relatively long conducting path (12 cm) resulted in a cell constant of 145.9 cm^{-1}, as determined in 0.1 demal KCl (prepared from single crystals). Use of platinized platinum electrodes and this particular cell design resulted in measured resistances independent of measuring frequency and depth of immersion ($< \pm 0.2\%$, frequency range 0.5–5 kHz, depth 3–7 mm) in the KCl solution. The large resistance of the aqueous solution permitted use of a Jones bridge in the cell constant determination without introduction of errors discussed previously.[54]

[53] BeF_2 obtained from Brush Beryllium Co., distilled by B. F. Hitch; Li_2BeF_4 prepared by J. H. Shaffer and co-workers.

[54] G. D. Robbins, *Electrical Conductivity of Molten Fluorides. A Review,* ORNL-TM-2180 (March 26, 1968); G. D. Robbins and J. Braunstein in *Proc. Symp. on Characterization and Analysis in Molten Salts, Sept. 8–13, 1968, 156th National ACS Meeting, Atlantic City, N.J.,* ed. by G. Mamantov, Marcel Dekker, New York, in press.

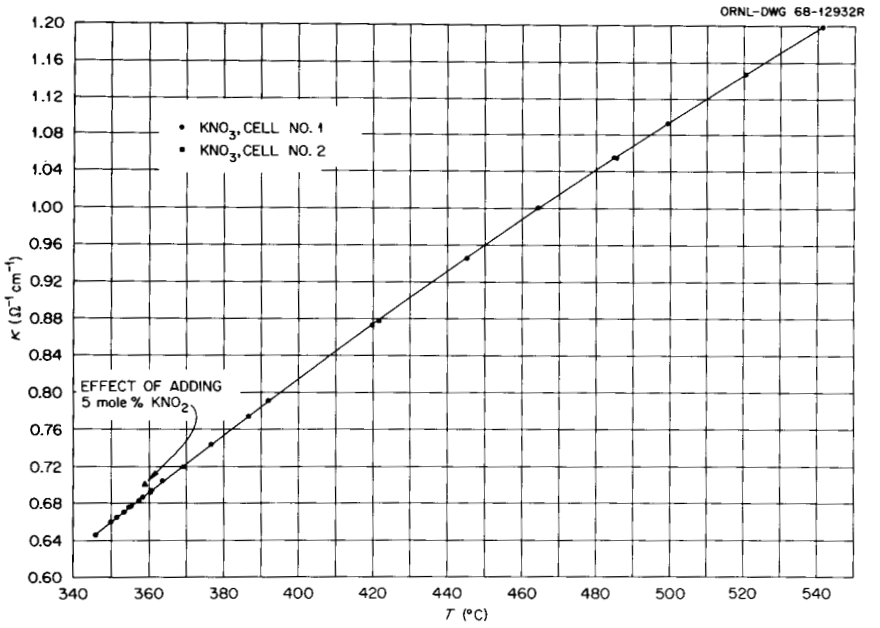

Fig. 1.12. Specific Conductance of Molten KNO_3 vs Temperature.

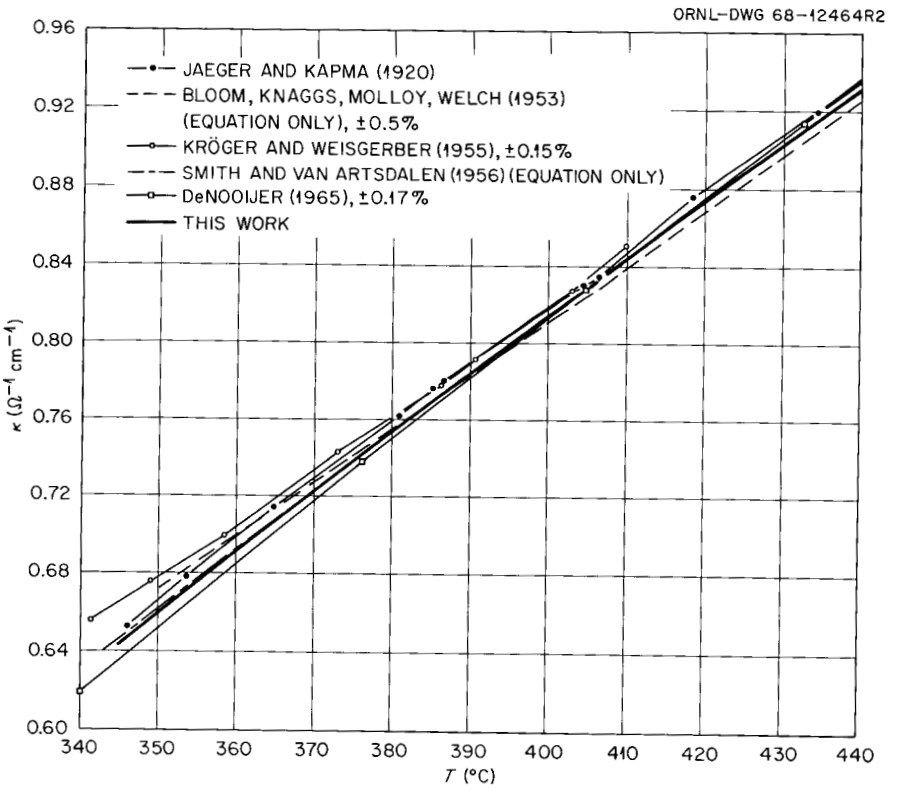

Fig. 1.13. Specific Conductance vs Temperature for Molten KNO_3. Comparison of this and previous work.

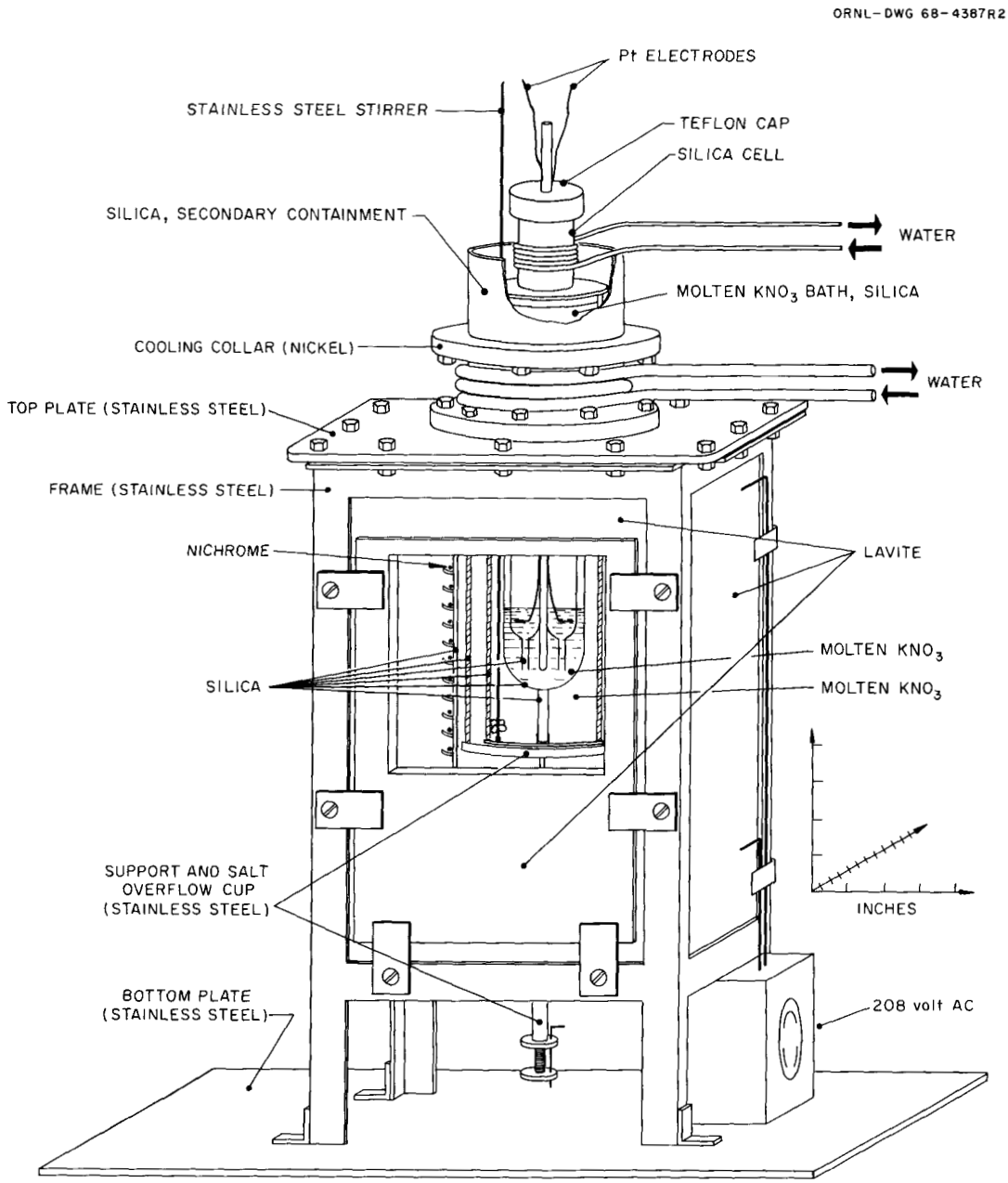

Fig. 1.14. Silica and Lavite Furnace.

For measurements of conductance in molten fluorides the entire cell assembly was immersed in a stirred molten KNO_3 bath and contained in the silica and Lavite furnace[55] shown in Fig. 1.14. A specially constructed measuring bridge[56] containing a series-component balancing arm determined resistance as a function of frequency. With this experimental arrangement, the measured resistance was stable, independent of depth of cell immersion, and varied less than 0.5% over the frequency range 1 to 10 kHz, the variation being approximately linear in $f^{-1/2}$. Values of measured resistance extrapolated to infinite frequency were less than 0.3% lower than the 10-kHz values.

The molten fluoride was contained in a closed silica cell (pressure = 1 atm) in which the low equilibrium

[55] K. A. Romberger, *MSR Program Semiann. Progr. Rept. Feb. 29, 1968*, ORNL-4254, p. 149.

[56] G. D. Robbins and J. Braunstein, *Reactor Chem. Div. Ann. Progr. Rept. Dec. 31, 1967*, ORNL-4229, p. 57.

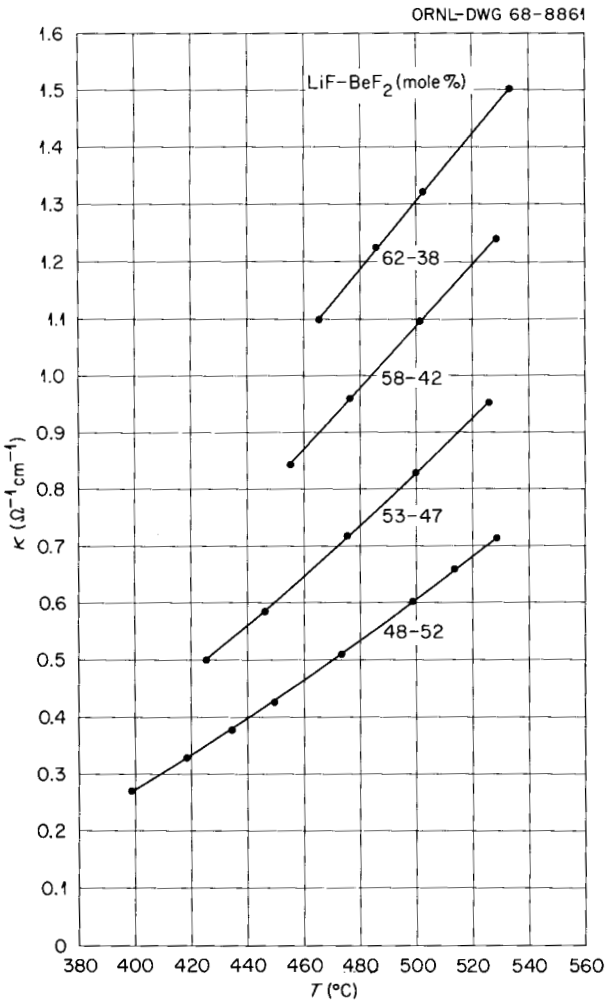

Fig. 1.15. Specific Conductance of LiF-BeF$_2$ Mixtures vs Temperature.

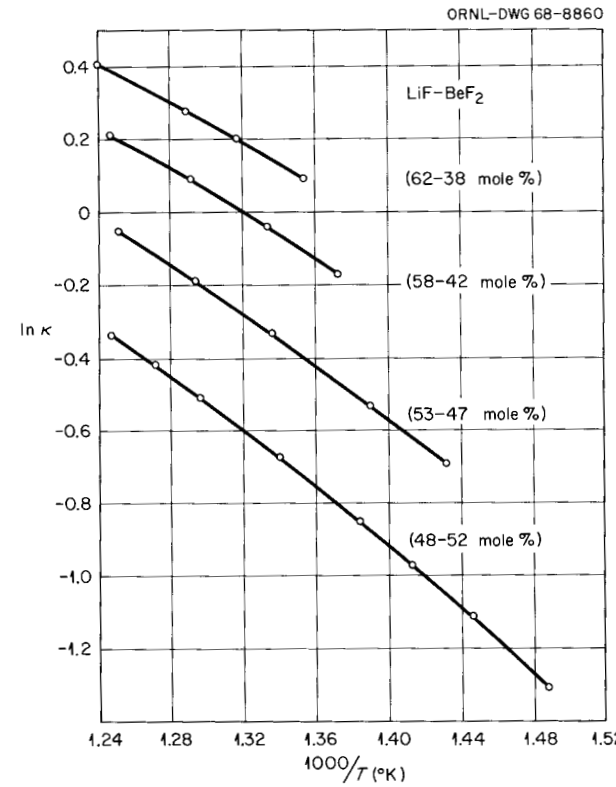

Fig. 1.16. Natural Logarithm of Specific Conductance vs $1/T$ for LiF-BeF$_2$ Mixtures.

partial pressure of SiF_4 (<1 mm at 500°C)[57] prevented major attack of the silica via the reaction

$$2BeF_2 + \underline{SiO_2} \rightarrow \underline{2BeO} + SiF_4 \uparrow . \qquad (34)$$

The slow solid-solid reaction

$$\underline{SiO_2} + \underline{2BeO} \rightarrow \underline{Be_2SiO_4} \qquad (35)$$

and the low solubility of BeO and Be_2SiO_4 (<0.01 mole/kg at 500°C)[58,59] should not affect the conductance measurements.

Specific conductance κ vs temperature data are listed in Table 1.3 and illustrated in Fig. 1.15. Plots of $\ln \kappa$ vs $1/T$, shown in Fig. 1.16, exhibit curvature, indicating temperature dependence of the conventional Arrhenius energy of activation for specific conductance, E_κ,

$$E_\kappa = -R \frac{d \ln \kappa}{d(1/T)} .$$

The variation of activation energy for conductance at low temperatures has been interpreted by Angell[60,61] in terms of a model, based on a theoretical glass transition temperature, which incorporates a non-Arrhenius form for the temperature dependence of transport properties. While there is as yet no completely satisfactory theoretical justification for the proposed equations, they have led to striking correlations in a

[57] C. E. Bamberger, R. B. Allen, and C. F. Baes, Jr., *Reactor Chem. Div. Ann. Progr. Rept. Dec. 31, 1967,* ORNL-4229, p. 60.

[58] B. F. Hitch and C. F. Baes, Jr., *Reactor Chem. Div. Ann. Progr. Rept. Dec. 31, 1966,* ORNL-4076, p. 19.

[59] C. E. Bamberger, private communication; C. E. Bamberger, C. F. Baes, Jr., and J. P. Young, *J. Inorg. Nucl. Chem.* 30, 1979 (1968).

[60] C. A. Angell, *J. Phys. Chem.* 68, 1917 (1964).

[61] C. A. Angell, *J. Phys. Chem.* 70, 2793 (1966).

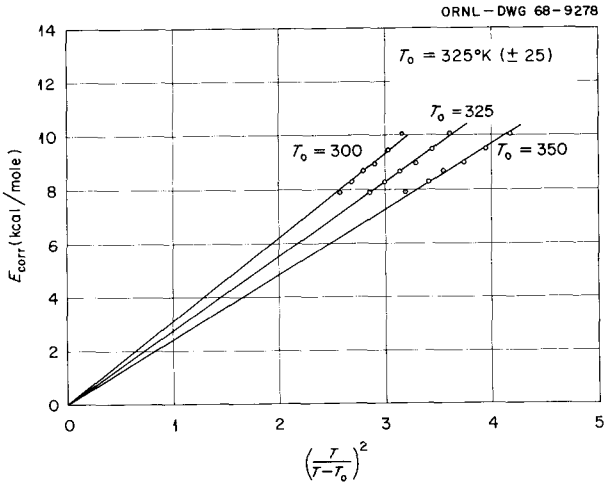

Fig. 1.17. Evaluation of T_0 from Plots of E_{corr} vs $[T/(T - T_0)]^2$.

number of systems. Since the eutectic composition of 52 mole % BeF_2 presents the largest temperature range, we have estimated the glass transition temperature for this composition. The temperature dependence of the corrected energy of activation is, according to the model,

$$E_{corr} = E_\kappa + \frac{1}{2}RT + \alpha RT^2 = kR\left(\frac{T}{T - T_0}\right)^2 ; \quad (36)$$

E_{corr} can be calculated, as indicated, from the conventional Arrhenius energy of activation for specific conductances, E_κ, and the expansivity α of the melt. A plot of E_{corr} vs $[T/(T - T_0)]^2$ should be linear with slope kR, and pass through the origin. T_0 is the zero mobility temperature (in degrees Kelvin), and k is a constant related to the potential energy of minimum-sized cooperatively rearranging groups. Figure 1.17 shows such a series of plots for different values of T_0. (Values of α were obtained from density data in fused fluoride melts.[62])

These plots result in a fit of the data corresponding to T_0 = 325 (±25)°K. The value of k thus determined is 1400 (±150)°K. The reduced temperature range of the measurements based on this value of T_0 is $2.1 \leqslant T/T_0 \leqslant 2.5$, which is slightly above the range of reduced temperatures for which Angell[60] found k to be constant in the molten $Ca(NO_3)_2$-KNO_3 system ($T \leqslant 1.7T_0$). Angell estimated an increase in k over the low-temperature value (obtained below $1.7T_0$) of about 10% at $2T_0$ and about 40% at $3T_0$. If a similar variation occurs in the fused fluoride system, a k of 1400 would be approximately 20% too large, indicating its correct value to be approximately 1170.

Since the assumptions of the model become more nearly valid at temperatures near T_0, one might expect the data in the lower half of the temperature range to provide a better estimate of T_0. It can be seen from Fig. 1.17 that the results of the three lowest temperatures (the three largest values of $[T/(T- T_0)]^2$) indicate a T_0 of 350 (±25)°K and a corresponding value of k = 1200 (±150)°K. (The range of values of T/T_0 would then be 1.9–2.1.) These estimates appear to be consistent with results in other systems, for example, T_0's of 200 to 330°K for the nitrates.[61] Values of k for the nitrates,[61] carbonates (estimated),[61] and a sodium silicate melt (viscosity)[61,63] are of the order of 700, 1400, and 5100°K respectively.

Experiments are currently in progress which encompass a composition range of 34–100 mole % BeF_2. These additional data should permit an interpretation of the composition dependence of the conductivities.

Electrical Conductances of Molten Salts at High Pressures

A. S. Quist

The investigation of properties of molten salts as a function of both temperature and pressure holds great promise in leading to a better understanding of the behavior of these systems. Conventional experiments are limited in that when measurements are made at 1 atm pressure as a function of temperature, the volume of the system also changes as a result of thermal expansion, thereby introducing a new variable. If both temperature and pressure (density) are changed in a regular manner, then the system parameters can be obtained at constant volume as a function of temperature. Such information obtained from electrical conductance measurements is of particular usefulness in evaluating models which have been proposed to describe migration processes in molten salts.

In collaboration with scientists at the Institut für Physikalische Chemie und Elektrochemie der Universität Karlsruhe, West Germany, an apparatus was constructed (at Karlsruhe) for measuring the electrical conductances of molten salts to 850°C and 8000 bars.

[62] B. C. Blanke *et al.*, MLM-1086 (1956).

[63] G. S. Fulcher, *J. Am. Ceram. Soc.* 8, 339 (1925).

Early experience at Karlsruhe with a piston-cylinder arrangement for generating the pressure and transmitting it to molten salts was unsatisfactory and led to the present development of an internally heated vessel pressurized by argon gas. The effect of the solubility of argon in the molten salt was circumvented by separating the gas-salt interface from the conductance cell compartment either by a sliding piston or by a relatively long capillary. Previous investigators found both arrangements to be satisfactory to pressures of 1000 bars.[64]

The main part of the apparatus is an internally heated cylindrical pressure vessel, 200 mm OD, 40 mm ID, 360 mm long, and weighing approximately 260 lb. This pressure vessel was made from two thick-walled stressed concentric cylinders. During assembly, the outer cylinder was heated (to about 370°C) until it had expanded enough so that the inner cylinder could be inserted. Upon cooling, the inner cylinder was put under compression. This technique of construction makes it possible to reduce the pressure vessel's outer diameter (as compared with normal construction where the vessel is made from a single cylinder) while retaining the same inner diameter and strength of the vessel. This technique is also advantageous because a corrosion-resistant alloy which also retains high mechanical strength to elevated temperatures can be used for the inner cylinder while using a normal steel for the outer cylinder. Usually these special alloys are not available in large diameters except at prohibitive expense.

The internal nickel-chromium resistance heater was spirally wound on a grooved alumina cylinder (15 mm ID, 21 mm OD, 160 mm long). This alumina tube was surrounded by a zirconia cylinder, and the annular space between the tubes was filled with alumina powder. The heater winding was divided into three separately controlled heating zones and required four separate leads. These leads were brought out the bottom of the pressure vessel using a Bridgman-type stem through which the pressurizing gas also passed. A separate closure was developed to bring the electrical leads from the high-pressure region to atmospheric pressure. The upper part of the pressure vessel assembly consisted of a similar closure through which a total of eight thermocouple and electrode leads could be passed. Water-cooled jackets were fitted to the exterior of the main pressure vessel.

The Pyrex conductance cell initially used in this apparatus for measurements on potassium nitrate to 400°C was designed to fit inside a 14-mm-ID, 15-mm-OD, 100-mm-long nickel cylinder which was in turn inserted into the alumina furnace described above. Platinum spheres approximately 2–3 mm in diameter served as the electrodes. They were contained in 6- to 7-mm-diam spherically shaped cell compartments which were separated by a 30-mm length of capillary (2 mm OD, 0.5 mm ID). The resulting cell constant was approximately 1800 cm^{-1}. The salt in the cell compartment was separated from the argon-salt interface by 180-mm lengths of the same capillary tubing in an arrangement similar to that described by Barton.[64]

Pressures to 2000 bars were generated by an air-driven diaphragm pump and measured by a Heise Bourdon tube gage. An air-driven oil pump was used with a mercury gas compressor to reach pressures of 6000 bars. These pressures were measured by a Manganin cell. Provision was made for later addition to the apparatus of an intensifier in order to reach pressures of 8000 bars. Valves and composite tubing (3/4 in. OD, 1/16 in. ID) rated for service to 15,000 bars were used in the section of this system subjected to the highest pressures. The apparatus was tested to pressures of 8000 bars and to temperatures of 850°C.

Using this apparatus, the electrical conductance of potassium nitrate has been measured to 4000 bars and 400°C. The results indicate that a longer uniform-temperature region needs to be established within the pressure vessel before sufficiently accurate conductance measurements can be obtained. The necessary modifications are being carried out at Karlsruhe, and the measurements will be continued by a graduate student as a thesis research project. A complete description of this apparatus and the potassium nitrate results will appear in the literature at a later date.

APPARATUS AND TECHNIQUES FOR SPECTROSCOPIC MEASUREMENTS IN FLUORIDE MEDIA

The Diamond Window Cell

L. M. Toth J. P. Young[65] G. P. Smith[66]

Until now the windowless container has been used extensively for measuring absorption spectra of ions in molten-fluoride solvents. There is, however, a need for a container or cell with fixed transparent windows. Such a container would provide a fixed and easily determined path length, the facility to bubble the melt with

[64] A. F. M. Barton, B. Cleaver, and G. J. Hills, *Trans. Faraday Soc.* 64, 208 (1968).

[65] Analytical Chemistry Division.

[66] Metals and Ceramics Division.

reactive gases, and better containment of volatile species. The problems encountered with such a cell have been to find windows which were optically transparent in the spectral range 200–250 mμ and which would resist the extremely corrosive action of molten fluorides. Also, it must be convenient to use so that the long-term applications of it to fluoride problems would be practical.

Initially we sought to use silica, platinum-coated silica,[67] and fluoride salt crystals as window materials. However, none of these were satisfactory for the general applications to fluoride spectroscopy which we sought.

Because it has long been recognized that diamond is perhaps the most ideal window material for molten fluorides, a diamond-window spectrophotometric cell was fabricated which satisfied the above design requirements (cf. Fig. 1.18). Except for the diamond windows, the cell is made entirely of graphite. It consists of a cell body, two retainers for the diamonds, a sleeve which holds the retainers in place, and a nut to secure the sleeve. The optical path length between the diamonds is 1.0 cm. The diamond windows are approximately 5 X 5 X 1 mm type IIa plates. Some variation in the diamond size from the above nominal value is unavoidable. Consequently the cell design allows appreciable variations in the window dimensions. For example, one of the plates we are now using measures 5.0 X 4.3 X 1.3 mm.

Positioning of a window in the cell is achieved by a horizontal groove on the body, which fixes the vertical position, and a vertical groove in the retainer, which fixes the horizontal position. The depth of each groove is one-half the window thickness (nominally 1 mm) while the width of each groove is, of course, the same as the width of the window, 5 mm. With this arrangement, the windows are not sealed gastight to the cell body but merely fit flush to the body with a force of a few grams exerted upon them. Fluid leakage around the windows does not occur because most molten fluoride salts do not wet graphite. The advantages of this arrangement are simplicity of design, ease of assembly and disassembly, and no significant danger of window breakage due to loading stresses.

This cell was successfully used in a number of tests.[68] A spectrophotometric base line for $LiF\text{-}BeF_2$ (66-34 mole %) and the spectra of NiF_2 and UF_4 in the $LiF\text{-}BeF_2$ solvent were recorded. Because of the reproducibility of the base line achieved with the diamond cell, a broad peak centered at 2.06 μ in the UF_4 solution spectrum was identified for the first time in a molten-fluoride system (cf. Fig. 1.19). This peak has been seen in noncorrosive systems before but has not been reported in molten fluorides because of the previous uncertainty in the base line.

The main disadvantage in using a graphite cell body centers around the difficulty in outgassing oxide-containing gases which otherwise exchange-react with fluoride solutes and cause their precipitation. Diffusion pumping at 700 to 900°C of the graphite has proven inadequate for our purposes. As an alternative, the graphite has been treated at 500 to 700°C with HF.[69]

ORNL-DWG 68-9074

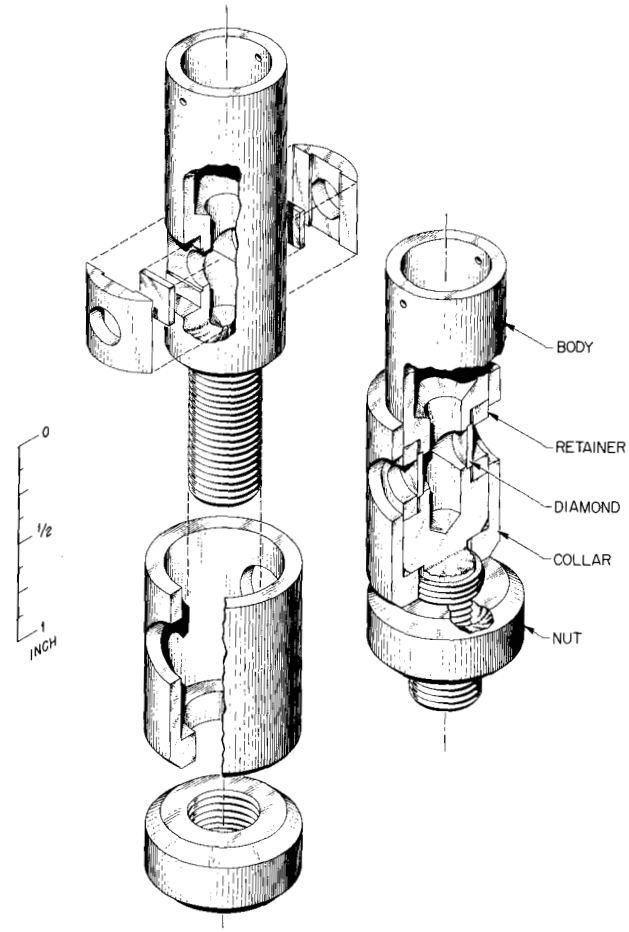

Fig. 1.18. Two Views of the Diamond-Windowed Cell.

[67] L. M. Toth and G. P. Smith, *Reactor Chem. Div. Ann. Progr. Rept. Dec. 31, 1967,* ORNL-4229, p. 63.

[68] See chap. 3, this report, for further data obtained by this scheme.

[69] *MSR Program Semiann. Progr. Rept. Feb. 28, 1962,* ORNL-3282, pp. 89–94.

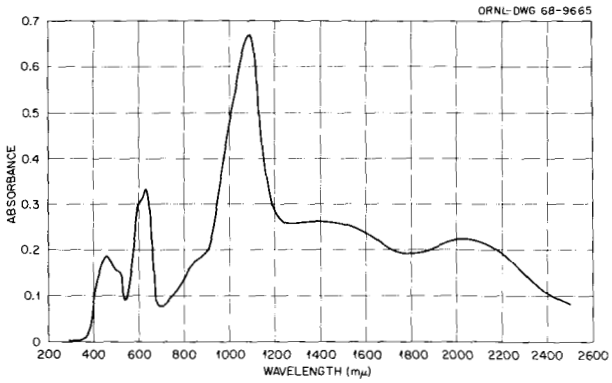

Fig. 1.19. Absorption Spectrum of a Dilute Solution of UF_4 in Molten $LiF-BeF_2$ (66-34 Mole %) at 650°C.

Although the complete removal of residual HF in the graphite might be as difficult as that of the oxides, residues of the former present fewer problems.

Salt Purification for Fluoride Spectroscopy

L. M. Toth

Melts which are both low in oxide content and free of suspended matter are a prerequisite for spectroscopy of dilute species in fluoride solvents. Even small amounts of solute which react with the soluble oxides and leave solution cause problems either by remaining suspended and scattering light or by precipitating and collecting on the windows of the cell.

The salts are best purified as individual components instead of as the mixed salts. We use the customary approach of subliming volatile fluorides and HF sparging nonvolatile fluorides.

In the past, volatile fluorides have been sublimed at rates which caused entrainment of impurities.[70] Baffle plates were used to partially remedy the entrainment. However, we find that low sublimation rates at pressures of 10^{-4} to 10^{-5} torr eliminate the need for baffles and produce much better results. For some very crude salts it has been necessary to sublime a second time (as in the case of ZrF_4). At these low sublimation rates we have been able to produce up to 50 g of salt in two to three days.

The results on some of these fluoride salts are listed in Table 1.4.

CRYSTAL STRUCTURES OF COMPLEX FLUORIDES

The crystal structures which follow are in different stages of refinement, and the parameters listed in the tables may be subject to minor changes. The discrepancy factor,

$$R = \Sigma \left| |F_o| - |F_c| \right| / \Sigma |F_o| ,$$

is listed in the tables for each structure.

The Crystal Structure of $NaBF_4$

G. D. Brunton

The lattice parameters and atomic parameters of $NaBF_4$ were refined (Table 1.5). (The temperature factor expression in Table 1.5 refers to all tables through Table 1.9.) The refined parameters are only slightly different from those determined by Weiss and Zohner[71] from two-dimensional Weissenberg data. The orthorhombic form of $NaBF_4$ crystallizes in the space group *Cmcm*; refined values for the unit cell parameters are a_0 = 6.8368(9) A, b_0 = 6.2619(7) A, and c_0 = 6.7916(4) A; calculated density is 2.5075 g/cm^3, Z = 4.

[70] L. B. Yeatts, Jr., and W. T. Rainey, Jr., *Reactor Chem. Div. Ann. Progr. Rept. Jan. 31, 1965,* ORNL-3789, p. 330.

[71] A. Weiss and K. Zohner, *Phys. Status Solidi* **21**, 257 (1967).

Table 1.4. Purification of Fluoride Salts

Salt	Purification Process			Product Evaluation	
	Method	Temperature (°C)	Process Time	General	$KBrF_4$ Oxide Analysis (ppm)
ZrF_4	Two sublimations	590–600	3 days each	TSC 0.25 g[a]	70
NbF_5	Sublimation	100	5 days	TSC 0.50	<50
LiF	HF sparging	900	1 hr	TSC	<50

[a]TSC 0.25 g, "transparent single crystals" followed by average weight of single crystals.

Table 1.5. Lattice and Atomic Parameters for $NaBF_4$

$R = 0.036$

Atom	x	y	z	β_{11}[a]	β_{22}	β_{33}	β_{12}	β_{13}	β_{23}
Na	0.0000	0.6552(2)[b]	0.2500	0.0136(2)	0.0121(2)	0.0089(2)	0.0000	0.0	0.0000
B	0.0000	0.1608(3)	0.2500	0.0085(3)	0.0078(3)	0.0076(3)	0.0000	0.0	0.0000
F(1)	0.0000	0.2920(2)	0.08458(0.9)	0.0185(3)	0.0137(2)	0.0087(2)	0.0000	0.0	0.0029
F(2)	0.1644(1)	0.0312(2)	0.2500	0.0121(2)	0.0156(3)	0.0201(3)	0.0054(2)	0.0	0.0000

[a]Coefficients in the temperature factor, $\exp[-(\beta_{11}h^2 + \beta_{22}k^2 + \beta_{33}l^2 + 2\beta_{12}hk + 2\beta_{13}hl + 2\beta_{23}kl)]$.
[b]The numbers in parentheses are $\sigma \times 10^4$.

ORNL-DWG 68-7964

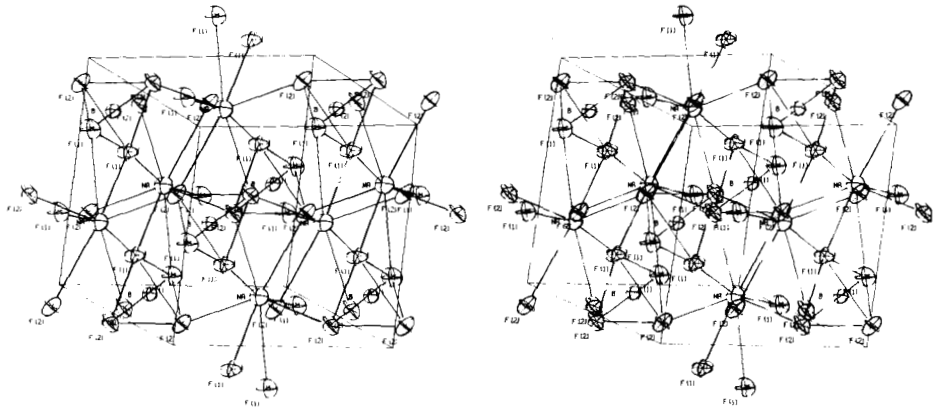

Fig. 1.20. A Stereoscopic Pair of Drawings of the Unit Cell of $NaBF_4$. The unit cell is outlined and has been tilted $-15°$ around the x axis and $-30°$ around the y axis of the drawing.

The structure is shown in Fig. 1.20. The BF_4 tetrahedra are slightly irregular with two $F(1)^-$ ions 0.006 A more distant from the B^{3+} ion than the two $F(2)^-$ ions. The Na^+ ions are coordinated by eight F^- ions which are at the corners of an irregular polyhedron which is neither a cube nor antiprism. The Na^+ polyhedron shares opposite edges with BF_4 tetrahedra, four corners with BF_4 tetrahedra, and edges with two other Na^+ polyhedra. The Na^+-F^- distances vary from 2.2963 to 2.609 A.

The Neutron and X-Ray Crystal Structure of $(Na,Li)_7Th_6F_{31}$

G. D. Brunton D. Richard Sears

The compound $(Na,Li)_7Th_6F_{31}$ crystallizes in space group $P3c1$ with $a_0 = 9.9056 \pm 0.0003$ A and $c_0 = 13.2820 \pm 0.0005$ A. The calculated density is 6.045 g/cm^3, and $Z = 2$. There are 18 atoms in the asymmetric unit. Two independent Th^{4+} ions and F(1) through F(10) are on the general position 6(d); Th(1) is coordinated by nine F^- and Th(2) is coordinated by ten F^-. Ion F(11) is on position 2(a). The three sodium ions Na(1), Na(2), and Na(3) occupy positions 2(c), 2(b), and 2(a) respectively. The ion Na(3) is surrounded by 12 F^-, and Na(2) and Na(1) are surrounded by six F^- at distances less than 3.0 A. Sodium(1) and sodium(2) have five and three more F^- nearest neighbors, respectively, between 3.0 and 3.5 A. Lithium(1) is octahedrally coordinated at position 2(a). Lithium(2) is at general position 6(d) and is surrounded by seven F^- nearest neighbors less than 3.0 A distant.

The atomic parameters derived from the x-ray and neutron data are listed in Table 1.6. The atomic parameters from the neutron data differ from those of the x-ray data because of false minima in the least-squares refinement. Figure 1.21 is a stereoscopic representation of one asymmetrical unit in the unit cell.

Table 1.6. Positional Parameters and Temperature Factors for $(Na, Li)_7Th_6F_{31}$

X, x ray ; N, Neutron

R x-ray = 0.050 ; R neutron = 0.096

ATOM		X	Y	Z	β_{11} [a]	β_{22}	β_{33}	β_{12}	β_{13}	β_{23}
Th(1)	X	0.0847(2) [b]	0.4094(2)	0.0 [c]	0.0044(2)	0.0039(3)	0.0007(1)	0.0024(2)	0.0000(2)	-0.0003(1)
	N	0.0782(4)	0.3954(4)	0.0	0.0012(3)	0.0012(3)	0.0006(2)	0.0006(3)	0.0002(2)	-0.0001(2)
Th(2)	X	0.9214(2)	0.6045(2)	0.2061(2)	0.0036(2)	0.0035(2)	0.00035(9)	0.0017(2)	0.0000(1)	0.0002(1)
	N	0.9148(4)	0.5911(4)	0.2059(2)	0.0008(3)	0.0017(3)	0.0003(2)	0.0007(3)	0.0001(2)	0.0003(2)
F(1)	X	0.139(4)	0.441(4)	-0.181(3)	0.002(1)	d				
	N	0.1370(7)	0.4291(8)	-0.1862(5)	0.0029(7)	0.0038(7)	0.0007(3)	0.0003(6)	-0.0005(4)	-0.0001(4)
F(2)	X	0.864(4)	0.563(4)	0.388(3)	0.002(1)	d				
	N	0.8658(8)	0.5552(7)	0.3853(6)	0.0036(7)	0.0030(7)	0.0009(3)	0.0007(6)	-0.0008(4)	-0.0002(4)
F(3)	X	0.129(5)	0.315(4)	-0.374(3)	0.003(2)	d				
	N	0.1191(8)	0.3061(8)	-0.3759(6)	0.0031(7)	0.0039(8)	0.0015(4)	0.0020(6)	0.0011(5)	0.0002(4)
F(4)	X	0.886(5)	0.690(4)	0.587(3)	0.003(2)	d				
	N	0.8781(8)	0.6893(8)	0.5827(6)	0.0037(8)	0.0028(7)	0.0012(4)	0.0015(6)	0.0006(4)	-0.0004(4)
F(5)	X	0.357(5)	0.459(5)	-0.062(3)	0.004(2)	d				
	N	0.3431(6)	0.5103(7)	-0.0444(5)	0.0015(6)	0.0047(7)	0.0022(3)	0.0001(5)	-0.0005(3)	0.0005(4)
F(6)	X	0.668(4)	0.493(5)	0.249(3)	0.004(2)	d				
	N	0.6479(8)	0.5494(7)	0.2615(5)	0.0069(9)	0.0038(7)	0.0021(3)	0.0006(7)	0.0004(4)	0.0003(4)
F(7)	X	0.079(4)	0.196(4)	-0.061(3)	0.0009(9)	d				
	N	0.1033(8)	0.1966(7)	-0.0655(6)	0.0059(8)	0.0025(7)	0.0015(3)	0.0031(7)	-0.0001(4)	-0.0006(4)
F(8)	X	0.893(4)	0.803(3)	0.267(3)	0.0003(9)	d				
	N	0.9191(7)	0.8111(7)	0.2643(7)	0.0014(6)	0.0031(7)	0.0018(3)	0.0005(6)	0.0009(4)	0.0001(4)
F(9)	X	0.117(4)	0.576(4)	-0.347(3)	0.001(1)	d				
	N	0.1295(8)	0.5851(7)	-0.3531(6)	0.0026(7)	0.0020(7)	0.0017(4)	0.0003(6)	-0.0014(4)	0.0004(4)
F(10)	X	0.868(5)	0.417(4)	0.555(4)	0.002(1)	d				
	N	0.8836(8)	0.4214(8)	0.5508(6)	0.0022(7)	0.0033(7)	0.0013(3)	0.0003(6)	-0.0007(4)	0.0008(4)
F(11)	X	0.66667	0.33333	-0.321(8)	0.012(4)	d				
	N	0.66667	0.33333	-0.306(1)	0.0038(7)	f	0.008(1)	f	f	f
Na(1)	X	0.66667	0.33333	-0.055(4)	0.001(2)	d				
	N	0.66667	0.33333	-0.047(2)	0.002(1)	f	0.003(2)	f	f	f
Na(2)	X	0.33333	0.66667	0.248(4)	0.001(1)	d				
	N	0.33333	0.66667	0.258(2)	0.005(2)	f	0.0006(8)	f	f	f
Na(3)	X	0.0	0.0	0.084(5)	0.009(3)	d				
	N	0.0	0.0	0.121(2)	0.006(2)	f	0.002(2)	f	f	f
Li(1)	X	0.0	0.0	-0.15(2)	0.008(6)	d				
	N	0.0	0.0	-0.139(3)	0.003(2)	f	0.002(2)	f	f	f
Li(2)	X	0.272(9)	0.310(9)	-0.221(8)	0.003(3)	d				
	N	0.233(4)	0.283(3)	-0.188(3)	0.027(6)	0.004(3)	0.014(4)	-0.011(4)	0.012(4)	-0.001(3)

[a] Coefficients in the Temperature Factor: $EXP-(\beta_{11}h^2+\beta_{22}k^2+\beta_{33}\ell^2+2\beta_{12}hk+2\beta_{13}h\ell+2\beta_{23}k\ell)$.

[b] Standard Error (in parentheses) Corresponds to Last Significant Digit in Parameter.

[c] Defines Origin Along Z.

[d] X-Ray Temperature Factors for F, Na, and Li are Constrained to be Isotropic.

[f] Only those β_{ij} Adjusted as Independent Variables are Shown. Symmetry Constraints Upon the β_{ij} of all Atoms in Special Positions are: $\beta_{11}=\beta_{22}=2\beta_{12}$ and $\beta_{13}=\beta_{23}=0$. (Levy (1956)).

ORNL-DWG 69-2079

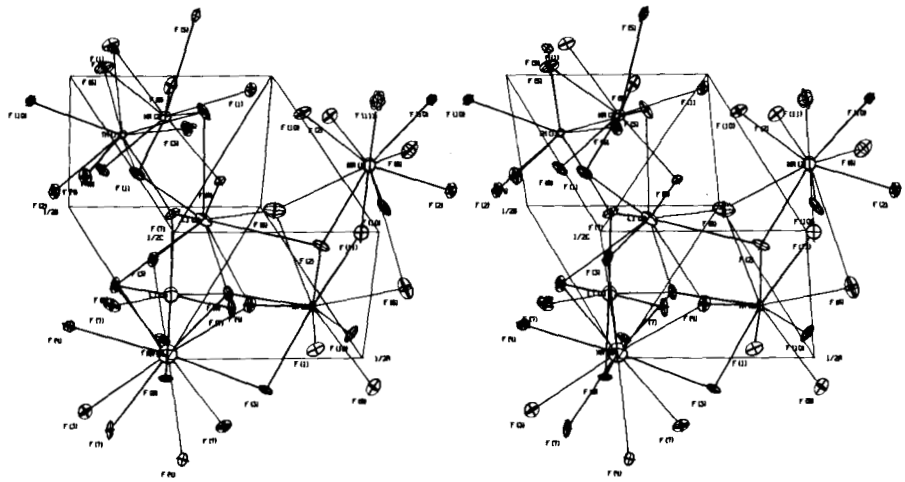

Fig. 1.21. One Asymmetrical Unit of $(Na,Li)_7Th_6F_{31}$. One-fourth unit cell outline.

Table 1.7. Atomic Parameters for Na_3CrF_6

$R = 0.061$

Atom	x	y	z	β_{11}	β_{22}	β_{33}	β_{12}	β_{13}	β_{23}
				$\times 10^{-4}$	$\times 10^{-4}$	$\times 10^{-4}$	$\times 10^{-4}$	$\times 10^{-4}$	$\times 10^{-4}$
Cr^{3+}	0.0	0.0	0.0	76(2)[a]	42.2(9)	23.5(4)	0.0	25.5(6)	0.0
Na(1)	0.5	0.0	0.5	125(5)	78(3)	43(2)	0.0	40(2)	0.0
Na(2)	0.7606(2)	−0.0552(3)	0.2458(2)	205(5)	96(3)	77(2)	−19(3)	81(2)	1(2)
F(1)	0.3375(3)	0.0538(3)	0.2251(2)	127(5)	115(4)	31(2)	5(3)	21(2)	−7(2)
F(2)	0.7661(3)	0.1761(3)	0.0504(2)	212(6)	104(4)	71(2)	60(4)	94(3)	17(2)
F(3)	0.0975(3)	0.2776(3)	0.9314(2)	160(5)	80(3)	75(2)	−4(3)	62(3)	31(2)

[a]The numbers in parentheses are the standard errors in terms of the least significant digit.

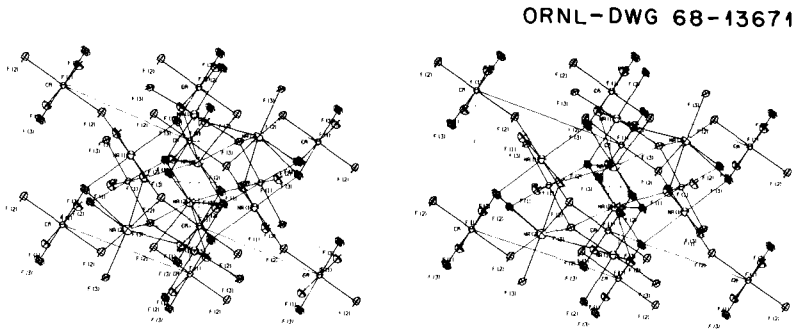

Fig. 1.22. One Asymmetrical Unit of Na_3CrF_6. One-fourth unit cell outline.

The Crystal Structure of Na_3CrF_6

G. D. Brunton

Single crystals of a compound identified as Na_3CrF_6 were recovered as corrosion products as a result of circulating a mixture of molten $NaBF_4$-KBF_4 in a Hastelloy N loop.[72] The results of a single-crystal x-ray analysis of the material show that the compound is isostructural with the low-temperature polymorph of Na_3AlF_6.[73] Similar compounds of Na_3CoF_6 and Na_3FeF_6 are cubic[74,75] and isostructural with the high-temperature polymorph of Na_3AlF_6. The complete three-dimensional structure of Na_3CrF_6 is illustrated in Fig. 1.22. The atomic parameters are listed in Table 1.7. The Cr^{3+} ion is coordinated by six F^- ions at the corners of a nearly regular octahedron; Cr-F distances, 1.904 to 1.908 A. The Na^+ ions are coordinated by six and eight F^- ions, respectively, at the corners of irregular polyhedra. The distances Na(1)-F are 2.227 to 2.293 A, and the distances Na(2)-F are 2.299 to 2.906 A. The unit cell parameters are a_0 = 5.4913(3), b_0 = 5.7021(3), c_0 = 9.6618(9) A, and β = 125.021(5)°. The space group is $P2_1/c$, and the x-ray density is 3.149 g/cm^3; $Z = 2$.

The Crystal Structure of $Cs_4Mg_3F_{10}$

H. Steinfink[76] G. D. Brunton

The compound $Cs_4Mg_3F_{10}$ crystallizes in space group *Cmca* with a_0 = 6.1333(3), b_0 = 14.561(2), and c_0 = 13.653(1) A. The observed density is 4.0 ± 0.4 g/cm^3, and the calculated density is 4.3276 g/cm^3; Z = 4.

The structure consists of corrugated sheets of linked MgF_6 octahedra parallel to (010) with the sheets held

[72]A. P. Litman, *MSR Program Semiann. Progr. Rept. Aug. 31, 1967*, ORNL-4191.

[73]S. Naray-Szabo and K. Sasvari, *Z. Krist.* 99, 27 (1937).

[74]R. Hoppe, *Rec. Trav. Chim.* 75, 569 (1956).

[75]W. Minder, *Z. Krist.* 96A, 15 (1937).

[76]Consultant, University of Texas.

together by the Cs^+ ions. The basic unit within a corrugated sheet consists of three articulated octahedra in which the central octahedron shares two opposing faces with the other two octahedra. The basic units are linked by the outside octahedra of each unit sharing corners with the outside octahedra of other basic units. The Mg^{2+}-F^- distances vary from 1.890 to 2.104 A. The Cs^+-F^- distances vary from 2.940 to 3.471 A. The atomic parameters are listed in Table 1.8, and the structure is shown in Fig. 1.23.

Table 1.8. Atomic Parameters and Their Standard Deviations for $Cs_4Mg_3F_{10}$

$R = 0.078$

Atom	x	y	z	β_{11}	β_{22}	β_{33}	β_{12}	β_{13}	β_{23}
	$\times 10^{-4}$	$\times 10^{-4}$	$\times 10^{-4}$	$\times 10^{-4}$	$\times 10^{-4}$	$\times 10^{-4}$	$\times 10^{-4}$	$\times 10^{-4}$	$\times 10^{-4}$
Cs_1	0	2542(0.4)[a]	3939(0.4)	86(1)	15(0.2)	28(0.3)	0	0	−3(0.2)
Cs_2	0	4482(0.3)	1389(0.3)	72(0.1)	15(0.2)	16(0.2)	0	0	−0.8(0.1)
Mg_1	0	1170(2)	1575(2)	57(5)	8(0.8)	12(1)	0	0	0(0.7)
Mg_2	0	0	0	48(7)	10(1)	11(1)	0	0	−0.3(1)
F_1	2100(6)	958(2)	403(2)	61(7)	19(1)	17(1)	−6(2)	9(3)	−2(1)
F_2	2500	1098(4)	2500	74(10)	19(2)	19(2)	0	−15(4)	0
F_3	0	4732(4)	3575(3)	107(12)	15(2)	16(2)	0	0	3(2)
F_4	0	2465(4)	1482(5)	126(15)	14(2)	38(4)	0	0	7(2)

[a]The numbers in parentheses are the standard errors in terms of the least significant digit.

ORNL-DWG 69-2080

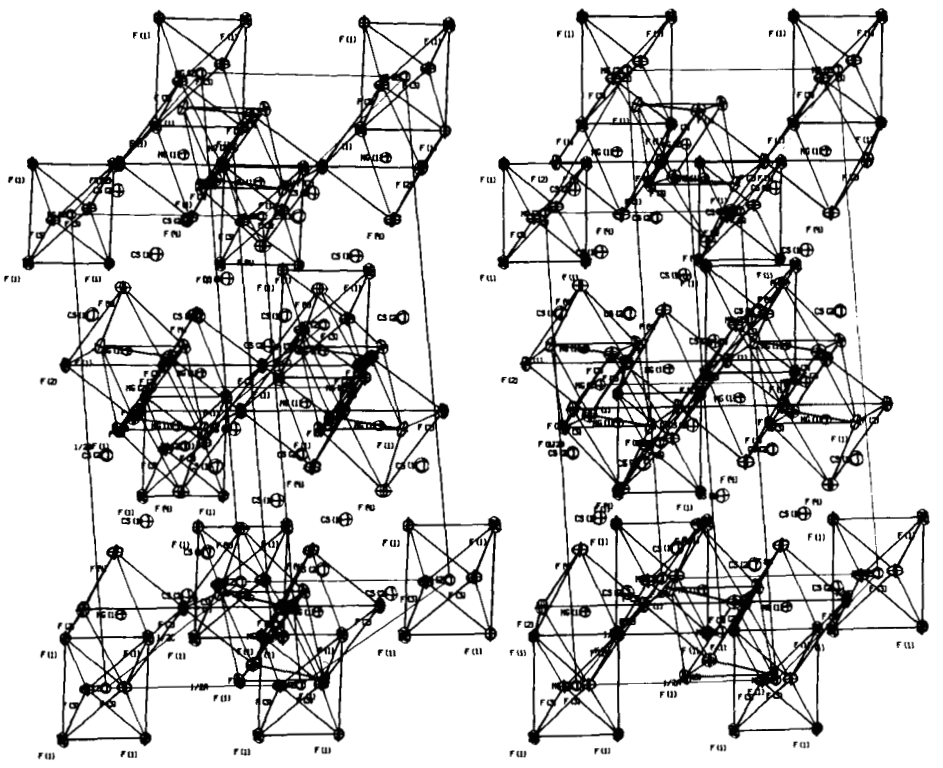

Fig. 1.23. One Asymmetrical Unit of $Cs_4Mg_3F_{10}$. One-fourth unit cell outline.

The Crystal Structure of K_3MoF_6

G. D. Brunton

The compound K_3MoF_6 crystallizes in space group *Fm3m* with a_0 = 8.7839(9) A and an x-ray density of 3.2066 g/cm^3; Z = 4. The compound is isostructural with $(NH_4)_3FeF_6$.[77] The Mo^{3+} and K(1) are octahedrally coordinated by six F^- each at 2.00(2) and 2.40(2) A respectively (Fig. 1.24). The K(2) ion is coordinated by 12 F^- at 3.112(2) A. The atomic parameters are listed in Table 1.9.

[77] L. Pauling, *J. Am. Chem. Soc.* **46**, 2738 (1924).

ORNL-DWG 69-2967

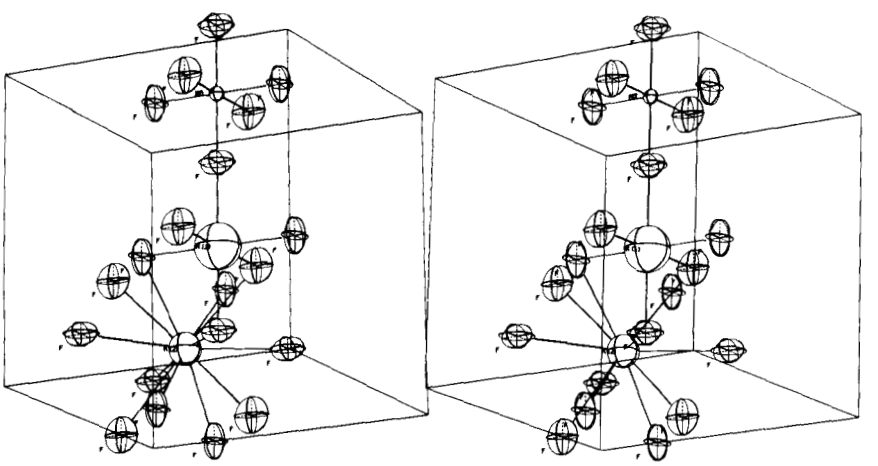

Fig. 1.24. Stereo View of the Crystal K_3MoF_6. One asymmetrical unit with the unit cell outlined.

Table 1.9. Lattice and Atomic Parameters for K_3MoF_6

R = 0.103

Atom	x	y	z	β_{11}	β_{22}	β_{33}
Mo	0.0	0.0	0.0	0.0049(0.3)[a]	0.0049(0.3)	0.0049(0.3)
K(1)	0.5	0.5	0.5	0.049(7)	0.049(7)	0.049(7)
K(2)	0.25	0.25	0.25	0.025(2)	0.025(2)	0.025(2)
F	0.226(3)	0.0	0.0	0.014(3)	0.029(3)	0.029(3)

[a] The numbers in parentheses are $\sigma \times 10^3$.

2. Direct Support for the Molten Salt Reactor Experiment

These studies will be reported in the Reactor Chemistry Division Annual Progress Report for Period Ending December 31, 1969.

3. Behavior of Fission Products and Protactinium in Molten Fluorides

Rather surprising amounts of gas-borne noble metal fission products have been observed in the MSRE. Various types of laboratory experiments have been performed in an effort to provide an adequate explanation of these observations. A study of the behavior of colloids and other small metal particles in molten salts was launched because it now seems probable that the gas-borne particles are metallic, but investigations of the behavior of noble metal fluorides have continued because they probably have at least a transitory existence in the reactor system.

One of the principal advantages offered by molten-salt breeder reactors is the promise of continuous removal of fission product poisons and protactinium, an intermediate product in the conversion of fertile ^{232}Th into fissionable ^{233}U. Reductive extraction processes appear feasible for protactinium and rare-earth removal, but they exhibit rather limited efficiency for the separation of rare earths and thorium from the single-region $LiF\text{-}BeF_2\text{-}ThF_4$ mixtures that are expected to be used in future molten-salt breeder reactors. Various expedients are being investigated for the purpose of alleviating this problem and are reported here in connection with the reprocessing studies.

STUDIES OF PARTICLES IN AND ABOVE MOLTEN SALTS

Radioaerosol Formation over Molten Salts

H. W. Kohn S. S. Kirslis
F. F. Blankenship

As an addendum to hot-cell tests previously reported[1] we have examined the behavior of ^{95}Zr decaying to ^{95}Nb in a typical fuel salt. The experimental procedure is similar to that used in the hot-cell tests, but the radioactivity is at tracer level (0.02 mc/g). The data are summarized in Fig. 3.1. The most important finding of these experiments was that small amounts of ^{95}Zr and ^{95}Nb escaped to the gas phase. Varying most of the parameters shown in the figure did not seem to affect this release; in particular, varying the reduction potential of the melt did not have any great effect. The aim here was to demonstrate that ^{95}Nb was not escaping as a volatile fluoride. The deposition of ^{95}Nb from the gas phase was much greater than that of ^{95}Zr. The rate of ^{95}Nb deposition was greatly increased by evacuating the apparatus; it could also be decreased by substituting argon blanket for the helium-hydrogen normally used. Hence we are led to the conclusion that the niobium travels as fine particles or critical nuclei of metal and that their rate of deposition is diffusion controlled.

The zirconium, on the other hand, seems to travel as fine particles of salt. If the Li, ^{95}Zr, and UF_4 deposited on the probe according to their respective vapor pressures,[2-4] the ratio of Li to Zr in the condensate would be about 1, but that of Li to U would have to be at least 10^3. Analysis of the material deposited in terms of calculated amounts of salt on the probes, as shown in Table 3.1, shows that this does not happen. The composition of the condensate is essentially that of the salt.

These results substantiate the results of the hot-cell tests reported previously, but exclude the intense radioactivity as a possible cause of the phenomenon.

Bubbles, Drops, and Entrainment in Molten Salts

H. W. Kohn

A report[5] was prepared on this subject. It includes a literature search, most of which is devoted to references to aqueous systems, and a discussion and description of a few crude but crucial experiments on molten nitrates.

---

[1] S. S. Kirslis and F. F. Blankenship, *MSR Program Semiann. Progr. Rept. Feb. 29, 1968*, ORNL-4524.

[2] S. Cantor *et al.*, *J. Phys. Chem.* **62**, 96 (1958).

[3] S. Langer and F. F. Blankenship, *J. Inorg. Nucl. Chem.* **14**, 26 (1960).

[4] S. Cantor *et al.*, *Physical Properties of Molten-Salt Reactor Fuel, Coolant and Flush Salts*, ORNL-TM-2316, p. 33 (August 1968).

[5] H. W. Kohn, *Bubbles, Drops and Entrainment in Molten Salts*, ORNL-TM-2373 (December 1968).

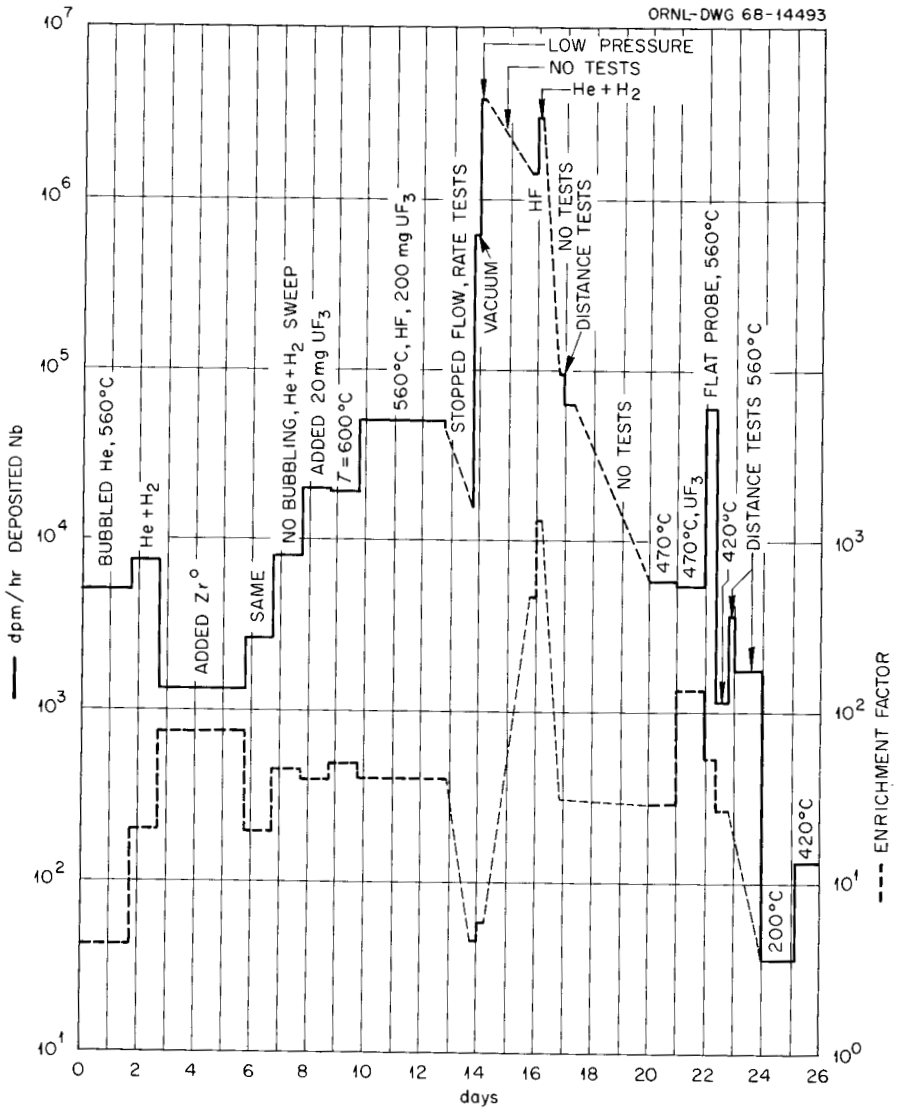

Fig. 3.1. Vapor Deposition of ^{95}Nb from Fuel Salt.

Table 3.1. Calculated Amount of Salt Deposited on Eight Different Probes

Calculations based on liquid salt composition

Sample	Micrograms of Salt Calculated from Lithium Analyses	Micrograms of Salt Calculated from Uranium Analyses	Micrograms of Salt Calculated from ^{95}Zr Activity	Treatment
6	3896	4300	315	UF_3
8	1840	7150	11640	HF, UF_3
14	21300	10800	15793	Vacuum
16	779	1114	656	HF sparge
17	619	796	472	He + H_2
18	330	334	315	
20	110	72	113	
21	458	477	364	480°C
22	183	584	66	480°C, 200 mg UF_3

There are three sorts of drops which can contribute to entrainment in the MSRE: jet drops from splashes and from the bursting of small recirculated bubbles, film drops from the breakup of the film cap of larger bubbles, and crown drops from the breakup of the crown from splash drops. In addition, there might be a considerable direct aerosol formation due to spray from the spray ring in the pump bowl of the MSRE, but we have, at present, no way of evaluating this. The amount of salt potentially available for entrainment from these sources is much larger than that actually lost from the reactor; hence the mist baffles provided must be very effective.

It was also shown experimentally that jet drops can preferentially remove a surface film from a molten-salt surface. This surface microtome effect might well have contributed to the loss of fission products to the gas stream (cf. "Fission Product Behavior in the MSRE"). The jet droplet behavior of the fuel salt can be well approximated by a 50% water-glycerol mixture.

Metallic Colloids in Molten Salts

H. W. Kohn F. F. Blankenship

In addition to the silver sols previously reported,[6] we also prepared silver iodide colloids and colloidal gold, both in mixed nitrate media. Gold colloids were formed by reduction of $AuCl_3$ solution by nitrite ion; silver iodide was formed by the addition of silver nitrate solution followed by potassium iodide solution. Gold sols prepared in $LiNO_3$-KNO_3 eutectic had a mean particle size of 300 A and a narrow particle size distribution determined by electron microscopy; those prepared in $NaNO_3$-KNO_3 eutectic had a wider range of sizes and a mean particle size of about 600 A. We were able to follow the coagulation of gold sol by observing the decrease in the absorption peak at 5750 A. Gold in $LiNO_3$-KNO_3 eutectic was usually stable for a day or two; even after a week there was still some unsettled gold in the solution. The gold did not react with aged silver iodide, although silver iodide was partially precipitated by freshly formed gold. A paper covering this portion of the work has been submitted for publication.[7]

We have also used three methods – reductive electrolysis, Bredig arc, and alternating current electrolysis – to prepare colloids of gold, titanium, niobium, molybdenum, platinum, and nickel in lithium beryllium fluoride. These colloids were not particularly stable: platinum and titanium sols were coagulated in less than 20 min; nickel and niobium were coagulated within an hour; gold and molybdenum sols were the most stable. The Bredig arc gave the most uniform particles, about 100 to 200 A across; the other methods gave large agglomerates, but again the individual particles, where discernible, were in the 100 to 200 A range. The colloids so observed were molybdenum particles that were separated by high-temperature centrifugation[8] followed by water washing.

SYNTHESIS OF NOBLE METAL FLUORIDES AND IDENTIFICATION OF SPECIES IN AND ABOVE MOLTEN FLUORIDES

Synthesis of MoF_4 and RuF_3; Kinetic and Mass Spectrophotometric Studies

C. F. Weaver

Previously reported studies of molybdenum fluoride chemistry, along with the reasons for initiating this work, may be found in refs. 9–17. The following subjects were discussed: synthesis of molybdenum fluorides, reactions of molybdenum fluorides with molten $2LiF$-BeF_2;[9,12,14,17] mass spectrometry of molybdenum fluorides;[10,13,15] potentiometric study of molybdenum in LiF-BeF_2 (67-33 mole %);[11] lithium

[6] H. W. Kohn *Reactor Chem. Div. Ann. Progr. Rept. Dec. 31, 1967*, ORNL-4229, p. 42.

[7] H. W. Kohn and T. E. Wilmarth, *Science*, in press.

[8] H. A. Friedman, *J. Sci. Instr.* **44**, 454 (1967)

[9] C. F. Weaver and H. A. Friedman, *MSR Program Semiann. Progr. Rept. Aug. 31, 1967*, ORNL-4191, pp. 142–44.

[10] R. A. Strehlow and J. D. Redman, *MSR Program Semiann. Progr. Rept. Aug. 31, 1967*, ORNL-4191, pp. 144–46.

[11] N. J. Meyer, C. F. Baes, Jr., and K. A. Romberger, *Reactor Chem. Div. Ann. Progr. Rept. Dec. 31, 1967*, ORNL-4229, pp. 32–33.

[12] C. F. Weaver, H. A. Friedman, and D. N. Hess, *Reactor Chem. Div. Ann. Progr. Rept., Dec. 31, 1967*, ORNL-4229, pp. 33–37.

[13] J. D. Redman and R. A. Strehlow, *Reactor Chem. Div. Ann. Progr. Rept. Dec. 31, 1967*, ORNL-4229, pp. 37–39.

[14] C. F. Weaver, H. A. Friedman, and D. N. Hess, *MSR Program Semiann. Progr. Rept. Feb. 29, 1968*, ORNL-4254, pp. 129–34.

[15] R. A. Strehlow and J. D. Redman, *MSR Program Semiann. Progr. Rept. Feb. 29, 1968*, ORNL-4254, pp. 134–36.

[16] L. M. Toth, J. P. Young, and G. P. Smith, *MSR Program Semiann. Progr. Rept. Feb. 29, 1968*, ORNL-4254, p. 136.

[17] C. F. Weaver, H. A. Friedman, and D. N. Hess, *MSR Program Semiann. Progr. Rept. Aug. 31, 1968*, ORNL-4344.

fluoromolybdates(III);[12,14] and absorption spectroscopy of MoF_5[14] and MoF_3.[16]

Synthesis of Molybdenum and Ruthenium Fluorides (H. A. Friedman, J. W. Gooch, Jr., and D. N. Hess). – Earlier work indicated that MoF_5 can be easily synthesized by refluxing purified commercial MoF_6 over Mo in Pyrex containers at temperatures less than 100°C. It was further shown that the MoF_5 may be disproportionated to produce MoF_3 and MoF_6, which when pumped from the system leaves pure MoF_3. Additional studies of this process have revealed that the solid product resulting from the disproportionation of MoF_5 depends on the pressure of MoF_6 which is maintained in the reaction vessel. If the MoF_6 pressure was kept in the micron range, the solid produced was MoF_3. If much higher pressures, on the order of an atmosphere, were maintained, the solid product was MoF_4, which displays 2θ values for the three most intense x-ray diffraction peaks (Cu radiation) of 23.23, 24.71, and 25.31°. The x-ray diffraction pattern for this material is very similar to that incorrectly reported[18,19] for MoF_3 several years before a satisfactory preparation was studied.[20] Analysis of the MoF_4 gave (wt %) Mo 55.9, F 44.0 compared with calculated values of 55.8 and 44.2 respectively. The compound was found to be stable for many days at a temperature of 200°C and pressures in the micron range, but it decomposed at somewhat higher temperatures (<300°C) to MoF_3 and a volatile product. The results for temperatures above 200°C are somewhat uncertain because the Pyrex container was attacked by the fluorides. These stability studies must be repeated in a metal container.

Synthesis studies of the volatile inorganic fluorides have been extended to the RuF_x family of compounds. An attempt, in accordance with the literature,[21–24] to produce RuF_5 by direct fluorination of Ru metal produced RuF_3 instead. The compound was identified by its x-ray diffraction pattern.[25]

It was indicated above that the products of an MoF_x synthesis were unusually dependent on experimental conditions. Apparently the RuF_x and MoF_x compounds are analogous in this respect. The RuF_3 produced will be used in investigations of the rate of removal of Ru^{3+} from molten $2LiF \cdot BeF_2$ and MSR fuels, paralleling the Mo^{3+} kinetic studies.

[18] H. J. Emeleus and V. Gutmann, *J. Chem. Soc.* 1949, 2979–82.

[19] V. Gutmann and K. H. Jack, *Acta Cryst.* 4, 244–46 (1951).

[20] D. E. Lavalle, *et al.*, *J. Am. Chem. Soc.* 82, 2433–34 (1960).

Kinetic Behavior of Trivalent Molybdenum in Molten $2LiF \cdot BeF_2$

H. A. Friedman J. W. Gooch, Jr.
D. N. Hess

Continued studies of the rate of removal of Mo^{3+} from molten $2LiF \cdot BeF_2$ have served to emphasize the complexity of molybdenum fluoride chemistry.

These experiments have shown that the order as well as the rate of removal vary with the experimental conditions. Figures 3.2 through 3.5 show second-, first-, half-, and half-order kinetics respectively.

It has become apparent that the initial removal rate at 700° is strongly enhanced by the hydrogen firing step, which was used on new batches but not thereafter. Experiments without hydrogen firing will provide a better reference system for kinetic studies involving MSR materials, since the gas is not involved in the reactor chemistry. The most stable conditions encountered thus far are at 500°C; neither the flow rate of He nor H_2 firing of the Cu container strongly affected either the order or rate constant for the Mo^{3+} removal from the molten $2LiF \cdot BeF_2$. The half-order rate constants associated with Figs. 3.4 and 3.5 are defined as

$$k = t^{-1/2}(C_0^{1/2} - C^{1/2})$$

and are 8.1×10^{-3} $ppm^{1/2}/hr$ and 7.3×10^{-3} $ppm^{1/2}/hr$ respectively. This system at 500°C is stable enough to serve as a reference for kinetic studies involving MSR fuels, graphite, and INOR-8, which we will now run in parallel with studies of the simpler systems.

Previously reported[12] evidence that Mo^{3+} was not removed from solution by reaction with the copper container indicated that a disproportionation reaction was involved. It has been reported[19] and we have confirmed by x-ray diffraction that MoF_3 decomposes in the temperature range 500 to 700°C to form Mo metal and a volatile product. It was also shown[26] by

[21] M. A. Hepworth, R. D. Peacock, and P. L. Robinson, *J. Chem. Soc.* 1954, 1197–1201.

[22] J. H. Holloway and R. D. Peacock, *J. Chem. Soc.* 1963, 527–30.

[23] J. H. Holloway, R. D. Peacock, and R. W. H. Small, *J. Chem. Soc.* 1964, 644–48.

[24] H. A. Porter, E. Greenberg, and W. N. Hubbard, *J. Phys. Chem.* 69, 2308–10 (1965).

[25] The aid and advice of H. L. Yakel, Jr., and R. M. Steele of the Metals and Ceramics Division with respect to the interpretation of x-ray diffraction data is gratefully acknowledged.

[26] J. P. Young, personal communication.

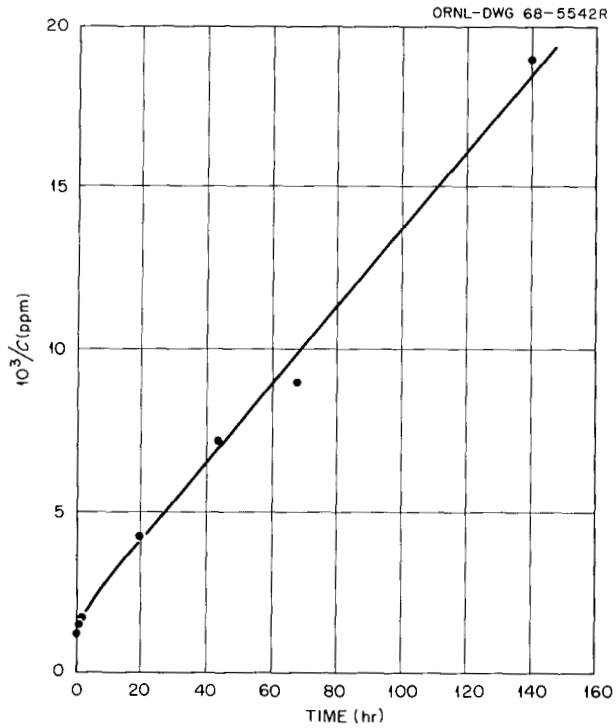

Fig. 3.2. Removal of Mo^{3+} from Molten $2LiF \cdot BeF_2$. Conditions: 700°C, ¾ liter/hr He flow, Cu container H_2 fired at 500°C.

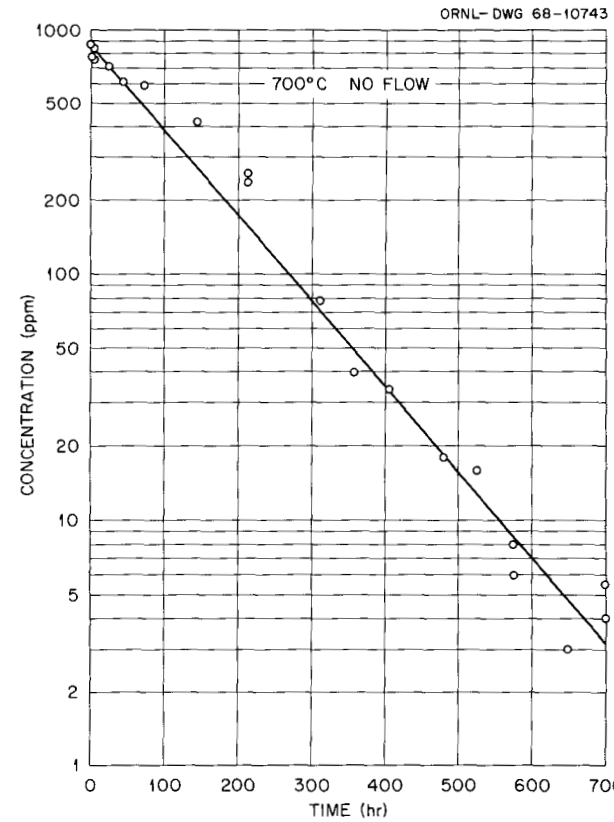

Fig. 3.3. Removal of Mo^{3+} from Molten $2LiF \cdot BeF_2$. Conditions: 700°C, no He flow, Cu container not H_2 fired.

electron probe analysis that a sample of $2LiF \cdot BeF_2$ and MoF_3 heated to 700°C in a graphite container under an He atmosphere had Mo metal on the He-salt interface after cooling. Since all of the intermediate-valence MoF_x ($3 < x < 6$) compounds are thermally unstable in bulk at temperatures well below 500–700°C, it was proposed that the reaction $2MoF_3 \rightarrow Mo + MoF_6$ occurred. However, efforts to collect the volatile species by trapping it in aqueous caustic solution were unsuccessful.[12] More recently, efforts to detect the volatile species under two different conditions with a spectrophotometer[27,28] were also unsuccessful. In one case the spectrophotometric cell was at room temperature, obviating the detection of species not volatile at room temperature. It is known from our own work[14] in cooperation with J. P. Young that MoF_5 does not have a high enough vapor pressure at room temperature to be detected in a 5-cm quartz cell by absorption spectroscopy. In the second case a

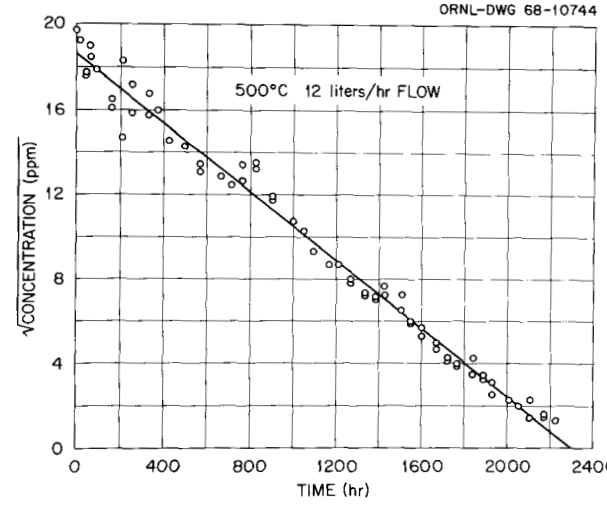

Fig. 3.4. Removal of Mo^{3+} from Molten $2LiF \cdot BeF_2$. Conditions: 500°C, 12 liters/hr He flow, Cu container H_2 fired at 500°C.

[27] L. M. Toth, J. P. Young, and G. P. Smith, personal communication.

[28] L. M. Toth, J. P. Young, and G. P. Smith, *MSR Program Semiann. Progr. Rept. Aug. 31, 1968*, ORNL-4344.

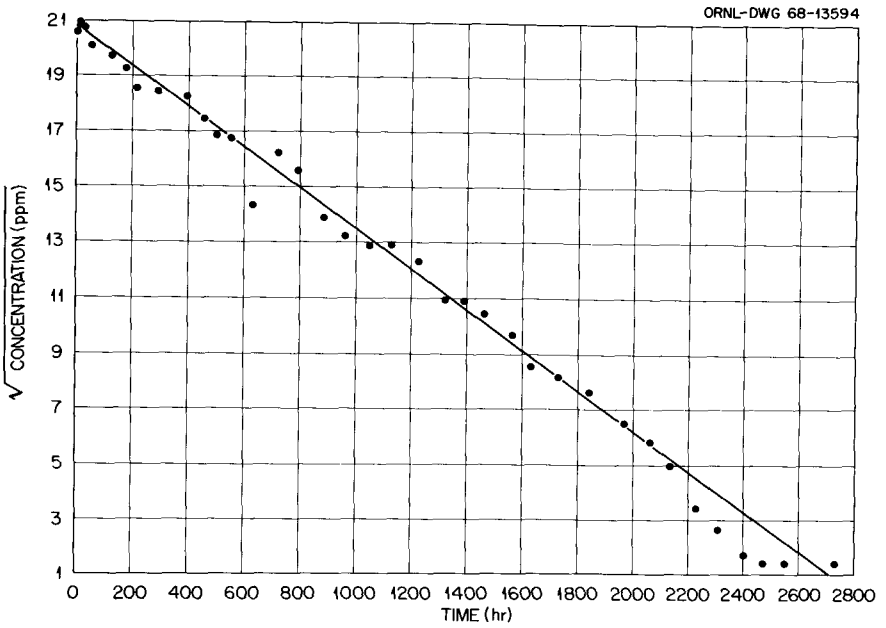

Fig. 3.5. Removal of Mo^{3+} from Molten $2LiF \cdot BeF_2$. Conditions: 500°C, no He flow, Cu container not H_2 fired.

windowless cell was used. The optical path was at melt temperature, but clearly volatile material could easily escape from the path.

On opening the systems used for the kinetic studies a blue coating typical of MoF_x hydrolysis product was found in the portion of the gas outlet line that was warmer than room temperature. This observation suggests that a volatile molybdenum compound did escape from the melt, condensed at lower temperature in the hot line, and hydrolyzed when the system was exposed to air at the end of the run. Since the volatile species cannot be MoF_6, we now believe that it is MoF_4 or MoF_5 and that their low partial pressures, on the order of 1 torr or less, either reduce their decomposition rates or shift the chemical equilibria in their favor, as indicated at even lower pressures by the following mass spectrometric studies.

Mass Spectrometric Studies of Fluorides

J. D. Redman

Mass spectrometric studies of pure MoF_3 have shown[15] (Fig. 3.6, dotted lines) that the gas escaping from a Knudsen cell in the temperature range 500 to 700°C was predominantly MoF_5 with lesser amounts of both MoF_6 and MoF_4 and that the ratio of MoF_4 to MoF_5 increased with temperature. Similar studies with $LiF\text{-}BeF_2\text{-}MoF_3$ (60-30-10 mole %) in the temperature range 500 to 800°C indicated (Fig. 3.6, solid lines) that the same three materials, MoF_4, MoF_5, and MoF_6, were present, but that the amount of MoF_4 was markedly increased at the expense of both MoF_5 and MoF_6, that the ratio of MoF_4 to MoF_5 again increased with temperature, and that the MoF_4 became the dominant species at ~590°C. The molybdenum fluoride dimer previously observed over pure MoF_3 was not observed with the $LiF\text{-}BeF_2\text{-}MoF_3$ mixture. Two groups of fragments with typical molybdenum isotopic ratios were observed at 600°C having 228 and 130 amu (for ^{98}Mo). Neither of these peaks was observed in previous studies involving molybdenum fluorides or oxyfluorides in the absence of molten $2LiF \cdot BeF_2$. It is possible that they represent the trimer fragments

$$^{7}LiF \cdot {}^{98}MoF_3 \cdot BeF_2^{+} \text{ and } \begin{matrix} Li \\ Li \end{matrix}\!\!>\!Mo\!<\!\!\begin{matrix} Be^{+} \\ Be \end{matrix} .$$

In any event they are a minor portion (~2%) of the effusing vapor. In addition, this study has shown that the molten $2LiF \cdot BeF_2$ solvent tends to stabilize Mo^{3+} and that copper is much superior to nickel as a container material. Both observations are consistent with our experience in synthesis and solution kinetics described above.

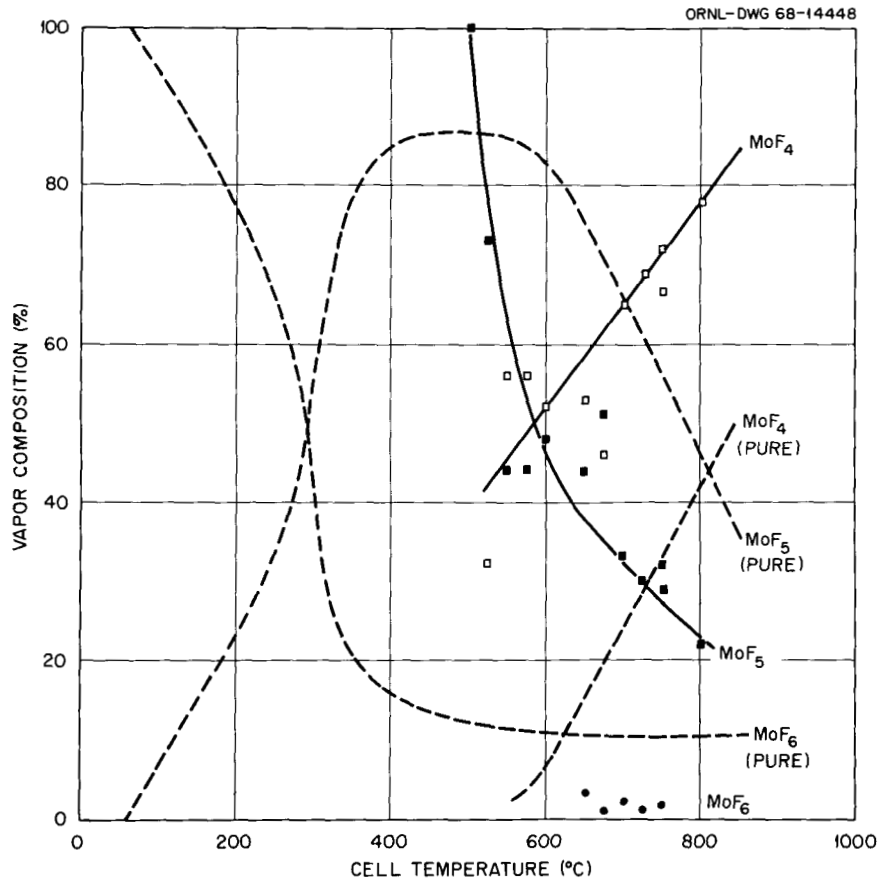

Fig. 3.6. Vapor Composition over MoF_3 in Molten $2LiF \cdot BeF_2$ Compared with That over Pure MoF_3.

We plan to pursue this and similar studies with other MSR materials, since at present mass spectrometry is the only approach which has provided definite information about the composition of the gas phase associated with Mo^{3+} solutions. For this reason the following work with RuF_3 and NbF_5 was done.

A sample of RuF_3, prepared by D. E. LaValle (Analytical Chemistry Division), disproportionated in the Knudsen cell at temperatures between 600 and 700°C forming Ru metal (identified by x-ray diffraction) and either RuF_4 or RuF_5. The total cell pressure at 650°C was estimated to be about 10^{-4} torr. Ionization efficiency curves at 650°C for the ion fragments are shown in Fig. 3.7. The appearance potentials, obtained by the vanishing-current technique, are listed in Table 3.2. The RuF_4^+ ion may be formed either by simple ionization of RuF_4 or by dissociative ionization of RuF_5. The latter method is characteristic of many metal halide systems,[29] including those of molybdenum and niobium.

In Table 3.3 are cracking patterns of the vapor species as a function of temperature (600 to 700°) for 75 ev electron energy and as a function of electron energy (18 to 75 ev) for 650°. Over the narrow 100° temperature range, within which the metal fluoride completely effused, no significant change in the relative abundance of the ions was seen. The temperature stability of the effusing Ru fluoride indicates the presence of only one neutral precursor. At lower electron energies (less than 30 ev) the RuF_3^+ to RuF_4^+ ratio decreased. This effect, as seen in the ionization efficiency curves for RuF_3^+ and RuF_4^+ in Fig. 3.7, could be expected for a parent ion as it undergoes less fragmenting at lower electron energies. It would appear, therefore, that RuF_4 undergoes the unusual simple ionization and that the disproportionation reaction is $4RuF_3 \rightarrow Ru + 3RuF_4$.

The sample of NbF_5, synthesized by L. M. Toth and H. A. Friedman, was sublimed in a Knudsen cell at 75°C, leaving a 1.6 wt % oxygen-containing residue

[29] K. F. Zmbov and J. L. Margrave, "Mass Spectrometric Studies of Scandium, Yttrium, Lanthanum, and Rare-Earth Fluorides," pp. 267–89 in *Mass Spectrometry in Inorganic Chemistry*, ed. by R. F. Gould, ACS, Washington, D.C., 1968.

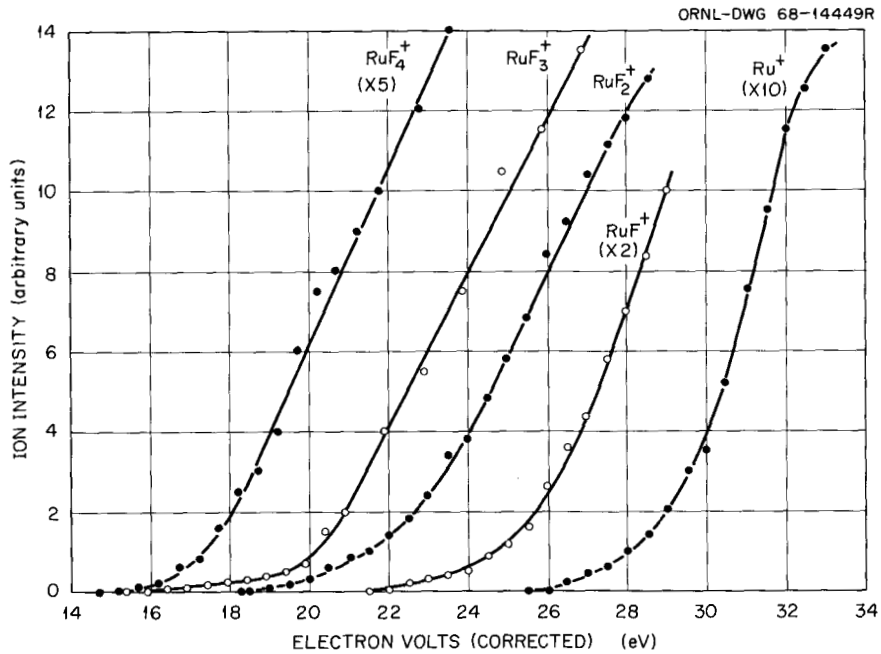

Fig. 3.7. Ionization Efficiency Curves for Vapor over RuF_3.

Table 3.2. Appearance Potentials for Ion Fragments from Vapor over RuF_3 at 650°C

Ion	Appearance Potential (ev)[a]
RuF_4^+	15.3
RuF_3^+	15.9
RuF_2^+	18.5
RuF^+	22.0
Ru^+	25.5

[a]Argon reference gas: Ar^+ at 15.75 ev.

Table 3.3. Cracking Patterns for the Vapor over RuF_3

Ion	Relative Abundance (75 ev) at Temperatures (°C) of –			Relative Abundance (650°C) at Energies (ev) of –					
	600	650	700	18	19	25	30	40	60
RuF_4^+	19	25	17	100	72	44	31	23	31
RuF_3^+	100	100	100	80	100	100	100	100	100
RuF_2^+	32	39	33				26	32	47
RuF^+	18	23	24				12	14	26
Ru^+	31	44	39				15	16	41

which was not volatile at this temperature. The residue gave off $NbOF_3$ in the temperature range 300 to 575°C and again above 700°C. The cell pressure at 75°C was estimated to be between 10^{-3} and 10^{-2} torr. The cracking patterns for NbF_5 and $NbOF_3$ at 75 ev are shown in Table 3.4. The ionization efficiency curves are given in Fig. 3.8. The appearance potentials obtained from these curves are listed in Table 3.4. Since the NbF_5^+ parent peak is absent, the NbF_5 must undergo dissociative ionization, typical of metal halides.[29] This suggests that the neutral precursors for the $Nb_2F_9^+$ and the $Nb_3F_{14}^+$ ions are the dimer Nb_2F_{10} and the trimer Nb_3F_{15} respectively.

The Nb, Mo, and Ru fluorides studied thus far are strikingly different in behavior. The Nb forms at least two polymers, Nb_2F_{10} and Nb_3F_{15}, the Mo forms Mo_2F_{10}, while Ru gives no evidence of polymerization. The strong tendency to form oxyfluorides is shared by all these elements, but the relative volatilities differ. In the case of Mo the oxyfluorides are somewhat more volatile than the fluorides but not sufficiently so to provide an easy separation of the species. On the other hand, both Ru and Nb form oxyfluorides which are much less volatile and allow complete separation of the fluorides. The probability that the Ru fluorides undergo simple rather than dissociative ionization, discussed above, distinguishes them from the Mo and Nb fluorides.

In addition to the noble metal fission product work, recent interest[30] in the use of aluminum halides to form volatile complexes with actinide or rare-earth fluorides prompted a mass spectrometric study of vapor species over $LiF\text{-}BeF_2\text{-}ThF_4$ (72-16-12 mole %) containing PrF_3 and AlF_3. The barren fuel, spiked with 10 wt % PrF_3 and 11 wt % AlF_3, was loaded in a nickel Knudsen cell crucible. Vapor species effusing from the cell were monitored over the temperature range 650 to 850°C. The total pressure inside the cell at 850°C was estimated to be near 0.2 μ. The only volatile aluminum complexes observed were $LiAlF_4$ and Li_2AlF_5 (about 8:1). No fragments containing Pr or Th were seen.

Table 3.4. Cracking Patterns for NbF_5 at 75°C and $NbOF_3$ at 800°C

Ion	Relative Intensity	Appearance Potential[a] (ev)
	NbF_5	
Nb^+	0.3	
NbF^+	1.0	
NbF_2^+	2.0	
NbF_3^+	14.0	21.2
NbF_4^+	100	14.5
$Nb_2F_6^+$	0.06	
$Nb_2F_7^+$	0.4	
$Nb_2F_8^+$	1.50	
$Nb_2F_9^+$	55.0	16.0
$Nb_3F_{13}^+$	0.06	
$Nb_3F_{14}^+$	2.0	18.7
	$NbOF_3$	
Nb^+	14.0	
NbO^+	8	
NbF^+	8	
$NbOF^+$	13	
NbF_2^+	13	
$NbOF_2^+$	100	
NbF_3^+	1.0	
$NbOF_3^+$	50	
NbF_4^+	<0.1	

[a]Argon reference gas: Ar^+ at 15.75 ev.

Spectrophotometric Examination of Molybdenum Fluorides in Molten $LiF\text{-}BeF_2$ Mixtures

MoF_3 Fluoride Solution Spectra (L. M. Toth, J. P. Young,[31] and G. P. Smith[32]). – Spectra of dilute solutions of MoF_3 in molten $LiF\text{-}BeF_2$ (66-34 mole %)[33] have been studied in order to demonstrate both the valence state and coordination of the molybdenum species. Peaks at 472 and 353 mμ with molar absorptivities of *ca.* 8 and 12 liters $mole^{-1}$ cm^{-1}, respectively, have been observed. The positions of these two transitions are consistent with what is predicted from the spectrochemical series.[34] On this basis it is possible to

[30]C. F. Weaver to H. F. McDuffie, personal communication, 1968; A. M. Weinberg to W. R. Grimes, personal communication, 1968; M. A. Bredig to W. R. Grimes, personal communication, 1968.

[31]Analytical Chemistry Division.

[32]Metals and Ceramics Division.

[33]Hereafter referred to as L_2B.

[34]C. K. Jorgensen, *Absorption Spectra and Chemical Bonding in Complexes*, p. 108, Pergamon, London, 1962.

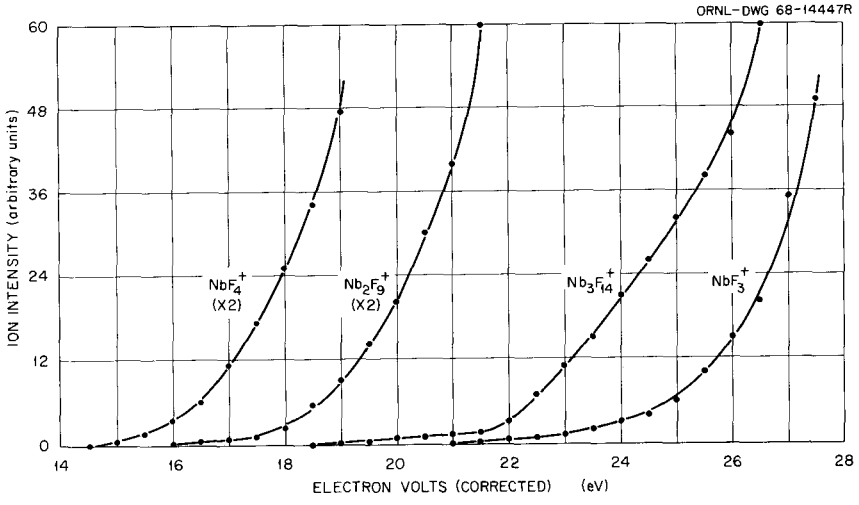

Fig. 3.8. Ionization Efficiency Curves for Vapor over NbF_5.

say that MoF_3 in L_2B is present as Mo^{3+} ions which are octahedrally coordinated to fluoride ions to form MoF_6^{3-}.

For these studies the melts have been contained in windowless cells[35] made from graphite, platinum, molybdenum, or copper. The variety of container materials were used in an unsuccessful effort to maintain stable MoF_3 solutions. Molybdenum was invariably lost from solution after 24 hr at 700°C due to an unexplained mechanism. Experience with the system has led us to believe that impurity reactions were involved.

K_3MoF_6 Synthesis and Spectrum (L. M. Toth and G. P. Smith). – As an independent demonstration that the melt spectrum of MoF_3 in L_2B was due to octahedrally coordinated Mo^{3+}, that is, MoF_6^{3-}, a spectrum of Mo^{3+} in a known chemical environment was required. It was predicted[36] that K_3MoF_6 would probably exhibit a cubic structure in which the Mo^{3+} ion was coordinated to six fluoride ligands. However, previously reported synthesis of K_3MoF_6[37] was actually found to produce an oxyfluoride compound that does not possess the required octahedral environment for Mo^{3+}. Therefore, K_3MoF_6 was prepared by mixing stoichiometric quantities of KF and MoF_3[38] and fusing in a sealed platinum tube at 880°C for ½ hr. A low (*ca.* 5%) yield of the product was obtained in the form of small crystals which measured approximately 0.3 mm in diameter. These crystals were hand picked and washed with ethanol and/or acetone.

Density measurements of the K_3MoF_6 gave a value of 3.23 ± 0.03 g/cm^3 at 25°C, which is consistent with the assumed stoichiometry and measured unit cell dimensions. The crystal structure[39] confirms that the compound is K_3MoF_6.

The diffuse reflectance spectrum of K_3MoF_6, shown in Fig. 3.9, has three broad absorption bands with maxima at 262 mμ (*ca.* 38,200 cm^{-1}), 337 mμ (*ca.* 29,700 cm^{-1}), and 425 mμ (*ca.* 23,500 cm^{-1}). The transmission spectrum of the polycrystalline particle had absorption maxima at 337 and 425 mμ, but light scatter at 262 mμ was too severe to permit absorption measurements at this wavelength.

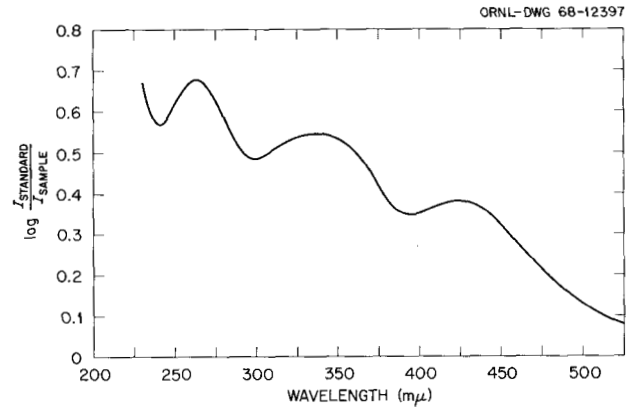

Fig. 3.9. Diffuse Reflectance Spectrum of K_3MoF_6.

We assign the two lowest-energy bands to the lowest-energy spin-allowed ligand-field transitions as follows: 23,500 cm^{-1} to $^4T_{2g}(t_{2g}^2e_g) \leftarrow {}^4A_{2g}(t_{2g}^3)$ and 29,700 cm^{-1} to $^4T_{1g}(t_{2g}^2e_g) \leftarrow {}^4A_{2g}(t_{2g}^3)$. The mean energy of the first of these transitions should approximate 10 Dq so that Dq is on the order of 2,350 cm^{-1}. By inserting this value of Dq and the energy of the second band into the appropriate Tanabe-Sugano[40] secular equation of a d^3 system, we obtain 570 cm^{-1} as an estimate of Racah's electronic repulsion parameter B. This value is 93% of a previous estimate of the free-ion value (610 cm^{-1}).[34]

These parameters can be compared with those previously reported[34,41] for MoX_6^{3-} complexes where X = Cl^- and Br^-. The Dq values for Cl^- and Br^- are 1910 and 1770 cm^{-1}, respectively, and their B values are 420 and 390 cm^{-1}. We find both the spectrochemical and the nephelauxetic series for Mo(III) to be $F^- > Cl^- > Br^-$, which is as expected.[34]

The assignment of the band at 38,200 cm^{-1} is less certain. The wave number is considerably lower than that predicted for the remaining spin-allowed transition, $^4T_{1g}(t_{2g}e_g^2) \leftarrow {}^4A_{2g}(t_{2g}^3)$, when the above values of Dq and B are substituted into the Tanabe-Sugano equation. (The predicted value is about 49,300 cm^{-1}.) Despite the deficiencies of the theory, this difference of about 10^4 cm^{-1} seems unreasonably large. Possibly this band is a spin-forbidden transition of the $t_{2g}^3 \rightarrow t_{2g}^2e_g$ type. Several of these should lie between the second and third spin-allowed transitions. The possibility of observing

[35] J. P. Young, *Anal. Chem.* **36**, 390 (1964).

[36] Private communication with H. L. Yakel, Metals and Ceramics Division.

[37] S. Aleonard, *Compt. Rend.* **260**, 1977 (1965).

[38] Materials supplied by S. Cantor and C. F. Weaver respectively.

[39] L. M. Toth, G. D. Brunton, and G. P. Smith, submitted to *Inorganic Chemistry*, November 1968.

[40] Y. Tanabe and S. Sugano, *J. Phys. Soc. Japan* **9**, 753 (1954).

[41] H. Hartman and H.-J. Schmidt, *Z. Physik. Chem. (Frankfort)* **11**, 234 (1957); T. Kormorita, S. Miki, and S. Yamada, *Bull. Chem. Soc. Japan* **38**, 123 (1965).

such a band would depend, of course, on the mixing of multiplicities as a consequence of the moderately large spin-orbit coupling constant for Mo(III). However, the band intensity appears to be much too large for such an assignment. The remaining possibility, and the one we regard as most plausible, is assigned as a charge-transfer absorption. Similar charge-transfer bands are known[40] for $MoCl_6^{3-}$.

The lowest-energy spin-forbidden transitions give rise to two relatively sharp low-energy bands in $MoCl_6^{3-}$. The one at 9500 cm^{-1} is almost certainly due to the pair of transitions $^2T_{1g}(t_{2g}^3)$, $^2E_g(t_{2g}^3) \leftarrow {}^4A_{2g}(t_{2g}^3)$, which are theoretically predicted to lie close together. The positions of these transitions are not influenced significantly by Dq at the 2000 cm^{-1} level. Hence, if we assume that the ratio of Racah parameters B/C is not very different in MoF_6^{3-} and $MoCl_6^{3-}$, these transitions should occur near the same positions in both complexes. Since 9500 cm^{-1} (1053 mμ) lies outside the range of our measurements, our failure to see this band is not surprising. The second spin-forbidden band in $MoCl_6^{3-}$ was found at 14,800 cm^{-1} (676 mμ). It should lie at a somewhat higher energy in MoF_6^{3-}, but because the longest accessible wavelength with our diffuse reflectance accuracy was 600 mμ, we did not observe this band either. In any event, a careful search for these spin-forbidden bands by transmission spectroscopy at low temperatures on specimens of higher optical quality than we were able to prepare is clearly worth while and, if successful, would permit estimation of Racah's C parameter.

With the crystal structure determination that the Mo^{3+} ion in K_3MoF_6 is surrounded in octahedral symmetry by six fluoride ligands as MoF_6^{3-}, a comparison between its spectrum and that of the high-temperature MoF_3 in L_2B spectrum gives conclusive evidence that the species present in the MoF_3-L_2B solution is MoF_6^{3-}.

Vapor-Phase Studies over MoF_3 Solutions (L. M. Toth, J. P. Young, and G. P. Smith). – Previously it was proposed that MoF_3 disappears from L_2B solutions by a disproportionation reaction:[42]

$$2MoF_3 \rightleftharpoons Mo + MoF_6 \ .$$

We sought to support this argument by measuring the spectrum of MoF_6 in the gas phase over a solution of MoF_3 in L_2B. MoF_6 has a strong charge-transfer absorption in the 200 mμ region ($\epsilon \sim 10^3$ liters $mole^{-1}$ cm^{-1}) with vibrational structure that provides a "fingerprint" for identification.

Initial attempts to measure MoF_6 spectra directly over the melt in a windowless container at 550 to 700°C revealed nothing. Because we knew neither our sensitivity limits nor the reason for losses of molybdenum from the MoF_3-L_2B solutions, we refined our approach in the following manner:

The procedure was simply to maintain an L_2B solution of MoF_3 at 700°C or greater in an appendix tube attached to the 10-cm-path-length gas cell fitted with quartz windows. The gas cell was kept at room temperature and fitted into the sample compartment of a Cary model 14 spectrometer. Any MoF_6 generated in the hot appendix tube was then expected to diffuse into the gas cell, where its spectrum could be measured.

The second-order rate constant data of Weaver, Hess, and Friedman[43] indicate that 1000 ppm of MoF_3 in L_2B would have an equilibrium pressure of at least 1 torr. A calibration of our system with MoF_6 gas showed that we could detect MoF_6 at pressures as low as 0.020 torr.

First, MoF_6 was introduced to demonstrate that pressures as low as 0.020 to 0.050 torr were stable in the system for 1 hr or more. Then solutions containing 0.1 to 1.0 wt % MoF_3 in L_2B were fused in the appendix tube and held at 700°C. Under no conditions was MoF_6 evolution from solution observed, not even when the solution temperature was raised to 900°C.

It has been concluded from this work that MoF_6, within detection limits, does not exist in equilibrium over solutions of MoF_3 in L_2B, and thus we have no basis to say that the above disproportionation occurs.

REPROCESSING STUDIES FOR MOLTEN-SALT BREEDER REACTORS

Reductive Extraction of ^{233}Pa, Uranium, and Zirconium from Molten LiF-BeF_2-ThF_4 Mixtures into Bismuth

D. M. Moulton W. R. Grimes
W. Jennings, Jr. J. H. Shaffer

In the single-fluid molten-salt breeder reactor the most important reprocessing step is the removal of protactinium from the salt at a rather low level (less than 100 ppm). Uranium at 0.3 mole % must be

[42] C. F. Weaver, D. N. Hess, and H. A. Friedman, *MSR Program Semiann. Progr. Rept. Feb. 29, 1968*, ORNL-4254, p. 133.

[43] Private communication with C. F. Weaver, D. N. Hess, and H. A. Friedman, Reactor Chemistry Division.

removed as well if reductive extraction is used as the reprocessing method. Zirconium is produced in substantial quantities as a fission product; though it is not a major reactor poison, it will be extracted in the vicinity of uranium and protactinium, and it is known to affect at least the solubility of uranium in bismuth quite substantially. In order for a workable process to be designed, the behavior of all of these metals singly and in combination needs to be investigated. Several experiments have been completed in a continuing program on this subject.

In the first experiment ^{233}Pa without uranium was extracted from $LiF\text{-}BeF_2\text{-}ThF_4$ (72-16-12 mole %) into bismuth in an all-graphite apparatus. After a point where 70.4% had been extracted at an overall balance of 93.8%, a temperature runaway made the rest of the data unreliable. A few analyses of the system after this excursion gave the ratio $D_{Pa}/D_{Th} = 280$ at 700°. The experiment was repeated with the addition of 0.3 mole % UF_4. The uranium balance was good, but the Pa balance began to decline at $D_{Pa} > 2$. The maximum extraction at 600° was 74%, with a balance of 86%. Both spectrochemical and chemical methods were used to determine Li and Th in the bismuth, and when they disagreed the former were preferred.

A different salt, $LiF\text{-}BeF_2\text{-}ThF_4$ (68-20-12 mole %), containing 1 wt % UF_4 and a Pa tracer, was also studied in the same way. At several points in the experiment the phases were sampled at 2, 4, and 20 hr after the addition of reductant to see whether there was any loss of reduced metal with time. The only significant change was a sharp rise of Pa concentration between the first two samples at the highest thorium concentration, due probably to the slow dissolution of the metallic thorium added. The Pa balance was good up to $D_{Pa} = 0.5$ and then fell slowly. The maximum extracted was 41% at a balance of 58%. The design of the seals for the all-graphite systems in this and the previous experiment did not allow firing the vessels at as high a temperature as desirable, and this may have left residual impurities which caused the apparent loss of Pa. Lithium and thorium analyses were made both by emission spectroscopy and by flame photometry (Li) and aqueous (Th) methods. The values obtained by these methods are listed as "spec" and "chem" in the Table 3.5.

For comparison we have also listed the values obtained in an extraction at 650° from $LiF\text{-}BeF_2\text{-}ThF_4$ (73-2-25 mole %), which are a recalculation of the numbers reported earlier.[44] The numbers at the bottom of the table are the Li-Th values obtained in some cerium reduction experiments reported elsewhere in this publication. Spectrochemical methods were used for Li and Th in these last three experiments. In all the valence of uranium has been taken as 3.0, and the error limits are the standard deviations of the measurements.

The inconsistency in the change in $\Delta\mathcal{E}'_0$ with temperature may reflect a systematic error in the analytical methods, but the differences are generally within the error limits of the measurements. The behavior is not so peculiar as it looks: the increasing multiplying constant RT/nF masks the fact that the logs of the equilibrium constants are decreasing in magnitude, that is, the actinides are becoming harder to reduce relative to lithium as the temperature rises.

The differences among the salts are probably real. If the free fluoride present in the 72-16-12% salt (ff = +4) does indeed stabilize the actinides, then $\mathcal{E}'_{0\,Li} - \mathcal{E}'_{0\,m}$ should be smaller with this salt than with the others. This does work with the 68-20-12% salt, and the 73-2-25% salt may be different enough to override the free-fluoride effect. Baes has found[45] in $LiF\text{-}BeF_2$ that stabilization by free fluoride is greater for those ions with a high charge-to-radius ratio. This predicts that the order of stabilization would be $U^{4+} > Pa > Th \gg U^{3+}$. The Pa-Th difference is observed, but the stabilization of U (which should be U^{3+}) is not explained by this model.

Zirconium without U or Pa has been extracted from $LiF\text{-}BeF_2\text{-}ThF_4$ (68-20-12 mole %) in graphite using both spectrochemical and radiochemical methods of Zr analysis. The latter involved counting the resolved $^{95}Zr\text{-}^{95}Nb$ peaks on a lithium-drifted germanium diode. The zirconium analyses were quite good, in contrast to some earlier experiments where they were not. The potential differences are tabulated below.

T	$\mathcal{E}'_{0\,Li} - \mathcal{E}'_{0\,Th}$	$\mathcal{E}'_{0\,Li} - \mathcal{E}'_{0\,Zr}$	$\mathcal{E}'_{0\,Th} - \mathcal{E}'_{0\,Zr}$
600	−0.366* ± 0.042	−0.532* ± 0.077	−0.145 ± 0.047
700	−0.433 ± 0.027	−0.615 ± 0.027	−0.166 ± 0.053

The lithium-thorium value at 600° is not as great as it had been in other experiments with this salt. In view of the rather large error, it seems reasonable to add 0.056 v to this and the Li-Zr potential, making them −0.422 and −0.588 v respectively. This experiment indicates that Zr should extract between U and Pa. What, if any, interaction occurs among these metals remains to be determined.

[44] D. M. Moulton *et al.*, *Reactor Chem. Div. Ann. Progr. Rept. Dec. 31, 1967*, ORNL-4229, p. 46.

[45] C. F. Baes, Jr., *Reactor Chem. Div. Ann. Progr. Rept. Dec. 31, 1965*, ORNL-3913, p. 21.

Table 3.5. Extraction Potential Differences for Protactinium and Uranium in $LiF-BeF_2-ThF_4$ Salts

Salt	Temperature	$\mathcal{E}'_{0\,Li} - \mathcal{E}'_{0\,Th}$	$\mathcal{E}'_{0\,Li} - \mathcal{E}'_{0\,Pa}$	$\mathcal{E}'_{0\,Li} - \mathcal{E}'_{0\,U}$	$\mathcal{E}'_{0\,Pa} - \mathcal{E}'_{0\,U}$
72-16-12	600	−0.392 ± 0.049	−0.477 ± 0.047	−0.551 ± 0.020	−0.065 ± 0.009
	700	−0.409 ± 0.051	−0.508 ± 0.018	−0.576 ± 0.014	−0.074 ± 0.011
68-20-12					
(Spec)	600	−0.422 ± 0.013	−0.544 ± 0.022	−0.611 ± 0.045	−0.067 ± 0.025
	700	−0.434 ± 0.019	−0.574 ± 0.016	−0.636 ± 0.033	−0.064 ± 0.029
(Chem)	600	−0.448 ± 0.031	−0.575 ± 0.034	−0.643 ± 0.030	−0.067 ± 0.025
	700	−0.431 ± 0.062	−0.561 ± 0.067	−0.630 ± 0.058	−0.064 ± 0.029
73-2-25	650	−0.340 ± 0.013	−0.483 ± 0.011	−0.540 ± 0.017	−0.056 ± 0.018
72-16-2	600	−0.381 ± 0.020			
	700	−0.392 ± 0.018			
68-20-12					
(Spec)	600	−0.415 ± 0.018			
	700	−0.399 ± 0.013			

Protactinium Studies in the High-Alpha Laboratory

C. J. Barton H. H. Stone J. C. Mailen[46]
R. G. Ross

Results of two experiments on the transfer of protactinium from molten fluoride mixtures to liquid bismuth containing either uranium or thorium were given in the last report.[47] Our attention has been focused exclusively on the liquid metal extraction method of recovering protactinium during the past year. Two experiments were performed with a fluoride blanket composition, and all others involved a single-fluid fuel composition. Most of the results have been discussed in other reports,[48,49] and the data will only be summarized here.

Experiments with a Blanket Composition. – The salt phase in two Bi-Th alloy extraction experiments was the two-region nuclear blanket composition $LiF-BeF_2-ThF_4$ (73-2-25 mole %). Graphite was the container material in both experiments. In the first experiment sufficient thorium was added to give a concentration of 2500 ppm (the approximate saturation value at the equilibration temperature, 625°C) after reducing the uranium and protactinium fluorides present. Reduction of protactinium and uranium and their transfer to the bismuth occurred quite rapidly, in 30 min or less. The concentration of protactinium in the bismuth decreased slowly during a period of 18 hr. Addition of more thorium at this juncture caused a drop in the protactinium concentration in both phases. The decrease in the bismuth is attributed to coprecipitation of protactinium with a Bi-Th intermetallic compound. The protactinium material balance (filtered samples) was close to 80%, and there appeared to be some insoluble protactinium present in the bismuth. Approximately 80% of the uranium was found in the bismuth, and there was little change in the uranium concentration in both phases during the last 17 hr of the initial equilibration period.

The second experiment essentially duplicated the first except that the reduction of protactinium and uranium was much slower. After the salt and Bi-Th alloy (0.17 wt % excess Th) had been in contact for 18⅛ hr, 58% of the protactinium was in the filtered bismuth and 35% in the filtered salt, making a total of 93%. At the conclusion of the experiment it was found that the graphite dip leg had broken at the point where it was sealed to ⅛-in. nickel tubing. Consequently, no mixing of the phases was effected in this experiment. The concentration of thorium in bismuth dropped from its initial value of 1760 ppm to about 1100 and then rose to the saturation value (2570 ppm) upon the addition of more thorium.

Experiments with Single-Fluid Fuel Composition. – Seven experiments were conducted with the single-fluid fuel composition $LiF-BeF_2-ThF_4$ (72-16-12 mole %). Most of the results obtained with this composition were quite poor in comparison with the above-reported data obtained with the blanket composition, which con-

[46] Chemical Technology Division.

[47] C. J. Barton and H. H. Stone, *Reactor Chem. Div. Ann. Progr. Rept. Dec. 31, 1967*, ORNL-4229, p. 47.

[48] C. J. Barton *et al.*, *MSR Program Semiann. Progr. Rept. Feb. 29, 1968*, ORNL-4254, pp. 159–65.

[49] C. J. Barton *et al.*, *MSR Program Semiann. Progr. Rept. Aug. 31, 1968*, ORNL-4344.

tained more ThF_4 and less BeF_2. No definitive reason can be given at present for the different behavior of the two compositions, which is especially evident in graphite containers. One experiment in a mild steel liner gave no better results than those conducted in graphite, but one highly successful experiment carried out in molybdenum-lined equipment gives hope that single-fluid compositions can be extracted in this or a similar container material.

The experiments in graphite were characterized by a slow but consistent loss of thorium from the bismuth phase, averaging about 100 ppm/hr. This resulted in incomplete transfer of protactinium and uranium to the bismuth and poor material balances. In some instances, a reversal was noted. That is, protactinium and uranium transferred from the salt phase to bismuth while the thorium was present in the metal and then went back to the salt as the thorium concentration in the bismuth dropped to a low level. We noticed that when thorium was added to the experiment in the form of crystal bar material, which dissolves slowly in bismuth, less reduction of protactinium and uranium occurred than when thorium turnings having a high surface-to-weight ratio were used as the reducing medium. This was interpreted as an indication that the unknown reaction that converted thorium into an insoluble form occurred more rapidly when the thorium was present as the metal than when it was dissolved in bismuth.

The principal difference noted when the container material was mild steel rather than graphite was that the thorium concentration in bismuth dropped to zero in the first hour that the alloy was in contact with the steel. This presumably was due to alloying of thorium with the iron liner. However, reduction of protactinium and uranium proceeded at a slow rate, indicating that the insoluble thorium still possessed reducing power.

The experiment in molybdenum was conducted in two stages. In the first stage, the salt solvent containing 8800 ppm ^{238}U (as UF_4) and 100 ppm ^{231}Pa (as PaF_4) was mixed with Bi-Th alloy containing 0.93 wt % Th, a slight excess over the amount required to reduce the uranium and protactinium. Protactinium distribution data obtained in this part of the experiment are shown in Fig. 3.10, while the uranium data are displayed in Fig. 3.11. It is apparent from these figures that reduction of protactinium and uranium was not complete when the first samples were taken after 0.8 hr contact between the salt and Bi-Th alloy. Equilibrium had been achieved by the time the second samples at 2.3 hr were taken. No change in protactinium or uranium distribution was found during four days under static argon and two days with flowing argon, but a

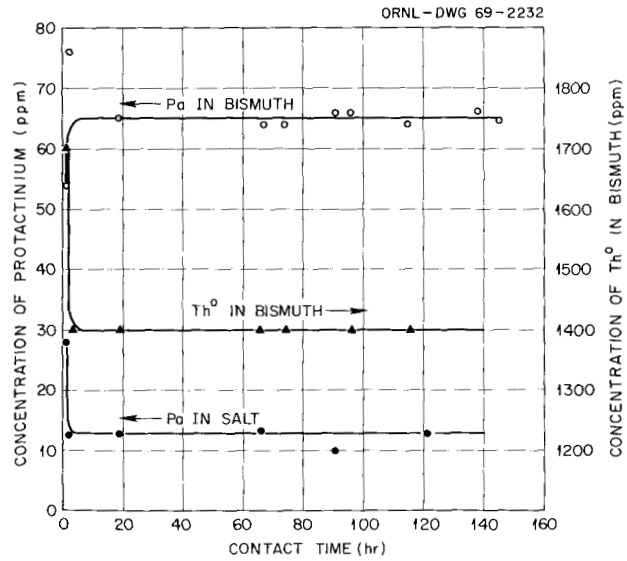

Fig. 3.10. Distribution of Protactinium Between LiF-BeF_2-ThF_4 (72-16-12 Mole %) and Bi-Th alloy.

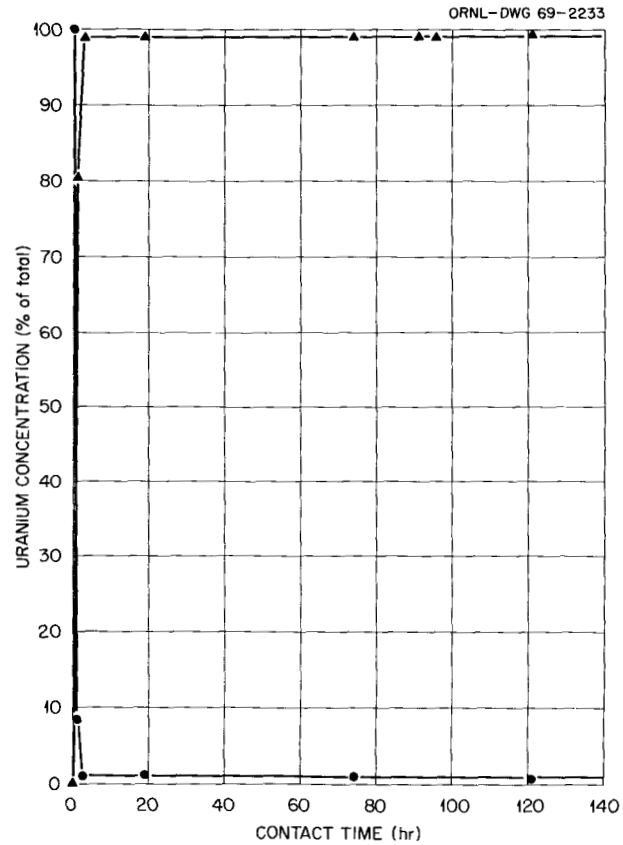

Fig. 3.11. Distribution of Uranium Between LiF-BeF_2-ThF_4 (72-16-12 Mole %) and Bi-Th alloy.

Table 3.6. Distribution Coefficients for Protactinium, Uranium, and Thorium During Incremental Addition of Thorium

Amount of Th^0 Added (g)	Time After Addition (hr)	$D_{Pa} = \frac{X_{Pa(Bi)}}{X_{Pa(salt)}}$	$D_U = \frac{X_{U(Bi)}}{X_{U(salt)}}$	$D_{Th} = \frac{X_{Th(Bi)}}{X_{Th(salt)}}$	$Q_{Th}^{Pa} = \frac{D_{Pa}}{D_{Th}}$	$Q_{Th}^{U} = \frac{D_U}{D_{Th}}$
0.481	2	0.0109	0.522	7.59×10^{-4}	14	690
	23	0.00668	0.701	3.40×10^{-3}	2	210
0.481	25	0.0575	4.34	1.51×10^{-3}	38	2,870
0.481	26	3.20	100	3.41×10^{-3}	940	29,300
0.105	25	9.05	211	7.74×10^{-3}	1170	27,300
0.301	24	19.5	243	1.47×10^{-2}	1250	16.500
0.112	42[a]	7.39	115	1.924×10^{-2}	380	6,000
	49	19.3	475	1.49×10^{-2}	1300	31,900

[a]At 805°C.

slight decrease in the protactinium concentration in bismuth was noticed after helium flowed through the vessel for one day. The argon received a more rigorous purification treatment than the helium used in this experiment, and the latter may have had a trace of an oxidizing impurity.

At the conclusion of the first stage of the experiment, the uranium and protactinium were returned to the salt phase by treating the mixture with gaseous HF diluted with hydrogen, followed by hydrogen alone. Metallic thorium was then added to the system in small increments. The results are given in Table 3.6. The distribution coefficients shown in the last two columns can be compared with the values of $Q_{Th}^{Pa} = 1680$ and $Q_{Th}^{U} = 25{,}800$ (the distribution coefficient of protactinium or uranium divided by that of thorium) obtained during the first stage of the experiment. The temperature was raised to 805°C during the latter part of the experiment to verify our belief that the drop in protactinium and uranium concentration in bismuth that occurred after the bismuth became saturated with thorium was due to coprecipitation of Pa and U with a Bi-Th intermetallic compound. The concentration of protactinium and uranium in the bismuth did increase with increasing temperature, but the concentration in the salt phase increased still more, causing a drop in the distribution coefficient.

We concluded from this experiment that molybdenum is a suitable container material for the reductive extraction of protactinium and uranium from single-fluid fuel compositions. Other investigators in the Chemical Technology Division of ORNL had previously arrived at a similar conclusion.[50] The factor of 20 difference between the distribution coefficients of protactinium and uranium shows that separation of these elements in a reductive extraction system should be easily effected.

[50]L. Ferris *et al.*, *MSR Program Semiann. Progr. Rept. Aug. 31, 1968*, ORNL-4344.

Further Studies of the Reductive Extraction of Protactinium from Single-Fluid MSBR Fuel Salt by Thorium in Molten Bismuth

R. G. Ross C. E. Bamberger C. F. Baes, Jr.

Successful reductive extraction of ^{231}Pa at the 100 ppm level from a single-fluid MSBR fuel composition by thorium in liquid bismuth has been demonstrated by Ferris *et al.*[50] and by Barton *et al.* (above). Additional measurements have since been undertaken by us to help determine accurately the equilibrium quotient for the extraction reaction

$$Pa^{4+}(F) + Th^0(Bi) \rightleftharpoons Pa^0(Bi) + Th^{4+}(F) , \qquad (1)$$

$$Q_{Th}^{Pa} = \frac{X_{Pa^0(Bi)}/X_{Pa^{4+}(F)}}{X_{Th^0(Bi)}/X_{Th^{4+}(F)}} ,$$

and to determine also whether this quotient depends significantly on the concentration of Pa^0 and/or U^0 in the bismuth phase. While the previous studies indicate that reproducible results should be obtained when molybdenum is used as a container material, such data in fact have been difficult to obtain. These additional measurements, therefore, seemed especially desirable in view of the importance of good equilibrium data to the development of a fuel reprocessing method employing reductive extraction.

The present measurements were performed in a molybdenum-lined nickel vessel (Fig. 3.12) equipped

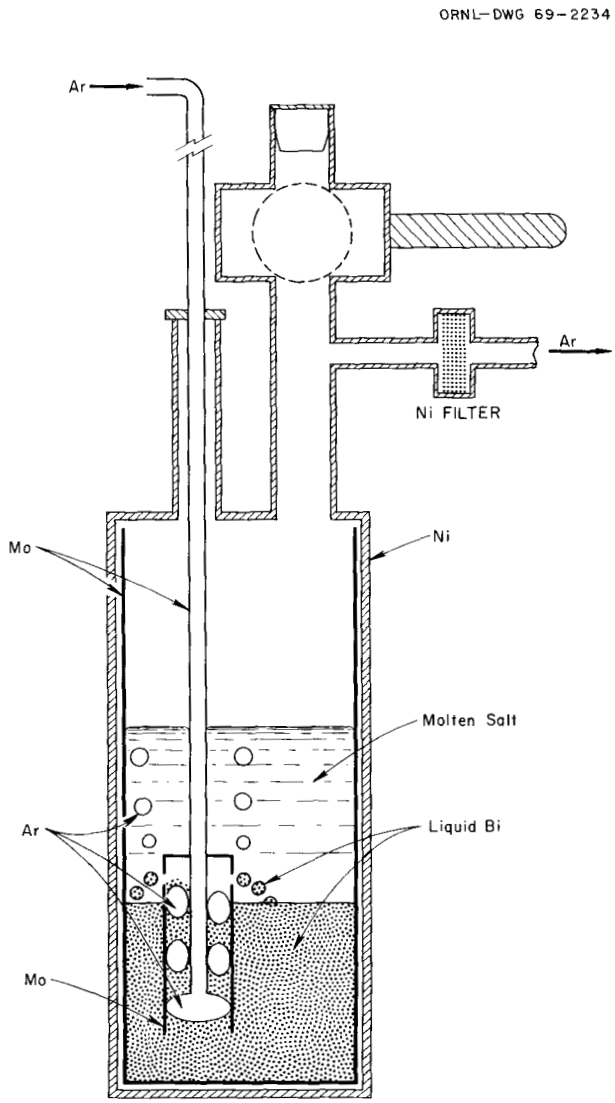

Fig. 3.12. Vessel for Reductive Extraction Experiments.

with a gas lift to provide improved mixing of the phases. (Tests in a silica container revealed that gas sparging alone produces negligible mixing of molten bismuth into the molten fluoride.) To avoid the possibly appreciable amounts of impurities such as water or oxygen which might be introduced by a once-through sparging gas system, a recirculating gas system was used. The circuit included a neoprene diaphragm pump, the gas lift in the extraction vessel, a fritted nickel filter in the gas exit line, an NaF trap (for any trace of HF), and an $Mg(ClO_4)_2$ trap. The experiments were performed at 625°C ± 2 using ~250 g of single-region salt, $LiF\text{-}BeF_2\text{-}ThF_4$ (72-16-12), to which ^{231}Pa and ^{233}Pa were added. This was hydrofluorinated in situ together with 250 g of Bi in the Mo liner. Hydrogen sparging for 4 to 6 hr followed, and then the H_2 was replaced by Ar at 4 to 5 psi before recirculation was started. Crystal bar thorium metal was added as the reducing agent. Stainless steel filter sticks were used for sampling the bismuth phase, and copper filter sticks were used for sampling the salt phase. Molybdenum filter sticks were also fabricated and tested by sampling both phases. These, unlike filter sticks of stainless steel or copper, are fully compatible with both phases. They were mechanically satisfactory, but the proper conditions for reduction of surface oxide by hydrogen have not yet been found.

Thus far, two runs have been made in the absence of uranium; these are compared with some earlier results of Barton in the presence of uranium in Fig. 3.13. Here we have plotted the distribution quotient for Pa,

$$D_{Pa} = X_{Pa^0(Bi)}/X_{Pa^{4+}(F)} ,$$

vs the mole fraction of thorium in the bismuth, determined for Barton's results by analysis and for our results by material balance (with allowance for the consumption of Th^0 by Li and Pa extraction). In the first series of measurements it was found, surprisingly, that quite large amounts of thorium could be added to the bismuth phase – $X_{Th^0(Bi)}$ calculated to reach 0.0014 – with very little Pa extraction, and even this small amount decreased slowly with time. It was surmised that the thorium was consumed by an oxidizing impurity present in relatively large amounts.

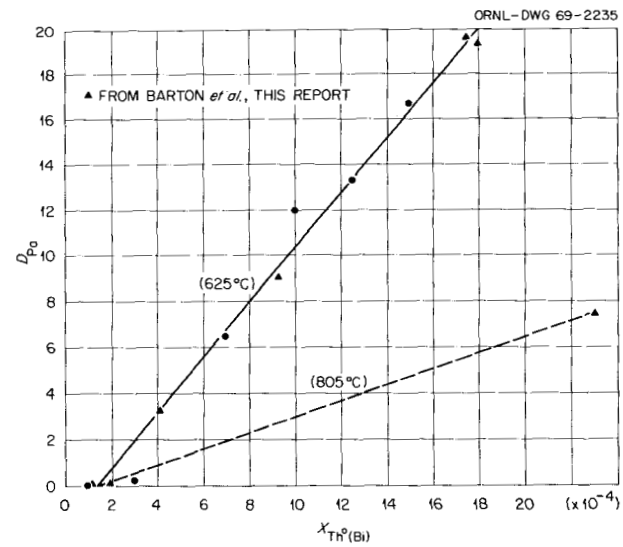

Fig. 3.13. Variation of Protactinium Extraction Coefficient with Mole Fraction of Thorium in the Bismuth Phase.

The contents of the vessel were re-treated with $HF-H_2$ and hydrogen. In a second series of measurements the increasing Pa extraction with successive Th^0 additions clearly indicates that the oxidant had been consumed. We are tempted to speculate that the cause of the difficulty was molybdenum oxide present initially which was fluorinated, but not completely reduced in the initial $HF-H_2$ treatment. At any rate, the points obtained during this series are in satisfying agreement with the results obtained previously by Barton *et al.*, wherein 0.24 mole % UF_4 was present initially in the salt phase.

Interestingly, it appears that in all of these measurements, $\sim 10^{-4}$ mole fraction of thorium was ineffective in extracting Pa. This could have been caused by a small amount of some unknown substance, present in reproducible amounts in the bismuth, which combined with this much thorium, the product remaining in solution. A more likely possibility, we think, is that this effect is caused by ZrF_4 which was present initially in the salt at ~150 ppm. This should have been extracted by the thorium, and then could have been mistaken for thorium in the subsequent colorimetric determinations. It would be included as well in the material balance calculation of the thorium in the bismuth phase.

Assuming that this small and reproducible "blank" may be subtracted from the thorium content of the bismuth, the Pa extraction quotient can be calculated from the slope of the line in Fig. 3.13,

$$Q_{Th}^{Pa} = 1450 \quad (625°C) .$$

One result reported by Barton *et al.* may be used to calculate

$$Q_{Th}^{Pa} = 414 \quad (805°C) .$$

The two results are given within their uncertainty by

$$\log Q_{Th}^{Pa} = 2830/T .$$

This would indicate that ΔS for the extraction reaction (1) is zero, a result which could well be general for such reactions which involve ions of similar size and valence in the salt phase and metals of similar character in the bismuth phase. From the measurements of Barton the value of Q_{Th}^{Pa} is apparently unaffected by the presence of up to 7000 ppm uranium in the bismuth phase.

In our future measurements, the extraction of uranium will be examined as well. Here behavior is complicated by the presence of two valence states in the salt phase at low extraction and by very low uranium levels in the salt phase when an excess of thorium is present. Finally, we wish to study the extraction behavior of Pa and U when they are present at high concentrations (e.g., 1500 ppm each) in the bismuth phase.

Reductive Extraction of Rare Earths from Molten Fluorides into Molten Metals

D. M. Moulton W. Jennings, Jr.
W. P. Teichert W. R. Grimes
W. K. R. Finnell J. H. Shaffer

Present nuclear and engineering studies for the proposed Molten-Salt Breeder Reactor Experiment are directed toward the design and construction of a two-region, single-fluid machine. By this concept the fissile and fertile materials will be combined in a single molten fluoride solvent having the approximate composition $LiF-BeF_2-ThF_4-UF_4$ (71.7-16-12-0.3 mole %). Since these design studies include provisions for chemically reprocessing the reactor fuel on a continuous basis, chemical researches have been concerned with the development of suitable reprocessing schemes for the selective removal of uranium, protactinium, and rare-earth fission products from the fluoride fuel solvent. The reductive extraction process, previously developed for the two-region, two-fluid MSBR,[51] is chemically feasible for removing protactinium and uranium from the single-fluid MSBR and is further described, separately, in this report. Since a three- to five-day process cycle is anticipated for ^{233}Pa and uranium separation, fission product removal, on much longer cycles, will very likely utilize the barren salt effluent stream from this process. Therefore this investigation has been directed toward an evaluation of rare-earth removal from mixtures of LiF, BeF_2, and ThF_4 by reductive extraction into molten metal mixtures.

The chemical feasibility of the reductive extraction method for rare-earth reprocessing schemes in the single-fluid reactor concept will depend, in part, on the magnitude of the distribution coefficients for the rare earths between the two liquid phases and the relative separation of these fission products from major constituents of the salt mixture. If reducing agents are limited to those metals whose cations are constituents of the salt phase, then the distribution of rare earths

[51] D. M. Moulton *et al.*, *Reactor Chem. Div. Ann. Progr. Rept. Dec. 31, 1967*, ORNL-4229, pp. 43–46.

between the two liquid phases at equilibrium can be simply described by equations of type

$$y\mathrm{LnF}_{x(\mathrm{salt})} + x\mathrm{R}^{0}_{(\mathrm{metal})} \rightleftharpoons y\mathrm{Ln}^{0}_{(\mathrm{metal})} + x\mathrm{RF}_{y(\mathrm{salt})}\,, \quad (1)$$

where Ln refers generally to rare-earth fission products; R denotes lithium, beryllium, or thorium; x and y are the respective valences of rare-earth and reductant cations in the salt phase. The thermodynamic activities of the reacting species can be equated to a constant by the relation

$$K = \frac{(a_{\mathrm{Ln}^0})^{y}_{\mathrm{metal}}\,(a_{\mathrm{RF}_y})^{x}_{\mathrm{salt}}}{(a_{\mathrm{LnF}_x})^{y}_{\mathrm{salt}}\,(a_{\mathrm{R}^0})^{x}_{\mathrm{metal}}}\,. \quad (2)$$

If the activity coefficients for the individual species remain constant over concentration ranges of interest, they may be included in the equilibrium constant and related to the chemical concentrations of the reactants by the equation

$$KQ = \frac{(N_{\mathrm{Ln}^0})^{y}_{\mathrm{metal}}\,(N_{\mathrm{R}}F_y)^{x}_{\mathrm{salt}}}{(N_{\mathrm{LnF}_x})^{y}_{\mathrm{salt}}\,(N_{\mathrm{R}^0})^{x}_{\mathrm{metal}}}, \quad (3)$$

where

$$KQ/K = \frac{(\gamma_{\mathrm{LnF}_x})^{y}_{\mathrm{salt}}\,(\gamma_{\mathrm{R}^0})^{x}_{\mathrm{metal}}}{(\gamma_{\mathrm{Ln}^0})^{y}_{\mathrm{metal}}\,(\gamma_{\mathrm{RF}_y})^{x}_{\mathrm{salt}}}\,. \quad (4)$$

In practice, separation factors and distribution coefficients for the reductive extraction process are based on chemical concentrations rather than on thermodynamic activities. Therefore this experimental program has considered methods for optimizing these process parameters by imposing changes in the activity coefficients of the chemical species in the two liquid phases. One part of this program has examined the effects of salt composition on the extraction of cerium into bismuth, and the comparative extractabilities of some important rare-earth fission products also into bismuth. A second phase of this program has considered various metals and metal mixtures as alternate choices for the molten metal extractant phase.

Effects of Salt Composition on the Reductive Extraction of Cerium from LiF-BeF$_2$-ThF$_4$ Mixtures into Bismuth. – In the reductive extraction system, where bismuth is used as the metal-phase extractant, the distribution of rare earths between the two liquid phases will be in equilibrium with realistic quantities of lithium and thorium according to Eq. (1). Beryllium does not form intermetallic compounds with bismuth and is essentially insoluble in molten bismuth at temperatures of interest to this program. Thus the chemical feasibility of this reductive extraction system will depend on the separability of rare-earth fission products from lithium and thorium. In addition, the degree to which rare earths can be extracted per equilibrium stage will be limited to a relatively low reduction potential corresponding to the solubility of thorium in the bismuth pool.

The fuel solvent for the single-fluid MSBR will be selected from the ternary system LiF-BeF$_2$-ThF$_4$, with probable concentrations of 10 to 12 mole % for thorium, 16 to 20 mole % for beryllium, and the balance of lithium fluoride. Within these restraints, however, activity coefficients for the individual salt constituents may be quite varied owing to the formation of coordinated species, BeF_4^{2-} and ThF_7^{3-}, in the fluoride melt. Therefore this phase of the experimental program has examined the extraction of cerium from various compositions of the ternary salt mixtures into bismuth under otherwise similar conditions.

The two liquid phases of each experiment were contained in an extraction vessel of 4-in. IPS stainless steel pipe about 14 in. long, with welded end closures of ¼-in. stainless steel plate. The top plate was penetrated in two places by ¾-in. steel pipe which extended to within ½ in. of the bottom plate. These ports were used separately for adding metal reducing agents (lithium or thorium) directly into the bismuth and for withdrawing samples of bismuth without contacting the salt phase. A third ¾-in. pipe just penetrated the top plate and was used for loading materials into the vessel and for withdrawing samples of the salt phase. Two additional small-diameter penetrations of the top plate were used for a thermowell and for inserting a reference electrode of beryllium into the salt phase. The extraction vessel was further provided with either a mild steel or graphite liner for primary containment of the liquid phases. Each experiment contained 3 kg of bismuth and 2 to 3 kg of salt solvent with 100 ppm of Ce and 5 mc of ^{144}Ce activity.

The experimental procedure was directed primarily toward the evaluation of equilibrium data according to Eq. (3). Values for the equilibrium quotients were derived from radiochemical analyses of samples taken from the salt and metal phases for cerium and from spectrochemical analyses of the metal-phase samples for lithium and thorium. Changes in the reduction potential were made by adding lithium or thorium in small tared increments and measured between the beryllium electrode and the extraction vessel.

Equilibrium quotients obtained for the various salt mixtures at 600°C are shown in Table 3.7. Distribution coefficients for lithium, thorium, and cerium and their separation factors when the bismuth pool was saturated with thorium[52] are shown in Table 3.8.

Although quantitative estimates of the formation of BeF_4^{2-} and ThF_7^{3-} ions are not available, the equilibrium quotients for the reduction of cerium by thorium could be fitted to an empirical model which assumed complete coordination of the two cation species.[53] This reference scale was defined as an excess or deficit in the "free fluoride" content of the salt mixture according to the equation

$$\text{excess free fluoride} = \text{mole \% LiF} - 2(\text{mole \% } BeF_2) - 3(\text{mole \% } ThF_4) .$$

Table 3.7. Equilibrium Quotients for the Reduction of Cerium, Lithium, and Thorium from $LiF\text{-}BeF_2\text{-}ThF_4$ Mixtures into Bismuth at 600°C

Salt Composition (mole %)			K_1[a]	K_2	K_3
LiF	BeF_2	ThF_4			
				$\times 10^{-8}$	$\times 10^{-10}$
72	16	12	3.81	14.9	15.9
65	23	12	0.13	2.67	0.43
64	30	6	0.80	1.14	0.29
70	21	9	1.92	3.94	2.14
68	20	12	0.62	5.73	2.61
75	16	9	14.04	20.7	37.6
74	20	6	46.67	7.21	14.0

[a] $K_1 = D^4_{Ce}/D^3_{Th}$, $K_2 = D^3_{Li}/D_{Ce}$, $K_3 = D^4_{Li}/D_{Th}$, where $D = N_{metal}/N_{salt}$.

Relations of this "free fluoride" model to the behavior of cerium and thorium are illustrated in Fig. 3.14 for the reaction equilibrium constants and in Fig. 3.15 for the separation of cerium from thorium. Data obtained for the behavior of lithium could not be correlated to the "free fluoride" model and suggest further complexities in the extraction system.

The Effect of Metal-Phase Composition on Rare-Earth Extraction. – The experiments on varying the salt composition have shown that this does not produce too great an improvement in the problem of extracting rare earths but not thorium from $LiF\text{-}BeF_2\text{-}ThF_4$ mixtures. Therefore an extensive program on varying the metal phase has been begun. Normally rare earths are about 0.25 v more difficult to reduce than thorium. The use of bismuth has reduced this potential difference to almost zero since the intermetallics formed by rare earths are stronger than those formed by bismuth. If a solvent or an additive to bismuth which strengthens the rare-earth compounds even a little more can be found, it will make the extraction process much more attractive.

The lanthanide-bismuth compounds are rather ionic in nature, with bismuth behaving somewhat like a Bi^{3-} anion. One approach therefore is to try to find an element which will be even more nonmetallic. This is supported by some very limited experience suggesting that lead is a poorer extractant than bismuth. Therefore 20.6 mole % of antimony was added to the bismuth in

[52] J. S. Bryner and M. B. Brodsky, *Proc. 2nd Intern. Conf. Peaceful Uses At. Energy* 7, 209 (1958).

[53] M. A. Bredig, memo to W. R. Grimes, MSR 68-75 (Apr. 26, 1968).

Table 3.8. Reductive Extraction of Cerium, Lithium, and Thorium from $LiF\text{-}BeF_2\text{-}ThF_4$ Mixtures into Bismuth at 600°C

Salt Composition (mole %)			Distribution Coefficients			Separation Factors		
LiF	BeF_2	ThF_4	D_{Ce}[a]	D_{Li}[a]	D_{Th}[b]	D_{Ce}/D_{Th}	D_{Ce}/D_{Li}	D_{Th}/D_{Li}
72	16	12	0.077	0.0024	0.021	3.67	32.1	8.75
65	23	12	0.033	0.00098	0.021	1.57	33.7	21.4
64	30	6	0.088	0.00105	0.042	2.10	83.8	40.0
70	21	9	0.081	0.00161	0.028	2.89	50.3	17.4
68	20	12	0.049	0.00153	0.021	2.33	32.0	13.7
75	16	9	0.133	0.0032	0.028	4.75	41.6	8.75
74	20	6	0.243	0.0028	0.042	5.79	86.8	15.0

[a] Based on Eq. (1) and KQ given in Table 3.7.

[b] Based on thorium solubility in bismuth by J. S. Bryner and M. B. Brodsky, *Proc. 2nd Intern. Conf. Peaceful Uses At. Energy* 7, 209 (1958).

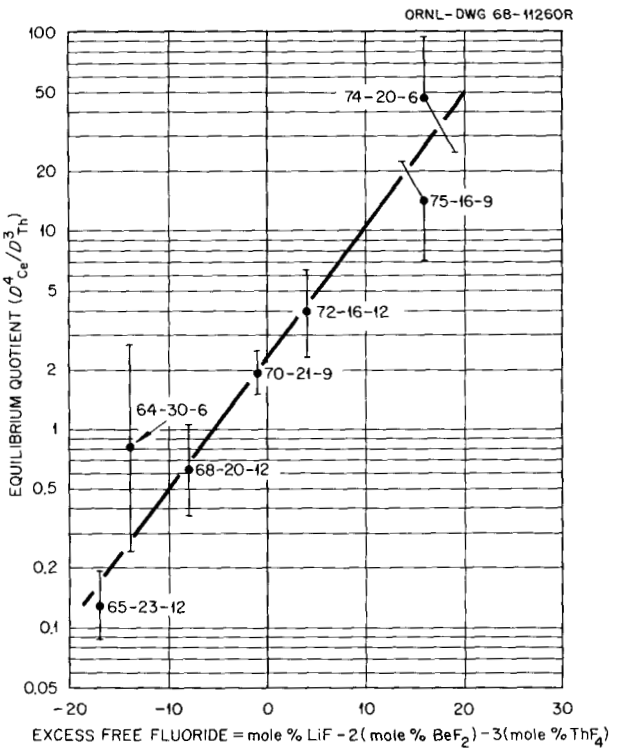

Fig. 3.14. Effect of Salt Composition on the Equilibrium Reduction of Cerium by Thorium from LiF-BeF_2-ThF_4 Mixtures into Bismuth at 600°C.

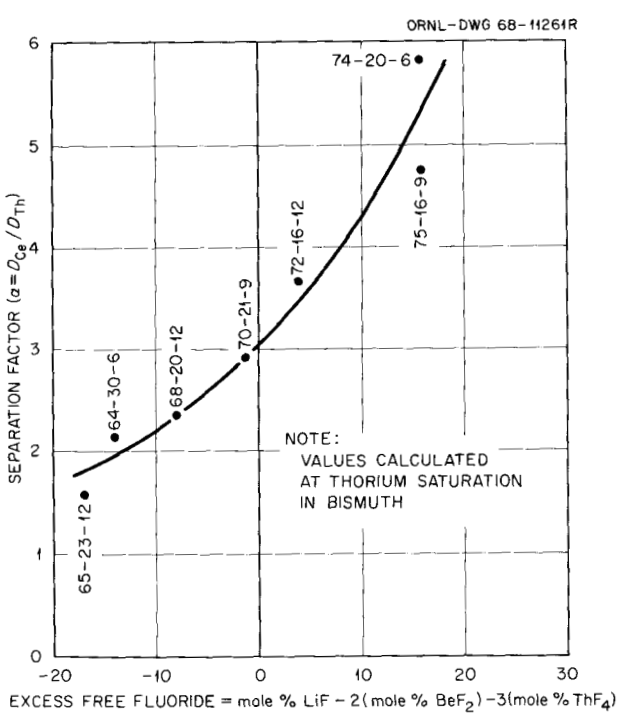

Fig. 3.15. Effect of Salt Composition on the Separation of Cerium from Thorium During Reductive Extraction of Cerium from LiF-BeF_2-ThF_4 Mixtures into Bismuth at 600°C.

two experiments. In the first we attempted to reduce europium from LiF-BeF_2-ThF_4 (72-16-12 mole %) at 600° with thorium metal. No detectable amount of europium was removed, but analyses of the lithium and thorium content of the metal and of a beryllium electrode potential showed $\mathcal{E}_{0Li} - \mathcal{E}_{0Be} = 0.00$ v and $\mathcal{E}_{0Be} - \mathcal{E}_{0Th} = -0.42$ to -0.44 v. With this salt and pure bismuth the differences are -0.11 and -0.28 v, so that both metals have become easier to reduce, but unfortunately the change was greater for thorium. The plateau of potential suggests thorium saturation at 0.22 at. %. In the second experiment with antimony, LiF-BeF_2-ThF_4 (65-23-12 mole %) containing cerium was used as the salt. Here there was appreciable extraction of cerium, but it was less than half that obtained between this salt and pure bismuth. The thorium content was higher, reaching saturation at 0.6 at. % at 600° and not reaching it at 0.75 at. % at 700°. This is probably a better measure of saturation than that obtained in the europium experiment, where the data had to be extrapolated. The lithium and thorium analyses showed too much scatter to permit comparison of the potential differences with the earlier experiment. In both cases the greatest increase in intermetallic compound strength upon adding antimony seemed to be with thorium, which is just the opposite of the desired effect. Therefore no further studies were made of this system.

A second type of strong intermetallic bond is formed between transition metals with nearly full and nearly empty *d* orbitals. Such compounds exist as solids, but the bonding might persist to a certain extent in solution. An attempt at utilizing this sort of behavior was made by adding 3% gold to bismuth in the extraction of neodymium from an LiF-BeF_2-ThF_4 (68-20-12 mole %) salt at 600 and 700°. The measured potential differences are shown in Table 3.9.

The lithium and thorium data are not very good, but it seems that the thorium is now relatively less easy to reduce; this is what we wanted. The thorium distribution at saturation at 600° was 0.037, corresponding to a neodymium distribution of 0.05 and a separation factor of 1.33. Thorium saturation was apparently not reached at 700°, but a D_{Nd} of 0.104 was attained. The distribution of neodymium between this salt and pure bismuth is not yet known. However, an experiment using LiF-BeF_2-ThF_4 (72-16-12 mole %) indicated that the maximum D_{Nd} is 0.050 at 600° and 0.132 at 700°. This latter is a more favorable salt for rare-earth extraction. If

$$D_{Nd}\,(\text{salt B})/D_{Nd}\,(\text{salt A}) = D_{Ce}\,(\text{salt B})/D_{Ce}\,(\text{salt A})\,,$$

Table 3.9. Extraction Potential Differences Between $LiF-BeF_2-ThF_4$ (68-20-12 mole %) and Bi-Au (97-3 mole %)

T	$\mathcal{E}'_{0Li} - \mathcal{E}'_{0Th}$	$\mathcal{E}'_{0Li} - \mathcal{E}'_{0Nd}$	$\mathcal{E}'_{0Nd} - \mathcal{E}'_{0Th}$
600°	−0.334 ± 0.42	−0.323 ± 0.040	−0.014 ± 0.007
700°	−0.372 ± 0.037	−0.331 ± 0.058	−0.015 ± 0.009

then in the 72-16-12 salt we would expect D_{Nd} with the bismuth-gold system to be 0.079 at 600° and at least 0.163 at 700°.

The antimony and gold additions have been attempts to lower rare-earth activity without affecting the thorium too much, thereby improving the rare-earth–thorium separation. Now the maximum rare-earth distribution, which is rather low, is set by the solubility of the thorium intermetallic. An alternative approach to the reprocessing problem is to increase the thorium solubility and thus the rare-earth distribution without worrying about the separation of the two metals. There seem to be only two metals which will dissolve an appreciable amount of thorium: these are aluminum and magnesium, dissolving, respectively, about 4 and 9 at. % at 700°. Disregarding the practical problems in handling these liquid metals, we have begun a study of them as solvents. The results to date are fragmentary, but two properties are indicated. Aluminum alloys with Au, Ag, and Cu do not seem to reduce Be from the 68-20-12% salt, and they can be made to extract cerium to a level (per weight of solvent) at least as high and probably higher than bismuth. These experiments have been performed with the metal contained in a small graphite dipper inserted into a large vessel of salt and connected electrically to a metallic beryllium anode. Such a system allows rapid trials of different metal systems, but it is not easy to tell when thorium saturation occurs. With aluminum alloys the rather low density means that salt-metal separation may not be very good, so that some of the measured cerium may be included salt. Nevertheless these systems remain the object of active study and interest because of the promising preliminary results.

The Behavior of Metals with Two Oxidation States upon Reduction from Molten Salts into Liquid Metals

D. M. Moulton

In the reductive extraction process for removing actinides and lanthanides from the salt streams of molten-salt reactors, there occur metals with more than one stable oxidation state, such as samarium, europium, and uranium. Under the strongly reducing conditions which prevail, one must also consider the possibility that these or other metals might form less stable lower oxidation states not found under ordinary circumstances.

The behavior in these systems of elements with two oxidation states of any relative stability can be described in a formal way. Consider a metal M with oxidation states $+m$ and $+n$ such that $m > n$. We can write standard half-cell potentials $\mathcal{E}_{0m}$ and $\mathcal{E}_{0n}$ for the reduction of each of these. The definition of the standard extraction potential $\mathcal{E}'_{0n}$ is

$$\mathcal{E}'_{0n} = \mathcal{E}_{0n} - \frac{RT}{nF} \ln \gamma_0/\gamma_n ,$$

where γ_0 and γ_n are the metal- and salt-phase activity coefficients. We can obtain $\mathcal{E}_{0R}$, the standard potential for the reduction of M^{m+} to M^{n+}, as

$$\mathcal{E}_{0R} = \frac{m\mathcal{E}_{0m} - n\mathcal{E}_{0n}}{m - n} .$$

The value of $\mathcal{E}_{0R}$ is unchanged by substituting $\mathcal{E}'_{0m}$, $\mathcal{E}'_{0n}$ into this expression, so that $\mathcal{E}_{0R}$ is unaffected by the metal phase. What does happen when a metal phase is present is that $\mathcal{E}_{0m}$ and $\mathcal{E}_{0n}$ both decrease in magnitude and approach $\mathcal{E}_{0R}$ for very small γ_0, which is the case for all of the elements of interest here. At the point where $\mathcal{E}_{0R} = \mathcal{E}'_{0m} = \mathcal{E}'_{0n}$ the disproportionation equilibrium constant has risen to unity because of the stabilization of one of the disproportionation products by the metal phase. Even before this point is reached the state M^{m+} becomes more favored relative to M^{n+} since the difference $\mathcal{E}_0 - \mathcal{E}'_0$ is less for m than for n.

The magnitude of this effect may be demonstrated as follows. At any point in the reduction we can write the equilibrium condition

$$\mathcal{E}'_{0n} - \frac{RT}{nF} \ln \frac{X_0}{X_n} = \mathcal{E}_{0R} - \frac{RT}{(m-n)F} \ln \frac{X_n}{X_m} ,$$

where X_0, X_n, X_m are mole fractions of M^0, M^{n+}, M^{m+}.

In most experiments the measured distribution of M is

$$D = \frac{X_0}{X_m + X_n},$$

because the measurement cannot distinguish between M^{m+} and M^{n+}. The observed valence n^* of M is found by

$$n^* = \frac{d \log D}{d \log D_{Li}}$$

or by a similar expression using the distribution of another metal or an electrode potential; n^* is just a weighted average valence:

$$n^* = n \cdot \frac{X_n}{X_n + X_m} + m \cdot \frac{X_m}{X_n + X_m}.$$

A relationship between n^* and D can be found: letting $n + 1 = m$ for convenience,

$$D = \frac{(m - n^*)^m}{(n^* - n)^n} \cdot \frac{1}{\gamma_0} \cdot \frac{\gamma_n{}^m}{\gamma_m{}^n} \cdot \exp\frac{nF}{RT}(\mathcal{E}_{0n} - \mathcal{E}_{0R}). \quad (1)$$

At a given salt composition the ratio $\gamma_n{}^m/\gamma_m{}^n$ is constant. Now an increase in the strength of the intermetallic, that is, a decrease in γ_0, means that D will be larger for a given n^*. The valence n^* will go from m to n during a reduction, but in the experimentally observable region (roughly, $10^{-2} \leqslant D \leqslant 10^2$) it may be in any portion of that range, depending on γ_0. At $\gamma_0 \approx 1$, D will be rather small until n^* is nearly equal to n. For a very small γ_0, n^* may not depart from m until nearly all of the extraction has been completed. Thus M may appear to have the valence $+n$, $+m$, or even sometimes a changing intermediate value.

It can be shown that the maximum fraction of the total M which can exist as M^{n+} will be given by

$$a = \frac{nP\gamma_0{}^{1/m}}{m + nP\gamma_0{}^{1/m}},$$

with

$$P = n^{-1/m} \exp\frac{nRT}{mF}(\mathcal{E}_{0R} - \mathcal{E}_{0n}),$$

where it is assumed that the total numbers of moles in the metal and salt phases are equal. For γ_0 not too small, M^{m+} will be completely reduced to M^{n+} before there is any extraction into the metal, but at very small γ this will no longer be the case, and M^{n+} will partially or even almost fully disproportionate.

Figure 3.16 is a plot of expression (1), using Baes' data[54] on uranium in $LiF\text{-}BeF_2$ (66.7-33.3 mole %) at 600°. The various values of γ_0 are equivalent to extracting uranium into different metals forming increasingly strong intermetallic compounds. Several authors have found γ_0 for U in Bi to be around 1×10^{-4}, so it would seem that the experimental n^* should range from about 3.4 to 3.05. If an n^* larger than this is found, it requires a smaller γ_0 and therefore a lower $\mathcal{E}_0'$ for uranium than the -1.26 for U^{3+} that these data predict (or -1.23 for U^{4+}).

[54] C. F. Baes, Jr., *Reactor Chem. Div. Ann. Progr. Rept. Dec. 31, 1965*, ORNL-3913, p. 21.

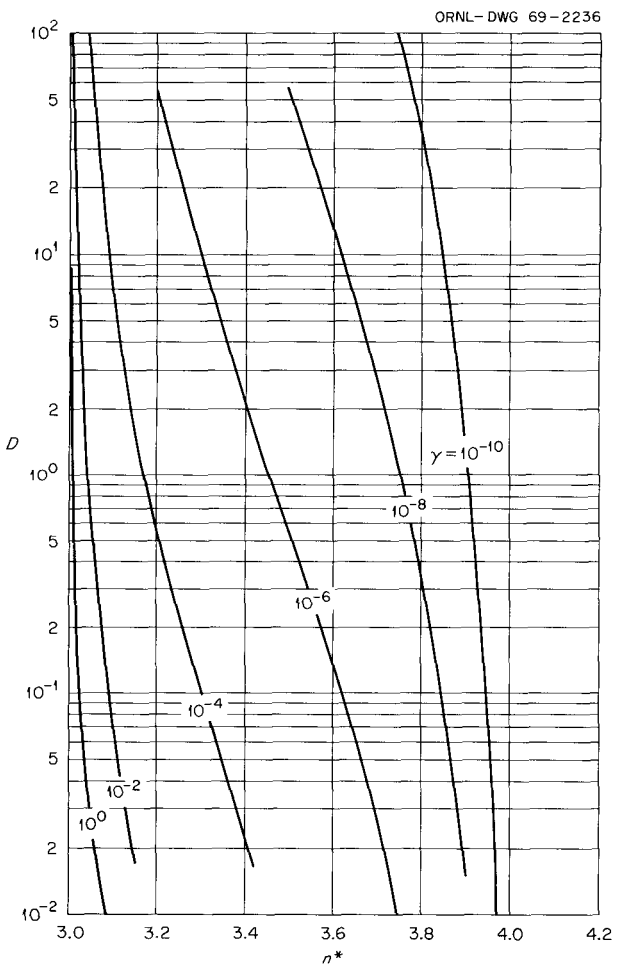

Fig. 3.16. The Effective Valence of Uranium Ion as a Function of the Experimental Distribution for Different Values of the Metal-Phase Activity Coefficient.

For the rare earths γ_0 in Bi is much smaller, of the order of 10^{-15}. If we consider reduction from the M^{3+} state to the M^{2+} state, it turns out that in order for the M^{2+} state to appear to any significant extent the value of $-(\mathcal{E}_{0n} - \mathcal{E}_{0m})$ must be at least about 0.2 v, while for the metal to be reduced completely to this lower state the potential difference must be at least 0.55 v. For Sm and Eu the valence seems to be no higher than 2, and a crude estimate from the aqueous systems is that $\mathcal{E}_{0n} - \mathcal{E}_{0m}$ is about 0.7 v or 16 kcal per fluoride. For the other rare earths the M^{2+} state would have to be about 5 kcal per fluoride more stable than M^{3+}. It is not likely that such states exist and have not yet been discovered. Therefore the fractionally low valence states which have sometimes been reported for rare earths must be actually due to some other phenomenon if they are in fact real at all.

Returning to uranium we can consider the salt activity coefficient ratio in expression (1). Using Baes' data,[54] we find that this ratio in $LiF\text{-}BeF_2$ is 1.12 at 31% BeF_2 and 0.48 at 39% BeF_2, if we assume with him that $\gamma_{U^{3+}} \approx \gamma_{Ce^{3+}}$. These compositions correspond to free fluoride values (ff = % Li − 2 × % Be) of +7 and −17 respectively. Such a variation is about as large as one might expect in $LiF\text{-}BeF_2\text{-}ThF_4$ mixtures suitable for the molten-salt breeder reactor. Now in these extreme cases n^* at $D = 1$ will go from 3.17 to 3.18 for ff = 7 and 3.14 at ff = −17. These are not insignificant changes (for example, a goes from 64 to 61 or 79%), but they do not affect the general conclusion that if a constant integral value must be chosen for uranium it should be 3 rather than 4.

Separation of Cerium from Thorium in Bismuth by Cold-Zone Deposition of Thorium Bismuthide

D. M. Richardson W. R. Grimes
W. K. R. Finnell J. H. Shaffer

In experiments conducted thus far on the reductive extraction of rare earths from $LiF\text{-}BeF_2\text{-}ThF_4$ mixtures into bismuth, separation factors (D_{Ln}/D_{Th}) of less than 10 have been found under equilibrium conditions and at temperatures from 500 to 800°C. Although these values may be sufficient for reprocessing the MSBR fuel solvent by the reductive extraction process, much higher values could greatly improve the plant efficiency. Accordingly, various parameters of the extraction process principle are being investigated to improve its application to the reprocessing requirements of the MSBR. To this end, an experiment is now in progress to examine the cold-zone deposition of thorium from bismuth which also contains a dissolved rare earth. The chemical feasibility of this application will depend on the precipitation of pure $ThBi_2$ rather than a coprecipitation with the metallic rare earth. The crystal structure of $ThBi_2$ is reported as tetragonal, while those of Bi(Ln) are all face-centered cubic. However, the structure of compounds Bi_3Ln_4, which are the probable high-temperature forms of trivalent rare-earth bismuthides, is not known. The experimental procedure embodies the extraction of cerium from a simulated MSBR fuel solvent at 700°C into flowing bismuth and its back-extraction by hydrofluorination into a recovery salt mixture. The recirculating bismuth stream will be contacted with solid thorium bismuthide at 700°C to achieve its saturation with thorium. The exit stream from the extraction vessel will pass through a cold trap (outlet temperature of about 400°C) before flowing to the recovery vessel. Thus the comparative transport of cerium and thorium to the recovery salt will indicate the effectiveness of the cold-zone deposition application. At the conclusion of the experiment the cold trap will be drained of bismuth and sacrificed for analyses of its cerium content and possibly the composition of the precipitating phase.

The objectives of this experiment have resulted in the construction of a simple pump loop which utilizes an electromagnetic device to achieve low flow rates of bismuth. The hot trap and cold trap are of identical construction and depend upon tightly packed stainless steel demister material (Yorkmesh) for the retention of solids. Each trap is equipped with Calrod heaters and will be cooled by a countercurrent flow of an external air-water stream. The extraction and recovery vessels were fabricated from 4-in. IPS 304L stainless steel pipe and are fitted with graphite cylinders of $^1/_8$-in. wall thickness for primary containment of the salt mixtures. Bottom penetrations provide for the circulation of bismuth through each vessel, while top penetrations provide for loading and sampling procedures.

The experimental assembly contains approximately 35 kg of bismuth, which provides an approximate depth of 1 in. of bismuth in each vessel. The fuel solvent mixture will be simulated by approximately 2 kg of $LiF\text{-}BeF_2\text{-}ThF_4$ (68-20-12 mole %) which contains 100 ppm cerium and about 5 mc of ^{144}Ce activity.

Since the transport of realistic fractions of cerium from the extractor is an objective of the experiment, an a priori evaluation of thorium inventory requirements of the bismuth system was necessary. The material balance of cerium in the extraction vessel at any time can be expressed as

$$X = y(1 + S/BD) = Ay ,$$

where X = total moles of Ce in vessel, y = moles of Ce in B moles of Bi in the vessel, S = the moles of salt, and D = the distribution coefficient of cerium between the two liquid phases. Since the thorium concentration in bismuth, N, should remain constant within the extractor under test conditions, the rate of cerium removal from the extractor can be expressed as a function of the moles of thorium, T, passing through the extractor. If the recovery of cerium from the bismuth by hydrofluorination is complete, the transport process at the extractor can be expressed as

$$\frac{dX}{dT} = -\frac{y}{BN} = -\frac{X}{ABN}.$$

The application of the integrated form of this equation for the experimental conditions is shown as Fig. 3.17. Because of these relatively large requirements, thorium will be introduced into the bismuth system by reduction from $LiF\text{-}BeF_2\text{-}ThF_4$ (68-20-12 mole %) by added beryllium metal in the recovery section of the apparatus. When thorium reduction is complete, the recovery salt will have a composition of approximately 60 mole % LiF and 40 mole % BeF_2 and a liquidus temperature of about 450°C.

Experimental progress thus far has included the circulation of bismuth in the system with the EM pump

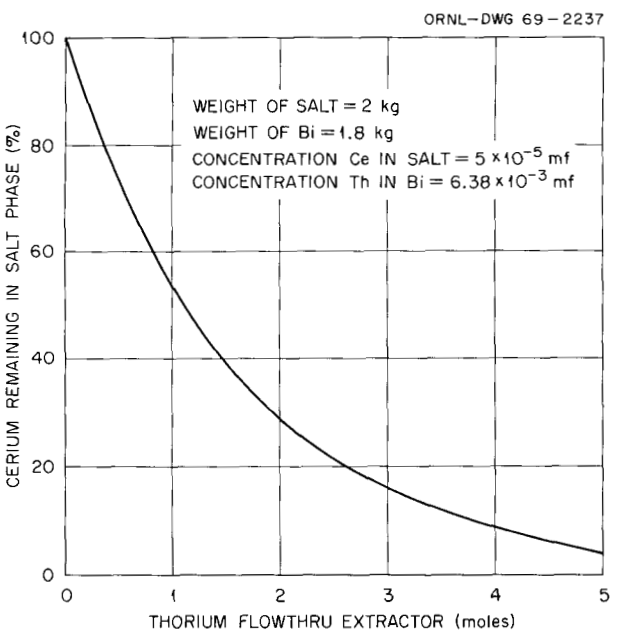

Fig. 3.17. Anticipated Rate of Cerium Removal from $LiF\text{-}BeF_2\text{-}ThF_4$ (68-20-12 Mole %) into Flowing Bismuth Saturated with Thorium at 700°C.

at rates of about 50 to 200 cm^3/min, the addition of the recovery salt mixture, and hydrofluorination of the recovery salt while recirculating bismuth to remove oxides from the metal phase. Beryllium metal is currently being added to the recovery salt mixture incrementally to achieve thorium reduction. Upon achievement of near-complete removal of thorium from the recovery salt and its collection in the appropriate trap, the fuel solvent mixture will be loaded into the extraction vessel. The progress of the experiment will be monitored from radiochemical analyses of samples taken periodically from each salt phase and at four locations in the metal phase system. The results of chemical and spectrographic analyses of these samples for thorium, lithium, and beryllium will provide further description of the experimental results.

Zone Melting of Fluoride Salts

E. L. Compere Terry Dorsett[55]

Zone melting[56] tests have been conducted on an $LiF\text{-}BeF_2\text{-}ThF_4$ mixture (72-16-12 mole %) to determine the separation of constituents under several conditions. In some tests the salt contained added cerium trifluoride at a concentration of 0.3 mole %, somewhat below its solubility limit in the melt. Since the solubility limit was exceeded after the melt was partially solidified, the experiments provide insight into phase behavior of this salt, but for the same reason these experiments do not provide a test of zone refining itself. Experiments at tenfold lower CeF_3 concentration were conducted to accomplish this.

Nickel tubes, 0.305 in. ID × 12 in. long, were filled with powdered salt and capped. After the melting cycles were completed, successive 1-in. sections were submitted for chemical analysis. Experiments described below typify the data obtained.

Composition of all tests remained within the phase field characterized by $3LiF \cdot ThF_4$ and $2LiF \cdot BeF_2$. The gradation in composition along the tube was fairly regular in all tests, the largest proportionate changes occurring for Be and Th. The greatest observed concentration extremes were $LiF\text{-}BeF_2\text{-}ThF_4\text{-}CeF_3$ (73.0-10.3-16.3-0.38 mole %) and (69.1-22.8-7.8-0.22) obtained with four nominally horizontal passes of a

[55] ORAU student participant, summer 1968 (present address, Maryville College, Maryville, Tenn.).

[56] A. J. Singh, R. G. Ross, and R. E. Thoma, *Zone Melting of Inorganic Fluorides*, ORNL-3658 (July 1965).

three-zone heater at 1.5 cm/hr. Salt in a duplicate tube was slowly melted and frozen 12 times in succession while the tube was mounted vertically in a furnace. Composition patterns were similar to those described above, the bottom sample having a composition LiF-BeF_2-ThF_4-CeF_3 (73.2-11.7-14.0-0.32 mole %) and the top (69.2-21.9-8.7-0.26 mole %).

Examination of recently available tie-line data of Thoma[57] and of CeF_3 solubility studies[58] permit explanation of these results. Soon after precipitation begins from the original melt, at about 490°C, two solid phases occur, one a $3LiF \cdot ThF_4$-based solid solution of composition LiF-BeF_2-ThF_4 about 69-7-24 mole %, the other solid phase being LiF. These are in equilibrium with a liquid phase which tends toward 67-28-5 mole %. In this melt phase CeF_3 solubility at 457°C (near the solidus temperature) is estimated by extrapolation to be 0.18 mole %. Thus the combination of lowered temperature and altered melt composition during solidification resulted in a diminished rare-earth solubility in the melt. The limit probably characterizes any melt-solidification process for this salt.

The separation by direct heating and cooling doubtless occurred because the solidifying phases were richer in thorium and thus more dense, and during freezing or melting the denser phase settled to the bottom.

A mixture of LiF-BeF_2-ThF_4 (71.2-16.3-12.5 mole %) was prepared containing ~0.03 mole % CeF_3. Analysis of cerium at this concentration level is regarded as reliable. The mixture was placed in three nickel tubes. One tube was given four horizontal passes (carefully leveled) of the three-zone heater; slightly higher concentrations of thorium and cerium appeared in the end fractions than in the center sections (14.0–14.5 vs 10.5 mole % Th, 0.044–0.028 vs 0.023–0.024 mole % Ce). A second tube was given a single upward pass of the three-zone heater; resultant tube bulging prevented more passes. Thorium concentrations ranged between 14.6 and 11.0 mole %, being slightly higher in both end fractions, and cerium concentrations between 0.020 and 0.026 mole % were found, with no evident trend. The third tube was slowly melted and frozen in a vertical position 12 times. The bottom section had a composition (LiF-BeF_2-ThF_4-CeF_3) of 73.2-9.4-17.4-0.028 mole %, while the top section had a composition of 70.5-24.6-4.9-0.016 mole %.

These data lead to the following view. The dominant effect in this system is the crystallization first of high-density phases, which settle to the bottom of the container. These fractions contain higher concentrations of thorium than those crystallizing later, in agreement with existing tie-line data. Cerium appears to accompany thorium to some extent even when its solubility is not exceeded, and it does not appear to be concentrated in the melt during crystallization or zone-melting processes.

Removal of Thorium from Single-Fluid Fuel Compositions by Fractional Crystallization

C. J. Barton

Another section of this chapter[59] gives results showing that it is difficult to separate rare-earth elements from single-fluid fuel compositions containing a high concentration of ThF_4. This problem would be alleviated if a simple process for removing a major fraction of the ThF_4 were available that would leave the rare earths in solution. Results of an effort toward effecting such a reduction in ThF_4 concentration by fractional crystallization are reported here.

Inspection of the LiF-BeF_2-ThF_4 phase diagram[60] showed that the composition LiF-BeF_2-ThF_4 (58-30-12 mole %), a possible single-fluid fuel composition, should be amenable to fractional crystallization because it is in the $LiF \cdot 2ThF_4$ primary phase field. The solubility of CeF_3 in this mixture, reported elsewhere in this document,[58] is 1.1 mole % at 600°C.

A mixture of about 450 g of this composition was prepared by adding ThF_4 to the previously purified mixture LiF-BeF_2 (66-34 mole %). Enough CeF_3 was added to give a concentration of 100 ppm, and about 0.5 mc of ^{144}Ce was introduced to permit radiochemical analysis for this element. The melt was treated at 650° with a gaseous HF-H_2 mixture to remove hydrolysis products and then with H_2 to reduce NiF_2 and any other easily reducible species present.

Two filtered samples were removed from the purified melt at 720°C to give representative samples that would permit a determination of the specific activity of the dissolved CeF_3. The melt was cooled to temperatures below the liquidus (595°C), held there for 30 to 45 min, and then filtered samples were removed for analysis. This procedure was later repeated, starting at

[57] R. E. Thoma, *Crystallization Reactions in the System LiF-BeF_2-ThF_4*, ORNL-TM report in preparation.

[58] L. O. Gilpatrick, J. Fredrickson, and C. J. Barton, "Solubility of CeF_3 in Molten Mixtures of LiF, BeF_2 and ThF_4," this report, chap. 2; see also the following section.

[59] D. M. Moulton *et al.*, "Reductive Extraction of Rare Earths from Molten Fluorides into Molten Metals," this chapter.

[60] R. E. Thoma *et al.*, *J. Phys. Chem.* **64**, 865 (1960).

640°C rather than 720°C. Table 3.10 gives the results obtained. It seems evident that the first ThF_4 phase that crystallizes does not remove CeF_3 from solution, but at a temperature between 517 and 490°C precipitation of CeF_3 begins. The phase diagram gives a clue as to the cause of the loss of CeF_3 in this temperature range. Secondary phase separation occurs at a composition very close to that of the filtrate obtained at 530°C. The phase diagram indicates that this separation takes place at a temperature of about 445°C. The data now available indicate that CeF_3 precipitation occurs in conjunction with the crystallization of the $3LiF \cdot ThF_4$ compound. The reason for the apparent discrepancy in the temperature of crystallization of the $3LiF \cdot ThF_4$ phase is not clear at present. The results in Table 3.10 indicate, however, that a large fraction of the ThF_4 content of this composition can be removed by fractional crystallization and filtration without significant removal of rare earths.

Data reported by Compere and Dorsett in the previous section are pertinent to this problem.

Table 3.10. Analysis of Filtered Samples of $LiF\text{-}BeF_2\text{-}ThF_4$

Sample Temperature (°C)	Sample Composition (mole %)			CeF_3 Concentration (ppm)
	LiF	BeF_2	ThF_4	
720	58.7	29.5	11.8	100
530	61.4	33.0	5.54	100[a]
490	56.7	39.3	4.0	55
640	61.3	26.8	11.9	100
555	62.0	30.5	7.5	100[a]
517	61.9	31.2	6.8	100[a]
460	64.0	32.7	3.3	68

[a]Cerium-144 count per milligram of sample higher than that of the original melt because of the lower thorium content (less internal absorption of the soft ^{144}Ce gamma radiation).

Part II. Aqueous Reactors and Desalination

4. Corrosion and Chemical Behavior in Reactor and Desalination Environments

ASSESSMENT OF WATER TECHNOLOGY IN BOILING- AND PRESSURIZED-WATER REACTORS

G. H. Jenks

Water reactors which would be of a sealed or low-leakage type and which would be capable of operating for long periods without operator attention are of possible interest in Army work. We are continuing[1,2] our review and assessment of water technology in pressurized- and boiling-water reactors with the objectives of (1) providing additional bases for judging the feasibility and merits of unattended reactors of either type; (2) recommending materials, coolant compositions, and operating procedures; and (3) recommending research and development work which would aid in the development of such reactors. Secondary steam systems as well as primary systems are to be included in this work.

WATER CHEMISTRY IN A SMALL STATE-OF-THE-ART PRESSURIZED-WATER REACTOR

G. H. Jenks

A study was undertaken by the Reactor Division at ORNL to provide a reference design for a small [1500 kw (electrical)] state-of-the-art pressurized-water reactor. In this study we had the responsibility of providing recommendations in areas related to water technology in the primary system. A report of our work is included in a comprehensive report of the reference design which has been submitted for review.[2] Some of the information and results of analyses which influenced our recommendations and which are of general interest are summarized below.

Tritium in Coolant[3]

Tritium is found in primary coolants of water reactors in amounts ranging from very low values up to about 10 μc per cubic centimeter of coolant. The maximum permissible concentrations within restricted and unrestricted areas are 0.1 and 0.003 $\mu c/cm^3$ respectively. The tritium is present as the oxide (HTO) and so is not easily separated. Accordingly, handling and disposal of coolant waters are made more complicated by the presence of tritium, especially if water for waste dilution is scarce at the reactor site. Thus one of the design objectives was the exclusion of tritium from the coolant.

Major potential sources of tritium in water reactors are (1) uranium fission ($\sim 10^{-4}$ T per fission) and (2)

[1] G. H. Jenks and J. C. Griess, *Water Chemistry in Pressurized and Boiling Water Power Reactors,* ORNL-4173 (November 1967).

[2] *Reference Design and Technology Assessment of a 1500 kw(e) State-of-the-Art Pressurized Water Reactor,* G. Samuels, Program Director, M. E. Lackey, report editor. To be published as ORNL report.

[3] A principal source of information on tritium formation reactions and on other aspects of the tritium-contamination problem is a report by J. W. Ray, R. O. Wooton, and R. H. Barnes, *Investigation of Tritium Generation and Release in PM Nuclear Power Plants,* BMI-1787 (October 1966); see also J. O. Blomeke and F. E. Harrington, *Management of Radioactive Wastes at Nuclear Power Stations,* ORNL-4070 (January 1968).

the neutron reactions

$$^{10}B(n,\alpha)^{7}Li(n,n\alpha)T$$

and

$$^{10}B(n,2\alpha)T\ ,$$

occurring within boron poison elements. The rate of tritium formation from the neutron reactions is typically about one-tenth that from fission in a given reactor. Contamination of coolant from these sources occurs only if the tritium diffuses through the cladding on the fuel and poison elements. The most commonly used fuel element cladding materials are Zircaloy and austenitic stainless steel. The latter is also a common cladding material for burnable poison elements. On the basis of a review of available information relating to tritium in reactor coolants, we concluded that tritium would be retained within Zircaloy-clad pin-type fuel and poison elements in the present reactor. We also concluded that with stainless-clad elements of the same type, some indeterminate but probably significant fraction of the tritium would enter the coolant. Accordingly, we recommended that Zircaloy cladding be used if tritium exclusion must be assured.

Tritium is also produced directly in coolants through neutron reactions with some of the chemical elements which may be present. The reaction

$$^{10}B(n,2\alpha)T$$

is the most important of these, the tritium formation rate at 1500 ppm natural boron being, typically, about one-tenth the ternary fission rate. Accordingly, boron shim control cannot be used when tritium must be excluded. The amounts of tritium formed from other elements, including ^{7}Li, ^{9}Be, ^{14}N, and ^{2}H at concentrations usually present, are small and would not create significant problems in light-water PWR's.

Crud Deposits in Reactor Core

It is well known that some of the products of corrosion of materials external to the core in PWR primary systems (principally stainless steel and Inconel 600) can be transported to and deposited on fuel element surfaces. These deposits can conceivably affect flow and heat transfer, and they might also affect corrosion of the cladding. The effect on corrosion could presumably occur in a coolant employing a strong-base additive (e.g., LiOH or KOH) if boiling within a porous deposit leads to an increase in concentration of base within the deposit. In the case of Zircaloy cladding in a coolant containing LiOH, an increase in corrosion rate over that in pure water is expected to be noticeable at a pH of about 11.3 to 11.7 (measured at room temperature), and the rate is expected to increase with increasing pH. In practice, reported information for several previous PWR's shows that in some systems the amounts of deposits were negligible with respect to such effects, while fairly heavy deposits were experienced in others. The amounts of deposits and their chemical and physical properties are apparently dependent in poorly defined ways upon the particular combination of primary system materials, coolant composition, and the core design used in the reactor.

The recommended combination for the state-of-the-art reactor most nearly resembles that of Shippingport core I, where deposits were minor. The systems are alike with respect to coolant composition (high pH with LiOH) and with respect to fuel element type and cladding (pin type, Zircaloy clad). Points of difference include, primarily, (1) occurrence of subcooled boiling in this core; (2) lower coolant velocities through the core, about 2.4 fps vs minimum of 4.4 fps in Shippingport core I; and (3) use of Inconel 600 steam generator tubing. Stainless steel tubing was used in the Shippingport reactor. The majority of other surfaces in contact with coolant are of stainless steel, and this was also true of the Shippingport reactor.

We concluded that the boiling and low velocities will not lead to detrimental effects on thermal, hydraulic, or corrosion properties of the core in the state-of-the-art reactor if the deposits are primarily of magnetite. The deposits are expected to be comprised primarily of this material if only stainless steel corrosion products are transported to the core. These conclusions were based on review and analysis of reported experimental information and reactor experience. They were also based, in part, on information on magnetite solubility reported recently by Sweeton, Baes, and Ray.[4] We will not review the information and analyses here except to show the solubility information which was used (Fig. 4.1).[5] The plots in Fig. 4.1 illustrate that the solubility of magnetite at reactor temperatures changes significantly with changes in pH and also that at most pH

[4] F. H. Sweeton, C. F. Baes, Jr., and R. W. Ray, chap. 6, this report.

[5] Plots made from data analyses of Sweeton, Baes, and Ray[4] and kindly furnished by F. H. Sweeton. The results of preliminary analyses which were used in the report on the state-of-the-art reactor[2] showed somewhat greater changes in solubility with pH and temperature.

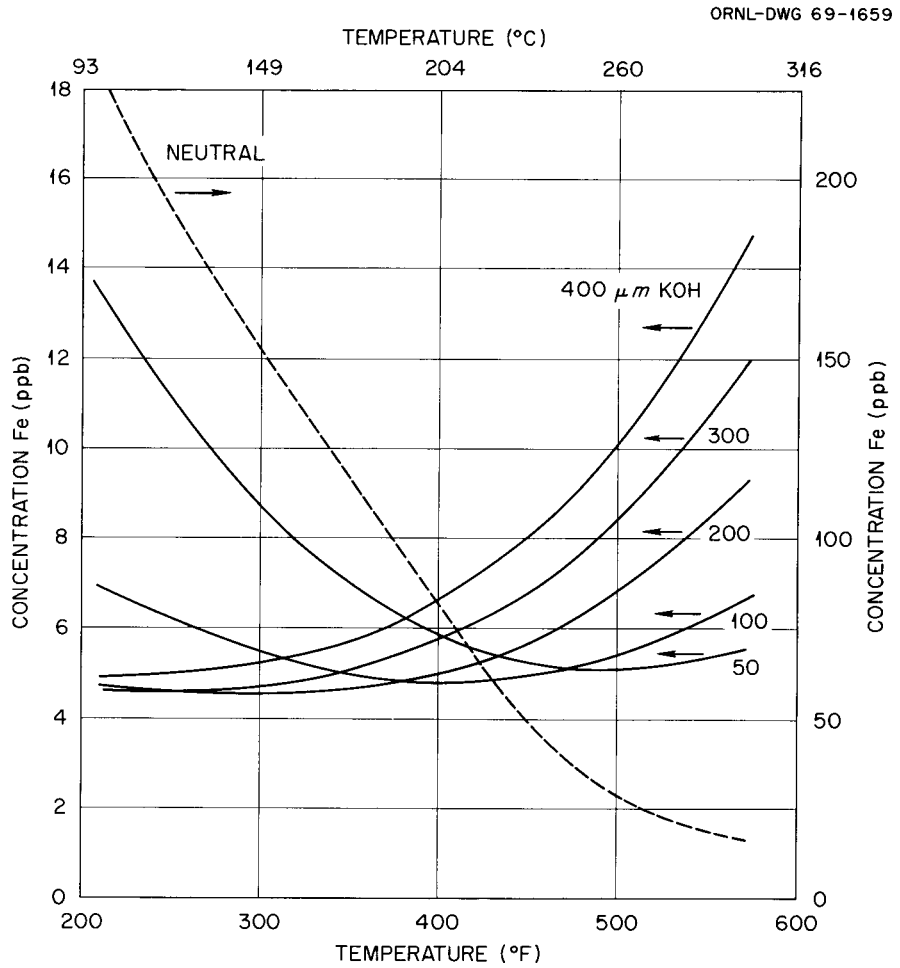

Fig. 4.1. Magnetite Solubility in Neutral and in 50, 100, 200, 300, and 400 μm KOH with 17.5 cm^3 H_2 per Kilogram.

values, the solubility differs significantly between the temperatures which prevail at core surfaces and those in adjacent coolant. The magnetite would be expected to transfer from one location to another under the influence of the solubility gradients created by the temperature gradients. The directions and magnitudes of the gradients would be determined by the pH.

The available information on Inconel corrosion product transport, deposition, and solubility was not sufficient to permit predictions of behavior of this material in the core of the state-of-the-art system. However, it is likely that the corrosion rate of Inconel will be very low in this system, so that the amount of corrosion product available for transport to the core will not cause hydraulic, thermal, or corrosion problems. However, since we could not exclude the possibilities of some effects, the actual performance of the system must be determined during operation of the reactor.

Gas Distribution in PWR Steam Pressurizers[6]

The steam pressurizer employed with a PWR is partially filled with reactor coolant water which is heated to produce the desired steam overpressure. The pressurizer also serves as a surge tank in which changes in reactor coolant volume are accommodated at more or less constant pressure by generation or condensation of steam. The thermal insulation on the pressurizer vessel is not perfect; so even at constant volume and pressure, condensation of steam occurs on the walls of the steam dome, and at the same time vaporization of liquid takes place to maintain constant pressure. That is, it is a refluxing system. If a dissolved gas, such as hydrogen, oxygen, or nitrogen, is initially present in the liquid, it will be transferred nearly quantitatively into

[6]With Garland Samuels of Reactor Division.

the vapor phase as a result of this continuous refluxing, unless means are provided for counteracting the transfer. Further, since there is always some interchange of liquid between the pressurizer and reactor vessel, nearly all gas within the reactor coolant eventually will be transported to the vapor phase. The PWR coolants invariably contain some gas (e.g., 25 to 50 cm^3 of H_2 per kilogram to suppress O_2 formation), so that gas transfer to the vapor phase can affect water chemistry control. It can also affect the performance of the pressurizer as a pressurizer and surge tank if there is insufficient leakage from the steam dome.

We analyzed the available theoretical and experimental information relating to gas distribution in steam pressurizers and from the results of this have proposed a design which will permit control of gas distribution and pressure in a zero-leakage steam pressurizer. In this design a small bypass stream from the reactor will spray into the top of the steam dome and circulate back to the reactor. A small trough is attached to the pressurizer wall to collect part of the condensate and spray and return this fraction, f, to the bottom of the pressurizer below the heaters. The temperature at which the spray enters the pressurizer will be that of the reactor water.

Analyses show that with the value of f approximately equal to 0.2, the pressure of gas in the steam dome will be higher than that in an equilibrium system by a factor of about 3. The value of this factor will be insensitive to changes in the spray and steam rates and to the effective value of the gas distribution coefficient. The spray rate should approximately equal 5×10^{-6} of the reactor coolant volume per second in order to achieve reasonable times of mixing between reactor and pressurizer fluids.

The benefits accruing from the use of this system are summarized below.

1. A stable and predictable distribution of gas between reactor coolant and steam dome is reached.
2. The concentration of gas in the steam dome is near that in an equilibrium system.
3. Gas in the steam dome will not interfere with the performance of the pressurizer.
4. The steam dome serves as a gas reservoir which will substantially reduce changes in gas concentration in the coolant with changes in total amount of gas in the system.

The performance of this pressurizer system in practice remains to be demonstrated.

RDT STANDARDS FOR PRIMARY COOLANT SYSTEMS OF WATER REACTORS

H. C. Savage P. D. Neumann G. H. Jenks

The AEC Division of Reactor Development and Technology (RDT) has set up a program to develop standards for water-cooled reactors.[7,8] An RDT Standards Program has been established at ORNL by the AEC to assist in the preparation, review, reproduction, distribution, and revision of standards for water-cooled reactors in cooperation with the AEC and reactor contractors.

As part of the RDT Standards Program at ORNL, we are preparing standards which will establish requirements for the coolant chemistry in primary systems of boiling-water, pressurized-water, and research or test reactors. The BWR's are direct-cycle power reactors in which steam produced in the reactor core is fed to the turbine generator. In this country, high-purity water without additives is used, and the steam condensate is returned to the reactor after purification and removal of radiolytic gases. The PWR's are power reactors using an indirect cycle in which heat is transferred to the steam system through a steam generator. Various additives are used in the primary coolant water. These include hydrogen gas to suppress the radiolytic decomposition of water; boric acid as a neutron absorber for "chemical shim" control in central station power reactors; and ammonium hydroxide, lithium hydroxide, or potassium hydroxide for pH adjustment. The pH adjustments are made to control corrosion and core deposits and to increase the nuclear reactivity of the core. The test reactors are typified by reactors such as the Oak Ridge Research Reactor and the High Flux Isotope Reactor which operate at low temperatures and do not produce electrical power. In this country aluminum-clad fuel elements are used, and the pH of the coolant water is kept on the acid side to control aluminum corrosion.

It is intended that our RDT standards will establish requirements for the chemistry of the primary coolants and will include accepted compositions, impurity limits, dissolved gas contents, and the purification systems and methods for control of coolant composition and purity. They are expected to reflect existing technology and

[7] M. Shaw, AEC Program in Nuclear Standards, Division of Reactor Development and Technology, *Nucl. News* 10(11), 41–44 (1967).

[8] M. Shaw, Standards and Reactor Safety, *Nucl. Safety* 9(5), 337 (1968).

provide a source of sound, proven information for use by designers, builders, and operators of reactor systems and components. In order to meet this objective, pertinent literature, research and operating reports, and design documents relating to water-cooled reactors are being reviewed. We have visited several nuclear power stations (Dresden, Yankee, and Connecticut Yankee) and have consulted with reactor designers, contractors, and operators to obtain current information on coolant composition control specifications in the present generation of water reactors.

Preliminary drafts of standards for these three reactor types are being prepared.

CORROSION OF ELECTROLESS PLATED NICKEL ON ALUMINUM AT HIGH HEAT FLUXES

J. C. Griess R. D. Cheverton[9] J. R. McGuffey[10]

The performance of aluminum-clad fuel elements in the HFIR has been satisfactory to this time, but any significant increase in either the power density or fuel element life could make aluminum unsatisfactory as a cladding material in high-performance reactors such as the HFIR. The reason for this is that the corrosion of aluminum in hot water produces an adherent layer of corrosion products that has a very low thermal conductivity, and the thickness of the layer, which is a function of surface temperature and exposure time, becomes significant in terms of fuel plate temperature for HFIR operating conditions. At high temperatures both corrosion and fuel plate instability, resulting from large temperature differences and lack of mechanical strength of the aluminum, can lead to fuel element failure. If the fuel element were coated with electroless nickel, which has a high degree of corrosion resistance in reactor water, the usefulness of aluminum as a cladding material could be significantly extended.

The use of electroless nickel plate to protect aluminum has been investigated previously. In one case it was shown that the nickel plate protected aluminum in isothermal tests at 300 to 330°C in water[11] with both as-plated and diffusion-bonded specimens. In another case fuel plates exposed in a reactor indicated that most of the nickel peeled from the surface shortly after the specimens were brought to power.[12] Although not stated, the pH of the water was probably 5.0 to 5.5. In this latter case the plated specimens were heat treated at temperatures in excess of 400°C to produce a diffusion bond between the aluminum and the nickel. Such a heat treatment produces nickel-aluminum intermetallic compounds which are brittle, a condition which may have contributed to the failures.

Tests of electroless nickel plate on aluminum under heat transfer conditions in the absence of radiation had not been made, and a test of such a nature was considered desirable. Also, since the time that the other tests had been conducted, an improved surface preparation technique had been developed.[13] Using this technique, personnel at K-25 plated several test coupons with about 1 mil of nickel. These coupons were exposed for one week to deionized water at 250°C and then examined. The results indicated that the as-plated specimens had fewer imperfections through which aluminum oxide protruded than did the heat-treated ones. On this basis it was decided to use the electroless plate in the as-plated condition for the heat flux test.

The corrosion test under high heat flux was conducted with the same type of specimen and in the same equipment previously described.[14] In general, the rate of oxide buildup on the surface of the specimen is obtained from temperature measurements on the outside of the insulated specimen, while the heat flux, flow rate, and coolant temperature are maintained constant. In this test, water flowed through the channel at a velocity of 30 fps, and at all times the specific resistivity of the water was $>10^6$ ohm-cm. During the first 68 hr a heat flux of 1.0×10^6 Btu hr^{-1} ft^{-2} was maintained; subsequently the heat flux was increased to 1.5×10^6 Btu hr^{-1} ft^{-2} for the remainder of the test, 459 hr. At the higher heat flux the calculated temperature at the nickel-water interface ranged from 229 to 242°C.

At each heat flux the temperatures on the outside of the specimen remained constant, indicating no formation of any significant deposit at the interface. Examination of the specimen surface at the conclusion of the test confirmed this, showing no evidence of aluminum oxide corrosion product; the nickel had developed only a slight surface discoloration. However, a few very fine cracks in the nickel were apparent. A cross-sectional

[9] Reactor Division.

[10] Inspection Engineering.

[11] A. B. Johnson, Jr., *Behavior of Chemical Nickel Plate on Aluminum Alloys in High Temperature, Dynamic, Aqueous Systems*, HW-81196 (April 1964).

[12] M. Zukor, *Annual Progress Report on Reactor Fuels and Materials Development for FY 1966*, IDO-17218, pp. 105–8.

[13] R. R. Wright *et al.*, memo to J. C. Barton, *Procedure for Electroless Nickel Plating on Aluminum Alloys*, KL-3088 (November 1968).

[14] J. C. Griess, H. C. Savage, and J. L. English, *Effect of Heat Flux on the Corrosion of Aluminum by Water. Part IV. Tests Relative to the Advanced Test Reactor and Correlation with Previous Results*, ORNL-3541 (February 1964).

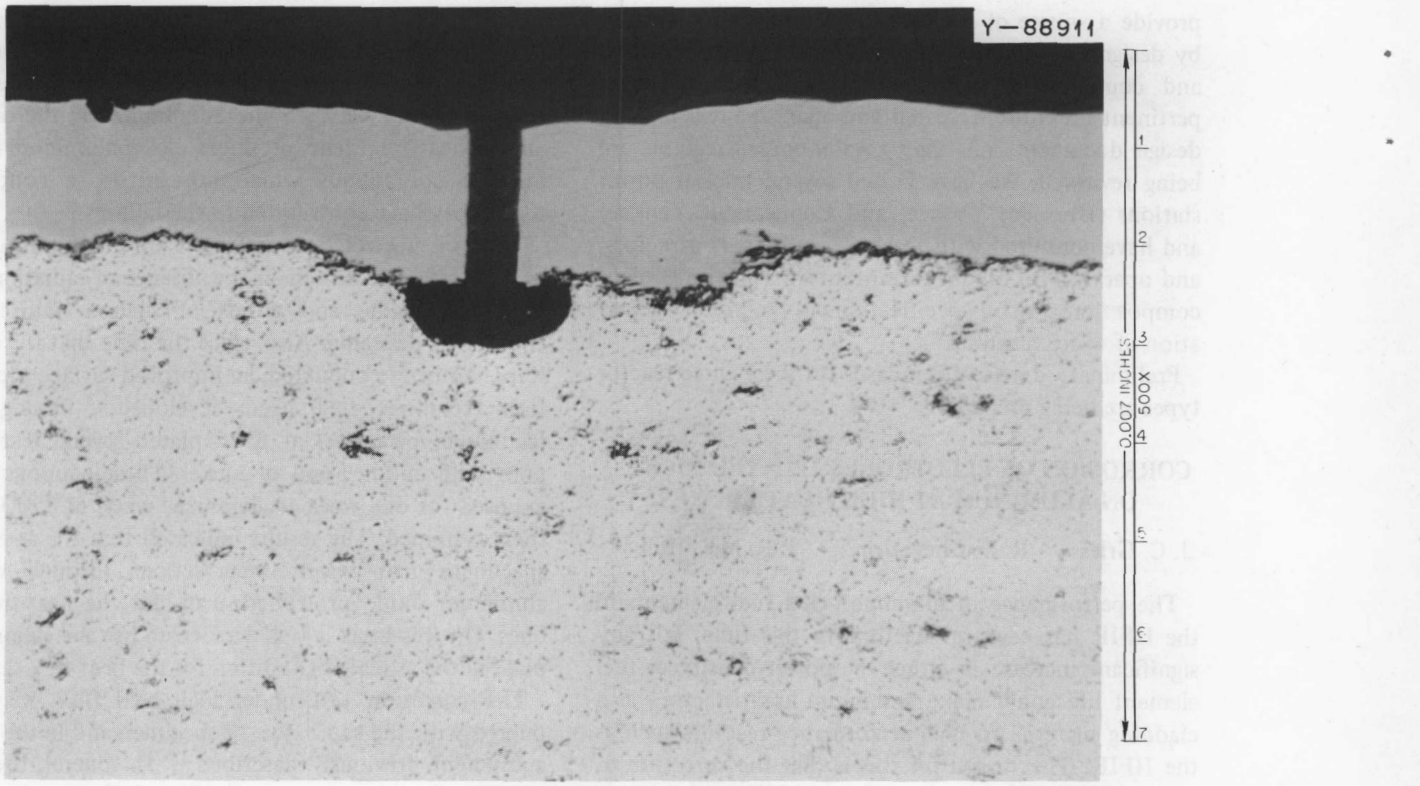

Fig. 4.2. Cross-Sectional View Through One of the Cracks on the Electroless Nickel-Coated Aluminum Specimens.

view through one of the cracks is shown in Fig. 4.2. Directly below the crack the aluminum had been attacked to a depth of about 0.5 mil. Part of the crack and the corroded volume were packed with aluminum corrosion products. At no place along any of the cracks was there evidence of the nickel showing a tendency to peel from the aluminum surface.

While the results of the above experiment are promising, much additional development work would be required to demonstrate the adequacy of electroless nickel plate as a means of protecting aluminum-clad fuel elements. In the only in-reactor experiments reported to date, the plate sloughed off. The differences, other than radiation, between those tests and the one reported here were: pH 5.0 to 5.5 vs 6.5 to 7.0 in the latter test; improved surface preparation used in the ex-reactor test; and diffusion bonding of the nickel to the clad in the in-reactor tests vs the as-plated condition for the ex-reactor tests. Which, if any, of these differences are of most significance is not apparent at the present time.

CORROSION OF MATERIALS IN IODINE-ABSORBING REACTOR CONTAINMENT SPRAY SOLUTIONS

J. C. Griess A. L. Bacarella

In the event of a catastrophic failure of a nuclear pressure vessel and subsequent meltdown of the fuel, volatile fission products, of which iodine is the most hazardous from a biological standpoint, would be released to the containment building. By scrubbing the containment building atmosphere with a spray capable of absorbing iodine and/or compounds of iodine, escape of iodine to the outside environment can be prevented. The purpose of this program is to determine the corrosion resistance of materials that would be present in power reactor systems containment vessels in iodine-absorbing sprays as well as in the liquid phase of such solutions.

To simulate the conditions that would exist in a reactor containment building during operation of a

spray system, a small stainless steel loop was constructed. The loop consisted of a small pump which recirculates the solution through a full-cone, center-jet spray nozzle, a spray chamber in which specimens are exposed both in the spray and totally submerged, and associated control equipment.

The two spray solutions used in tests to this time had the following compositions: 0.15 *m* NaOH–0.28 *m* H_3BO_3 and the same solution containing 0.064 *m* $Na_2S_2O_3$. Both solutions had pH values of 9.3. The materials investigated included types 304 and 316 stainless steel, A-108 and A-210 carbon steel, 90-10 and 70-30 cupronickel, Inconel 600 and 718, copper, Monel 400, Zircaloy-2, and several different aluminum alloys. In nearly all tests, four identical specimens were exposed to the spray and two were exposed totally submerged in the solution in the bottom of the spray chamber.

If a spray system were actually used, the initial maximum temperature of the environment would be about 140°C, which would decrease to 55°C or less within a few days. For that reason specimens have been exposed to both solutions at 140, 100, and 55°C for 1, 7, and 21 days respectively. In all cases an atmosphere of air (room temperature) filled the spray chamber at the start of a test.

The results showed that under all conditions the aluminum alloys were unsatisfactory. In the solution without thiosulfate, corrosion rates of all aluminum alloys except the 5052 alloy (2.5% Mg, 0.25% Cr, balance Al) corroded at rates in the range of several inches penetration per year; the 5052 alloy was considerably more resistant than the others, but even this alloy corroded at about 60 mils/year. At 55°C all aluminum alloys corroded at rates as high as 200 mils/year, with no significant differences among the alloys. In a brief test in the thiosulfate-containing solution, the corrosion rates of the aluminum alloys appeared to be similar to those in the absence of thiosulfate. In the latter test, aluminum reduced some of the thiosulfate to sulfide, which reacted with copper corrosion products to form copper sulfide. The coarse copper sulfide particles lodged in the nozzle and within a short time completely stopped the spray.

Under all test conditions the stainless steels, the Inconels, and the Zircaloy-2 specimens showed no significant effect from being exposed to the spray or being totally immersed in either solution. At the highest temperature very light tarnish films occasionally formed, but within the weighing precision no weight changes were observed. In the absence of thiosulfate, only copper and its alloys showed detectable corrosion rates. The same was true for the thiosulfate-containing solution, except at 100°C the carbon-steel specimens developed pits as deep as 5 mils and showed average corrosion rates as high as 11 mils/year. These carbon-steel specimens were in the system during the brief time (one day) that aluminum specimens were also in the

Table 4.1. Corrosion Rates of Copper Alloys in Iodine-Absorbing Spray Solutions

Material	Corrosion Rate (mils/year) at Temperatures of:					
	140°C[a]		100°C[b]		55°C[c]	
	Spray	Solution	Spray	Solution	Spray	Solution
	0.15 *m* NaOH–0.28 *m* H_3BO_3					
Copper	7.1	1.8	1.7	0.5	0.8	0.3
90-10 cupronickel	1.3	4.9	0	0	0.06	0.03
70-30 cupronickel	0.3	0	0	0	0.02	0.02
Monel 400	0	0	0	0	0	0
	0.15 *m* NaOH–0.28 *m* H_3BO_3–0.064 *m* $Na_2S_2O_3$					
Copper	1200	18	210	11	76	3.9
90-10 cupronickel	190	1.5	1.8	1.1	0.2	0.2
70-30 cupronickel	1.3	0.3	0.2	0.9	0.02	0.03
Monel 400	0.2	0.2	0.2	0.2	0	0

[a]Tests lasted 1 day.

[b]Tests lasted 7 days.

[c]Test lasted 21 days in 0.15 *m* NaOH–0.28 *m* H_3BO_3. In thiosulfate solution, results based on 15-day exposure; the test is continuing.

system. At the higher and lower temperatures, there was no significant attack, and it is probable that the sulfide ions that were formed when aluminum was in the system were responsible for the attack noted. Table 4.1 shows the average corrosion rates observed on copper and copper alloy specimens in both solutions.

It is interesting to note that in all cases copper was the least corrosion resistant, followed in order by 90-10, 70-30, and Monel 400 (~35% Cu). Thus the higher the nickel content, the higher the corrosion resistance of the alloy. In addition, the corrosion rate of any alloy was usually higher in the spray than in the solution, and the solution with thiosulfate was more corrosive than the same solution without thiosulfate.

The results obtained to date indicate that only the aluminum alloys have excessively high corrosion rates in both solutions and that copper is heavily corroded by solutions that contain thiosulfate. Reactors that will incorporate spray systems will not use aluminum in the containment vessel. The chief use of copper is for electrical conductors, and those that must be used in the event of a catastrophic failure will be enclosed in stainless steel conduit. With the above two precautions, it appears that none of the materials in the containment vessel will suffer significant corrosion damage during operation of a spray system.

The 0.15 *m* NaOH–0.28 *m* H_3BO_3 solutions were stable at all temperatures. The pH remained constant, and no loss of boron from the solution was observed. The thiosulfate solutions were slightly unstable even in the absence of aluminum. At 100°C the thiosulfate concentration decreased to 85% of its starting value in 96 hr; at 140°C about the same loss was observed in 24 hr. In neither case was any boron lost from solution. These observations are in good agreement with those obtained in an all-glass system under similar conditions[15] and indicate that metallic surfaces or insoluble corrosion products suspended in solution have no appreciable effect on thiosulfate stability.

CORROSION OF COPPER ALLOYS IN SODIUM CHLORIDE SOLUTIONS

J. C. Griess E. G. Bohlmann

In spite of the fact that copper alloys have been used for many years in saline water environments, very little quantitative information exists on the corrosion of this class of alloys, especially at temperatures above 100°C. As part of the corrosion program conducted for the Office of Saline Water, the corrosion behavior of four copper alloys is being determined in sodium chloride solutions under controlled conditions. Data are being obtained in two ways: weight loss measurements resulting from exposure of specimens to flowing salt water in a titanium pump loop, and electrochemical polarization studies with single specimens in a small Hastelloy C pump loop. The latter studies have usually been conducted potentiostatically. With both loops, fresh solution is continuously pumped into, and an equal volume removed from, the loops so that the solution composition remains essentially constant during a test.

The alloys under investigation are Admiralty brass, 90-10 and 70-30 cupronickel, and Monel 400, and to this time principally 1 *m* NaCl at 125°C has been used. In all cases oxygen was removed from the solution by sparging with pure nitrogen, and in some cases low concentrations of other compounds were added to the solution. Specimens for weight loss determinations were exposed with solution flowing past them at 3, 7, and 15 fps. The velocity of the solution past the specimens on which electrochemical measurements were made was 4 fps, although velocities as high as 12 fps can be achieved.

The tests in which corrosion rates were determined from weight loss data lasted for ~1500 hr, with some specimens of each alloy being replaced with new ones at intermediate times. In all cases weight losses at five or more time intervals were recorded for all four alloys. Plots of weight loss vs time yielded straight lines after an initial period, and from the slopes of these lines corrosion rates were obtained. Table 4.2 shows the corrosion rates for the four alloys in oxygen-free 1 *m* NaCl and in 1 *m* NaCl with either 10 ppm sulfide (as Na_2S) or 10 ppm cystine $[-S-CH_2-CH(NH_2)-COOH]_2$ added to it. Only the rates observed at 3 and 15 fps are reported; at 7 fps, rates were between the other two.

In deaerated 1 *m* NaCl all materials developed very thin corrosion-product films and, with the exception of Admiralty brass, had very low corrosion rates. There was no evidence of localized attack on any specimen. With 10 ppm sulfide present, both cupronickels underwent heavy attack and developed poorly adherent, heavy black scales which contained sulfides of copper and nickel. Of the four alloys, only the 90-10 alloy underwent localized attack; several relatively deep pits were present on all specimens. Monel 400 also corroded appreciably more in the presence of sulfide than in its absence, but Admiralty brass corroded less. With 10

[15] H. E. Zittel, *ORNL Nuclear Safety Research and Development Program Bimonthly Report for March–April 1968*, ORNL-TM-2230, pp. 77–81 (June 26, 1968).

Table 4.2. *Corrosion of Copper Alloys* in Flowing Oxygen-Free 1 *m* NaCl at 125°C

Additive	Corrosion Rate (mils/year)			
	Admiralty Brass	90-10 Cupronickel	70-30 Cupronickel	Monel 400
None	2.2–3.3	0.8–0.7	0.1–0.3	0.1–0.1
10 ppm sulfide	0.8–1.7	7–20	9–16	1.9–3.1
10 ppm cystine	2.8–5.6	2.8–5.6	2.8–5.6	2.8–5.6

ppm cystine in the solution all four alloys corroded to about the same extent, and none of the specimens developed heavy corrosion-product scales. A few pits were occasionally found on the Admiralty brass specimens, and at the higher flow rates there was a slight indication of a velocity effect on the same specimens. No other specimens underwent localized attack. Sulfides of both copper and nickel were identified in the corrosion products, indicating at least partial decomposition of the cystine.

Although the data presented above were obtained in sodium chloride solutions, they are generally consistent with observations made on seawater condensers and on evaporator tubes in desalination plants. Thus experience has shown that in unpolluted water both 90-10 and 70-30 cupronickels are superior to Admiralty brass, with the 70-30 alloy generally a better choice (from a corrosion standpoint) than the 90-10 alloy. On the other hand, it is generally known that in sulfide-containing waters Admiralty brass performs better than the cupronickels.

Electrochemical polarization studies with the same alloys are in progress, with only 90-10 cupronickel having been thoroughly investigated to this time. Figure 4.3 shows typical polarization curves of 90-10 cupronickel in deaerated 1 *m* NaCl at 125°C. The reduction of water constituted the primary cathodic reaction, although at lower potentials some other reduction process also occurred. For example, extrapolation of the first linear portion of the cathodic curve to the open-circuit or corrosion potential yields a current density of 1.3×10^{-6} amp/cm^2, which corresponds to a corrosion rate of 1 mil/year; this is in good agreement with the value of 0.8 mil/year shown in Table 4.2. At lower cathodic potentials (–0.7 to –0.8 v vs S.C.E.), a region in which the current increased rapidly with small changes in potential was observed. At still lower cathodic potentials the curve became steeper. Reversing the polarization sequence produced only one linear region of about the same slope as the first. There was no evidence of the plateau at –0.7 to –0.8 v.

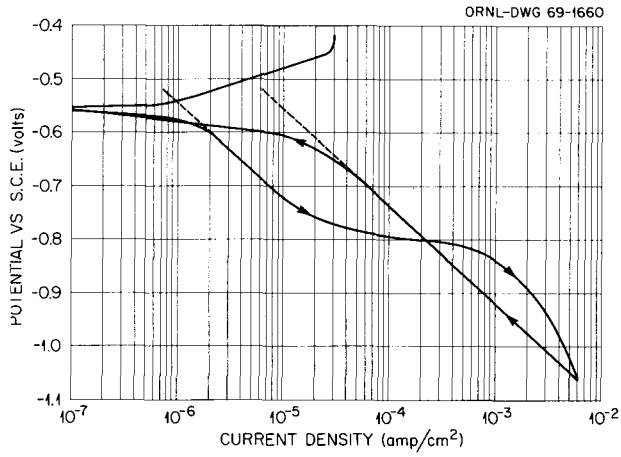

Fig. 4.3. The Polarization of 90-10 Cupronickel at 125°C in Deaerated 1 *m* NaCl Flowing at 4 fps.

An explanation of the cathodic curve is as follows: The initial linear portion represented the reduction of water on a surface mostly covered with corrosion products, the plateau represented the reduction of corrosion products on the surface, and the linear region obtained when proceeding from cathodic to anodic potentials corresponded to reduction of water on a film-free surface. A similar type of cathodic behavior was observed when the system contained low concentrations of sulfide; that is, there was evidence of reduction of solid corrosion products (–0.9 to –1.0 v vs S.C.E.) when proceeding from the corrosion potential in a cathodic direction and no such evidence when the polarization sequence was reversed. As in the absence of sulfide, extrapolation of the initial linear portion of the cathodic curve to the corrosion potential indicated a corrosion rate in reasonable agreement with that shown in Table 4.2 (12 vs 7 mils/year), whereas extrapolation of the second linear portion intersected the corrosion potential at a current density about an order of magnitude greater.

As shown in Fig. 4.3 the anodic polarization curves in deaerated 1 *m* NaCl were linear over some region, but at

higher current densities the curves deviated from linearity. The current density where deviation from linearity started varied randomly from about 3×10^{-5} to 3×10^{-4} amp/cm^2. The average slope of the linear portions was 73 mv per decade. The presence of 10 ppm sulfide in the solution depressed the corrosion potential of the 90-10 cupronickel by about 300 mv. Anodic polarization curves showed limiting diffusion current densities, the magnitudes of which were dependent on the sulfide concentration.

Based on the experience with 90-10 cupronickel, it appears that electrochemical measurements can be adequately correlated with the results of weight loss measurements, which in turn are in reasonable agreement with industrial experience in saline water environments. If similar results are obtained with other alloys, an electrochemical technique involving small current polarization should be most useful in evaluating the effects of many variables on existing alloys and in assessing the merits of new alloys in situ under conditions of flow and high temperature.

CARBON DIOXIDE SCALE SUPPRESSION STUDIES

S. A. Reed D. M. Eissenberg[9]
C. C. Littlefield[16]

Experiments have been conducted at Oak Ridge and at the Office of Saline Water Test Station at Wrightsville Beach, North Carolina, to determine the technical feasibility of using carbon dioxide as a scale suppressant in distillation-type desalination plants.

The objectives of the experiments were (1) to verify that CO_2 injected into the feed seawater upstream of a brine heater will prevent alkaline scale from forming on the heat exchange surfaces at temperatures up to 290°F, (2) to devise a method of handling the solids which precipitate when the CO_2 overpressure on the hot brine is removed, and (3) to demonstrate that the CO_2 stripped from the brine can be economically recovered for reuse.

The first objective has been accomplished. It was shown that seawater containing sufficient CO_2 to depress the pH to 6.6 or less prevented the formation of alkaline scale on heat exchange surfaces at least up to brine temperatures of 300 to 315°F.

The second objective is being investigated, and the results to date have been encouraging.[17] A dealkalizer test apparatus was constructed in Oak Ridge to strip the CO_2 from synthetic seawater by countercurrent gas/liquid contacting and to precipitate the scale, which rapidly formed, on a bed of solids. Outlet alkalinities as low as 20 ppm were obtained in this manner using various configurations of dealkalizers.

Tests using low-surface-area packing materials, including ½-in. limestone gravel and ¼-in. Intalox saddles, gave higher alkalinities leaving the stripper than tests with activated alumina. However, the use of Intalox saddles in the stripper permitted higher specific liquid flow rates at lower pressure drops compared with the alumina.

Carbon dioxide was stripped from solution equally well using either steam, air, or nitrogen. Lowering of alkalinity was found to be essentially unaffected by steam flow rate over the range investigated, that is, 25 to 125 lb hr^{-1} ft^{-2}.

Tests were carried out in packed column strippers using both continuous-gas-phase and continuous-liquid-phase types of operation. The continuous-liquid-phase mode of operation resulted in lower residual alkalinity. This was attributed to the longer liquid residence times obtained with a continuous-liquid column. However, the higher pressure drop of the continuous-liquid-phase column is likely to be uneconomical in large plants. Therefore a combination continuous-gas-phase CO_2 stripper and continuous-liquid-phase contactor was evolved to permit both the low pressure drop of continuous-gas-phase stripping and the needed residence time for $CaCO_3$ precipitation. This also permitted the use of a different type of packing for each section of the dealkalizer, that is, Intalox or other conventional tower packing for the CO_2 stripper and activated alumina for the contactor.

The $CaCO_3$ solids left in the dealkalizer beds of a desalination plant need to be removed periodically. This can be accomplished by dissolution of the precipitate using blowdown brine which has been acidified with the excess CO_2 from the stripping column. The blowdown brine in which the $CaCO_3$ is dissolved is returned to the ocean.

The third objective, to prove that the recovery and recycle of CO_2 can be achieved without affecting the economics of distillation desalination plants, has not been verified as yet. However, flowsheets have been developed which indicate that no difficulties should be encountered with CO_2 recycle.

Further testing of the use of steam for stripping the CO_2 is required. The relatively low quantities of steam needed in the small test apparatus and the difficulties inherent in metering such low flows, plus the need to

[16] ORGDP.

[17] C. C. Littlefield, D. M. Eissenberg, and S. A. Reed, *Control of Alkaline Scale Using CO_2 Suppression,* ORNL-TM-2415 (to be published).

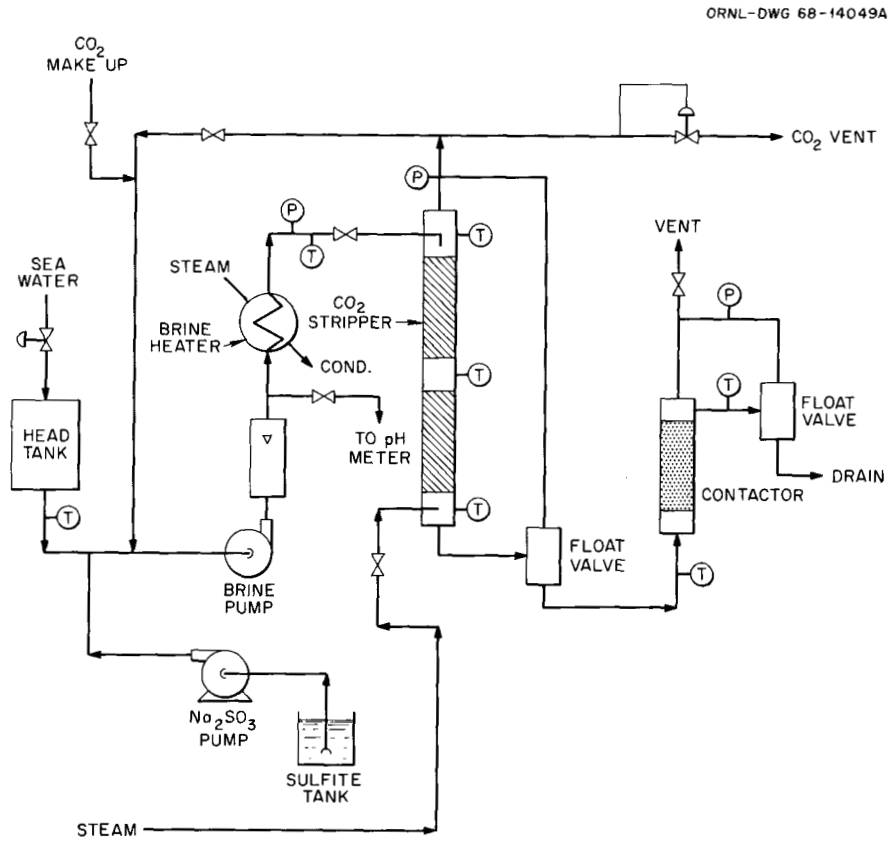

Fig. 4.4. Modified Wrightsville Beach Test Rig.

determine design parameters for large plants, make it desirable to increase the scale of the test operations and to use actual seawater rather than the artificial salt water used in the bench-scale studies at Oak Ridge. Further testing will be done during 1969 using the 6-in.-diam Wrightsville Beach unit (Fig. 4.4) after modification to permit the use of both a CO_2 stripper and a contactor at seawater flows of 1 to 5 gpm. Completion of testing on the unit will lead to the design of a 30-gpm unit which may be tied in to either the vertical tube evaporator or the multistage flash evaporator pilot plants at Wrightsville Beach. Final scaleup parameters and sufficient operating experience will be accumulated with the 30-gpm unit to permit design of the process as it would be applied to a larger desalination plant.

OSW MATERIALS INFORMATION CENTER

J. L. English S. A. Reed

In 1967, the Office of Saline Water, U.S. Department of the Interior, requested Oak Ridge National Laboratory to proceed with the establishment of a Materials Information Center for the purpose of developing procedures for the collection, indexing, abstracting, retrieval, evaluation, and dissemination of information relating to the corrosion performance of materials used in distillation processes for the desalination of seawater. A manual information storage and retrieval system was designed to fulfill this objective.

However, in mid-1968 a decision was made by the Office of Saline Water to expand the initial objective to include all saline-water conversion processes rather than just distillation processes and to change from a manual to a computerized system for information storage and retrieval. A thesaurus of descriptive key words numbering 612 was prepared and is being expanded as necessary. Bibliographic codes to aid in retrieval of information were prepared also. For the present, computer facilities of the Computing Technology Center located at the Oak Ridge Gaseous Diffusion Plant are being utilized to accommodate the needs of the Materials Information Center.

The Center will maintain a permanent file of all material processed, such as reports, journal articles, etc. The immediate-term objective has been to concentrate on pertinent information contained in reports issued by the Office of Saline Water. Thus far, 360 such reports have been reviewed, of which 174 were found to contain information relevant to the corrosion performance of materials. These reports have been ordered and received and are being processed. It is planned to issue quarterly indexed bibliographic reports, with the initial publication scheduled for release early in 1969.

Upon completion of the processing of the Office of Saline Water reports, efforts of the Center will be directed to the open literature concerned with materials performance in saline-water conversion processes.

Among other activities undertaken at the request of the Office of Saline Water has been the development of a two-page set of forms which will be used for inspection and equipment performance reports at all test-bed plants. These forms are designated as the "Office of Saline Water Materials Performance Reporting System" and will be coded for computerization of information storage and retrieval. Personnel of the Materials Information Center visited the Freeport Test Bed Plant and the Senator Clair Engle Test Bed Plant to explain and field-evaluate the forms. Final revision of the forms has been accomplished, and printing for distribution to the concerned test-bed plants will be completed early in 1969. The Center will maintain a permanent file of the inspection report forms, laboratory reports, photographs, and any other information generated during future inspections of equipment at the various installations. The Center has on hand approximately 1000 inspection forms of a different type which have been used for previous plant inspections. Information from these forms will be transcribed to the new forms for computerization.

The Materials Information Center will be in full operation by the end of fiscal year 1969.

5. Electrical Conductance of Aqueous Electrolytes to 800°C and 4000 Bars

ELECTRICAL CONDUCTANCES OF AQUEOUS SODIUM IODIDE AND THE COMPARATIVE THERMODYNAMIC BEHAVIOR OF AQUEOUS SODIUM HALIDE SOLUTIONS TO 800°C AND 4000 BARS

L. A. Dunn W. L. Marshall

The properties of aqueous electrolyte solutions at high temperatures and pressures, particularly in the supercritical region, are amenable to investigation by conductance techniques. This method has been applied in several recent papers from this Division to the study of the behavior of dilute aqueous solutions of $KHSO_4$,[1] NaCl,[2] NaBr,[3] and HBr[4] to 800°C and to a pressure of 4000 bars. These studies have indicated that, at high temperatures and pressures, aqueous electrolyte solutions exhibit a simplified behavior not evident at lower temperatures.[5] It was found that the isothermal limiting equivalent conductances of these salts in the temperature range 100 to 800°C are linear functions of the solvent density.[1-4] Moreover, at temperatures from 400 to 800°C the limiting equivalent conductances for a particular electrolyte were found to be independent of the temperature at constant solvent density.[1-4]

During the past year, conductance measurements of dilute (0.001 to 0.10 *m*) aqueous NaI solutions were made at temperatures from 0 to 800°C and at pressures to 4000 bars. A paper on this study is in press,[6] from which the following summary is taken. An example of equivalent conductances for 0.05 *m* NaI vs density at several temperatures is shown in Fig. 5.1. From these and measurements for the other molalities, limiting equivalent conductances (Λ_0) of NaI were obtained over a range of temperature and density. Figure 5.2 shows the linear relationship observed when isothermal values of Λ_0(NaI) are plotted against the density of the solvent. For NaI, this relationship is represented by

$$\Lambda_0(\mathrm{NaI}) = 1897 - 1210d\,, \qquad (1)$$

where d is the density; the two parameters are within 10% of those found previously for $KHSO_4$,[1] NaCl,[2] and NaBr.[3] The significance of this similarity in behavior of 1-1 electrolytes has already been discussed.[2-4]

With the concept of the complete ionization constant (including hydration),[7,8] isothermal plots of log K against log C_{H_2O}, where C_{H_2O} is the molar concentration of water, provided linear relationships at the several temperatures, as shown in Fig. 5.3. The slope k for NaI was independent of temperature in the range 400 to 800°C, having an average least-squares value of 9.67 ± 0.08. This value of k has been proposed to represent the net change in waters of solvation on ionization of one mole of the electrolyte.[7,8]

Comparative Thermodynamic Behavior of the Alkali Halides

From this and the previous work[2,3] over the entire range of temperature (T) and density (d) studied, the order of association at constant T and d is NaCl > NaBr > NaI. This behavior can be observed from a comparison of both the conventional ionization constants, shown in Fig. 5.2 for NaI and previously for the other

[1] A. S. Quist and W. L. Marshall, *J. Phys. Chem.* 70, 3714 (1966).

[2] A. S. Quist and W. L. Marshall, *J. Phys. Chem.* 72, 684 (1968).

[3] A. S. Quist and W. L. Marshall, *J. Phys. Chem.* 72, 2100 (1968).

[4] A. S. Quist and W. L. Marshall, *J. Phys. Chem.* 72, 1545 (1968).

[5] W. L. Marshall, *Rev. Pure Appl. Chem.* 18, 167 (1968).

[6] L. A. Dunn and W. L. Marshall, "Electrical Conductances of Aqueous Sodium Iodide and the Comparative Thermodynamic Behavior of Aqueous Sodium Halide Solutions to 800°C and 4000 Bars," *J. Phys. Chem.*, in press (1968).

[7] W. L. Marshall and A. S. Quist, *Proc. Natl. Acad. Sci.* 58, 901 (1967).

[8] A. S. Quist and W. L. Marshall, *J. Phys. Chem.* 72, 1536 (1969).

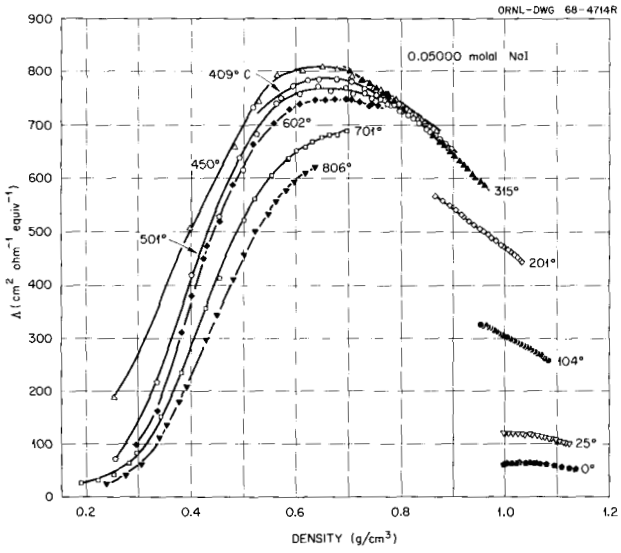

Fig. 5.1. Equivalent Conductances of 0.05000 *m* NaI Solutions as a Function of Density at Several Temperatures.

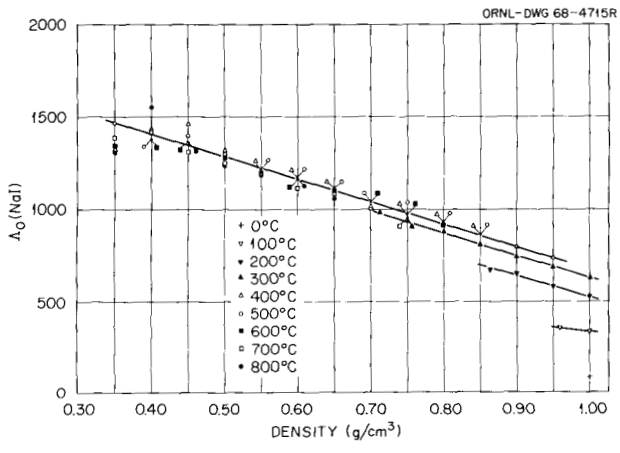

Fig. 5.2. Limiting Equivalent Conductances of NaI as a Function of Density at Temperatures to 800°C.

two halides,[2,3] and the complete constants for the three alkali halides. Thus NaI is the most highly ionized electrolyte, while NaCl is the most highly associated electrolyte, with NaBr occupying an intermediate position. This pattern observed over an extreme range of temperature and density implies that the halogen ion sizes, independent of the degree of hydration, remain in the order $I^- > Br^- > Cl^-$, where the extent of association is expected to be inversely proportional to the ion sizes.

The approximate constancy of k between 400 and 800°C allows a simple comparison of the thermodynamic functions over this range of temperature, since

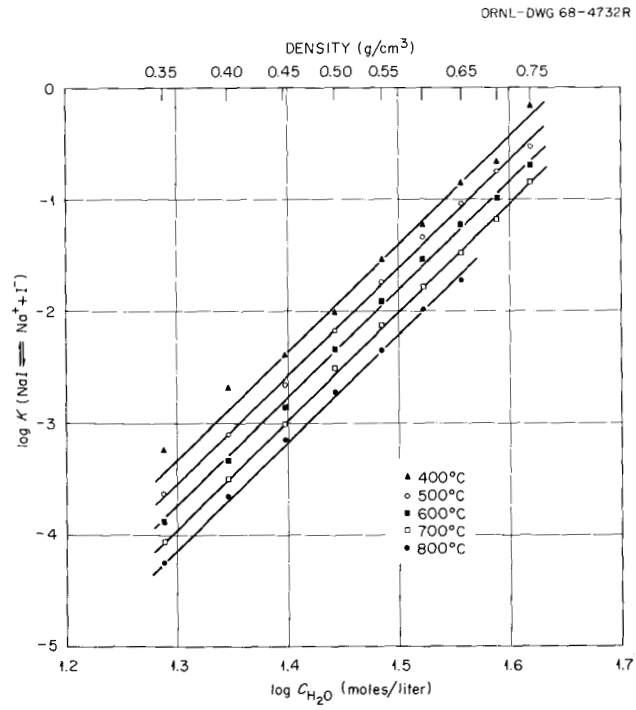

Fig. 5.3. Log K (Molar Units) for the Equilibrium NaI $\rightleftharpoons Na^+ + I^-$ as a Function of the Logarithm of the Molar Concentration of Water at Temperatures from 400 to 800°C.

for each electrolyte the respective equilibrium does not change in stoichiometry. Plots of the log K° data against T^{-1} (°K) are shown in Fig. 5.4 for the three sodium halides. Least-squares analysis of the data indicated an average slope of 1540 for each of the three electrolytes, within the precision of the measurements. This value of the slope yielded a single value of −7.0 kcal/mole for ΔH° for the complete equilibria for the three electrolytes. With this value of ΔH° and the ΔG° values obtained from the K°'s, values for ΔS° for the complete reactions were calculated and were found, within the precision of the measurements, to be independent of both density and temperature (400–800°C). Comparative values for k, ΔH°, and ΔS° are given in Table 5.1 for the three electrolytes. For the complete equilibria,

$$(\partial \ln K^\circ/\partial P)_T = -\Delta V^\circ/RT = 0 . \qquad (2)$$

Thus $\Delta H^\circ = \Delta E^\circ + P\,\Delta V^\circ = \Delta E^\circ$. The negative values of ΔS°, approximately proportional to k, show that increase in solvation upon ionization of the ion pairs provides greater order in the respective systems.

Table 5.1. Thermodynamic Values (ΔH°, ΔS°) and k for the NaCl, NaBr, and NaI Equilibria

Electrolyte	k	ΔH° (kcal/mole)	ΔS° (cal mole^{-1} deg^{-1})
NaCl	10.20 ± 0.15	−7.0 ± 0.7	−88.3 ± 0.1
NaBr	9.94 ± 0.48	−7.0 ± 0.7	−86.2 ± 0.3
NaI	9.67 ± 0.08	−7.0 ± 0.7	−82.9 ± 0.1

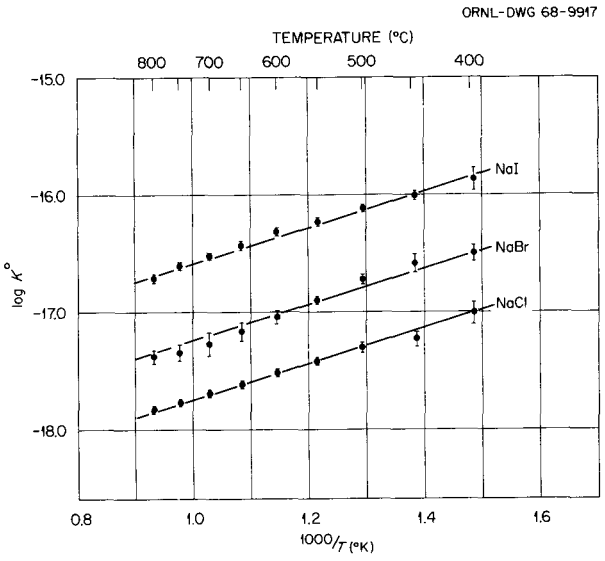

Fig. 5.4. Log K° (Molar Units) for the Equilibrium $NaX(H_2O)_j + kH_2O \rightleftharpoons Na(H_2O)_m^+ + X(H_2O)_n^-$ as a Function of T^{-1} (°K) for NaCl, NaBr, and NaI.

Simple Description of Alkali Halide Behavior

By obtaining complete ionization constants, it has been found that at high temperatures not only does k become constant with temperature and density, but also ΔH° and ΔS°. Since ΔH° is a constant, independent of density and temperature (400–800°C), within the precision of the measurements for all three 1-1 salts, only ΔS° needs to be known for the particular salt in order to specify K° or ΔG°. To specify the fraction ionized at a particular temperature and pressure, we must know the additional single value for k.

The closeness in values of k and ΔS° and the essentially identical value of ΔH° for these three alkali halides suggest that the degree of ionization for most 1-1 salts is approximately identical in this high-temperature range and can be specified approximately by the above relationships and averaged values of ΔS° and k from those in Table 5.1. This nearly identical behavior has been observed from the conductance study of many 1-1 electrolytes,[9] and also in the observed linear relationships of Λ_0 vs density, where the intercept and slope of the equations like Eq. (1) are approximately the same for the several electrolytes studied.[1–3]

The thermodynamic relationships presented might well be expected to exist at pressures approaching zero. With this assumption the fraction of ionization can easily be calculated for cases of immediate applied interest, for example, in geochemistry or pressurized water technology, where pressures of 200 to 400 bars might be the range to be considered. Thus at 200 bars and at 400°C, sodium iodide (and the other 1-1 electrolytes investigated) is an extremely weak electrolyte, showing about the same extent of dissociation as water at 25°C.

THE ELECTRICAL CONDUCTANCES OF SOME ALKALI-METAL HALIDES IN AQUEOUS SOLUTIONS FROM 0 TO 800°C AND AT PRESSURES TO 4000 BARS

A. S. Quist W. Jennings, Jr. W. L. Marshall

Electrical conductance measurements of 0.01 m aqueous solutions of LiCl, NaCl, NaBr, NaI, KCl, KBr, KI, RbF, RbCl, RbBr, RbI, CsCl, CsBr, and CsI from 0 to 800°C and at pressures to 4000 bars have been presented in previous annual reports.[10,11] A paper on this subject is in press[9] that provides the complete information from which the following summary was obtained. Evaluation of the conductance results indicates that in general all these electrolytes exhibit the same type of conductance behavior at elevated temperatures and pressures. Thus at high temperatures, where

[9] A. S. Quist and W. L. Marshall, "The Electrical Conductances of Some Alkali Metal Halides in Aqueous Solutions from 0 to 800°C and at Pressures to 4000 Bars," *J. Phys. Chem.*, in press (1969).

[10] A. S. Quist, W. Jennings, Jr., and W. L. Marshall, *Reactor Chem. Div. Ann. Progr. Rept. Dec. 31, 1967*, ORNL-4229, pp. 88–90.

[11] A. S. Quist, W. Jennings, Jr., and W. L. Marshall, *Reactor Chem. Div. Ann. Progr. Rept. Dec. 31, 1966*, ORNL-4076, pp. 65–66.

most of the long-range structure of water appears to be destroyed, the relative order of the specific conductances of these electrolytes remains constant – except for some instances at the highest temperatures, when association effects appear to change this order. At temperatures below 100°C, comparative changes in the specific conductances of these electrolytes both with temperature and pressure can be correlated with the apparent disruption of the structure of water by the ions, by pressure, and by temperature. Thus these measurements indicate that the simpler behavior observed quantitatively in previous extensive measurements on several electrolytes at high temperatures and pressures[1–4] probably can be extended to include all of the alkali metals. With the exception of KCl,[12] NaCl,[2] and NaBr,[3] to our knowledge these conductances are the first experimental measurements that have been reported for these salts at supercritical temperatures and pressures.

A complete description of the equipment and procedures used for these measurements is contained in a recent paper.[2] A conductance cell having no pressure seals in the high-temperature region was used for all experiments. The precision of the high-temperature (200–800°C), high-pressure measurements for each experimental run was about ±0.7% at the lowest temperatures to ±1–2% at 800°C, with an estimated overall accuracy of ±2% or better. The precision of the measurements for each run at 0–120°C was better than ±0.5%; however, the accuracy may not have been better than ±1–2%.

Comparisons of the isobaric specific conductances of most of the alkali-metal halides, grouped according to anion, are given in Fig. 5.5, where specific conductance is plotted against temperature at a pressure of 4000 bars. This behavior is characteristic of salts of strong acids and bases and can be explained in terms of the

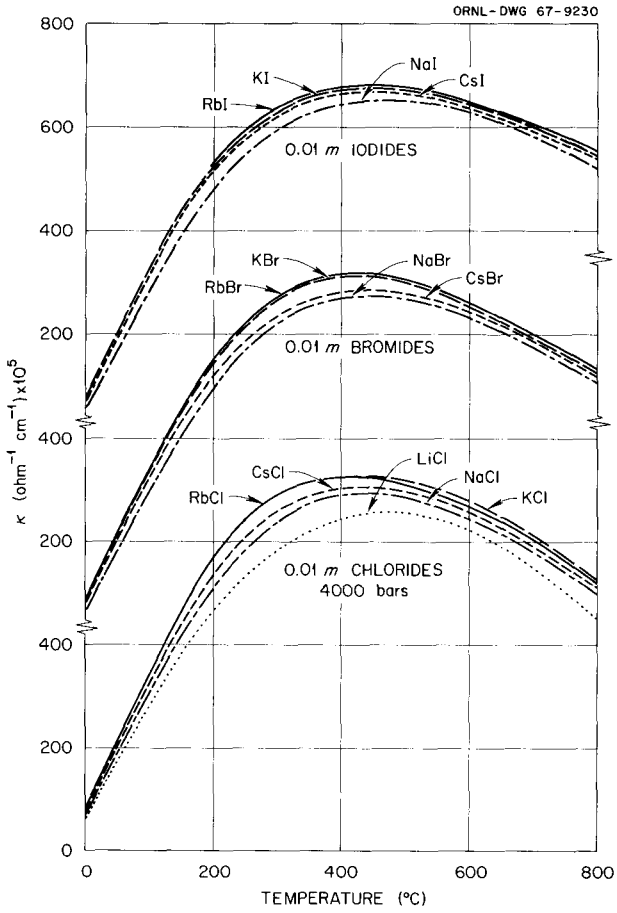

Fig. 5.5. Isobaric Specific Conductances of 0.01000 *m* Aqueous Solutions of Some Alkali Metal Halides as a Function of Temperature. Pressure = 4000 bars.

offset by a decrease in ionic concentration due to density and association effects.

Figure 5.6 illustrates the effect of pressure on the conductances of the alkali-metal chlorides at 25°C.[13]

with previously postulated structure-making and structure-breaking effects of ions as deduced from their viscosity *B* coefficients near room temperature and atmospheric pressure. At elevated temperatures, where there no longer appears to be any significant long-range water structure, the relative behavior of these ions remains constant – under all conditions when cation behavior is compared, and until appreciable but slightly different extents of association occur in the case of anions. Earlier quantitative results on NaCl[2] and NaBr,[3] and recent results on NaI,[6] indicated that the hydration numbers of these ions were unaffected by pressure and temperature from 400 to 800°C and to 4000 bars. Therefore the present measurements indicate that, for all of the alkali-metal halides presently studied, the

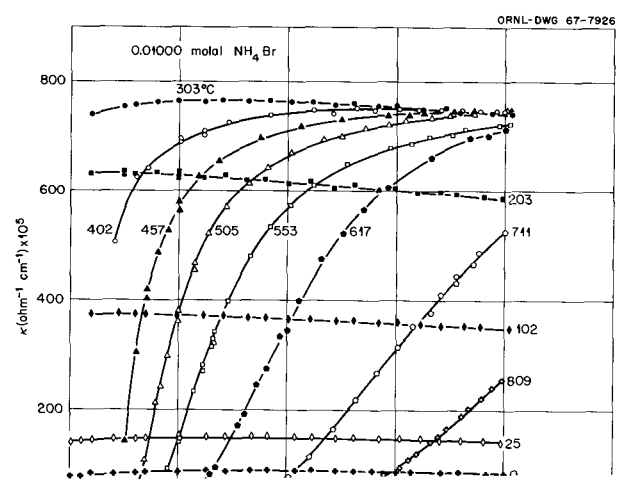

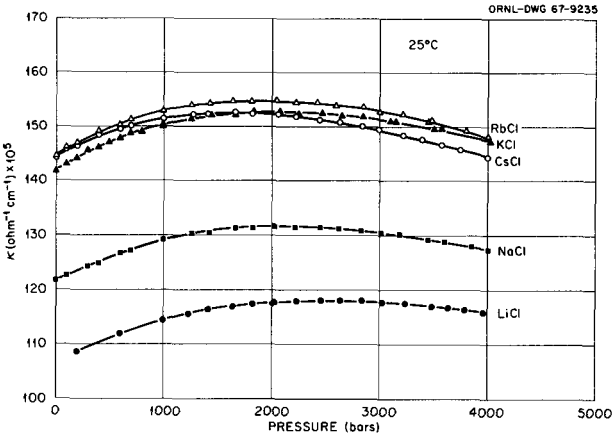

Fig. 5.6. Isothermal Specific Conductances of 0.01000 *m* Alkali Metal Chloride Solutions as a Function of Pressure. Temperature = 25°C.

Stokes and Mills[14] described the cesium ion as having a large disruptive effect on the structure of water in the immediate vicinity of the ion. This structure-breaking effect leads to a reduction in viscosity in the neighborhood of the ion and thus gives the cesium ion a greater mobility than it might be expected to have on the basis of ion size. Since increasing the pressure tends to break up the structure present in liquid water, the cesium ion will have less structure to break at high pressures, and so its "excess" mobility will be diminished. The potassium ion has only a small effect on the structure of water, and therefore the change in its conductance with increasing pressure is close to "normal." Consequently, when the pressure is increased, the conductance of the cesium ion near room temperature will decrease relative to that of the potassium ion, as shown in Fig. 5.6. The rubidium ion is slightly structure breaking (a *B* coefficient midway between K^+ and Cs^+), and therefore it also loses some of its excess mobility with increasing pressure. The conductance of the rubidium ion relative to that of the potassium ion has decreased until they are nearly the same at 4000 bars (Fig. 5.6). The much lower conductances of LiCl and NaCl in Fig. 5.6 probably reflect chiefly a stronger hydration of Li^+ and Na^+ compared with K^+, Rb^+, and Cs^+, with Li^+ being the more strongly hydrated of the two ions.[14]

The relative conductances of the halide anions at elevated temperatures and pressures may be compared with their relative values near room temperature and atmospheric pressure. Aside from small crossovers near 600–700°C at 4000 bars (shown in Fig. 5.5) and 450°C at 1000 bars (not shown), believed to be caused by small differences in association, the order of conductance of the halide ions at elevated temperatures and pressures is

$$Cl^- > Br^- > I^- > F^- .$$

The order at 25°C, 1 atm pressure, is[15]

$$Br^-(78.14) > I^-(76.84) > Cl^-(76.35) > F^-(55.4) ,$$

but at 55°C it has changed to[15]

$$Br^-(127.86) > Cl^-(126.40) > I^-(125.44) > F^- .$$

Let us assume that the normal order, without regard to any influence of the ions on the structure of water, is given by the high-temperature results. Then the order found near 25°C may be explained in relation to the effect of the bromide and iodide ions on the structure of water. Both of these halide ions have negative *B* coefficients, with that of the iodide ion being more negative than that of the bromide ion.[14] Thus both of these ions reduce the viscosity in their vicinity, leading to an excess mobility for these ions. The *B* coefficients become more positive with increasing temperature, indicating the diminution of this effect at higher temperatures and an approach to more normal behavior. This approach to normality occurs because the structure of water is destroyed by increasing temperature, and consequently these ions have less or very little structure to break. Thus the iodide ion, with the larger excess mobility, has reached its normal position in the ranking of the halide ions when a temperature of 55°C has been attained, but higher temperatures (and greater disruption of the water structure) are required in order that the mobility of the chloride ion will exceed that of the bromide ion.

Further discussion of the various effects of pressure and temperature on the relative conductances of alkali-metal halides is given in the complete paper.[9] In summary, by comparing the effect of pressure on alkali-metal halide conductances at 0 and 25°C, it appears that most of the long-range structure of water has been destroyed by the time pressures of 4000 bars have been reached. These pressure effects at 0 and 25°C, as well as the relative changes in conductance with increasing temperature, appear to be consistent

[14] R. H. Stokes and R. Mills, *Viscosity of Electrolytes and Related Properties,* Pergamon, Oxford, England, 1965.

[15] R. A. Robinson and R. H. Stokes, *Electrolyte Solutions,* 2d ed., revised, p. 465, Butterworth, London, 1965.

with previously postulated structure-making and structure-breaking effects of ions as deduced from their viscosity B coefficients near room temperature and atmospheric pressure. At elevated temperatures, where there no longer appears to be any significant long-range water structure, the relative behavior of these ions remains constant – under all conditions when cation behavior is compared, and until appreciable but slightly different extents of association occur in the case of anions. Earlier quantitative results on NaCl[2] and NaBr,[3] and recent results on NaI,[6] indicated that the hydration numbers of these ions were unaffected by pressure and temperature from 400 to 800°C and to 4000 bars. Therefore the present measurements indicate that, for all of the alkali-metal halides presently studied, the ion-solvent interactions remain constant in the temperature region 400 to 800°C.

ION PRODUCT OF WATER TO 800°C FROM ELECTRICAL CONDUCTANCE BEHAVIOR OF AMMONIUM BROMIDE SOLUTIONS AND RELATED ELECTROLYTES

A. S. Quist W. Jennings, Jr. W. L. Marshall

The conductance behavior of many alkali-metal halides,[2,3,6,9] some acids (H_2SO_4,[16] HBr[4]), a neutral salt (K_2SO_4),[17] an acidic salt ($KHSO_4$),[1] and a weak base (NH_4OH)[18] have been investigated in this program at temperatures from 0 to 800°C and at pressures from 1 to 4000 bars. These studies have led to a better understanding of the behavior of electrolyte solutions at high temperatures and pressures. In order to provide a wider spectrum of information, the conductance behavior of aqueous ammonium bromide solutions was studied over the same range of temperature and pressure. An example of the specific conductances obtained for 0.01 m NH_4Br is shown in Fig. 5.7. These values were converted to equivalent conductances by the methods described previously[2] and are shown as a function of density in Fig. 5.8 for comparison. Measurements were also made on 0.002008, 0.00508, and 0.01500 m solutions.

A comparison of the specific conductances of a 0.01 m NH_4Br solution with those of NaBr,[3] HBr,[4] and NH_4OH[18] solutions is given in Fig. 5.9 as a function of

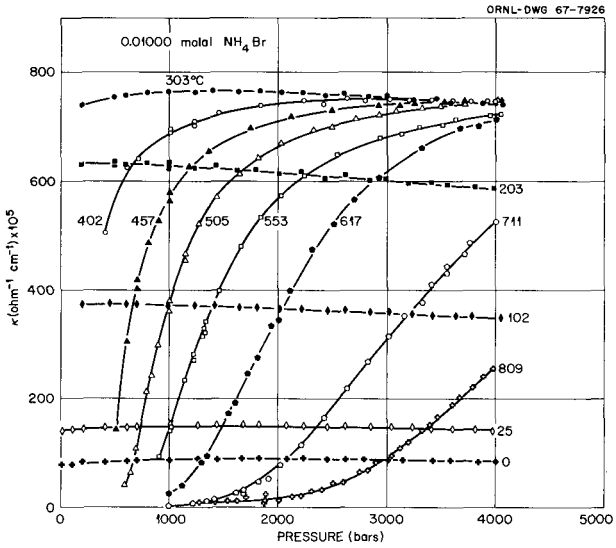

Fig. 5.7. Specific Conductances of 0.01000 m NH_4Br Solutions as a Function of Pressure at Several Temperatures.

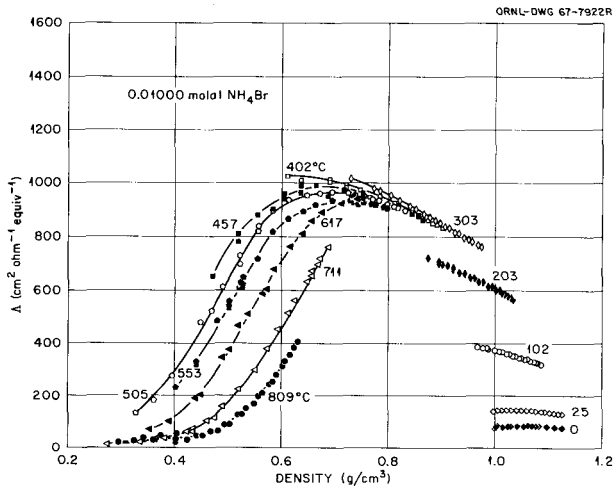

Fig. 5.8. Equivalent Conductances of 0.01000 m NH_4Br Solutions as a Function of Density at Several Temperatures.

temperature at a pressure of 4000 bars. At high temperature, the ammonium ion hydrolyzes extensively according to the following reaction:

$$NH_4^+ + xH_2O \rightleftharpoons NH_3 + H(H_2O)_x^+ .$$

Under conditions where there is insignificant association of hydrogen ions and bromide ions, the extent of hydrolysis is indicated by an increase in conductance over that expected for an unhydrolyzed ammonium bromide solution. This increase is a result of replacing

[16] A. S. Quist, W. L. Marshall, and H. S. Jolley, *J. Phys. Chem.* 69, 2726 (1965).

[17] A. S. Quist *et al.*, *J. Phys. Chem.* 67, 2453 (1963).

[18] A. S. Quist and W. L. Marshall, *J. Phys. Chem.* 72, 3122 (1968).

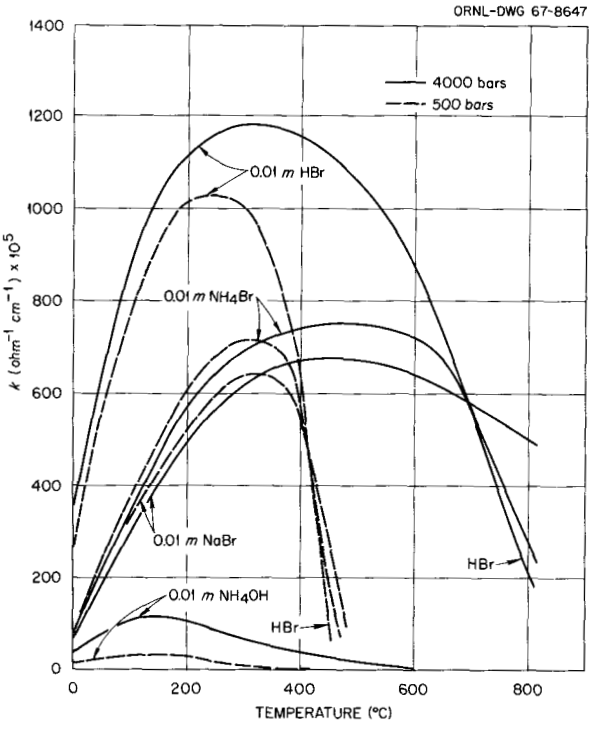

Fig. 5.9. Comparison of the Specific Conductances of 0.01 *m* HBr, NaBr, NH_4Br, and NH_4OH Solutions as a Function of Temperature at Pressures of 500 and 4000 bars.

ammonium ions by the more mobile protons. At higher temperatures, there is considerable association of hydrogen ions and bromide ions.[4] This behavior is qualitatively observed in Fig. 5.9 at temperatures above 600°C.

From these measurements on 0.01 *m* NH_4Br solutions and by using the conductances and ionization constants reported earlier for HBr,[4] NH_4OH,[18] NaBr,[3] and KBr[9] solutions, it was possible to calculate the ion product of water from 300 to 800°C and at densities from 0.45 to 0.90 g/cm^3. These values are given in Table 5.2 and represent the first reported values of K_w at these temperatures and densities as determined from experimental measurements.

Table 5.2. Negative Logarithms of the Thermodynamic Ionization Constant of Water (Molar Concentrations) at Several Temperatures and Densities

Density (g/cm^3)	Temperature (°C) 300	400	500	600	700	800
0.45			13.40	13.12	12.70	
0.50			12.51	12.39	12.00	11.68
0.55			11.80	11.66	11.28	10.98
0.60				10.96	10.54	10.36
0.65				10.14	9.70	
0.70		10.73			9.58	
0.75		10.16				
0.80		9.73				
0.85	9.43	9.25				
0.90	9.16	8.97				

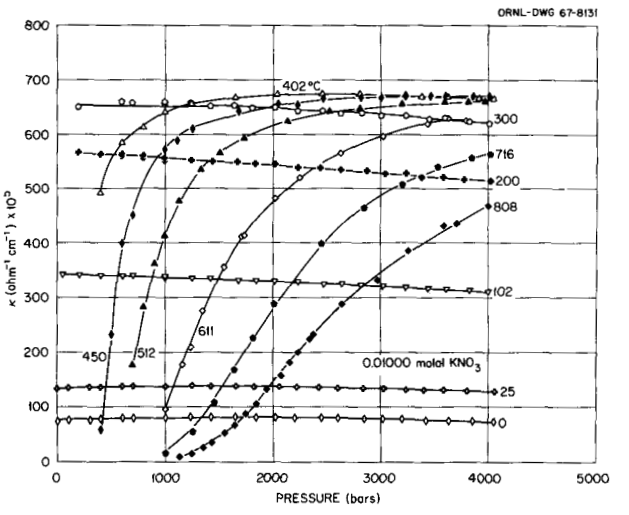

Fig. 5.10. Specific Conductances of 0.01000 *m* Solutions of KNO_3 as a Function of Pressure at Several Temperatures.

ELECTRICAL CONDUCTANCES OF 0.01 *m* KNO_3 SOLUTIONS TO 800°C AND 4000 BARS

A. S. Quist W. Jennings, Jr. W. L. Marshall

In connection with our experimental studies of the behavior of aqueous electrolyte solutions at high temperatures and pressures, it was of interest to measure the conductances of a 0.01 *m* potassium nitrate solution to 800°C and 4000 bars and to compare its behavior with that previously observed with other potassium halide solutions. This comparison would indicate whether or not extensive hydrolysis or decomposition of the nitrate ion occurred under these conditions. The results of these measurements are shown in Fig. 5.10, where the specific conductances of this solution are plotted as a function of pressure at the various temperatures of the experimental measurements. Figure 5.11 shows a comparison of the specific conductances of 0.01 *m* KNO_3 and KCl[11] solutions as a function of temperature at a pressure of 4000 bars. The behavior of these two electrolytes seems to be qualitatively very similar, indicating no unusual behavior (hydrolysis or decomposition) of KNO_3 under these conditions.

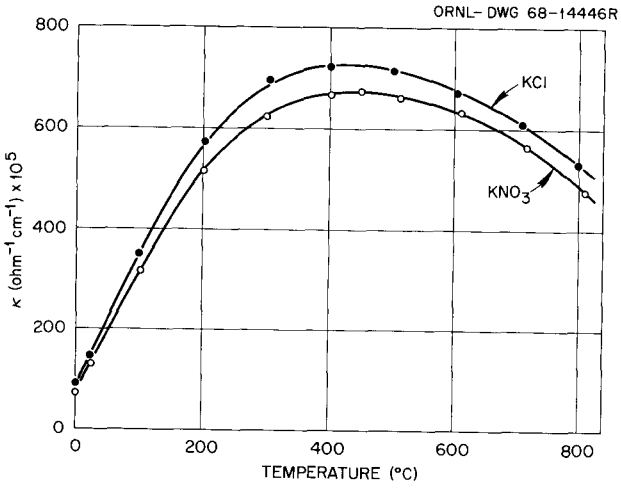

Fig. 5.11. Comparison of the Specific Conductances of 0.01 *m* KNO_3 and KCl Solutions as a Function of Temperature at a Pressure of 4000 Bars.

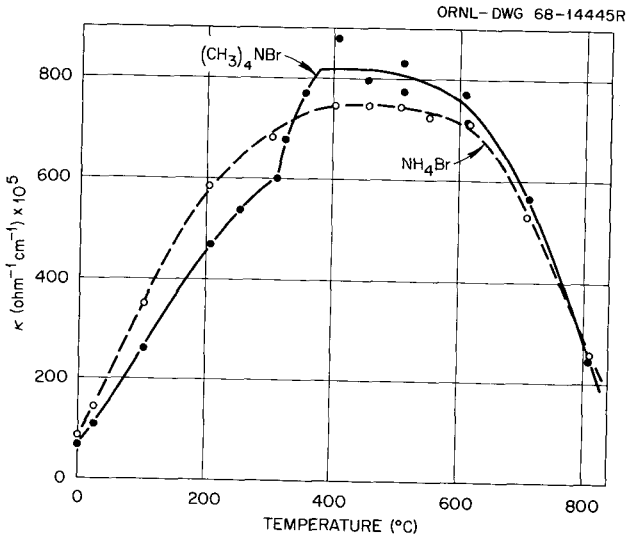

Fig. 5.12. Comparison of the Specific Conductances of 0.01 *m* $(CH_3)_4NBr$ and NH_4Br Solutions as a Function of Temperature at a Pressure of 4000 Bars.

ELECTRICAL CONDUCTANCES OF 0.01 *m* AQUEOUS $(CH_3)_4NBr$ SOLUTIONS TO 800°C AND 4000 BARS

A. S. Quist W. Jennings, Jr.

The electrical conductances of 0.01 *m* aqueous solutions of tetramethylammonium bromide have been measured to 800°C and 4000 bars and were compared with those obtained previously for other electrolytes. A comparison of the specific conductances of $(CH_3)_4NBr$ with those of NH_4Br as a function of temperature at a pressure of 4000 bars is given in Fig. 5.12. Below 300°C the conductance of $(CH_3)_4NBr$ is considerably less than that of NH_4Br, primarily because of the larger size of the tetramethylammonium ion as compared with the ammonium ion. Above approximately 300°C, the conductance of the tetramethylammonium salt increases rapidly, indicating extensive decomposition or hydrolysis of this ion. Although the results are somewhat erratic in the temperature range 400–600°C, the conductance of the $(CH_3)_4NBr$ solution is essentially the same as that of the NH_4Br solution at higher temperatures. This perhaps indicates that the products of the hydrolysis of the tetramethylammonium ion are likely to be four molecules of CH_3OH and the NH_4^+ ion.

6. Physical Chemistry of High-Temperature Aqueous Solutions

EQUILIBRIUM QUOTIENTS AT 25°C FOR $CaSO_4$ IN SEVERAL AQUEOUS MIXED-ELECTROLYTE SOLUTIONS

L. B. Yeatts W. L. Marshall

A study[1-3] of the system $CaSO_4$-Na_2SO_4-$NaNO_3$-H_2O led to the conclusion that the activity coefficients of Ca^{2+}, SO_4^{2-}, and $CaSO_4^0$ are apparently constant as the $Na_2SO_4/NaNO_3$ ratio is varied widely at constant ionic strengths (I) that range from 0.25 to 6 over the temperature range 0 to 350°C. This unusual result led us to question the uniqueness of the particular system and then to investigate the solubility of calcium sulfate in other alkali-metal salt solutions for comparison. Reported here are the results for the four systems $CaSO_4$-Na_2SO_4-$NaNO_3$-H_2O, $CaSO_4$-Na_2SO_4-NaCl-H_2O, $CaSO_4$-Li_2SO_4-$LiNO_3$-H_2O, and $CaSO_4$-Li_2SO_4-LiCl-H_2O determined at 25° and ionic strengths of approximately 0.5, 2, and 6.

Again, the postulated solubility equilibria[4] are

$$CaSO_4(s) \overset{Q_u}{\rightleftharpoons} CaSO_4^0(aq) \tag{1}$$

and

$$CaSO_4^0 \overset{Q_d}{\rightleftharpoons} Ca^{2+} + SO_4^{2-} ; \tag{2}$$

so that the net equilibrium is

$$CaSO_4(s) \overset{Q_{isp}}{\rightleftharpoons} Ca^{2+} + SO_4^{2-} . \tag{3}$$

Here Q_u, Q_d, and Q_{isp} are equilibrium quotients, where Q_u = molality of $CaSO_4^0$ and $Q_{isp} = Q_d Q_u$. Therefore the analytical molality of total dissolved calcium, s, can be expressed as

$$s = [CaSO_4^0] + [Ca^{2+}] \tag{4}$$

$$= Q_u + Q_d Q_u/(\text{total sulfate} - Q_u) \tag{5}$$

$$= Q_u + Q_{isp}/[SO_4^{2-}] . \tag{6}$$

In Figs. 6.1 to 6.3 the solubility data at the three different ionic strengths are plotted as a function of $1/[SO_4^{2-}]$ to test the validity of Eq. (6). The straight lines determined by a method of least squares are seen to fit the experimental results well in all cases. Calculated values for Q_u (the intercept) and Q_{isp} (the slope) are listed in Table 6.1 for each set of measurements; included here also are the corresponding Q_d values. The data for a given line in Fig. 6.1 show the changing solubility of calcium sulfate dihydrate in mixed-electrolyte solutions at I = 0.5 as the electrolyte solution composition is varied from alkali-metal sulfate, at the left, through alkali-metal sulfate + 1-1 electrolyte, to the 1-1 electrolyte solution, on the right. At the latter points the solubilities among the four systems vary 5% at most. The average values for Q_u, Q_{isp}, and Q_d at I = 0.5 would adequately describe any of the four systems in most instances (see Table 6.1 also). However, at I = 2.1 and particularly at I = 6.0, large differences in the solubilities at constant SO_4^{2-} appear among the systems (see Figs. 6.2 and 6.3). The solubilities of the dihydrate at constant I and SO_4^{2-} are nearly the same for the two nitrate systems and much greater in the presence of nitrate than chloride. In contrast to the nitrate systems, the sodium chloride system dissolves markedly more dihydrate at these ionic strengths than does the corresponding lithium chloride system. Furthermore, as the ionic strength increases from 0.5 to 6.0, the solubilities in the two nitrate systems increase

[1] L. B. Yeatts and W. L. Marshall, *Reactor Chem. Div. Ann. Progr. Rept. Dec. 31, 1966*, ORNL-4076, pp. 68–70.

[2] L. B. Yeatts and W. L. Marshall, *Reactor Chem. Div. Ann. Progr. Rept. Dec. 31, 1967*, ORNL-4229, pp. 92–95.

[3] L. B. Yeatts and W. L. Marshall, *J. Phys. Chem.* 73, 81 (1969).

[4] The equilibrium quotients are expressed in molal units; hence the constant value for the molality of water was not used to calculate the quotients presented here. For this reason, also, equilibria (1) and (3) are not written in terms of the stable solid phase $CaSO_4 \cdot 2H_2O$. See ref. 3 for further discussion of this point.

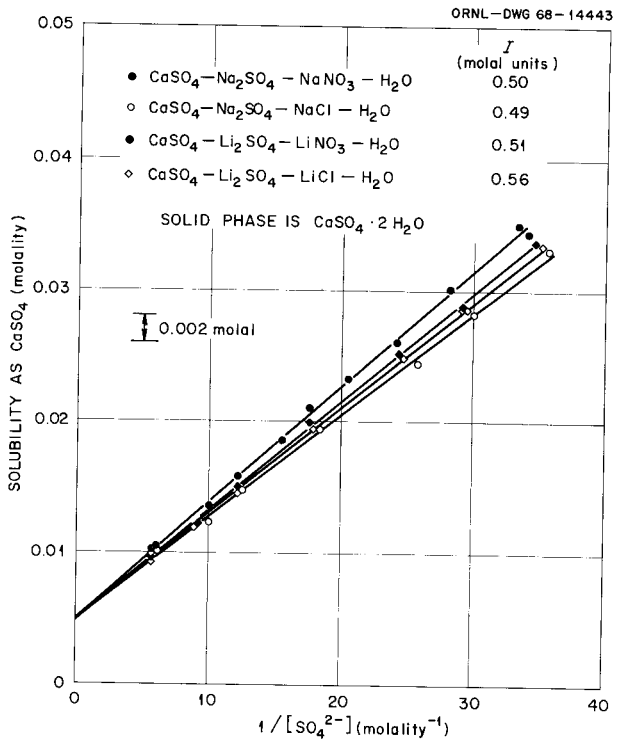

Fig. 6.1. Solubility of $CaSO_4 \cdot 2H_2O$ in Mixed Electrolytes at 25°C and at an Ionic Strength (I) of 0.5.

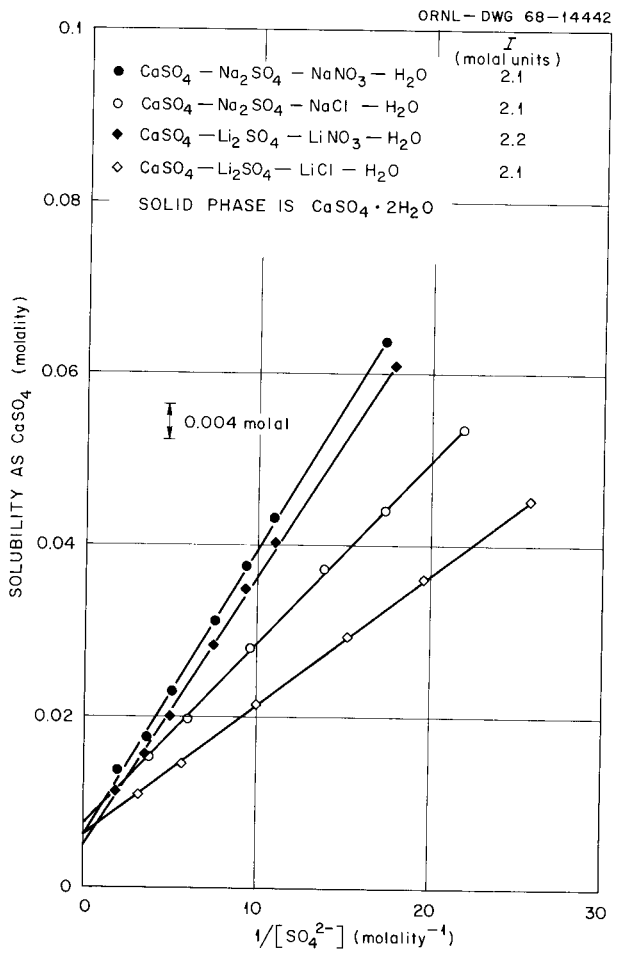

Fig. 6.2. Solubility of $CaSO_4 \cdot 2H_2O$ in Mixed Electrolytes at 25°C and an Ionic Strength (I) of 2.

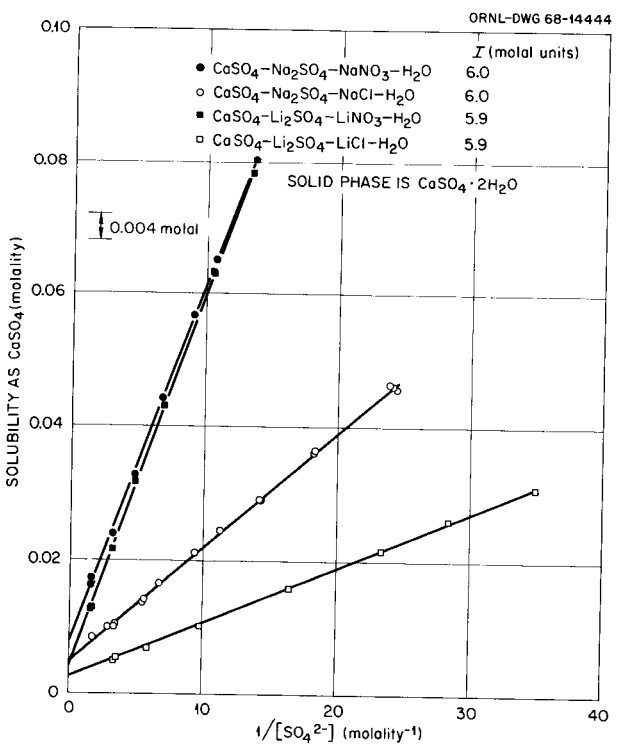

Fig. 6.3. Solubility of $CaSO_4 \cdot 2H_2O$ in Mixed Electrolytes at 25°C and an Ionic Strength (I) of 6.

Table 6.1. Equilibrium Quotients at 25°C for $CaSO_4$ in Several Aqueous Mixed-Electrolyte Systems

Mixed Electrolyte	$I = 0.5$			$I = 2.1$			$I = 6.0$		
	Q_u	Q_{isp}	Q_d	Q_u	Q_{isp}	Q_d	Q_u	Q_{isp}	Q_d
	$\times 10^{10-3}$	$\times 10^{-4}$		$\times 10^{-3}$	$\times 10^{-3}$		$\times 10^{-3}$	$\times 10^{-3}$	
Na_2SO_4-$NaNO_3$	5.08	8.80	0.173	6.07	3.32	0.547	7.28	5.38	0.739
Na_2SO_4-NaCl	5.14	7.74	0.150	7.42	2.10	0.283	4.73	1.72	0.363
Li_2SO_4-$LiNO_3$	4.81	8.34	0.174	4.91	3.14	0.639	3.43	5.68	1.65
Li_2SO_4-LiCl	4.99	8.02	0.161	6.20	1.51	0.243	2.23	0.827	0.371

steadily, but in the chloride system they decrease in going from $I = 2.1$ to $I = 6.0$. In fact, the solubilities of dihydrate in the lithium sulfate–lithium chloride system at $I = 6.0$ are lower than at $I = 0.5$ when the SO_4^{2-} concentration is constant. Although the interpretation of these results is incomplete at this time, it certainly appears that the effect of the uncommon anion upon the solubility is the dominating factor to be considered.

SOLUBILITY OF Fe_3O_4 AT ELEVATED TEMPERATURES

F. H. Sweeton R. W. Ray C. F. Baes, Jr.

The previously reported data[5] on the solubility of Fe_3O_4 in acid and basic solutions has been extended by some additional measurements at the relatively low temperatures of 50, 100, and 150°C and at the relatively high KOH concentration of about 400 μm. By means of least-squares fitting procedures,[6] various schemes of complexes have been fitted to the accumulated Fe_3O_4 solubility data. The reaction by which a species is formed was written:

$$\tfrac{1}{3}Fe_3O_4(s) + (2-b)H^+ + \tfrac{1}{3}H_2(g) = Fe(OH)_b^{(2-b)+} + (\tfrac{4}{3} - b)H_2O \,. \quad (7)$$

The equilibrium constant K_b for this reaction is

$$K_b = \frac{[Fe(OH)_b^{(2-b)+}]}{[H^+]^{(2-b)}\, P_{H_2}^{1/3}} \,. \quad (8)$$

The standard heat and entropy changes associated with this reaction were expressed in terms of parameters A, B, and D:

$$\Delta H_b^\circ = A_b + B_b T \,, \quad (9)$$

$$\Delta S_b^\circ = B_b \ln T + D_b \,, \quad (10)$$

where T is the absolute tempeature, on the assumption that ΔC_p of reaction ($= B_b$) is independent of temperature. The corresponding expression for log K_b, expressed in molal concentrations and atmospheric pressure, is

$$\log K_b = \frac{1}{2.303 \cdot R}\left[-\frac{A_b}{T} + B_b(\ln T - 1) + D_b\right] . \quad (11)$$

The schemes we have tried have involved only species containing one iron atom, since the concentration of iron in solution was always less than 100 μm. The two cationic species Fe^{2+} and $FeOH^+$ were both included in all schemes tried, since each was needed to explain the data for the acid solutions. One additional species, $Fe(OH)_2^0$, $Fe(OH)_3^-$, or $Fe(OH)_4^{2-}$, was essential to fit the data in the alkaline region, but a significant improvement in fit was obtained by going to a four-species scheme that included $Fe(OH)_2^0$ and either $Fe(OH)_3^-$ or $Fe(OH)_4^{2-}$. Since the fit of the data was found to be insensitive to the value of ΔS_0° for Fe^{2+} at 25°C, the parameters for this ion have been restricted to values corresponding to a ΔS_0° at 25° of −25.3 cal deg^{-1} mole^{-1}, which is consistent with the literature values of S° for the reactants and products, including a new value[7] of −25.6 cal deg^{-1} mole^{-1} for $S^\circ(Fe^{2+})$. The $Fe(OH)_3^-$ species has been chosen in preference to

[5] F. H. Sweeton, R. W. Ray, and C. F. Baes, Jr., *Reactor Chem. Div. Ann. Progr. Rept. Dec. 31, 1967,* ORNL-4229, pp. 84–86.

[6] W. R. Busing and H. A. Levy, *ORGLS, a General Fortran Least Squares Program,* ORNL-TM-271 (Aug. 7, 1962).

[7] J. W. Larson *et al., J. Phys. Chem.* 72, 2902 (1968).

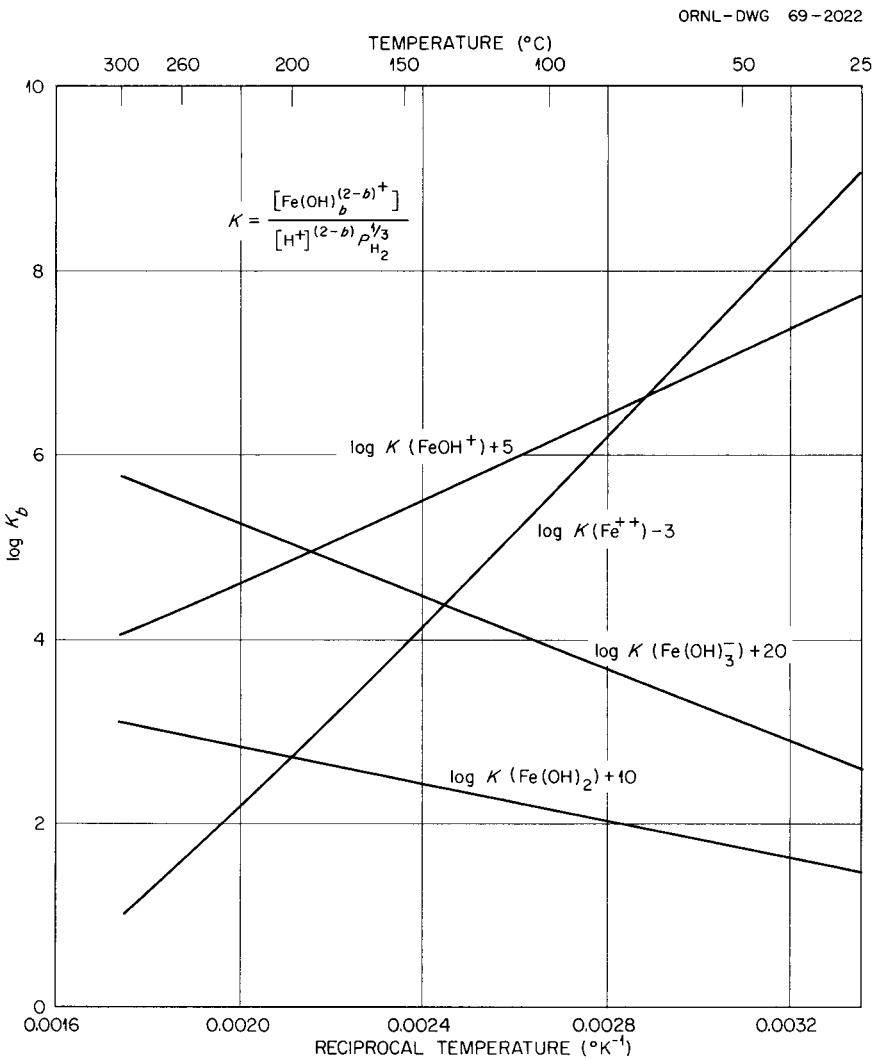

Fig. 6.4. Least-Squares Fit of Fe_3O_4 Data by Fe^{2+}-$FeOH^+$-$Fe(OH)_2{}^0$-$Fe(OH)_3^-$ Scheme.

Table 6.2. Values of Parameters After Least-Squares Fit to Fe_3O_4 Solubility Data

Species	Parameter Values		
	A	*B*	*D*
Fe^{2+}	−26876	9.812	−81.206
$FeOH^+$	−11733	3.3545	−42.723
$Fe(OH)_2{}^0$	+4615	0[a]	−23.575
$Fe(OH)_3^-$	+9045	0[a]	−49.366

[a]Not allowed to vary during least-squaring.

$Fe(OH)_4{}^{2-}$ because it is immediately next in sequence after the other three species.

The values of the fitted parameters for the species of the preferred scheme are given in Table 6.2, and the corresponding values of $\log K_b$ are plotted in Fig. 6.4 as a function of temperature.

Calculation of Thermodynamic Quantities for Fe^{2+} and $FeOH^+$

By combining the solubility data with other data in the following way we can calculate the thermodynamic quantities for the formation of Fe^{2+} and $FeOH^+$:

Table 6.3. Thermodynamic Quantities for Formation of Fe^{2+} and $FeOH^+$ by Eq. (15)

Temperature (°C)	Fe^{2+}			$FeOH^+$		
	ΔF° (cal/mole)	ΔH° (cal/mole)	ΔS° [cal mole^{-1} (°C)$^{-1}$]	ΔF° (cal/mole)	ΔH° (cal/mole)	ΔS° [cal mole^{-1} (°C)$^{-1}$]
25	−21929	−21825	(+0.3)[a]	−9214	−8678	+1.8
100	−21896	−22269	−1.0	−9251	−9549	−0.8
150	−21855	−22109	−0.6	−9203	−9709	−1.2
200	−21834	−21976	−0.3	−9134	−9890	−1.6
250	−21831	−21726	+0.2	−9050	−9992	−1.8
300	−21855	−21339	+0.9	−8963	−9994	−1.8

[a] ΔS° for formation of Fe^{2+} by solution of Fe_3O_4 was set to be −25.3 cal/mole.

$$\tfrac{1}{3}Fe_3O_4(s) + (2-b)H^+ + \tfrac{1}{3}H_2(g) = Fe(OH)_b^{(2-b)+} + (\tfrac{4}{3}-b)H_2O(l) \quad (12)$$

$$Fe(s) + \tfrac{4}{3}H_2O(g) = \tfrac{1}{3}Fe_3O_4(s) + \tfrac{4}{3}H_2(g) \quad (13)$$

$$\tfrac{4}{3}H_2O(l) = \tfrac{4}{3}H_2O(g) \quad (14)$$

$$Fe(s) + (2-b)H^+ + bH_2O(l) = Fe(OH)_b^{(2-b)+} + H_2(g) \quad (15)$$

The equilibrium of the second reaction has been determined by Emmett and Shultz[8] and by Fricke, Walter, and Lohrer.[9] We have taken $\Delta G^\circ = -4150$ cal/mole at 400°C as an average of their results. Combining this with our values of ΔG° for reaction (12) and table values of the changes with temperature of ΔG° for the various reactants and products of reactions (13) and (14), we obtain the values shown in Table 6.3 for ΔG° for the formation of Fe^{2+} and $FeOH^+$ by Eq. (15). Our result at 25°C is equivalent to an $E^\circ(Fe^{2+})$ of 0.475 v, which is in good agreement with $0.47_3 \pm 0.010$ v calculated recently by Larson *et al.*[7] and 0.467 v obtained by Hurlen[10] using voltage-current measurements. Randall and Frandsen[11] and Patrick and Thompson[12] found considerably lower values (0.440 and 0.409 v respectively) by direct measurement in sealed cells using iron electrodes, but we believe that their results are probably low because of a spontaneous reaction of the iron with the water.

The values of ΔS° listed in Table 6.3 for the formation of Fe^{2+} and $FeOH^+$ by Eq. (15) have been determined by reading the slopes of ΔG_f° against temperature. The values of ΔH° listed in the table were calculated from the ΔG° and ΔS° values.

Hydrolysis of the Fe^{2+} Ion at 25°C

The $\log K_h$ for the hydrolysis of Fe^{2+} ion,

$$Fe^{2+} + H_2O = FeOH^+ + H^+, \quad (16)$$

has been variously reported[13,14] to be anywhere between −6.7 and −9.5, and because of this we have made some tests to determine it directly at 25°C. We measured the conductance of an iron solution generated in our solubility system by pumping pure H_2O through a column of Fe_3O_4 held at 150°C. The solution, after being cooled to 25°C, flowed through a conductivity cell, through a pH cell containing platinum and calomel electrodes, and finally through a cation exchanger column, where the iron was collected for analysis. We could not use the pH cell data to determine the hydrolysis, as planned, because of O_2 contamination through the seals of the cell; the oxygen in only 0.05 ml of air was sufficient to completely oxidize and precipitate the Fe^{2+} ion in 1 liter of our solution. From the measured conductivity we calculated the extent of hydrolysis by algebraically determining the relative

[8] P. H. Emmett and J. F. Shultz, *J. Am. Chem. Soc.* 55, 1376 (1933).

[9] R. Fricke, K. Walter, and W. Lohrer, *Z. Elektrochem.* 47, 487 (1941).

[10] Tor Hurlen, *Acta Chem. Scand.* 14, 1533 (1960).

[11] Merle Randall and Mikkel Frandsen, *J. Am. Chem. Soc.* 54, 47 (1932).

[12] W. A. Patrick and W. E. Thompson, *J. Am. Chem. Soc.* 75, 1184 (1953).

[13] B. O. A. Hedstrom, *Arkiv Kemi* 5, 457 (1953).

[14] N. Lofman, *Z. Anorg. Allgem. Chem.* 107, 241 (1919); D. L. Leussing and I. M. Kolthoff, *J. Am. Chem. Soc.* 75, 2476 (1953); K. H. Gayer and L. Woontner, *J. Am. Chem. Soc.* 78, 3944 (1956); J. A. Bolzan and A. J. Arvia, *Electrochim. Acta* 8, 375 (1963).

concentration of Fe^{2+} and $FeOH^+$ (together with their corresponding OH^- ions) necessary to explain the observed conductivity. We used 55 mho-cm^2 as the equivalent conductivity for both the Fe^{2+} and $FeOH^+$ ions, estimating this value from data for the Co^{2+} ion, and 198 for the OH^- ion. The calculated $\log K_h$ for five tests averaged -8.4_5 and varied between -8.0 and -8.6.

The value of $\log K_h$ at 25°C from the Fe_3O_4 solubility determinations is $\log K_1 - \log K_0$ and amounts to -9.3. As a result of these two methods of determination we believe the best value of $\log K_h$ with zero ionic strength is -9.1 with an estimated uncertainty of 0.5.

Our value of $\log K_h$ agrees with the most negative of the reported values[13] but is more negative than the rest.[14] We believe the more negative values are to be preferred because hydrolyzable impurities, a likely source of error in such determinations, act in the positive direction.

FLUORIDE COMPLEXES OF BERYLLIUM(II) IN AQUEOUS MEDIA[15]

R. E. Mesmer C. F. Baes, Jr.

The investigation of the fluoride complexing behavior of beryllium(II), described previously, has been completed.[16] These complexes are uniquely stable among the fluoride complexes of divalent cations, and precise equilibrium measurements in this system over a range of temperature permit an interesting examination of the separate contributions of the entropy and enthalpy changes to the stability of each successive complex.

Previous equilibrium studies in this system, largely confined to 25°, have led to rather discordant results; for example, values reported for $\log Q_1$ for the first stepwise formation reaction range from 5.89 to 3.64. This lack of accord may be attributed mainly to the difficulties of the several indirect methods of measurement used for the studies of fluoride complexing. Until now the most widely used and probably the most reliable such method has been that first employed by Brosset and Orring,[17] who used the ferric-ferrous electrode as an indirect measure of the fluoride ion activity.

[15] R. E. Mesmer and C. F. Baes, Jr., *Inorg. Chem.*, in press (1968).

[16] R. E. Mesmer and C. F. Baes, Jr., *Reactor Chem. Div. Ann. Progr. Rept. Dec. 31, 1967*, ORNL-4229, pp. 96–97.

[17] C. Brosset and G. Orring, *Svensk. Kem. Tidskr.* 55, 101 (1943).

ORNL-DWG 68-6883

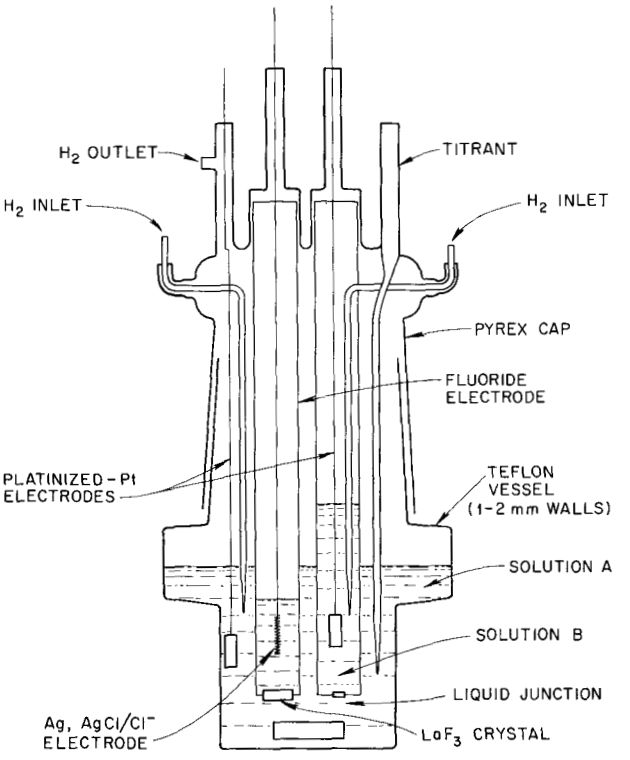

Fig. 6.5. Sketch of Potentiometric Cell.

In the present study we employed the recently developed lanthanum fluoride solid-state electrode, demonstrating it to be a suitable fluoride-ion reversible electrode for precise physical chemical measurements. Hydrogen electrodes, as indicator and reference electrodes, were also included in the cells used so that the hydrogen ion concentration as well as the fluoride concentration could be followed directly. The apparatus illustrated in Fig. 6.5 consisted of a Teflon vessel with a Pyrex cap constructed with several ground glass inlets for introducing the hydrogen gas, the titrant, and the electrode leads. The cell representations in 1 *m* NaCl are given below:

	Solution A	Solution B	
LaF_3	$(1 - 2a)$ *m* NaCl	$(1 - d)$ *m* NaCl	
and	*a m* $BeCl_2$	*d m* HCl	H_2,Pt
	b m HF		
Pt,H_2	*c m* NaF		

The internal Ag, $AgCl/Cl^-$ electrode of the LaF_3 electrode (Orion model 94-09) is not represented. The liquid junction (Fig. 6.5) was a porous Teflon plug compressed to produce a satisfactorily low flow rate (about 0.002 g per centimeter head of water per hour).

Most of the measurements of beryllium fluoride complex stability in this study were conducted in acidity ranges where the fluoride ion itself becomes protonated to some extent. Precise determination of the hydrogen fluoride equilibria in similar media is therefore essential to the correct analysis of the data. The beryllium, fluoride, and hydrogen ion concentrations were varied over wide ranges to identify the significant species of type

$$Be_xF_y(OH)_z^{(2x-y-z)+} ,$$

where z can be positive or negative, representing complexes containing hydroxide ions or hydrogen ions (as would be the case if HF or HF_2^- were a ligand). In experiments at 25°C in 1 m NaCl the concentration ranges investigated were: beryllium concentrations from 2×10^{-4} to 1.7×10^{-2} m, total fluoride concentrations from 6×10^{-4} to 4.4×10^{-2} m, and free fluoride concentrations from 1.6×10^{-6} to 1.0×10^{-2} m. The maximum value of $\bar{n}$ obtained was 3.46.

Figure 6.6 shows clearly that x, the number of beryllium ions in the complexes, is unity since for polynuclear complexes a series of approximately parallel curves for different beryllium ion concentrations is expected. This conclusion is also verified by the excellent fit of all the data at the three temperatures to the curves which were calculated for schemes containing only mononuclear species. The complete absence of fluoride bridges is surprising in view of the strong tendency of OH^- to form bridges in aqueous solution.

The absence of OH^- or ligands containing hydrogen ions was very sensitively determined in experiments carried out in which $BeCl_2$ or $Be(ClO_4)_2$ solutions (with very small amount of free acid present) were added to approximately neutral sodium fluoride solutions in the 1 m chloride or perchlorate media. Under these conditions, any small amount of bound OH^- or H^+ would have produced an easily detectable change in pH. The small pH changes which occurred vividly illustrate that at $\bar{n} \geqslant 1.5$ the amount of hydroxide complexed is less than 0.5% of the beryllium complexed. These data, as well as the previous work by us,[16] show that hydrolysis at these very low concentrations of free beryllium ion is negligible. (In such experiments, the highest values of $\bar{n}$, *ca.* 3.4, were attained, and uncertainties due to errors in the formation quotients for the hydrogen fluoride species are minimal.)

The lines (dotted, dashed, and solid) drawn on Fig. 6.6 represent $\bar{n}_c$ calculated by least-squares analysis for three different schemes of complexes. The BeF_4^{2-} species was included in all three to account for $\bar{n}_o$ above 3.0, and this species was combined with BeF^+ and BeF_2 in one case and BeF^+ and BeF_3^- in the other. The omission of either BeF_2 or BeF_3^- from the current scheme produces large systematic deviations in the $\bar{n}_c$.

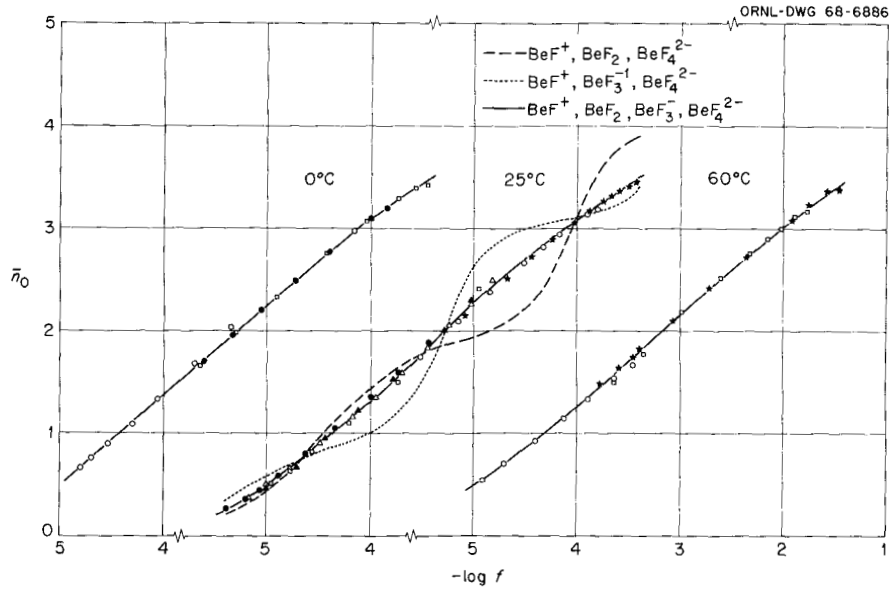

Fig. 6.6. The Average Number of Fluorides Complexed per Beryllium, $\bar{n}$, as a Function of $-\log f$ from Experiments in 1 m NaCl at 0, 25, and 60°.

Table 6.4. Thermodynamic Properties for Stepwise Equilibria of Beryllium Fluoride Species in 1.0 *m* Chloride at 25°

$$BeF_{y-1}^{(3-y)+} + F^- = BeF_y^{(2-y)+}$$

y	$\log Q_y$	ΔH (kcal)	ΔS (eu)
1	4.900 ± 0.014	−0.35 ± 0.32	21.2 ± 1.1
2	3.762 ± 0.016	−1.16 ± 0.24	13.3 ± 0.8
3	2.788 ± 0.017	−0.29 ± 0.23	11.8 ± 0.8
4	1.426 ± 0.020	−0.46 ± 0.25	5.0 ± 0.9

The corresponding effect is obtained if BeF^+ is omitted from the scheme of four species. The three-species schemes give an agreement factor of *ca.* 0.2, whereas with the four-species scheme a value of 0.03 is obtained. This clearly demonstrates that none of the four species can be omitted.

From our data in both chloride and perchlorate media at 25°, it is evident that the amount of beryllium complexing by chloride is very small. We have attributed the small differences which occur to activity coefficient differences between the media.

The ΔH and ΔS values derived from the data at 0, 25, and 60° in 1 *m* NaCl are given in Table 6.4. The nearly regular variation in log Q for the successive stepwise reactions is also reflected in the behavior of ΔH and ΔS. The equilibria are all slightly exothermic with heats less than −1.5 kcal, and ΔS varies from 21 eu for the first step to 5 eu for the fourth stepwise reaction. A regular trend in the stabilities is also predicted from a tetrahedral model of the hydrated complexes in which all the interactions of successive species are considered.

CORRELATION OF ΔH AND ΔS FOR THE ASSOCIATION OF THE RARE-EARTH(III) IONS WITH FLUORIDE

R. E. Mesmer C. F. Baes, Jr.

In the extensive literature on the stabilities of rare-earth complexes in solution, the absence of fundamental relationships representing their behavior is disappointing. Moeller *et al.*[18] attributed this situation to the concentration of effort on relatively complicated organic and polydentate ligands before the behavior of simple ligands is well understood. An important contribution has recently been made toward alleviating this deficiency by Walker and Choppin,[19] who reported

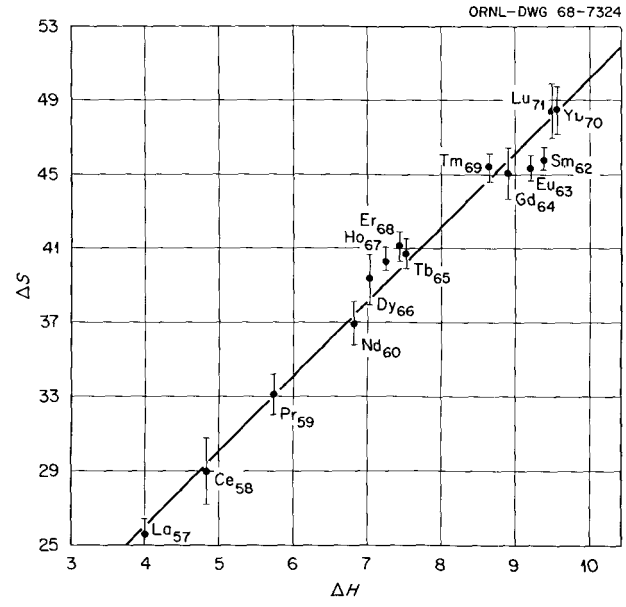

Fig. 6.7. The Change in Enthalpy vs the Change in Entropy for the Formation of the 1:1 Complex Between the Rare Earths and Fluoride.[19]

stability and calorimetric data on the first stepwise association reactions of the tripositive rare-earth cations with fluoride ion. Walker and Choppin pointed out the irregular variation with the atomic number (Z) of the ΔH and ΔS associated with complex formation. They accounted for the differences in the variation of ΔH for fluoride complexes and the variation of ΔH for acetate complexes in terms of the greater amount of covalent character in bonding of the acetate ion to the rare earths. They attribute the relatively large ΔS values associated with the formation of the fluoride complexes to a "dehydration" of the fluoride ion on complexing.

We wish to point out the very striking linear correlation which exists between ΔH and ΔS for the rare-earth fluoride complexes, LnF^{2+} (Fig. 6.7). Over the relatively wide ranges of enthalpy and entropy changes involved, the following expression represents the ΔS and ΔH values of Walker and Choppin within experimental error:

$$\Delta H\,(\text{kcal/mole}) = -2.38 + 0.246\,\Delta S\,. \qquad (17)$$

The experimental log K for the 1:1 rare-earth fluoride complexes increases with Z from 2.6 to 3.6; ΔH is positive, however, varying from 4.0 to 9.6 kcal/mole, and it is the large positive value of ΔS which accounts for the stability of these complexes.

The correlation between ΔH and ΔS is the more remarkable in view of the variations with Z of both ΔH

[18] T. Moeller *et al.*, *Chem. Rev.* 65, 1 (1965).

[19] J. B. Walker and G. R. Choppin, "Thermodynamic Parameters of Fluoride Complexes of the Lanthanides," in *Lanthanide/Actinide Chemistry*, ed by P. R. Fields and T. Moeller, *Advan. Chem. Ser.* 71, 127–38 (1967).

and ΔS. The following trends, pointed out by Walker and Choppin, can be seen in Fig. 6.7: in going from La_{57}^{3+} to Sm_{62}^{3+} (atomic numbers are written as subscripts to aid the reader), both ΔH and ΔS become more positive, then from Eu_{63}^{3+} to Dy_{66}^{3+} both become less positive, and finally from Ho_{67}^{3+} to Lu_{71}^{3+} both become more positive again.

The complexing reaction in general can be written

$$Ln(H_2O)_n^{3+} + F(H_2O)_m^- \rightleftharpoons LnF(H_2O)_p^{2+} + (n + m - p)H_2O\,, \qquad (18)$$

where n, m, and p are unspecified hydration numbers. The number of water molecules liberated by complex formation $(n + m - p)$ should be at least 2, since the F^- ion would displace at least one water from $Ln(H_2O)_n^{3+}$ and would give up at least one hydrate water of its own in forming the complex. Actually, the number of water molecules liberated should be considerably higher because of the reduction in outer-sphere hydration which ought to accompany the reaction of a trivalent cation with a monovalent anion to produce a divalent cationic complex. Thus it is reasonable that ΔS and ΔH values accompanying such a reaction are positive.

The *changes* in ΔS and ΔH as one proceeds through the series require a more detailed interpretation, however. Their steady increase with Z early in the rare-earth series would suggest either (1) that the strength of the ion-dipole Ln^{3+}-OH_2 bond increases more rapidly than does the strength of the ion-ion Ln^{3+}-F^- bond, that is, initially a fixed number of hydrate water molecules are bound increasingly more strongly relative to fluoride ion as Z increases, or (2) that an increasing amount of water is liberated by complex formation as Z increases. In either case the reversal in the upward trends of ΔS and ΔH beginning at Gd^{3+} and extending to Dy^{3+} could indicate a decrease in the amount of water released by complex formation. In the first case, this would suggest a decrease in the hydration number of the cation $Ln(H_2O)_n^{3+}$, induced by the decrease in ion size, beginning at about Gd^{3+} and completed at Dy^{3+}. In the second instance, wherein the hydration numbers of both Ln^{3+} and LnF^{2+} are viewed as being more variable, the reversal could indicate simply that the hydration number of Ln^{3+} decreases relative to that of LnF^{2+}.

Spedding *et al.*[20] have pointed out that the partial molal volumes of the rare-earth chlorides show a break equivalent to about 8 cc/mole between Nd^{3+} and Tb^{3+} superimposed on the regular decrease of $\bar{V}_2$ with Z. They have attributed this behavior to a reduction in hydration number of Ln^{3+} near the center of the series. Grenthe[21] and Edelin De La Praudiere *et al.*[22] similarly have invoked changes in hydration to account for the variation of ΔS and ΔH values associated with the formation of rare-earth complexes with carboxylated ligands.

Although many have been inclined to attribute trends in the stability of rare-earth complexes to ligand field effects, there is no compelling evidence at the present time that ligand field effects are significant. The ligand field effects in the first transition series are large because the d electrons are external in the ions; but in the rare earths, shielding by the $5s^2\ 5p^6$ octet should make ligand field effects produced by the f electrons very small.[18]

EMPIRICAL RELATIONSHIPS FOR STABILITY OF INORGANIC FLUORIDE COMPLEXES

R. E. Mesmer C. F. Baes, Jr.

After having carefully determined the stabilities of the beryllium fluoride complexes as discussed above, we hoped to relate these data with the published data on other metal fluorides. Figure 6.8 shows that for the systems for which the most reliable data are available the $\Delta \log Q_y$ values for stepwise fluoride complex reactions are well represented by the expression

$$\Delta \log Q_y = -1.1\ \Delta y\,, \qquad (19)$$

where y is the number of fluorides in the complex formed (or the number of the step). We have also found that an excellent empirical correlation is obtained if log Q_1 for the formation of the first fluoride complex of the 28 metal ions for which the most reliable fluoride complexing data are available is plotted as a function of Z_+^2/r_+ (see Fig. 6.9), where Z_+ and r_+ are the charge and radius of the cation. Log Q_1 values can be predicted with an average deviation of 0.3 log unit for the 28 examples shown in Fig. 6.9 from the relationship

$$\log Q_1 = -1.56 + 0.48 Z_+^2/r_+\,. \qquad (20)$$

[20] F. H. Spedding, M. J. Pikal, and B. O. Ayers, *J. Phys. Chem.* 70, 2440 (1966).

[21] I. Grenthe, *Acta Chem. Scand.* 18, 293 (1964).

[22] P. L. Edelin De La Praudiere and L. A. K. Staveley, *J. Inorg. Nucl. Chem.* 26, 1713 (1964).

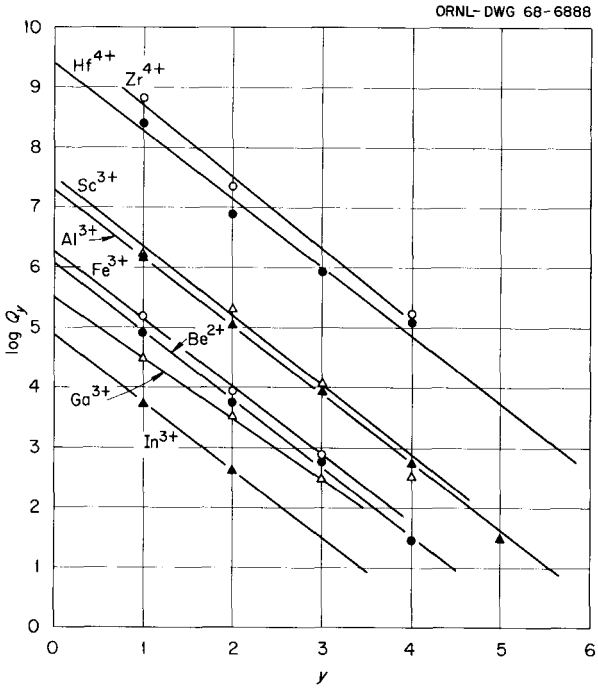

Fig. 6.8. Correlation of Stepwise Formation Quotients for Several +2, +3, and +4 Cations with y, the Number of Fluorides on the Complex (or the Number of the Step in Stepwise Equilibria).

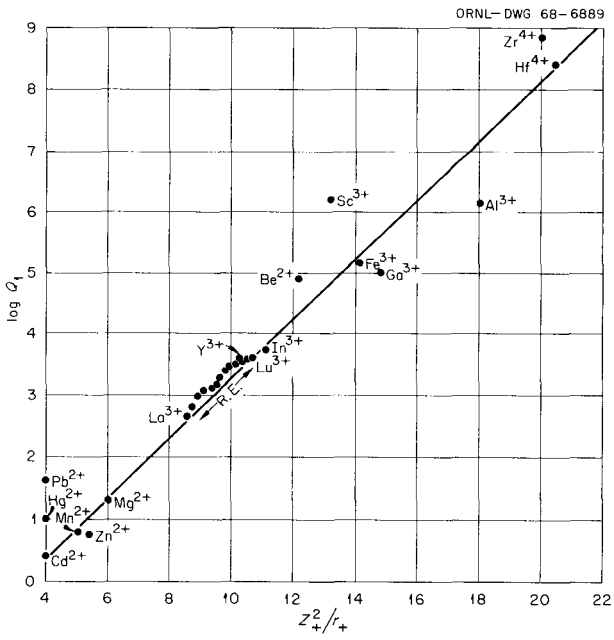

Fig. 6.9. Correlation of log Q_1 for the First Stepwise Fluoride Complex with Z_+^2/r_+ for 28 +2, +3, or +4 Cations, Where Z_+ and r_+ Refer to the Cation.

A somewhat poorer correlation was found between log Q_1 and $Z_+/(r_+ + r_-)$, which might be expected from a simple Coulombic picture of the ion association reaction. From Eqs. (19) and (20), we may write the following expression which should approximate the stepwise formation quotient of any given fluoride complex $MF_y^{(n-y)+}$:

$$\log Q_{1,y} = -0.46 - 1.1y + 0.48Z_+^2/r_+ \ . \qquad (21)$$

These correlations are remarkable in view of the wide variations in cation size and charge represented in the systems compared and in view of the uncertainty of the cation sizes in solution.

One limiting factor on the formation of fluoride complexes with cations of high charge and small size is the competing tendency of the cations to hydrolyze even at high acidities in water. One would predict from Eq. (21) very strong fluoride complexes for Si(IV) and B(III), and even with their strong tendency for hydrolysis to form oxyanions, indeed very stable fluoride complexes, SiF_6^{2-} and BF_4^-, are formed.

APPARATUS FOR EMF TITRATIONS AT ELEVATED TEMPERATURES

R. E. Mesmer F. H. Sweeton
C. F. Baes, Jr.

The design and construction of apparatus for the measurement of hydrolytic equilibria by titration experiments was reported previously.[23] The apparatus has now been tested by measuring the ion product of water as a function of temperature to 292°C. The hydrogen–hydrogen-ion concentration cell was found to produce results of very high precision.

The vessel, illustrated in Fig. 6.10, consists of a 6-in.-long cylinder of Hastelloy B 4 in. in diameter. The bore is lined with a Teflon cup and is covered with a Teflon cap from which is suspended a smaller inner Teflon compartment. The liquid junction is made with a porous Teflon plug. Each compartment contains a 0.040-in.-diam platinum-sheathed Chromel-Alumel thermocouple purchased from American Standard. The thermocouple leads are insulated from the sheath by MgO insulation, and the sheath doubles as the H_2 electrode. The platinum is insulated from the reactor vessel with Teflon packing and Teflon sheaths. An

[23] R. E. Mesmer and C. F. Baes, Jr., *Reactor Chem. Div. Ann. Progr. Rept. Dec. 31, 1967*, ORNL-4229, p. 100.

ORNL-DWG 69-2023

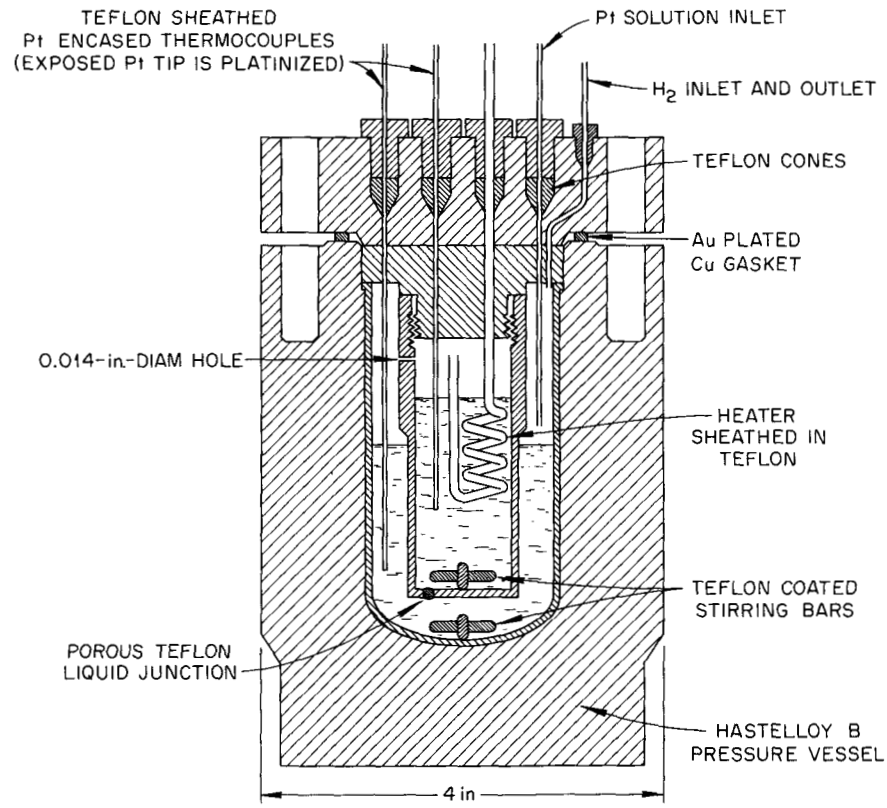

Fig. 6.10. High-Temperature EMF Titration Cell Assembly.

Inconel heater, 0.63 in. in diameter, is sheathed with Teflon tubing and wound in a spiral, which enables us to provide heat in the inner compartment to minimize the ΔT between the compartments during the heatup operation. The agitation in both compartments is accomplished with magnetic stirrers driven by a large magnet from below the oil bath. The temperature is maintained in a Haake thermostated bath containing Dow Corning 550 silicone oil.

As a test of the electrodes, the inertness of container materials, and the behavior of this liquid junction, a study of the ion product of water was conducted up to 292°C. We did not employ the titration assembly in order to simplify the test. Solutions containing 0.008245 *m* KOH in 1.00 *m* KCl and 0.009170 *m* HCl in 1.00 *m* KCl were placed in the outer and inner compartments respectively. About 500 psi of H_2 was placed over the solutions at the beginning of each experiment. During initial experiments an unknown source of CO_2 was encountered which could not be identified. However, it was learned that with new Teflon throughout, with pretreatment of the assembly by evacuation at 200°C, and with prolonged treatment with dilute acid, the difficulty was eliminated.

The emf of this hydrogen–hydrogen-ion concentration cell is given by

$$\Delta E = \frac{RT}{F} \ln \frac{(m_{H^+})(m_{OH^-})}{Q_w} - \Sigma D_i(m_{r,i} - m_i) , \quad (22)$$

where Q_w is the ion concentration product of water and complete dissociation of HCl and NaOH is assumed. The last term is a liquid junction term.[24] By use of the data obtained recently at this Laboratory by Quist and Marshall[25] on the limiting equivalent conductances of the H^+, OH^-, K^+, and Cl^- ions, the liquid junction term was evaluated. (The contribution is 0.4 to 0.5 mv over

[24] C. F. Baes, Jr., and N. J. Meyer, *Inorg. Chem.* 1, 780 (1962).

[25] A. S. Quist and W. L. Marshall, *J. Phys. Chem.* 69, 2984 (1964).

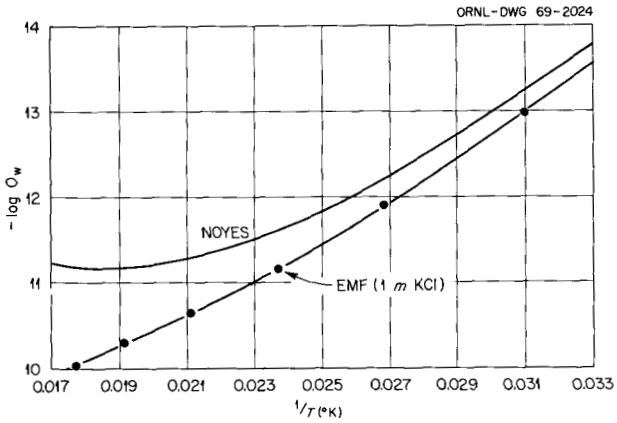

Fig. 6.11. The Variation of $-\log Q_w$ from 50 to 292°C as a Function of $1/T$. Upper curve for conductance data of Noyes *et al.* in dilute solutions. Lower curve for our emf data in 1 *m* KCl.

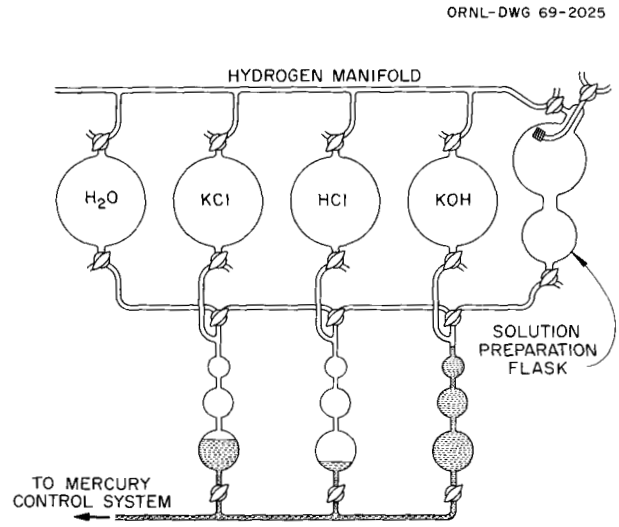

Fig. 6.12. Solution-Preparation System.

the temperature range investigated.) The results obtained for Q_w are believed to be good to at least ±0.01 log unit up to 250°C and about ±0.03 log unit at 292°C, where an extrapolation of the data was needed because of the drift resulting from the distillation of HCl to the base solution. The data are shown in Fig. 6.11 along with the data of Noyes *et al.*[26] for K_w (dilute solutions). An analysis of the difference has not yet been made, but it may contain contributions both from activity coefficients and from association, particularly of the hydroxide.

The extension of these measurements to obtain K_w (infinite dilution) will be conducted with the flowing cell (discussed next), in which impurities are expected to be less a problem, so that more dilute solutions can be investigated.

This cell has been found to produce data of sufficiently high precision that meaningful hydrolysis studies can now be pursued at temperatures where no knowledge is presently available. The study of the hydrolysis of aluminum ion is being initiated.

A FLOWING EMF CELL FOR MEASUREMENTS AT ELEVATED TEMPERATURES

F. H. Sweeton R. W. Ray
R. E. Mesmer C. F. Baes, Jr.

The design of an emf cell for measuring the dissociation constant of H_2O has been described previously.[27] The emf is measured between two H_2 electrodes in two flowing solutions, one acid and one alkaline, which then join to form the liquid junction before being discharged from the cell. The solutions are preequilibrated with hydrogen at low temperature and pressure before being pumped into the cell. The cell is capable of operation at temperatures up to 300°C. Tests of the pressure seals of the cell show that they remain tight after being held at 300°C under pressure for a time sufficient for a number of measurements.

Since this cell requires a separately prepared solution for each concentration studied, it is important to be able to prepare solutions of precisely known composition without having to analyze each one. For this purpose we have constructed the solution-preparation system shown schematically in Fig. 6.12. Known volumes of standardized stock solutions of KCl and HCl or KOH are displaced from calibrated bulbs by means of mercury into the capillary tubing connecting the H_2O reservoir to the test-solution flask. Water from the reservoir is used to flush the stock solutions into the test flask, and enough more is added to fill the calibrated lower section of the flask. Then the solution is transferred to the upper section for equilibration with H_2 before being transferred to the high-pressure system for pumping through the cell. This preparation system has been calibrated and is ready for use.

To make a run, two solutions will be prepared such that they have the same concentration of KCl as a supporting electrolyte. One will contain in addition a much smaller concentration of HCl, and the other a similar concentration of KOH. After these solutions are

[26] A. A. Noyes, Y. Kato, and R. B. Sosman, *J. Am. Chem. Soc.* 32, 159 (1910).

[27] F. H. Sweeton and R. W. Ray, *Reactor Chem. Div. Ann. Progr. Rept. Dec. 31, 1967,* ORNL-4229, pp. 100–102.

transferred to two titanium storage vessels in the high-pressure system, they will be displaced slowly by mercury from a double-cylinder pump and will be forced through the emf cell at flow rates of up to 4 ml/min. An automatic valve will adjust the discharge of mixed solutions to maintain the desired pressure in the cell.

This high-pressure system has been assembled and is ready for use, as are also the thermostat, the recording resistance thermometer, and the recording potentiometer system, which has a preamplifier with high impedance on both input terminals.

EFFECT OF SOLVENT ON THE ELECTROCHEMISTRY OF IRON

A. L. Bacarella A. L. Sutton

A study has been made of the electrochemical behavior of the active iron electrode in acidic ethanol-water media. The purpose of the investigation was to examine the changes in the corrosion kinetics and mechanism as a result of the addition of ethanol to the pure water solvent and to test the applicability of an "absolute acidity scale" postulated for ethanol-water mixtures.[28]

It has been shown by Kelly[29] that the steady-state anodic dissolution of zone-refined iron in aqueous acidic sulfate solutions is characterized by a Tafel slope of $^2/_3$ ($2.303RT/F$), that is, 40 mv per decade of current, and a first-order dependency on the hydroxyl ion activity. The results were interpreted in terms of the following mechanism:

$$Fe + H_2O \rightleftharpoons Fe(H_2O)_{ad} , \tag{23}$$

$$Fe(H_2O)_{ad} \rightleftharpoons Fe(OH^-)_{ad} + H^+ , \tag{24}$$

$$Fe(OH^-)_{ad} \rightleftharpoons Fe(OH)_{ad} + e , \tag{25}$$

$$Fe(OH)_{ad} \rightarrow (FeOH)^+ + e \quad \text{(rate determining)} , \tag{26}$$

$$(FeOH)^+ + H^+ \rightleftharpoons Fe^{2+} + H_2O . \tag{27}$$

These equations take formal account of the simultaneous coverage of the surface by adsorbed water molecules, hydroxyl ions, and the surface intermediate $(FeOH)_{ad}$. A less formal description combines Eqs. (23) through (25) into an overall equilibrium expression,

$$Fe + H_2O \rightleftharpoons (FeOH)_{ad} + H^+ + e , \tag{28}$$

which when followed by the rate-determining reaction [Eq. (26)] leads to the kinetic expression

$$i_+ = k_4 \frac{K_6 a_{Fe} \cdot a_{H_2O}}{a_{H^+}} \exp \frac{3}{2} \frac{F(E_{cell} + E_{0cal})}{RT} . \tag{29}$$

The above mechanism serves as a base for the kinetic analysis in the EtOH-HOH system. Results are reported for the anodic dissolution of zone-refined iron in hydrogen-saturated 0.50 M H_2SO_4 in EtOH-HOH solvents at 30°C. An analysis of the steady-state galvanostatic polarization data is made using extrathermodynamic relations postulated[28] for an absolute acidity scale in ethanol-water solutions.

In solvents other than water it is useful to distinguish between two acidity-measuring functions, pA and pH,[30] defined as follows:

$$pA = -\log a_+ = -\log cyf_H , \tag{30}$$

$$pH = -\log a_{H^+} = -\log cy , \tag{31}$$

where a_+ is the proton activity referred to water as the standard state, y is the conventional molar lyonium ion activity coefficient in solvent S, and f_H is the "degenerate activity coefficient" for the transfer of proton from infinite dilution in solvent S to infinite dilution in water. The parameter f_H is also referred to as the "medium effect" term.

Grunwald[28,31] and coworkers Berkowitz and Gutbezahl have collected and analyzed data for the dissociation constants of weak uncharged acids HA (acetic acid type) and cation acids HA^+ (ammonium-ion type) in ethanol-water mixtures. Values for the individual medium effects of hydrogen ion in these media were derived from the regularities observed in the solvent effect on pK by a method which presupposes the existence of certain linear free energy relationships.[28]

Values of f_H are listed in Table 6.5 together with values for the residual liquid junction error.[28] The liquid junction potentials, E_J, represent the difference between the potentials across the junctions:

[28] Boris Gutbezahl and Ernest Grunwald, *J. Am. Chem. Soc.* 75, 565 (1953).

[29] E. J. Kelly, *J. Electrochem. Soc.* 112, 124 (1965).

[30] A. L. Bacarella *et al.*, *J. Org. Chem.* 20, 747 (1955).

[31] Ernest Grunwald and B. J. Berkowitz, *J. Am. Chem. Soc.* 73, 4939 (1951).

soln X(ethanolic solvent)||KCl(sat aq)

and

soln X(aq)||KCl(sat aq) .

With this background and Table 6.5, the analysis of the anodic dissolution of iron is made.

The experimental system can be represented as:

Table 6.5. Values[a] of Log f_H and E_J in EtOH-HOH

EtOH (wt %)	$\log f_H$	E_J (mv)
0.0	0.000	0.0
20.0	0.008	−1.4
35.0	0.042	+6.4
50.0	0.251	+24.9
65.0	0.542	+43.5
80.0	1.152	+74.8
100.0	4.707	+139

[a]Boris Gutbezahl and Ernest Grunwald, *J. Am. Chem. Soc.* 75, 565 (1953).

(Pt or Fe) − H_2(1 atm)|0.50 M H_2SO_4 in ethanol-water solvent|E_J|KCl(sat aq)|Hg_2Cl_2 − Hg , (32)

where

$$E_{\text{cell(Pt)}} = (2.303\,RT/F)\log(cyf_{\text{H}}) - (E_{\text{0cal}} + E_J) \quad (33)$$

and

$$E_{\text{cell(Fe)}} = E_{\text{Fe}} - (E_{\text{0cal}} + E_J) . \quad (34)$$

An additional iron electrode is included in the cell for the polarization measurements. From Table 6.5 and Eq. (33) the activity of the proton referred to H_2O as the standard state is

$$\log cyf_{\text{H}} = \log a_+ = \frac{E_{\text{cell(Pt)}} + (E_{\text{0cal}} + E_J)}{0.060} . \quad (35)$$

The polarization data in the several solvents are shown in Fig. 6.13. Included are the experimental and theoretical estimates of the proton activity. The theoretical values in the ethanolic solvents were estimated

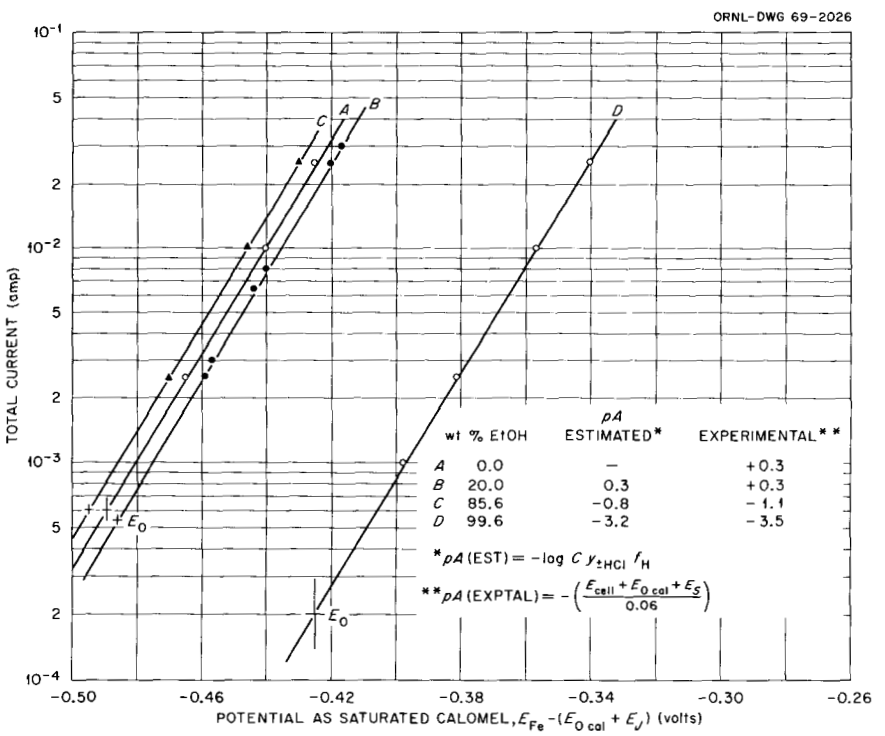

Fig. 6.13. Anodic Polarization of Iron in H_2-Saturated 0.50 M H_2SO_4 in 0.0, 20.0, 85.6, and 99.6 wt % EtOH–HOH at 30°C.

assuming H_2SO_4 is a uni-univalent electrolyte whose mean ionic activity coefficient $y_{\pm H(HSO_4)}$ is approximately equal to the mean ionic activity coefficient of HCl, $y_{\pm HCl}$, in the ethanolic solvents. These values are obtained from Harned and Owen.[32]

Based on the results shown in Fig. 6.13, that is, the Tafel slope is 40 mv/decade for all solvent compositions, it is assumed that the mechanism in the ethanolic solvent is the same as in water and that the rate is dependent on the adsorbed intermediate $(FeOH)_{ad}$. The rate constant for a possible $(FeOEt)_{ad}$ intermediate is therefore assumed much less than for the intermediate derived from water. Consequently, the rate expression [Eq. (29)] can be rewritten with superscript s to denote the changing solvent and also to take into account the liquid junction potential E_J:

$$i_+^s = k_4^s K_6 \frac{a_{Fe}^s a_{H_2O}^s}{a_{H^+}^s} \frac{f_{Fe} f_{H_2O}}{f_{H^+} \cdot f_{FeOH}} \times \exp \frac{3F}{2RT} [E_{cell} + (E_{ocal} + E_J)] \,. \quad (36)$$

The activities a^s refer to infinite dilution in solvent s, the "medium effect" terms f refer the activities to infinitely dilute water solutions as the reference state, and K_6 is therefore identically K_6 in pure water solvent. A knowledge of the liquid junction potential E_J is necessary since the measured currents are compared at constant iron potential,

$$E_{Fe} = E_{cell} + (E_{ocal} + E_J) \,. \quad (37)$$

Dividing Eq. (36) by the rate expression for pure water, written with superscript w, and expressing the result logarithmically, one obtains

$$\log i_+^s = \log i_+^w + \log (k_4^s/k_4^w) + \log (a_{Fe}^s/a_{Fe}^w) + \log (a_{H_2O}^s/a_{H_2O}^w) + \log a_{H^+}^w - \log (a_{H^+}^s f_{H^+}) + \log \left(\frac{f_{Fe} f_{H_2O}}{f_{FeOH}}\right) + \frac{1}{2.303}\left(\frac{3}{2}\right)\frac{FE_J}{RT} \,. \quad (38)$$

The factor containing E_J corrects the measured rates to constant E_{Fe}; $a_{H^+}^w$ is the activity of the proton in water, and $a_{H^+}^s f_{H^+} = a_+$ is the "absolute" activity of the proton. Assuming

$$\frac{a_{Fe}^s}{a_{Fe}^w} \sim 1 \,,$$

$$a_{H_2O}^w \sim 1 \,,$$

$$\frac{f_{Fe} \cdot f_{H_2O}}{f_{FeOH}} \sim 1 \,,$$

and

$$\frac{k_4^s}{k_4^w} \sim 1 \,,$$

Eq. (38) becomes

$$\log i_+^s = \log i_+^w + \log a_{H_2O}^s + \log a_{H^+}^w - \log a_+ + \frac{3}{2}(2.303RT/F)E_J \,. \quad (39)$$

That $k_4^s/k_4^w \sim 1$ implies that $\Delta F^\ddagger$ for the transition of $(FeOH)_{ad}$ to the activated state does not involve the participation of solvent. Therefore, if the activity of water $a_{H_2O}^s \cong N_{H_2O}^s$, where $N_{H_2O}^s$ is the mole fraction of water in the ethanolic solution, Eq. (39) becomes

$$\log i_+^s = \log i_+^w + \log N_{H_2O}^s + \log a_{H^+}^w - \log a_+^s + \frac{1.5(F/RT)\,E_J}{2.303} \,. \quad (40)$$

The agreement obtained between the experimental and predicted values, based on Eq. (40), is shown in Table 6.6. Two values of the calculated anodic current are presented: one value is calculated using a theoretical estimate of the proton activity referred to water as the standard state using Eq. (30); the second value is calculated using the experimentally measured proton activity using Eq. (35). Values for E_J and f_H as a function of weight percent EtOH were obtained from large-scale plots of the data in Table 6.5. The agreement is satisfactory considering the several assumptions used in their prediction. The results suggest a definite correlation between the rates and the absolute acidity scale for EtOH-HOH.

Summarizing the results, it is found that the mechanism for the anodic dissolution of iron in H_2-saturated

[32] H. S. Harned and B. B. Owen, *The Physical Chemistry of Electrolytic Solutions*, p. 550, Reinhold, New York, 1950.

Table 6.6. Comparison of the Observed Current with That Calculated from Eq. (40) at −0.440 v vs S.C.E. at 30°C

EtOH (wt %)	i_+^S(obs) (amp)	i_+^S(calcd) (amp)	
		a_+(estd)[a]	a_+(exptl)[b]
0	1.0×10^{-2}		
20.0	8.0×10^{-3}	1.0×10^{-2}	1.3×10^{-2}
85.6	1.4×10^{-2}	3.8×10^{-2}	1.9×10^{-2}
99.6	1.0×10^{-4}	8×10^{-5}	4×10^{-5}

[a]Note: a_+ from Eq. (38) using values of f_H in Table 6.5 and y values for HCl (see ref. 32).

[b]Note: a_+ determined with Pt-H_2 electrode.

acidic sulfate solution is unchanged by the addition of ethanol. In addition, it is found that the rate is proportional to the activity of H_2O in the ethanol-water solutions, as implied by Eq. (39) and the mechanism of Eqs. (23) through (27). The results suggest that changes in rates of certain electrochemical reactions with solvent may be understood on the basis of corresponding changes in the activities of reactants and that such changes may be calculated to a reasonable approximation using an "absolute" acidity scale.

AN IMPROVED HIGH-TEMPERATURE ISOPIESTIC UNIT

H. F. McDuffie[33] P. B. Bien[34] R. W. Ray
J. Braunstein

An improved electromagnetic balance has been installed in the pressure vessel designed for isopiestic studies at temperatures up to 200°C and pressures up to 15.6 bars[35] and has been tested at elevated temperatures, both dry and with steam pressures up to 4 psig. The overall sensitivity of the electromagnetic balance, with the electronic servo circuit controlling the coil current, is lower than the sensitivity of the undamped mechanical system. Some long-time drift of the readout circuit persisted, but tests with standard weights in the pans under operating conditions of 110°C and 4 psig steam pressure indicated that a precision better than ±1 mg could be expected. The apparatus is now being tested with aqueous solutions for which isopiestic data are available.[36]

[33]Presently on leave with USAEC.

[34]Retired.

[35]H. F. McDuffie and P. B. Bien, *Reactor Chem. Div. Ann. Progr. Rept. Dec. 31, 1967*, ORNL-4229, p. 102.

[36]C. S. Patterson, L. O. Gilpatrick, and B. A. Soldano, *J. Chem. Soc.* 1960, p. 2730.

Part III. Chemical Support for High-Temperature Solid-Fueled Reactors

7. Diffusion Processes

DIFFUSION STUDIES IN NOBLE-GAS SYSTEMS

M. D. Silverman A. P. Malinauskas

Gaseous diffusion is defined as the transport of mass or identity from one region in space to another as the result of a gradient in concentration. In a two-component closed system under isobaric, isothermal conditions, the characteristic parameter is the mutual diffusion coefficient D_{12}, which is defined through the phenomenological relationship, in one dimension,

$$J_1 = -D_{12}\,(\partial n_1/\partial z)\,, \tag{1}$$

where J_1 represents the flux of component 1 molecules due to the molecular density gradient $\partial n_1/\partial z$. A similar expression can of course be written for component 2, and it becomes a relatively simple matter to demonstrate that $D_{12} = D_{21}$.

From an applied viewpoint, the diffusion process is an important contributory mechanism in the description of a wide variety of problems, including such apparently unrelated topics as the kinetics of chemical reaction (particularly at elevated temperatures), the migration of gaseous fission products in nuclear reactors, and the dispersal of pollutants in the atmosphere. From a theoretical point of view, investigations of the diffusion phenomenon are primarily associated with studies of intermolecular forces. The dependence of D_{12} on molecular interactions is clearly seen in the Chapman-Enskog expression, which, in first approximation, is of the form

$$pD_{12} = \frac{0.0026280(T^3/2M)^{1/2}}{\sigma_{12}^2\,\Omega^{(1,1)*}(T_{12}^*)}\,, \tag{2}$$

where M is the reduced molecular weight,

$$1/M = (1/M_1) + (1/M_2)\,, \tag{3}$$

T is the temperature (°K), and the numerical constant has been evaluated under the restriction that the pressure p be in atmospheres and σ_{12} in Angstrom units. The quantity $\Omega^{(1,1)*}(T_{12}^*)$, the so-called "reduced collision integral for diffusion," is in essence a measure of the departure of a given molecular model from the idealized rigid-sphere (billiard ball) case. If the potential energy of interaction $\phi_{12}(r)$ at the separation distance r between the molecules is expressed in terms of the Lennard-Jones (12-6) function,

$$\phi_{12}(r) = 4\epsilon_{12}\,[(\sigma_{12}/r)^{12} - (\sigma_{12}/r)^6]\,, \tag{4}$$

then $\Omega^{(1,1)*}$ depends only upon the reduced temperature $T_{12}^* = kT/\epsilon_{12}$, where k is Boltzmann's constant.

The unique feature of the diffusion phenomenon is that the process is almost completely governed by unlike-molecule collisions; that is, terms involving $\sigma_{11}^2\,\Omega^{(1,1)*}(T_{11}^*)$ and $\sigma_{22}^2\,\Omega^{(1,1)*}(T_{22}^*)$ appear only in higher-order approximations and at most account for only about 5% of a given value of D_{12}. In fact, it is these terms which cause D_{12} to be mildly concentration-dependent. If the diffusion coefficient is referred to trace composition of the heavier component, then Eq. (2) is essentially correct as written.

For a rigid-sphere interaction potential,

$$\phi_{12}(r) = 0\,,\quad r > \sigma_{12}\,,$$

$$\phi_{12}(r) = \infty\,,\quad r \leqslant \sigma_{12}\,,$$

Table 7.1. Observed[1–3] Temperature Dependence of the Diffusion Coefficient[a] Characteristic of Noble-Gas Mixtures

Component 1	Component 2				
	He	Ne	Ar	Kr	Xe
He		1.63	1.68	1.69	1.70
Ne	1.63		1.67	1.76	1.69
Ar	1.68	1.67		1.92	1.94
Kr	1.69	1.76	1.92		1.86
Xe	1.70	1.69	1.94	1.86	

[a]Referred to trace composition of the heavier component.

the reduced collision integral $\Omega^{(1,1)*}$ is unity, and in this case the diffusion coefficient is predicted to increase with temperature as $T^{3/2}$. Deviations from rigid-sphere ideality should therefore be readily manifest in the observed temperature dependence of this parameter. Experimental data[1–3] involving all of the possible binary combinations among the noble gases, excepting radon, are displayed in Table 7.1.

In principle, then, experimental studies of the temperature dependence of D_{12} can be employed to yield information regarding bimolecular encounters between nonidentical molecules. Unfortunately, the potential utility of the phenomenon in this context is somewhat difficult to realize in practice; the experimental data must be extremely accurate.[4] However, this restriction can be mitigated provided the investigations are performed over a very wide temperature range.

In spite of the deceptively simple types of diffusion apparatus which have been designed, accurate determinations of D_{12} are difficult to obtain even at temperatures not too far removed from room temperature; thus methods have been sought to supplement directly measured values of the diffusion coefficient with indirect determinations. The most promising technique to date involves measurements of the composition dependence of the corresponding viscosity coefficient.[5] The attractiveness of the method is in large part due to the relative experimental ease with which highly accurate viscosity coefficient data can be obtained at both temperature extremes.

One of the primary aspects of the current studies concerned the resolution of some discrepancies which existed between previously measured values of D_{12} and the indirect determinations,[1] as well as the clarification of theoretical aspects regarding the method.[6,7] The present work, in addition to recent measurements by Van Heijningen *et al.*,[8] has proven the reliability of the technique. In fact, in some instances the results derived from viscosity data have proven to be superior to directly measured values of the diffusion coefficient.[1,3]

A similar method has also been proposed using composition dependence measurements of the thermal conductivities of gas mixtures.[9] The utility of this technique, however, has been challenged on practical grounds,[3] but it may be employed as a test of the consistency between diffusion and thermal conductivity measurements.[3]

THERMAL TRANSPIRATION

B. K. Annis R. E. Fuson[10]
J. W. Gooch A. P. Malinauskas

The establishment of a pressure difference in a closed volume of gas due to the application of a thermal gradient is known as thermal transpiration. In addition to the obvious dependence upon the gradient of temperature, the magnitude of the pressure difference is a sensitive function of the apparatus geometry, pressure, and properties of the gas. Moreover, the phenomenon itself occurs in the mathematically awkward pressure range below the region described by ordinary gas dynamics.

Recently, however, a mathematical formalism has been developed which adequately describes the essential features characteristic of the process; in addition, the mathematical treatment has uncovered a previously

[1]A. P. Malinauskas, *J. Chem. Phys.* **42**, 156 (1965).

[2]A. P. Malinauskas, *J. Chem. Phys.* **45**, 4074 (1966).

[3]A. P. Malinauskas and M. D. Silverman, *J. Chem. Phys.* (to be published).

[4]S. K. Kim and J. Ross, *J. Chem. Phys.* **46**, 818 (1967).

[5]S. Weissman and E. A. Mason, *J. Chem. Phys.* **37**, 1289 (1962).

[6]D. Burnett, *J. Chem. Phys.* **42**, 2533 (1965).

[7]T. S. Storvick and E. A. Mason, *J. Chem. Phys.* **45**, 3752 (1966).

[8]R. J. J. Van Heijningen, J. P. Harpe, and J. J. M. Beenakker, *Physica* 38, 1 (1968).

[9]S. Weissman, *Advances in Thermophysical Properties at Extreme Temperatures and Pressures*, pp. 12–18, American Society of Mechanical Engineers, New York, 1965.

[10]Summer Research Participant, Physics Department, Tennessee Technological University.

unsuspected dependence upon inelastic collisions among the gas molecules.[11,12] Experimental tests of the proposed relationship indicate that thermal transpiration measurements yield inelastic collision data relative to rotational excitation which are at least of equal accuracy as that obtained by the more conventional, and experimentally more elaborate, techniques.[13–15]

However, detailed studies[14,16,17] of the phenomenon have pointed out a defect in the current theory which has yet to be resolved satisfactorily.[18] This concerns the limiting expression as the total pressure approaches zero. Historically, the result deduced from simple kinetic theory arguments had been accepted as the correct limit, namely,

$$p_1/p_2 = (T_1/T_2)^{1/2} , \tag{5}$$

where $\Delta p = p_2 - p_1$ is the pressure difference resulting from the application of the temperature difference $\Delta T = T_2 - T_1$. In terms of the newly developed dusty-gas theory, the limit is of the form

$$p_1/p_2 = (T_1/T_2)^{\alpha_L} , \tag{6}$$

in which α_L reflects the type of scattering pattern which the gas molecules undergo in colliding with the available surfaces. For elastic isotropic scattering, $\alpha_L = 1/2$ and Eq. (5) is recovered.

Experiments conducted in this Laboratory with all of the noble gases as well as N_2, O_2, CO, and CO_2 indicate α_L to be considerably less than 0.5, ranging between 0.30 and 0.37, under conditions in which the thermal gradient was developed across 0.2-mm-ID glass capillaries by maintaining the end temperatures at 335.6 and 569.8°K. At this point it is difficult to ascertain whether the observed variation in α_L is actual or largely a manifestation of weaknesses in the approximations which were employed in the mathematical formulation. Work is currently in progress to resolve this aspect of the problem and to clarify its consequences on the relationships from which inelastic collision data are obtained.

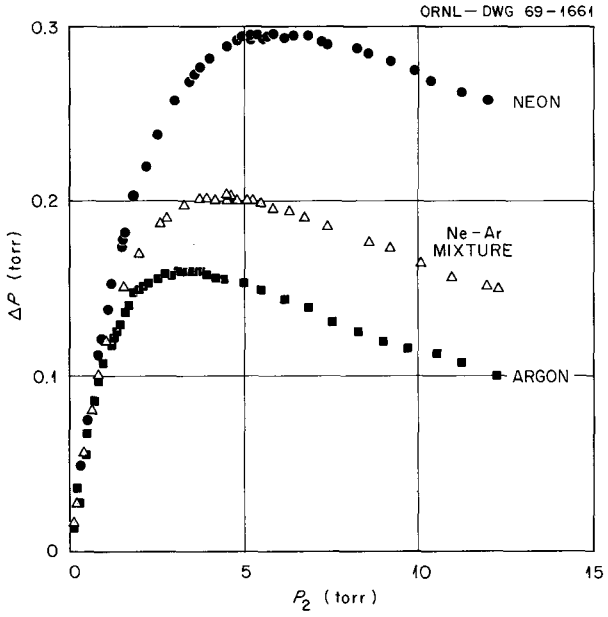

Fig. 7.1. A Comparison of Thermal Transpiration Data for a 46% Ne–54% Ar Gas Mixture with Corresponding Results for the Pure Gases. The effect was generated by maintaining the temperatures at the two ends of 0.2-mm-ID glass capillaries at 335.6 and 569.8°K.

The mathematical treatment of the thermal transpiration phenomenon has also been extended to include binary gas mixtures,[12,19] and an experimental verification of the theoretical results has been initiated. Some of the initial data are shown in Fig. 7.1, in which the pressure dependence of the steady-state values of Δp for a 46% Ne–54% Ar mixture are compared with similar data for the pure gases. The experimental conditions are identical with those quoted above. Analysis of the data with respect to theory has not yet been performed. Insofar as we are aware, these are the first thermal transpiration data ever obtained on gas mixtures.

[11] E. A. Mason, R. B. Evans III, and G. M. Watson, *J. Chem. Phys.* 38, 1808 (1963).

[12] E. A. Mason, A. P. Malinauskas, and R. B. Evans III, *J. Chem. Phys.* 46, 3199 (1967).

[13] E. A. Mason, *J. Chem. Phys.* 39, 522 (1963).

[14] A. P. Malinauskas, *J. Chem. Phys.* 44, 1196 (1966).

[15] A. Tip, J. Los, and A. E. de Vries, *Physica* 35, 489 (1967).

[16] J. P. Hobson, T. Edmonds, and R. Verreault, *Can. J. Phys.* 41, 983 (1963).

[17] T. Edmonds and J. P. Hobson, *J. Vacuum Sci. Technol.* 2, 182 (1965).

[18] E. A. Mason and A. P. Malinauskas, *The Effect of Accommodation on Thermal Transpiration: Limitations of the "Dusty-Gas" Model in the Description of Surface Scattering*, ORNL-3796 (April 1965).

[19] R. E. Jenkins, M.S. thesis, University of Maryland, 1967.

DETERMINATION OF THE VISCOSITY COEFFICIENTS OF GASES[20]

S. J. Whisenhunt, Jr.[21] J. Q. Searcy[22]
A. P. Malinauskas

A simple, inexpensive apparatus has been developed for the determination of viscosity coefficients of gases at room temperature. The method yields reasonably accurate values of the viscosity coefficient; in the present work, agreement with results which were obtained by more elaborate methods was found to be within about 2%.

The apparatus is sketched in Fig. 7.2. The gas under investigation is admitted into the graduated leg of a glass U-tube containing a suitable fluid and allowed to expand into the atmosphere through a short length of capillary tubing. During the course of the expansion, the rate of transport of the gas through the capillary is monitored by noting the rise of the liquid meniscus in the graduated leg of the U-tube. Through a judicious choice of fluid for use in the U-tube, which functions as both a volumeter and manometer, it is possible to employ sufficiently small pressure drops across the capillary that the rate of rise of the meniscus is given in good approximation by the expression[20]

$$\ln l = \ln l_0 - (K/\eta)t \,, \tag{7}$$

in which l represents the distance at time t between the fluid meniscus and some fiducial mark at which the liquid level in the ungraduated leg of the U-tube is maintained, l_0 is the corresponding distance at zero time, K is an apparatus constant, and η is the viscosity coefficient of the gas.

Although K can be evaluated by direct measurement, greater accuracy is attained if only relative values of the viscosity coefficients are determined. In our experimental verification of Eq. (7), we therefore chose argon as the "calibration gas" and referred all of the viscosity determinations to the viscosity of argon. This was done by noting that Eq. (7) is a linear relation between $\ln l$ and t, with slope

$$S = -K/\eta \,. \tag{8}$$

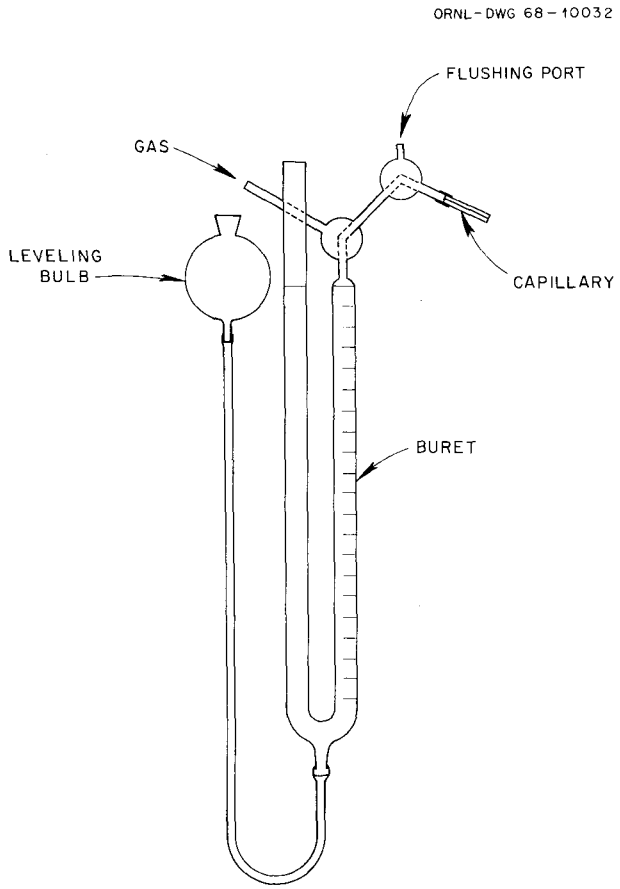

Fig. 7.2. Sketch of the Viscosity Apparatus.

It therefore follows that

$$S_{\mathrm{Ar}}/S_i = \eta_i/\eta_{\mathrm{Ar}} \,, \tag{9}$$

in which the subscript i refers to any gas other than argon. Experimental values of the slope ratio are compared with the corresponding literature values of the viscosity ratio in Table 7.2, in which the former results were derived from experiments in which water was employed as the manometric fluid.

A most remarkable effect was observed with helium, however. With this gas the transport behavior was described by Eq. (7), with the prescribed slope (see Table 7.2), until the water meniscus corresponded to a pressure drop across the capillary of about 6 torrs. At this point the water level came to a complete stop and remained at the same level over a prolonged period of time.

This stationary condition can only be regarded as one of zero net flux through the capillary; the most obvious manner in which this can occur requires that the air

[20] A. P. Malinauskas, S. J. Whisenhunt, Jr., and J. Q. Searcy, *J. Chem. Educ.* (to be published).

[21] Research Participant, summer 1968, Chemistry Department, Knoxville College, Knoxville, Tenn.

[22] Research Participant, summer 1967, Chemistry Department, Purdue University, Lafayette, Ind.

Table 7.2. Viscosity Coefficients at 23°C as Determined with Water as the Manometric Fluid

Gas i	S_{Ar}/S_i	η_i/η_{Ar}[a]
Ar	(1.000)	1.000
CO_2	0.654 ± 0.007	0.661
N_2	0.790 ± 0.006	0.793
Air	0.814 ± 0.005	0.818
He	0.880 ± 0.003	0.877
	0.875 ± 0.003[b]	
O_2	0.908 ± 0.007	0.914
Ne	1.382 ± 0.005	1.400

[a]Literature values. The viscosity coefficients at 23°C were interpolated from Il. F. Golubev, *Viscosities of Gases and Gas Mixtures,* chap. 3, Gosudarstvennoe Izdatel'stvo Fiziko-Matematicheskoi Literatury, Moscow, 1959. At this temperature, the viscosity coefficient of argon is 2235×10^{-7} poise.

[b]Data taken with a plastic bag over the capillary. See text.

molecules at the exit side of the capillary diffuse into the U-tube, against the pressure gradient, as rapidly as the helium molecules exit. This type of phenomenon is well known,[23,24] but in the present case it appears at a pressure drop which is about 100 times that expected. Moreover, the pressure drop is in the opposite direction. Although such an unexplained reversal has been observed for the case involving argon and carbon dioxide,[24] the same investigators found no reversal for the helium-nitrogen pair. This pair should behave similarly to helium-air.

Nonetheless, we tested the hypothesis by placing a plastic bag over the end of the capillary and flushing the bag with helium prior to the experiment. The bag was purposely punctured to ensure that there be no pressure buildup in the enclosed region. Under this circumstance, the anomaly was not observed, and the data yielded an excellent value of the viscosity coefficient of helium, as can be seen in Table 7.2.

On the other hand, if our proposed mechanism to account for the anomaly were correct, the same behavior should have been observed using dibutyl phthalate rather than water as the manometric fluid (without the plastic bag). In this case the anomalous transport of helium was not observed. The nature of the anomaly thus remains unexplained.

The apparatus and method, however, afford an excellent experiment, particularly for use in student laboratories, for demonstrations of laminar gas flow through capillaries and as an aid in understanding kinetic theory principles with regard to the viscosity coefficient.

SELF-DIFFUSION OF ^{14}C IN PYROCARBON STRUCTURES

R. B. Evans III L. D. Love[25]
E. H. Kobisk[26]

Studies of the self-diffusion behavior of carbon in graphites and pyrocarbons should provide information of fundamental importance regarding diverse chemical and solid-state reactions; yet the number of direct measurements of the self-diffusion phenomena is quite limited. The first set of measurements reported[27] concerned thin-layer experiments with a highly permeable graphite structure. The second set involved constant-potential experiments[28] with small graphite crystals selected from limestone near Ogdensburg, New Jersey. Finally, and most recently, two successful etching-decoration[29] experiments based on thin-layer boundary condition were performed[30] with small graphite crystals selected from pre-Cambrian rock at Ticonderoga, New York.

The most meaningful results obtained prior to our work seem to have come from the Ogdensburg-crystal experiments. These can be summarized as four points on an Arrhenius plot that permit calculation of the activation energy E_a through the relationship

$$D = D_0 \exp(-E_a/RT) ,$$

where D is the self-diffusion coefficient and T is the absolute temperature.

The reported[28] E_a was 163 ± 12 kcal/mole. This value appears reasonable in view of (1) early theoretical predictions,[31] later refined,[28] and (2) measured values of low-concentration thorium diffusion coefficients in pyrocarbons.[32] The preexponential D_0 value could not

[23]E. A. Mason, A. P. Malinauskas, and R. B. Evans III, *J. Chem. Phys.* **46**, 3199 (1967).

[24]L. Waldmann and K. H. Schmitt, *Z. Naturforsch.* **16a**, 1343 (1961).

[25]Plant and Equipment Division.

[26]Isotopes Division.

[27]M. H. Feldman *et al., J. Appl. Phys.* **23**, 1200 (1952).

[28]M. A. Kanter, *Diffusion of Carbon Atoms in Natural Graphite Crystals,* thesis issued as ANL-5433 (May 1955); also, M. A. Kanter, *Phys. Rev.* **107**, 655 (1957).

[29]G. R. Hennig, *J. Appl. Phys. Letters* **4**, 52 (1964).

[30]F. S. Feates, staff member of AERE, Harwell, U.K., Chemistry Division (private communication, March 1968).

[31]G. J. Dienes, *J. Appl. Phys.* **23**, 1194 (1952).

[32]R. B. Evans III, J. L. Rutherford, and F. L. Carlsen, Jr., *Reactor Chem. Div. Ann. Progr. Rept. Dec. 31, 1965,* ORNL-3913.

be determined with any certainty because the method employed required an estimate of irregular surface areas. Classical measurements based on sectioning of bulk structures were performed only in the porous graphite work.[27] Unfortunately grain-boundary, surface, and pore-diffusion effects seem to have dominated in these early experiments.

In our work the classical approach is also attempted. This turns out to be a formidable task in all aspects of the experimental manipulations starting with the labeling of specimens with a thin layer of ^{14}C. After some unsuccessful attempts to utilize the technique of Feldman *et al.*,[27] we have devised a very satisfactory method based on the glow discharge of labeled acetylene. Barium carbonate (85% total carbon as ^{14}C) is converted to calcium carbide by pyrolytic reaction with calcium metal in vacuum. Under a pressure of 1 to 2 μ (air), a mixture of calcium metal and the carbonate (200 and 97.3 mg respectively) is fused with a torch until the reaction is initiated; a quartz tube ~6 in. long and 60 mm in diameter is employed as the reaction vessel. The fused mixture can be stored indefinitely provided it is not in contact with a moist or oxidizing atmosphere.

As shown in Fig. 7.3, a Pyrex hydrolysis vessel is used to generate the acetylene by dropwise addition of distilled water to the fused reaction mixture in the quartz tube (a total of 500 ml is added to complete the reaction). In practice, the lower 2 in. of the quartz reactor is cut from the fusion tube and placed in the water reactor. Preceding water addition, the acetylene generator is evacuated to ~20 μ Hg, and a finger trap, shown in Fig. 7.3, is precooled with liquid nitrogen. Upon addition of water to the acetylene generator, a mixture of acetylene gas, water vapor, and hydrogen is discharged from the system by pumping on the frozen mixture of acetylene and water in the finger trap.

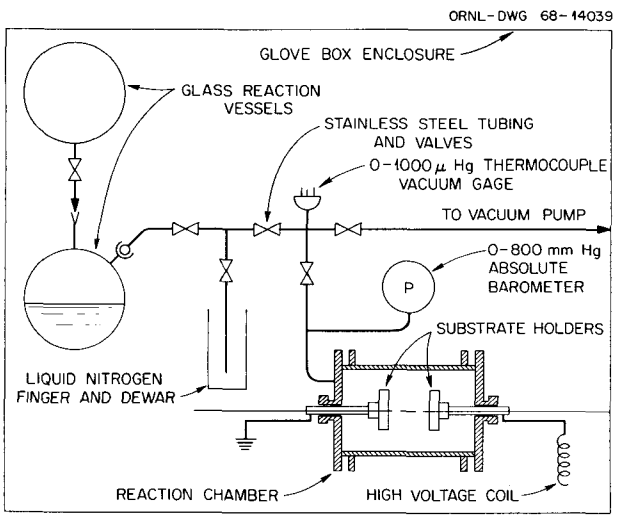

Fig. 7.3. Apparatus Used to Label Source Coupons with ^{14}C. The entire system is operated at pressures slightly below atmospheric. Noxious radioactive components are swept away by a constant air flow through the containment system. Absolute filters are present at the inlet and outlet ports. No external ^{14}C contamination has been encountered.

Two fixtures, each holding sixteen 1-cm^2 pyrocarbon coupons, are mounted in the reaction chamber as shown in Fig. 7.3 so that the faces to be coated are parallel and separated by a distance of ~2 cm. After evacuation of the glow discharge chamber to about 1 μ pressure, a small amount (900 μ) of the acetylene–water-vapor mixture is released. Considerable separation of acetylene from water vapor was achieved by virtue of the difference in vapor pressures of the two components. Residual water vapor does not interfere with subsequent glow discharge. Using the voltage derived from a Tesla coil, glow discharge was initiated in the chamber, wherein free radical polymerization reactions take place on exposed surfaces in the immediate region of the discharge. Infrared lamps are focused on the coupons to ensure the formation of low polymers, perhaps approaching elemental carbon. Otherwise the activity will be lost because higher polymers will volatize during subsequent high-temperature procedures.

Generally 15 min of glow discharge is required to obtain 200 μg of polymerized film. Each coupon in our initial experiments bore 6 to 60 μg. Since this was far in excess of our safety requirements, the coupons as treated above were used as source specimens. Activity was exchanged from source to diffusion specimens by placing the prepared surfaces in intimate contact for 10 min at 2000°C.

Exploratory experiments with several *porous graphites* revealed unusually deep penetrations at temperatures ranging from 2394 to 2902°C. This undoubtedly resulted from volatile species (CO-CO_2) moving through pores coupled with surface diffusion effects. On the basis of Feldman's efforts,[27] one might have expected such results.

Attempts to perform ⟨*c*⟩ direction experiments with *hot-pressed* and *columnar pyrocarbons* failed for the same reasons, but with opposite results. The tracer refused to penetrate in the ⟨*c*⟩ direction. Similar behavior has been observed for ⟨*c*⟩ direction movement of actinides in heat-treated pyrocarbons. Furthermore, the tracer either volatilized away from the basal surfaces and/or moved to and activated surfaces normal

to the "*a* direction." Movement from activated ⟨*a*⟩ surfaces to ⟨*c*⟩ edges is clearly shown by the autoradiograph in Fig. 7.4. We conclude that foreign carbon atoms are most prone to adhere to crystal edges and that they prefer to move along basal surfaces as opposed to crossing them.

A few quantitative results are available from this first exploratory series. They comprise data for ⟨*a*⟩ *direction* diffusion in *columnar pyrocarbon* specimens, all of which are preannealed (with tracer) at 2505°C for 15 min before being subjected to the actual diffusion anneal temperatures. A carbon resistance furnace operating at a positive helium pressure was employed in these experiments. One preannealed set was retained to furnish blank information to correct for diffusion during approach to diffusion temperatures and other experimental imperfections. The blanks gave a fictitious $(4Dt)_0$ value employed in the calculations as described below.

PHOTO 93697

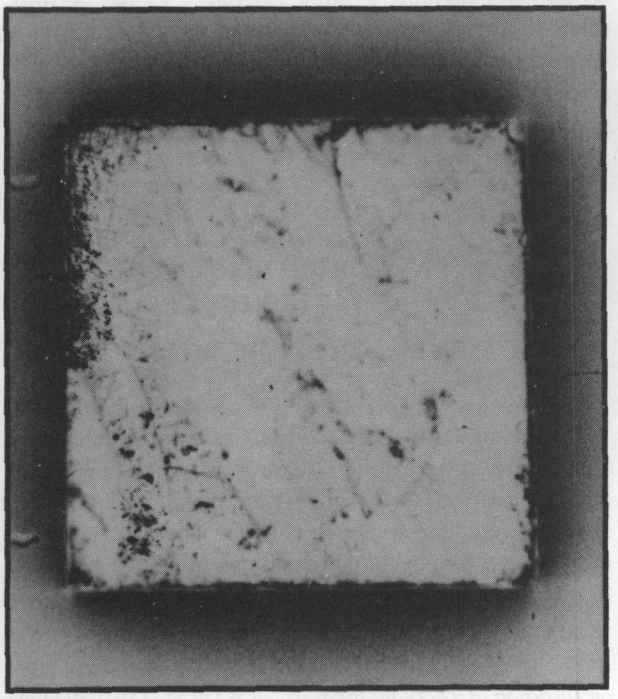

Fig. 7.4. Autoradiograph of a ⟨*c*⟩ Direction Specimen of Hot-Pressed Graphite After Diffusion Anneal at 2902°C. Originally the entire surface viewed by the reader was black, indicating a uniform layer of tracer. After high-temperature exposure, this surface is relatively clean; all the tracer present resides at the edges, as indicated by the black halo around the specimen.

Coefficients for actual experiments were obtained from the diffusion data (shown in Fig. 7.5) by taking the argument of erfc u to be $x[(4Dt)_0 + 4Dt]^{-1/2}$, where x is the penetration at various F.R. values, D is the coefficient sought, and t is the annealing time. This is a rigorously justifiable procedure used by Gruzin[33] and others. One merely matches tabulated u and measured x values at common F.R. values to compute D. Descriptions of the as-deposited pyrocarbon used, and the sectioning techniques employed, are given elsewhere in recently published papers[34] covering a project specially designed to prepare us for the present investigation involving very low penetrations as demonstrated by the plots shown in Fig. 7.5.

We suspect severe oxidation and volatilization effects were present in our initial experiments, because many specimens suffered weight changes, lost total activity, had sooty surfaces, and finally demonstrated shapes of concentration profiles that are characteristic of systems wherein activity is being lost.[35] Notice the drooping points near F.R. = 1 on two of the curves in Fig. 7.5. Errors associated with the "droop" can be circumvented by extrapolating the lower values to a new $x = 0$, F.R. = 1.0 point which amounts to translating the curves to the left. Surprisingly enough, profiles subject to activity loss tend to give deeper apparent penetrations on F.R. curves than on ideal curves,[35] but the translation generally gives very good estimates of the latter. In view of these results, the diffusion annealing furnace is being rebuilt to operate under a vacuum. Nonetheless, we have enough confidence in our tentative results to present in Fig. 7.6 a comparison of our results with those reported by Kanter. The similarity of slopes, coupled with the fact that no ⟨*c*⟩ direction results could be obtained in our experiments, prompts us to agree with Kanter in that an interstitial mechanism might be excluded for self-diffusion of carbon in graphite and that vacancy diffusion is the most likely mechanism.

---

[33] R. L. Gruzin, Yu. A. Polikarpov, and G. B. Fedorov, *The Study of Diffusion of Carbon in Nickel and Its Alloys Using the Radioactive Isotope* ^{14}C, AERE Lib/Trans 783 (March 1958).

[34] R. B. Evans III, J. L. Rutherford, and R. B. Perez, *J. Appl. Phys.* 38, 3127 (1967); *J. Appl. Phys.* 39, 3253 (1968).

[35] J. H. DeVan and R. B. Evans III, "Corrosion Behavior of Reactor Materials in Fluoride Salt Mixtures," pp. 557–79 in *Conference on Corrosion of Reactor Materials, June 4–8, 1962;* pp. 559–74 in *Conference on the Use of Radioisotopes in the Physical Sciences and Industry,* Sept. 16–17, 1960. Proceedings (vol. II and III, respectively) published by the International Atomic Energy Agency, Vienna, 1962.

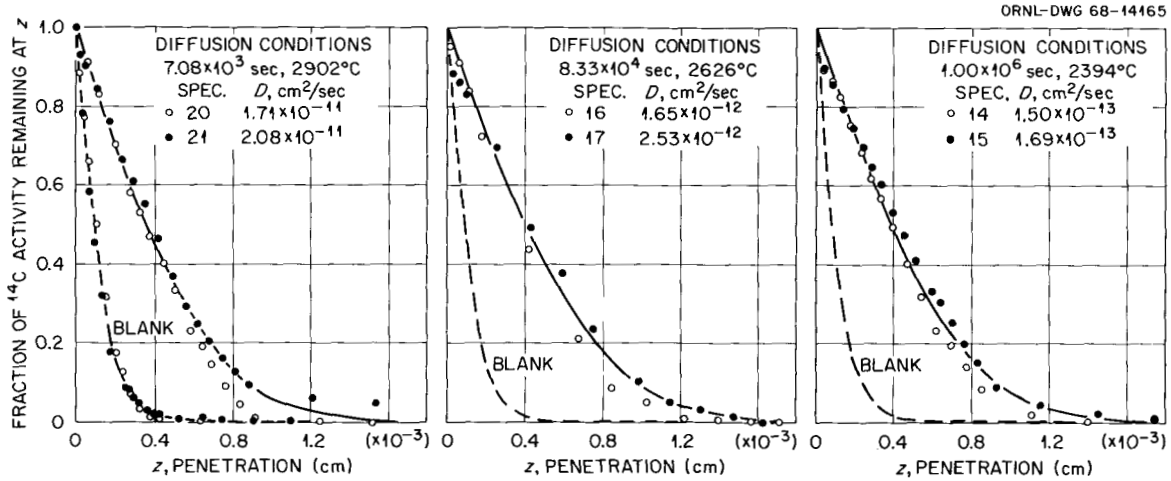

Fig. 7.5. Penetration Profiles for ⟨a⟩ Direction ^{14}C Diffusion in G.E. Pyrocarbon. Solid curves represent ideal profiles based on the average behavior of the two specimens comprising the diffusion couples. The blank curve resulted from a 15-min exposure at 2505°C; the $(4Dt)_0$ blank correction was 2.84×10^{-8} cm^2.

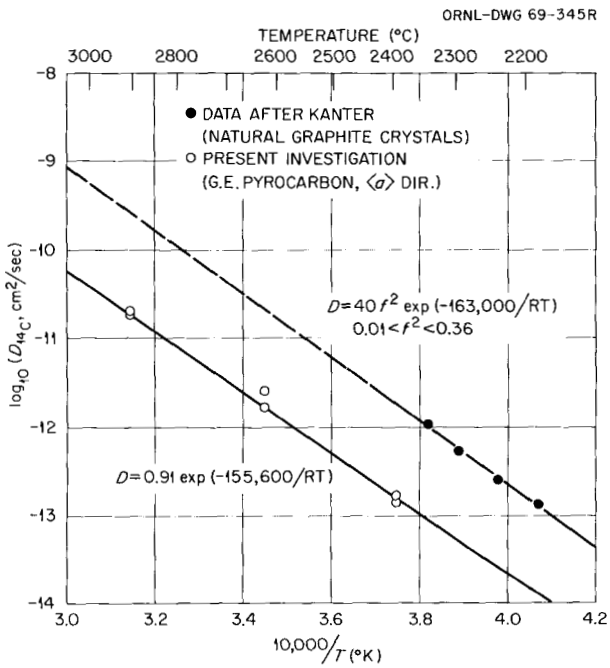

Fig. 7.6. Arrhenius Plots of Self-Diffusion Coefficients for Graphite Crystals and G.E. Pyrocarbons. The crystal values of Kanter[28] are at the top; the ⟨a⟩ direction pyrocarbon values (tentative) are at the bottom.

We should point out that the structure of the 2902°C diffusion-anneal specimen is undoubtedly quite different[36] with respect to low-order defects from those subjected to lower diffusion temperatures; normally one would not expect all three points to fall on the same curve. Wolfe *et al.*[37] have reported, however, nearly identical D_0 and E_a values for actinides in two entirely different structures (ZTA polycrystalline graphite and ⟨a⟩ direction G.E. pyrocarbon). Furthermore, Kanter has favored a value of $40f^2 = 5$ for entropy calculations; if this is a reasonable estimate, Kanter's data on Fig. 7.6 would displace down and nearly coincide with the curve corresponding to our data. The implication here is that the pyrocarbon results might not be too far removed from single-crystal results.

GAS TRANSPORT IN VENTED FUEL ELEMENTS AND CONTROL RODS

R. B. Evans III D. E. Bruins[38]
E. A. Mason[39]

The use of vents in the cladding around fuel elements and control-rod absorbers to prevent pressure buildup due to gas release is an attractive idea, since the cladding can then be much simpler. The problem is to design a venting system that allows pressure equalization without release of too much activity.

---

[36] F. L. Carlsen, Jr., *Effects of Pyrolytic-Graphite Structure on Diffusion of Thorium,* thesis issued as ORNL-TM-1080 (June 1965).

[37] J. R. Wolfe, D. R. McKenzie, and R. J. Borg, *The Diffusion of Nonvolatile Metallic Elements in Graphite,* UCRL-7324 (Apr. 29, 1964); also *J. Appl. Phys.* 36, 1906 (1965).

[38] Summer Participant, Carnegie Institute of Technology, Pittsburgh, Pa.

[39] Consultant, Brown University, Providence, R.I.

For fuel elements, the use of decay chambers or traps in conjunction with a vent that restricts diffusive flow can reduce activity release to a reasonable level. The designs of the vent and the decay chamber must be considered together for maximum efficiency. It was found that a cascade of decay volume and at least two vent sections represents the most efficient configuration. Design of the vent itself is important, since it must exhibit selective flow characteristics. The vent should permit enough forced flow to prevent pressure buildup but should restrict diffusion enough to permit short-lived fission products to decay in the chambers. These requirements are essentially contradictory, and only an optimum compromise can be hoped for. Gas-flow theory is thus of importance in the vent design; fortunately a generalized treatment of gas transport in porous media had previously been developed,[40] so that a discussion could be given of combined forced and diffusive flows, together with the complicated effects of temperature gradients and thermal diffusion. An effort was also made to develop the simplest possible explanations for this generalized treatment; these were essentially correct without resort to the heavy mathematical artillery of the Chapman-Enskog theory of gases. It is remarkable how far one can go in this way.[41] Numerical examples based on these equations gave considerable insight as to the proper vent construction.

It was found, in contradiction to the usual intuitive approach of trying to work in the Knudsen or free-molecule region, that the optimum design would involve working in the normal or hydrodynamic region. The best physical configuration would thus appear to be a small cylindrical hole (capillary) drilled in a solid metal cap with properly selected porous metallic filters at each end of the hole. The filters should guard against plugging of the capillary and excessive "breathing" of the decay chamber without introducing Knudsen flow characteristics. Although the theory will describe gas flow and diffusion in such porous filters, it does so in terms of unknown parameters (at least three) characteristic of the microscopic geometry of the filters; these parameters must be found experimentally. A number of stainless steel porous filters were acquired, and experimental study of their flow and diffusion characteristics for gases was begun. These porous filters were made by cold-pressing and then sintering a 23-μ stainless steel powder, yielding samples with a range from 18 to 31% voids and mean pore radii from 1.8 to 3.1 μ. Experiments will also cover scaled portions of venting devices, as well as individual components. The exact specification of the type of filter one might employ will depend to a large extent on criteria for plugging and allowable pressure drops, which do not seem to have yet been formulated.

Hopefully, the studies of the flow and diffusion properties of gases in vents for fuel elements and control rods will lead to relationships (either empirical or theoretical) among the three parameters characterizing porous media, or to relations that permit these parameters to be predicted from other measurable characteristics of the media. Eventually only a minimum of measurements would be necessary to characterize a given porous medium.

SIMPLIFIED COUNTERDIFFUSION APPARATUS FOR CHARACTERIZING VENTS AND VENT COMPONENTS

R. B. Evans III E. A. Mason[39]

The need for extensive experimental studies on the diffusion of gases in porous media being considered for use in vents for fuel elements and control rods makes it imperative to devise simple experimental techniques. The usual gas-sweep methods[42,43] are not well suited for the small and/or tight specimens encountered in vent studies, nor are they convenient for testing a large number of specimens in a reasonable time. A much simpler apparatus has been devised and tested and found to be suitable for such studies.

A crucial aspect of counterdiffusion experiments is that the total gas pressure must be kept uniform, in order that forced flow be absent and diffusion alone be measured. The very simple device used goes back to Thomas Graham in 1833, but it seems to have been largely forgotten in recent times in favor of more complicated apparatus.[44] All that is needed is a calibrated glass tube with an arrangement for mounting the porous sample on one end, and the other end immersed in a vessel of water. Figure 7.7 shows a prototype apparatus with a sintered glass frit in place of the test specimen. Helium is added to the tube by displacement of water and its volume noted. As

[40] E. A. Mason, A. P. Malinauskas, and R. B. Evans III, *J. Chem. Phys.* 46, 3199 (1967).

[41] E. A. Mason and R. B. Evans III, accepted for publication in the *Journal of Chemical Education.*

[42] R. B. Evans III, J. Truitt, and G. M. Watson, *J. Chem. Eng. Data* 6, 522 (1961).

[43] R. B. Evans III, G. M. Watson, and J. Truitt, *J. Appl. Phys.* 33, 2682 (1962).

[44] E. A. Mason, *Am. J. Phys.* 35, 434 (1967).

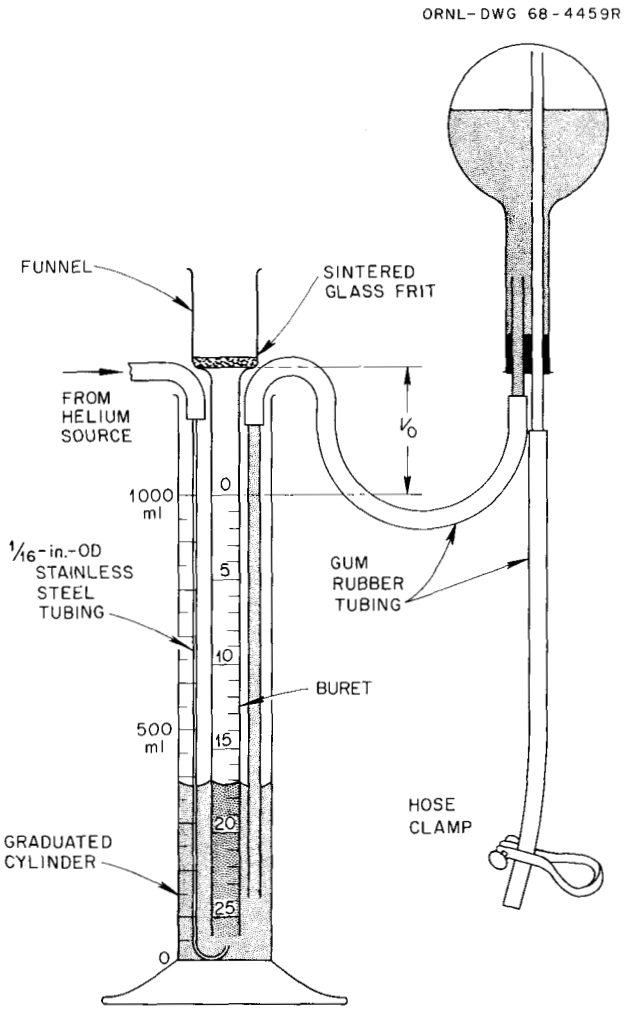

Fig. 7.7. Diffusion Tube and Auxiliary Equipment Used to Perform Graham's Diffusive Experiment. Gas is added to the buret through a piece of bent tubing. The inverted flask serves as a water reservoir to maintain equal water levels in the cylinder and buret.

diffusion through the specimen occurs, the water tends to rise as the helium diffuses out faster than the air diffuses in. The pressure is kept uniform by flowing water into the outer vessel from the inverted flask, so as to keep the water level outside the diffusion tube the

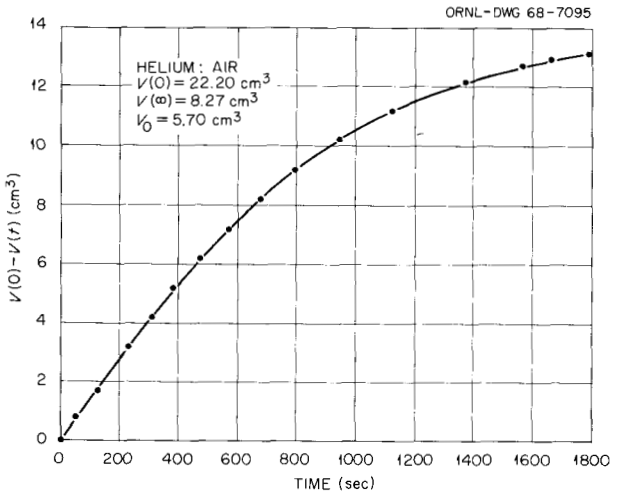

Fig. 7.8. Typical Volume Change as a Function of Time in a Graham Uniform-Pressure Diffusion Experiment.

same as the level inside. The volume of gas remaining in the diffusion tube is observed as a function of time, producing results similar to those shown in Fig. 7.8 (again for the prototype glass frit).

The effective helium-air diffusion coefficient for the porous test specimen can be determined from the slopes of the curve of Fig. 7.8 at various times, with a reproducibility of about 3%. Knowing the free-space value of the helium-air diffusion coefficient, we thus obtain the value of the porosity/tortuosity ratio, ϵ/q, for the test specimen.

The experiments with the prototype apparatus proved sufficiently successful and educational that the results have been prepared for publication.[45] The more extensive work on the apparatus for use with actual test specimens remains to be prepared for publication. Combined with standard gas permeability measurements, the present technique permits essentially complete characterization of a porous medium for gas flow and diffusion. Its great advantages over other types of apparatus are simplicity and accuracy.

[45] R. B. Evans III, L. D. Love, and E. A. Mason, accepted for publication in the *Journal of Chemical Education.*

8. Irradiation Behavior of High-Temperature Fuel Materials

O. Sisman

IN-PILE TESTS OF COATED FUEL PARTICLES

P. E. Reagan E. L. Long, Jr. J. G. Morgan
T. W. Fulton

We have continued the study of irradiation effects on coated fuel particles by measuring the fission gas release rates during irradiation at high temperature and by postirradiation examination. In this series of in-pile tests, we have (1) studied the effect of pyrolytic carbon coating thickness on coating stability, (2) determined the integrity of conventional isotropic-buffer coated uranium oxide fuel particles operating at low temperature, and (3) tested the performance of thorium-uranium oxide particles coated in the Thorium-Uranium Recycle Facility (TURF).

An optimum-coating-thickness test was conducted by irradiating uranium oxide particles having three pyrolytic carbon coating thicknesses (capsule B9-38).[1] Each batch of the uranium oxide particles had a 243-μ-diam core, coated with an average 25-μ porous buffer, and a 20-, 40-, or 60-μ isotropic carbon layer. These coated particles, designated OR-1044, -45, and -46, respectively, were irradiated at 1400°C to 7.8 at. % uranium burnup. The fractional fission gas release (R/B) was near 1×10^{-4} at the beginning of the test and remained nearly constant throughout the test. Postirradiation examination revealed no coating failures, and metallographic examination of the 60-μ coated particles showed no significant microstructural changes. However, the high fission gas release rates gave evidence that the thin (20-μ) isotropic coatings are not sufficient to retain fission gas within present reactor design criteria. Test results are given in Table 8.1.

An integrity test on buffer-isotropic coated uranium oxide particles was conducted at low temperature. These coated particles, designated OR-654, were coated at low temperature at a high deposition rate from propylene. The coated particles were irradiated at 900°C in capsule B9-39 (ref. 2) to 13 at. % uranium burnup, with very low fission gas release, as shown in Table 8.1. Postirradiation metallography found no evidence of coating failure and only slight densification of the inner buffer region.

A performance test was conducted on pyrolytic-carbon-coated thorium-uranium oxide particles (coated by the Remote Fabrication Group) as a demonstration of the capability of the TURF. Except for the remote fabrication technique, these were conventional buffer-isotropic coatings from propylene applied to large (428-μ) fuel particles. The coated particles, designated OR-CR707, were irradiated in capsule A9-14 (ref. 3) at

[1] P. E. Reagan *et al.*, *GCR Program Semiann. Progr. Rept. Mar. 31, 1968*, ORNL-4266, pp. 11–14.

[2] P. E. Reagan *et al.*, *GCR Program Semiann. Progr. Rept. Sept. 30, 1968*, ORNL-4353.

[3] P. E. Reagan *et al.*, *GCR Program Semiann. Progr. Rept. Mar. 31, 1968*, ORNL-4266, pp. 7–10.

Table 8.1. Test Results – HTGR Fuel Materials

Experiment No.	Batch	Fuel	Heavy Metal Burnup (%)	Irradiation Temperature (°C)	Fractional Fission Gas Release, R/B for ^{88}Kr
B9-38	OR-1044 OR-1045 OR-1046	UO_2	7.8	1400	1.1×10^{-4}
B9-39	OR-654	UO_2	13.0	900	2.4×10^{-8}
A9-14	OR-CR707	$(Th,U)O_2$	1.8	1250	9.0×10^{-8}

1250°C. Because of the low enrichment, 23.3% ^{235}U, only 1.8 at. % heavy metal burnup was attained. The fission gas release rates remained low throughout the test, as shown in Table 8.1. Metallographic examination found no microstructural changes. These coated particles performed as well in-pile as conventional laboratory-made coated fuel particles.

IN-PILE TESTS OF BONDED BEDS OF COATED FUEL PARTICLES

P. E. Reagan E. L. Long, Jr.[4] J. G. Morgan
T. W. Fulton

The fuel element design for the Fort St. Vrain High-Temperature Gas-Cooled Reactor consists of coated fuel particles bonded with a graphite matrix into a fuel stick or bonded bed. We have conducted in-pile tests on two such bonded beds of coated particles at high temperature and high burnup, and at burnup rates four to eight times the burnup rates in an operating HTGR. These tests were conducted to determine the performance of this type of fuel element at high burnup and at high temperature.

A high-burnup irradiation test was conducted to study the stability of a bonded bed of pyrolytic-carbon-coated uranium oxide particles. The coated particles, designated OR-1010, consisted of a 43-μ porous carbon buffer and an 80-μ dense isotropic pyrolytic carbon coating, plus a thin anisotropic sacrificial layer. This thin coating adheres to the bonding matrix and is pulled away from the isotropic coating during the bonding process. This bonded bed was irradiated in capsule A9-15 (ref. 2) at 1250°C to 35 at. % uranium burnup, which required over 4800 hr at power. Based on the low fission gas release (2.5×10^{-8} R/B for ^{88}Kr) at the beginning of the irradiation test, it was concluded that none of the coatings were damaged in the bonding process. There was no appreciable increase in fission gas release during the entire test.

Postirradiation examination found the bonded bed intact. There were many discontinuous cracks in the bed, particularly near the ends, but these cracks were noted in the unirradiated bonded bed. In general, this bonded bed showed no serious damage by irradiation. A transverse section was taken at about midlength of the bonded bed and examined metallographically. Forty-one of the pyrolytic-carbon-coated UO_2 particles were exposed in this section, and there were no failures or indications of potential failures. The only significant change in the fuel was the appearance of noticeable metallic fission products (primarily Mo and Ru)[5] and small fission gas bubbles. After etching we noted that the metallic fission products had collected in the grain boundaries and that equiaxed grain growth had occurred during irradiation. The fission gas bubbles were distributed throughout the fuel. Examination of the coatings revealed that the inner regions of the buffer coating had densified; about one-third of the thickness of the buffer coating had been affected. No change in the isotropic coating was noted.

A Nuclear Safety irradiation test was conducted to determine the coated particle failure rate in an HTGR-design bonded bed as a function of temperatures that would be expected in a blocked-channel incident in an operating reactor. The bonded bed consisted of coated particles, designated OR-793, in a graphite matrix. These were 212-μ-diam uranium carbide particles, with a 43-μ porous carbon buffer, a 22-μ silicon carbide barrier layer, a 69-μ isotropic layer, and a thin sacrificial layer. This bonded bed was irradiated in capsule B9-40 (ref. 2), first at 1350°C for 2526 hr to 13.3% heavy metal burnup. The temperature was then increased in steps to 1450, 1550, 1600, 1650, and 1700°C, returning to 1350°C between steps. Each time the temperature was returned to 1350°C after a higher temperature irradiation, the fission gas release at 1350°C was measured, as shown in Fig. 8.1, to estimate the amount of coating damage at the higher temperature. The curve of Fig. 8.1 was made from a continuous activity recorder normalized to ^{88}Kr values determined on periodic gas samples. Fission gas release continuously increased for 24 hr at 1550°C and at higher temperatures. After approximately 160 hr at 1700°C, a steady-state release rate was reached. Based on the fractional ^{88}Kr released from bare uranium carbide in a previous experiment, the number of damaged particles at the end of the experiment was 520 (about 10%). Postirradiation examination found the bonded bed intact. Metallographic examination is in progress.

[4] Metals and Ceramics Division.

[5] B. D. Bradbury, J. T. Demant, and P. M. Martin, *Solid Fission Products in Irradiated Uranium Dioxide*, AERE-R-5149 (1966).

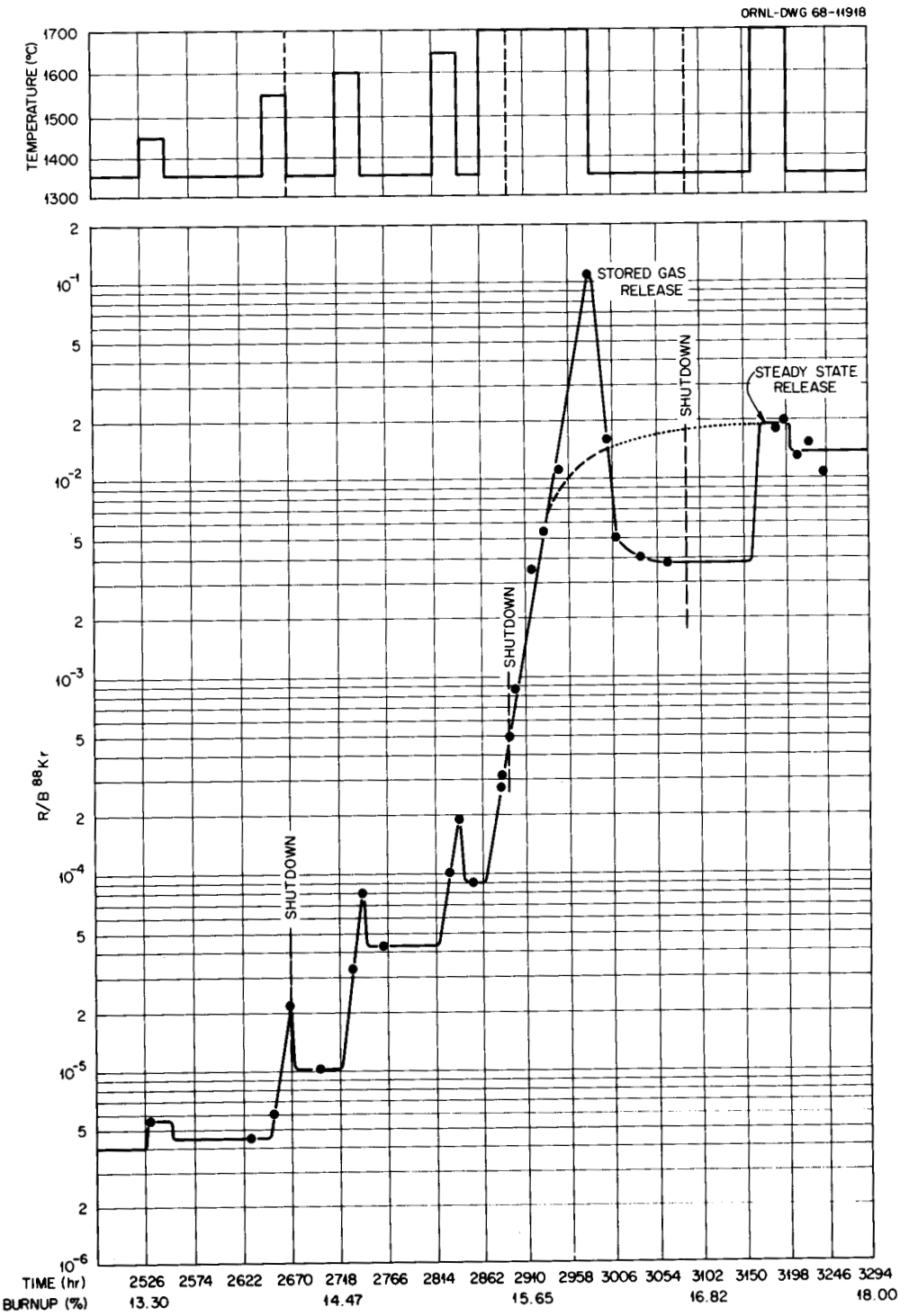

Fig. 8.1. Fission-Gas Release During Irradiation of a Bonded-Bed Fuel Containing OR-793 Coated Particles, Experiment B9-40.

FISSION PRODUCT RELEASE BY POSTIRRADIATION ANNEALING OF COATED FUEL PARTICLES

M. T. Morgan J. G. Morgan
R. L. Towns

Postirradiation anneals of coated fuel particles are being made to study the fission product retention of various coatings as a function of irradiation dose and temperature. The present program is concerned with Biso and Triso coatings applied to $(Th,U)C_2$, ThO_2, UC_2, or UO_2 microspheres. The Biso coating consists of a buffer layer of porous carbon and an outer layer of high-density isotropic pyrolytic carbon.[6,7] The Triso coating consists of a buffer layer of porous carbon, a layer of high-density isotropic pyrolytic carbon, an SiC barrier layer, and an outer layer of high-density isotropic pyrolytic carbon.[7] The microspheres range from 150 to 500 μ in diameter, while the coatings are from 70 to 130 μ in total thickness.

The retention of ^{137}Cs and ^{90}Sr in nuclear fuel elements is of considerable interest because of the long half-lives of these fission products (30 and 28.8 years respectively). A previous experiment with Triso-coated $(Th,U)C_2$ particles indicated that coated fuel particles with SiC barrier layers would retain all the prominent fission products except ^{137}Cs at temperatures to 1700°C and for short periods at 2000°C as long as the coatings remained intact.[8] Recent incomplete experiments on other Triso-coated fuel particles which showed that ^{137}Cs was retained prompted a repeat of the earlier experiment. Fifty additional Triso-coated $(Th,U)C_2$ particles from the same irradiation capsule as the earlier experiment with a burnup of 3.2% heavy metal were annealed for 6 hr at 2000°C. The ^{137}Cs release was less than 50 ppm. We are unable to account for the discrepancy in the earlier experiment, but believe that ^{137}Cs contamination of sample containers may have caused the high analysis.

The principal strontium fission products are ^{89}Sr and ^{90}Sr, but both are beta emitters. Since gamma spectrometry is the most accurate method of fission product analysis, we have been neutron activating small samples of unirradiated and irradiated coated fuel particles to produce fresh ^{91}Sr (half-life 9.7 hr) for annealing experiments. Activated Triso-coated $(Th,U)O_2$ particles were annealed for 19 hr at 2000°C. No ^{91}Sr was detected, but a significant fraction of ^{99}Mo was released. There was not enough ^{137}Cs produced in this activation to permit cesium analysis.

The annealing experiments to study cesium and strontium release will continue during the next year and will be expanded to study the retention of these fission products in bonded bed fuel elements. Some of these bonded bed fuel elements containing Biso- and Triso-coated UO_2 particles are now being irradiated in the B-9 facility of the ORR. It is planned to study the fission product retention as a function of irradiation time and annealing temperature by annealing bonded bed fuels with zero, medium, and high burnups and determining the fission products retained in the coated fuel particles, the matrix, and the graphite walls containing the bed.

MECHANISM OF FISSION GAS RELEASE FROM FUELED PYROCARBON-COATED MICROSPHERES

C. D. Baumann P. E. Reagan

Highly enriched UC_2-fueled pyrocarbon-coated microspheres with slightly contaminated coatings were irradiated in the A-9 facility of the ORR to determine the mechanism of fission gas release.[9] The postulated models for low krypton release rates, along with the resulting criteria for analyzing the release data, are summarized in Table 8.2.

It was found that the krypton release below 1600°C was by diffusion from contaminated outer coatings (model A-2) and that above 1600°C the release rate increased drastically with temperature and was by either Knudsen flow or solid-state diffusion through the outer coating (model B-1 or B-2). We were not willing to jeopardize the experiment by operating for long periods at high temperature. Therefore not enough high-temperature data were taken to determine which of these two possible mechanisms was the mode of release.

It was also found that when the temperature was reduced from above 1600°C to 1150°C the mechanism of krypton release gradually changed from diffusion through the coating back to diffusion from the coating.

The krypton release increased markedly with time, starting from the very beginning of irradiation. This is believed to be due to (1) the migration of the ^{235}U

[6] W. V. Goeddel, *Nucl. Appl.* 3, 599 (1967).

[7] *Summary Report on the Use of Triso-Coated Particles in the PSC Reactor Plant*, GA-8467, pp. 1–3 (Jan. 31, 1968).

[8] M. T. Morgan and R. L. Towns, *Reactor Chem. Div. Ann. Progr. Rept. Dec. 31, 1967*, ORNL-4229, pp. 128–31.

[9] C. D. Baumann and P. E. Reagan, *Reactor Chem. Div. Ann. Progr. Rept. Dec. 31, 1967*, ORNL-4229, pp. 130–32.

Table 8.2. Models for Low Krypton Release Rates from Fueled Pyrocarbon-Coated Microspheres

A. All release due to fissions that occur in contaminated coatings

Mode of Release	Fractional Release, f	Criterion
1. Direct recoil only	$f = \frac{3}{4}\frac{\delta}{c}\left[1 - \frac{1}{12}\left(\frac{\delta}{c}\right)^2\right]$	f same for all isotopes
2. Solid state diffusion	$f \xrightarrow[f<0.3]{} 3\sqrt{D/\lambda c^2}$	$\sqrt{\lambda_i} f_i = 3\sqrt{\frac{D}{c^2}}$, $i = 1, 2, \ldots$, number of isotopes
3. Combined recoil and diffusion	$f \rightarrow C\sqrt{D/\lambda c^2} + \frac{3}{4}\frac{\delta}{c}$	$\frac{f_i - f_j}{1/\sqrt{\lambda_i} - 1/\sqrt{\lambda_j}} = C\sqrt{\frac{D}{c^2}}$, $i, j = 1, 2, \ldots$, number of isotopes, $i \neq j$

B. All release due to fissions that occur in fueled core and product migrates through outer coating

Mode of Migration	Fractional Release, f	Criterion
1. Solid state diffusion	$f \rightarrow \frac{C}{\lambda}\sqrt{D_f D_c}\exp(-l\sqrt{\lambda/D_c})$	$\frac{\ln\frac{\lambda_i f_i}{\lambda_j f_j}}{\sqrt{\lambda_i} - \sqrt{\lambda_j}} = \frac{-l}{\sqrt{D_{0c}}}\exp(\Delta E/2RT)$
2. Knudsen flow through micropores in coating	$f \rightarrow \frac{C}{\lambda}\sqrt{D_f \frac{K}{\epsilon_c}}\exp(-l\sqrt{\lambda\epsilon_c/K})$	$\frac{\ln\frac{\lambda_i f_i}{\lambda_j f_j}}{\sqrt{\lambda_i} - \sqrt{\lambda_j}} = \frac{\text{const}}{T^{1/4}}$

δ = fission product recoil range in outer coating
c = radius of coated particle
D = diffusion coefficient (c = coating, f = fuel)
$= D_0 \exp(-\Delta E/RT)$
$C, D_0, \Delta E, R$ = constants
T = absolute temperature of fuel
λ = decay constant
l = thickness of outer coating
K = Knudsen flow coefficient
ϵ_c = open porosity of outer coating

which initially contaminated the outer coating, as well as (2) the increase of ^{235}U contamination (over fivefold) during the course of the experiment.

The xenon-iodine release model assumed that the parent iodine release plated out on the system walls and there decayed to xenon. Under steady-state conditions, the xenon decay rate equals the parent iodine release rate. Also, some xenon will be released directly from the coated particles. It is the sum of these two releases which is measured. When fissioning stops, the direct release of iodine and xenon ceases, but the iodine that plated out will continue to decay to xenon, the rate decreasing as exp $(-\lambda_I t)$. Thus one can determine the steady-state iodine release by extrapolating the xenon release back to time of shutdown.

By assuming the iodine and xenon release mechanism below 1600°C to be the same as that for krypton, that is, diffusion from contaminated coatings, one obtains for steady-state fractional releases

$$f_I = 3\sqrt{D_I/\lambda_I c^2}$$

and

$$f_x = 3\sqrt{\frac{D_x}{\lambda_x c^2}}\left(\frac{1}{1+\sqrt{\lambda_x D_I/\lambda_I D_x}}\right).$$

This model can be validated by examining the $\sqrt{\lambda}\, f$ for two or more iodine-xenon pairs. Table 8.3 lists the results of two measurements along with krypton data for comparison. From the constancy of the numbers for different isotopes of the same element, it is seen that the mode of release for iodine and xenon (as well as krypton) at about 1150°C appears to be by diffusion from contaminated coatings.

A postirradiation metallographic examination of slightly less than 2% of the irradiated particles disclosed no failures or evidence of potential failures, even though the experiment operated for about 500 hr above 1500°C.

RELEASE OF IODINE FROM BROKEN COATED PARTICLES

M. T. Morgan J. G. Morgan
R. L. Towns

Pyrolytic-carbon-coated fuel particles retain practically all the fission product iodine as long as the coatings remain intact. It was desired to find out how much iodine would escape if the coatings were fractured. We attempted to answer this question by postirradiation heating of cracked coated particles.[10]

Our experiments included UO_2 particles with an inner buffer coating of porous carbon and an outer coating of isotropic pyrolytic carbon, irradiated to a burnup of 10% ^{235}U, and UC_2 particles with a low-density isotropic inner coating and a high-density isotropic outer coating irradiated to a burnup of 14% ^{235}U. After the original ^{131}I had decayed, the coated particles were reirradiated to an additional burnup of 1% at a low temperature to produce fresh fission product iodine for the postirradiation experiments. The

[10] M. T. Morgan *et al.*, *Reactor Chem. Div. Ann. Progr. Rept. Dec. 31, 1967*, ORNL-4229, p. 132.

Table 8.3. Summary of Iodine-Xenon Experiments

Isotope	6/6 Experiment		6/22 Experiment	
	$\sqrt{\lambda}\, f \approx 3\sqrt{D/c^2}$ (min$^{-1/2}$)	T (°C)	$\sqrt{\lambda}\, f \approx 3\sqrt{D/c^2}$ (min$^{-1/2}$)	T (°C)
^{85m}Kr	5.20×10^{-6}	1140	2.18×10^{-5}	1167
^{88}Kr	4.99×10^{-6}		2.02×10^{-5}	
^{87}Kr	4.40×10^{-6}		2.23×10^{-5}	
^{133}I	4.65×10^{-6}		1.38×10^{-5}	
^{135}I	4.19×10^{-6}		1.61×10^{-5}	
^{133}Xe	5.84×10^{-6}		2.03×10^{-5}	
$^{135}Xe^{a,b}$	6.02×10^{-6}		1.78×10^{-5}	
$^{135}Xe^{a,c}$	6.48×10^{-6}		1.91×10^{-5}	

[a] For ^{135}Xe, $\lambda = \lambda + \sigma\phi$.
[b] $\sigma = 3.0 \times 10^6$ barns.
[c] $\sigma = 3.6 \times 10^6$ barns.

coatings were cracked after irradiation to simulate coating failures, and the particles with their coatings were then annealed to determine the ^{131}I release. We annealed one particle at a time, and the ^{131}I analyses were made on the particles before and after the anneals and on the furnace components after the anneals.

The iodine release from UO_2 is compared with that from UC_2 in Table 8.4. The fractional release of iodine from UC_2 was a factor of 10 to 17 lower than that from the UO_2. Most of the iodine release occurred during the first 2 hr at lower temperatures. The release in 8 hr was double that in 2 hr at the higher temperatures.

Some of the coatings of UO_2 particles were annealed separately from the cores. These data are listed in Table 8.5. The coatings from irradiated coated particles reirradiated at low temperature contained an average of 3.6% of the total iodine in the coated particle. This is much less than the 45% found in the coatings of the F-9 coated particles irradiated at 1250°C to a high burnup and reported previously.[11] This variation in iodine distribution in the coated particle resulted primarily because of the difference in irradiation time and temperature. If the fractional release of iodine from the coatings and cores of low-temperature-irradiated particles in Table 8.4 is applied to the iodine distribution found in the high-burnup coated particles, we find that the release of iodine in 2 hr at 1200°C would be about six times as much as for the low-temperature-irradiated particles. This difference would be greater at lower annealing temperatures and less at the higher temperatures. These differences should be considered in extrapolating results of postirradiation experiments on coated particles irradiated at low temperatures to the release expected under reactor operating conditions.

Table 8.4. Average Iodine Release from Cracked Coated Particles During Postirradiation Anneals

Temperature (°C)	Fuel Material	Percent of Total Released in –	
		2 hr	8 hr
1000	UO_2	0.9	1.0
	UC_2	0.08	0.1
1300	UO_2	7	11
	UC_2	0.4	0.9
1400	UO_2	17[a]	
	UC_2	1	2

[a]Extrapolated from 1-hr anneals.

POSTIRRADIATION STUDIES OF HIGH-BURNUP COATED PARTICLES

D. R. Cuneo J. H. Coobs[13]
J. A. Conlin[12] E. L. Long, Jr.[13]
H. E. Robertson

Three high-burnup coated particle irradiation experiments have been carried out in the ORR as part of the HTGR fuel program. The first two experiments were fueled by beds of loose coated particles, and the results were reported previously.[14] The third experiment was fueled by two in-line bonded beds containing a mixture of OR-1010-SB sol-gel UO_2 (93% enriched) and OR-1002-SB sol-gel ThO_2 coated particles (Th:U ratio was 16.6:1). The fuel cylinders, coated particles bonded

[11]M. T. Morgan *et al.*, *Reactor Chem. Div. Ann. Progr. Rept. Dec. 31, 1967*, ORNL-4229, p. 133.

[12]Reactor Division.

[13]Metals and Ceramics Division.

[14]D. R. Cuneo *et al.*, *Reactor Chem. Div. Ann. Progr. Rept. Dec. 31, 1967*, ORNL-4229, pp. 133–35.

Table 8.5. Iodine Release from Separated Coatings and Cores of Cracked Coated UO_2 Particles During 2-hr Postirradiation Anneals

Sample No.	Annealing Temperature (°C)	Percent of ^{131}I in As-Irradiated Coating	^{131}I Release	
			Coating (% of total in coating)	Core (% of total in core)
S20	1100	3.6	14	0.2
S21	1100	2.1	18	0.2
S19	1200	3.5	23	1
S18	1500	5.1	63	25

Table 8.6. Metallographic Observations of Pyrolytic-Carbon-Coated OR-1010-SB UO_2 and OR-1002-SB ThO_2 Particles Irradiated to a Fluence of 1×10^{21} neutrons/cm^2 at 1150 to 1300°C in Experiment F1-3

UO_2 Particles

1. Failed particles in upper and lower fuel cylinders similar in appearance
2. UO_2 converted to UC_2 in failed particles (Fig. 8.2*c*)
3. Relatively large fission gas bubbles observed in fuel cores as well as metallic globules of fission products
4. Inner buffer coatings had undergone densification for about half their thickness
5. Small metallic globules, less than 2 μ in diameter, could be seen in densified region of some buffer coatings
6. A few short microcracks observed in some isotropic coatings; these originated at the inner surface of the coatings
7. Separation of the nonbond (sacrificial) coatings observed
8. In a few particles, unilateral movement of the fuel cores toward the center line of the fuel cylinder was observed (Fig. 8.2*b*)

ThO_2 Particles

1. No significant microstructural changes noted
2. No potential failures found in 500 particles examined

together with resin containing graphite, were 1.74 in. long and 0.37 in. in diameter. The lower one also contained 10% maleic anhydride, which reduced curing time for the bonding matrix from 22 to 2 hr.

Details of the irradiation history and postirradiation findings have been given elsewhere.[15,16] The midplane central temperature of the fuel cylinders was maintained at 1150 to 1300°C during irradiation at a thermal neutron flux of 6.3×10^{13} neutrons cm^{-2} sec^{-1} ± 10%. The integrated thermal flux was 1×10^{21} neutrons/cm^2. Burnups ranged from 36 to 41% (upper to lower region) of the uranium in the UO_2 particles.

Upon disassembly of the experiment we found that the lower fuel cylinder (with maleic anhydride) had separated radially into three roughly equal-size pieces. The upper cylinder, initially found intact, separated into two pieces during dimensioning. Also, coated particles in the upper cylinder did not break away from the rough edges as they did in the lower cylinder. No unusual dimensional changes were found for other components of the experiments (various graphites and ZrC).

Gamma scans, narrow-range and multirange, gave locations of fission product and activated structural metal nuclides. Portions of experiment components were analyzed for fission product concentrations. While the gamma scans showed nonuniform distribution of fission products to varying extents, greater concentrations of the fission products were found in the graphite fuel holder and porous carbon insulators than in other components. About 10% of the ^{89}Sr and 2 to 3% of each of several other nuclides were found in the graphite fuel holder. About 15% of the ^{137}Cs was found in each of the two porous carbon insulators.

Leaching of three fuel-cylinder samples (8 *N* HNO_3 at 95°C for 8 hr) indicated UO_2 particle coating failures of 3.5, 5.3, and 12% for upper, central, and lower regions respectively. Metallographic examination of relatively few UO_2 coated particles revealed upper cylinder coating failures of about 10% and lower cylinder failures of about 23%. This lack of correlation is not too surprising, since the possibility of complete penetration of the acid through the bonding matrix and into very small cracks in the coatings is not too great. By the end of irradiation the fission gas release values (R/B) were in the range of 1 to 7%; from this it was estimated that 15 to 30% of the UO_2 particle coatings had failed.

Results of metallographic examinations of tranverse sections through the upper and lower fuel cylinders are

[15] A. W. Longest *et al.*, *GCR Program Semiann. Progr. Rept. Sept. 30, 1968*, ORNL-4353.

[16] D. R. Cuneo *et al.*, "High-Burnup Coated Particle Experiment No. 3," 14th Coated Particle Fuels Working Group Meeting, Nov. 20–21, 1968, ORNL.

R-46049

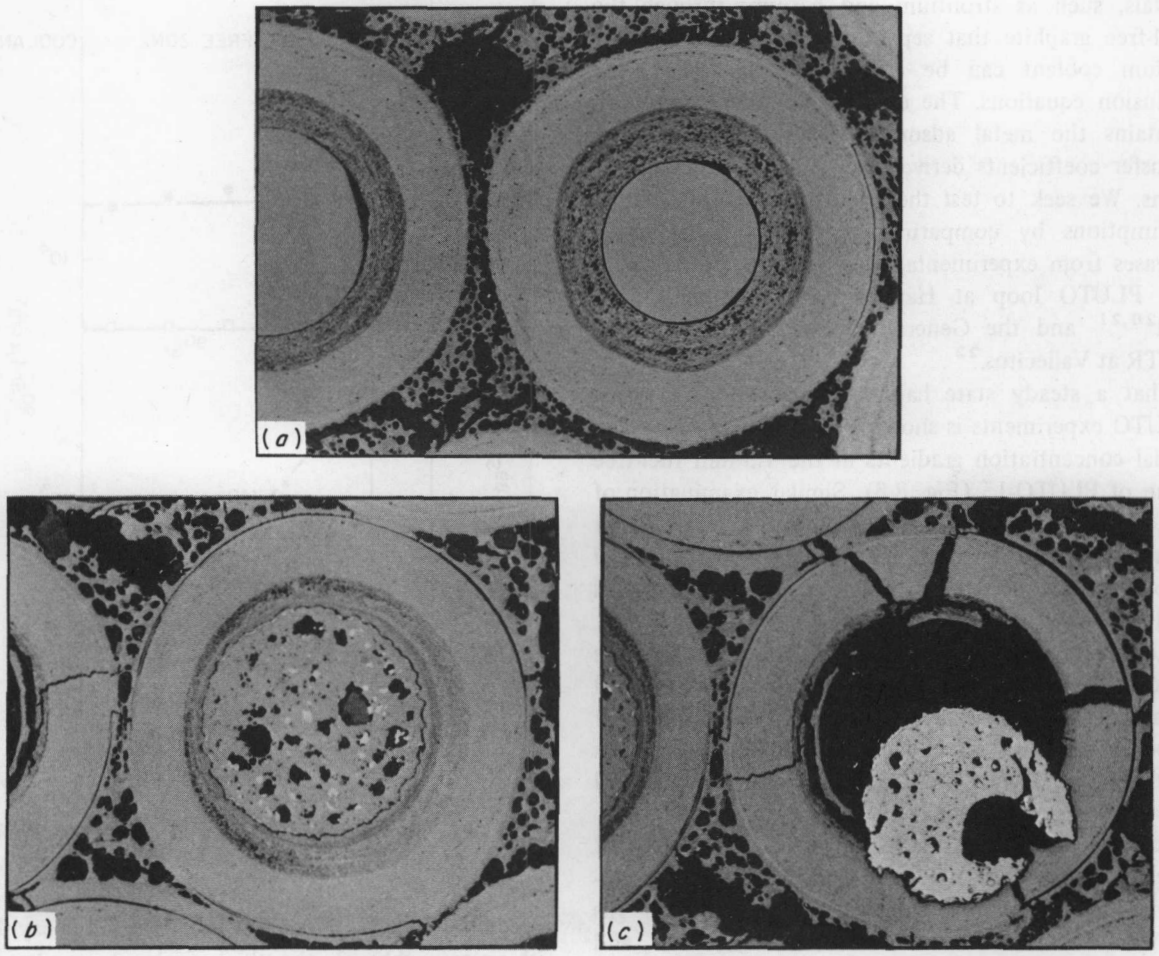

Fig. 8.2. OR-1010-SB UO_2-Coated Particles, Experiment F1-3. (*a*) Unirradiated control. (*b*) Particle irradiated to about 36% burnup. Note metallic globules in fuel core and its 10% displacement toward center line of lower fuel cylinder. (*c*) Failed particle irradiated to about 41% burnup. Note conversion of UO_2 to UC_2 and separation of nonbond (sacrificial) coating, now part of bed matrix.

reported in Table 8.6. Photomicrographs of the coated particles are shown in Fig. 8.2.

This experiment showed that OR-1010-SB UO_2 coated particles operated at 1150–1300°C to 35–38% burnup with 5–10% coating failures, and to 39–41% burnup with 15–25% failures. Fuel core movement within the coated particles was established as being unilateral toward the fuel cylinder center line. Weakness of the lower fuel cylinder (shorter curing time) was apparent; however, it underwent somewhat higher burnup and sustained more broken coated particles than the upper cylinder.

EXPERIMENTAL TEST OF THE FREVAP-8 CODE FOR CALCULATING METAL FISSION PRODUCT RELEASE FROM HTGR FUEL ELEMENTS

H. J. deNordwall V. H. Pierce[17]
L. R. Zumwalt[18]

In the FREVAP-8 (ref. 19) calculation, it is assumed for simplicity that the migration of fission product

[17] Gulf General Atomic, Inc.

[18] North Carolina State University, consultant.

[19] L. R. Zumwalt, *FREVAP-8 Code for Estimating the Release of Metallic Fission Products from HTGR Fuel Elements*, GAMD-7535 (December 1966).

metals, such as strontium and barium, through the fuel-free graphite that separates HTGR fuel from its helium coolant can be represented by steady-state diffusion equations. The external boundary condition contains the metal adsorption isotherms and mass transfer coefficients derived using known heat correlations. We seek to test these and other more detailed assumptions by comparing observed and calculated releases from experimental fuel elements irradiated in the PLUTO loop at Harwell for the Dragon Project[20,21] and the General Atomic (GAIL) loop in GETR at Vallecitos.[22]

That a steady state had been reached in the two PLUTO experiments is shown by the forms of observed radial concentration gradients in the 1.3-mm fuel-free zone of PLUTO-15 (Fig. 8.3). Similar examination of the GAIL element (Fig. 8.4) indicated clearly that steady state had not been achieved for the longer-lived strontium isotopes in the thicker graphite between fuel and coolant.[22]

Release rates for the fuels and diffusion coefficients used in the calculations were derived from unpublished measurements made on components of these and other experiments both in- and out-of-pile. The adsorption isotherms used were those determined at Gulf General Atomic for a nuclear-grade (TS-688) graphite.[23]

Table 8.7 describes the experiments, and Table 8.8 gives the results of the comparisons between experiment and calculation. Analyses of the coolant gas showed that the rates of release of ^{89}Kr, ^{90}Kr, and ^{140}Xe were insufficient to account for the ^{89}Sr, ^{90}Sr, and ^{140}Ba found in the PLUTO coolant circuits. The large differences between observed and calculated releases of ^{140}Ba are ascribed to uncertainties in the barium adsorption isotherm.

The FREVAP-8 calculation for the GAIL element yielded strontium releases which were very much higher than those observed. Here, neglect of transient diffusion for strontium has resulted in a calculated strontium release >100 times that observed. For the short-lived ^{140}Ba the situation is reversed because the calculation

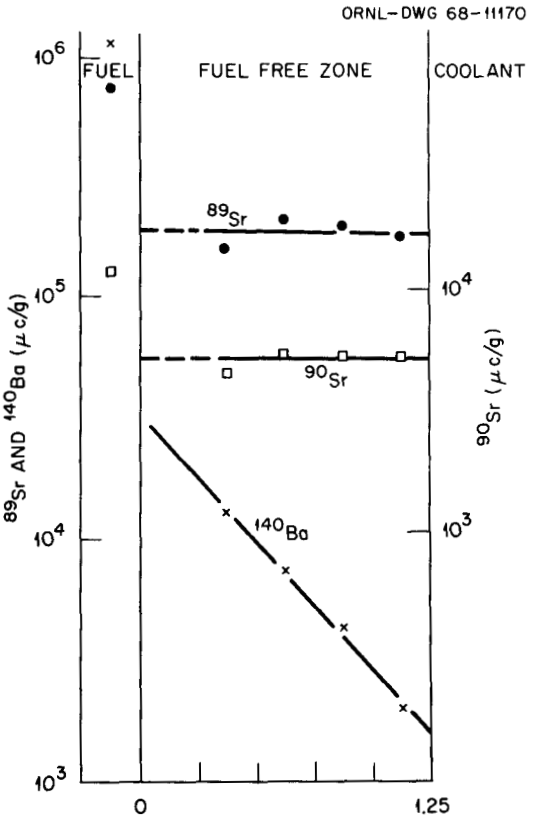

Fig. 8.3. Strontium and Barium Concentration Profiles in PLUTO 15 Fuel-Free Zone at 1120°C.

predicts that effectively all the ^{140}Ba will decay during its passage through the thick fuel tube, as is in fact found experimentally, whereas in reality there is a small release of ^{140}Ba as ^{140}Xe. Confirmation that ^{140}Xe release can account for observed ^{140}Ba has been obtained from GAIL and other experiments with similar thick fuel tubes.

We conclude that estimates of release from HTGR fuel elements in general were quite conservative. Methods of calculation taking into account transient behavior are recommended so that economic penalties from overdesign or the overestimation of hazards associated with ^{90}Sr in the coolant will be avoided.

Further comparisons between computed releases and experiment are being made in collaboration with Gulf General Atomic using the FIPER[24] code, which can handle transient situations. In addition, laboratory tests of the FREVAP and FIPER are in progress at ORNL.[25]

[20] P. E. Brown and H. J. deNordwall, *Postirradiation Radiochemical Analysis of Charge 8 for PLUTO Loop A*, AERE-R-5040 (1965); DP Report 388.

[21] H. J. deNordwall, *Postirradiation Radiochemical Analysis of Charge 15 of PLUTO Loop A*, AERE-R-5405 (1967).

[22] W. E. Bell, E. E. Anderson, and C. E. Milstead, *Postirradiation Chemical Examination of the GAIL IV Fuel Element*, GA-8588 (1968).

[23] J. H. Norman, D. A. Bafus, C. E. Milstead, and H. G. Staley, unpublished data, Gulf General Atomic, Inc.

[24] J. Appel and B. Roos, *A Study of the Release of Radioactive Metallic Isotopes from High Temperature Gas-Cooled Reactors*, GA-8399 (1967).

[25] F. H. Neill and M. D. Silverman, *GCR Program Semiann. Progr. Rept. Sept. 30, 1968*, ORNL-4353.

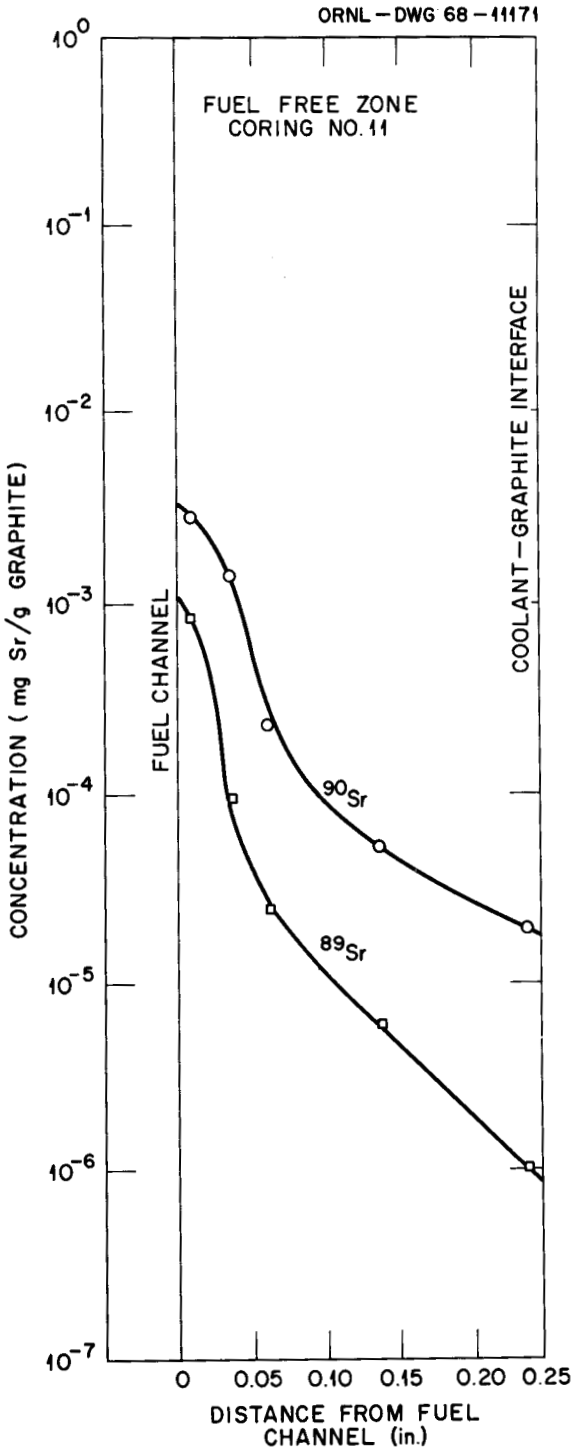

Fig. 8.4. Strontium Concentration Profiles in GAIL 4 Graphite at 950-900°C.

Table 8.7. Description of In-Pile Loop Experiments

Experiment	Fuel Coating[a]	Irradiation Time (days)	Peak Fuel Temperature (°C)	Peak Surface Temperature (°C)	Fuel-Free Zone Thickness,[b] L (mm)	Coolant Flow Rate (g/sec)
PLUTO 8	Pyc/SiC/PyC	173	1400	1350	1.25	18
PLUTO 15	PyC/Pyc	162	1370	1320	1.25	18
GAIL 4	PyC/PyC	400	1450	1100	$\leqslant$6.35	35

[a]PyC = pyrocarbon.

[b]For a PLUTO element L^2/D is $>$1/23 that for GAIL 4; hence a PLUTO element is that much closer to steady state. Alternatively a PLUTO element represents the behavior of an element with a 6-mm fuel-free zone after more than ten years irradiation, other things being equal.

Table 8.8. Comparison of Observed vs FREVAP Calculated Strontium and Barium Activity Release (in curies) for PLUTO 8, PLUTO 15, and GAIL IV

Nuclide	Experimental Data	Based on FREVAP
	PLUTO 8	
^{90}Sr – to FFZ[a]	2.7×10^{-2}	8.4×10^{-3}
^{90}Sr – to coolant	7.3×10^{-3}	6.9×10^{-3}
^{89}Sr – to FFZ	1.2	3.4×10^{-1}
^{89}Sr – to coolant	3.2×10^{-1}	2.7×10^{-1}
^{140}Ba – to FFZ	5.2×10^{-2}	3.4×10^{-2}
^{140}Ba – to coolant	2.2×10^{-3}	1.8×10^{-5}
	PLUTO 15	
^{90}Sr – to FFZ	Not determined	7.0×10^{-1}
^{90}Sr – to coolant	Not determined	6.5×10^{-1}
^{89}Sr – to FFZ	4.4×10^{1}	3.6×10^{1}
^{89}Sr – to coolant	3.5×10^{1}	3.3×10^{1}
^{140}Ba – to FFZ	4.8	9.2
^{140}Ba – to coolant	5×10^{-2}	5.0
	GAIL IV	
^{90}Sr – to FFZ	4.7	6.4×10^{1}[b]
^{90}Sr – to coolant	2.8×10^{-2}	5.2
^{140}Ba – to coolant	$(3 \text{ to } 12) \times 10^{-5}$	5.8×10^{-11}

[a]Fuel-free zone (to FFZ signifies the total quantity entering zone).

[b]Based on a conservative (high) estimate of "release constants." A calculated release of 2.4 curies is obtained using release data from in-pile experiments.

FISSION GAS RELEASE AND PHYSICAL PROPERTIES DURING IRRADIATION

Fission Gas Release During Fissioning of UO_2

R. M. Carroll R. B. Perez
O. Sisman

We have proposed a defect-trap model for the behavior of fission gas in UO_2 during irradiation.[26] The model uses the concept that fissioning will create defects in the fuel structure and will retard the migration of fission product atoms by trapping them at the defects. The population of the defects will vary with temperature, fission density, and irradiation history.

The effect of burnup on gas release is difficult to obtain with natural enrichment fuel, which we had used in prior experiments. On the other hand, enriched fuel would generate so much power that thermal stresses would fracture our usual-size specimens. We therefore obtained an enriched single-crystal specimen of UO_2 from which we cut highly polished spheres 0.0997 cm OD. Thirty-six of these spheres were placed in a tungsten holder and irradiated at power levels where thermal stresses would not break them.

The fission density within the spheres was higher than in any of our previous specimens, and we found that, in contrast to our earlier experiments, increasing the fission density accelerated the fission gas release. By combining all our experimental results with those from other workers, we have obtained the relation between fission density and the fractional release rate shown in Fig. 8.5 for specimens being irradiated at 1400°C. These results imply that at fission densities a little greater than 10^{14} fissions cm^{-3} sec^{-1} the fission gas release will become very high.[27]

The data of Fig. 8.5 are consistent with the defect-trap model in that at low fission densities ($<5 \times 10^{11}$) the fission-created defects have little effect on gas release. As fission densities increase, in the 10^{12} range, the increasing population of the defect traps becomes the dominating factor controlling the gas release rate. At about the 10^{14} fission density range, the fission-created defects are so dense that they interact with each other, thus accelerating the gas release.

The effect of burnup on the single-crystal spheres of UO_2 is shown in Fig. 8.6. Initially the fission gas release rate decreased because irradiation changed the surface structure of the spheres. This initial reduction has often been observed before.[28] As burnup progressed, an equilibrium release rate was obtained.

[26] R. M. Carroll and O. Sisman, *Nucl. Sci. Eng.* **21**, 147 (1965).

[27] R. M. Carroll, O. Sisman, and R. B. Perez, *Nucl. Sci. Eng.* **32**, 430 (1968).

[28] R. M. Carroll, *Nucl. Safety* 8(4), 345 (1967).

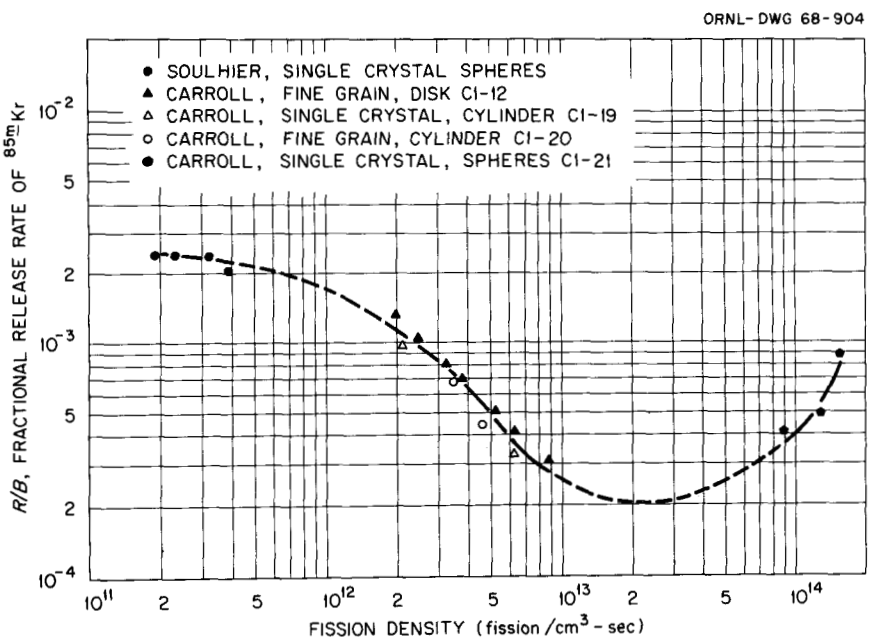

Fig. 8.5. Fractional Release of ^{85m}Kr from High-Density Stoichiometric UO_2 During Irradiation at 1400°C.

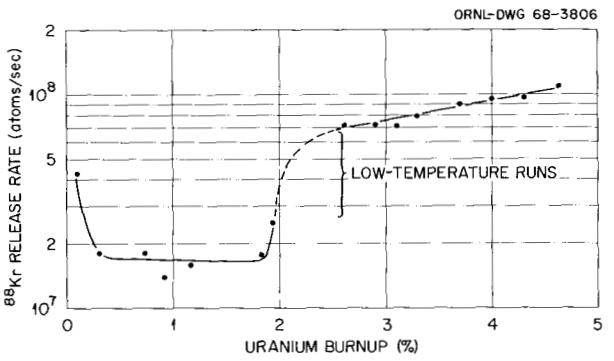

Fig. 8.6. ^{88}Kr Release from Single-Crystal UO_2 Normalized to 820°C and 1.5 × 10^{14} fissions cm^{-3} sec^{-1} as a Function of Uranium Burnup.

After about 1.9% uranium burnup, the gas release rate increased sharply with burnup. The increase is postulated to be caused by fission products which concentrated in defects, eventually causing enough stress to fracture the spheres. The increased surface area of the broken spheres resulted in an increased fission gas release. With more burnup the spheres continued to fracture into smaller and smaller fragments, thus causing an ever increasing fission gas release. The lack of internal porosity and grain boundaries, where fission products could be concentrated without creating stresses, undoubtedly contributed to the rupture of the single-crystal spheres at this comparatively low burnup.

Fission Gas Release During Fissioning of UN and $(Pu,U)O_2$

R. M. Carroll R. B. Perez
O. Sisman

Three UN pellets, each 19.77% enriched with ^{235}U, were stacked inside an Al_2O_3 holder and irradiated for the dual purpose of measuring thermal diffusivity and fission gas release. The pressed and sintered pellets, manufactured by the Metals and Ceramics Division, had a density of 13.56 g/cm^3 (94.7% of theoretical) and were each 0.65 cm OD. The three-pellet stack formed a hollow cylinder 2.27 cm long with a 0.26-cm-ID axial hole.

The UN pellets were irradiated to 9.8 × 10^{19} fissions/cm^3 (0.31% uranium burnup) at temperatures varying from 200 to 1500°C. After only 2.8 × 10^{18} fissions/cm^3 burnup at temperatures less than 600°C, we detected step increases of fission gas release, which indicated that the specimen was cracking. This was unexpected because of the low burnup, low thermal stresses, and low temperatures. As the burnup continued the amount of cracking continued.

There was some evidence that the cracks were healing when the specimen was irradiated at temperatures of 1300°C or above, thus implying that the cracks were very small. Any sudden change of temperature caused new cracks, resulting in a burst of fission gas as the specimen heated or cooled. A typical gas release as the specimen cooled is shown in Fig. 8.7, where it is apparent that spontaneous cracking occurred almost an hour after the specimen had cooled off. The continued escape of gas after the specimen cooled is from gas diffusing out of cracks in the UN specimen. The cause of the cracking is unknown at present, although metallographic examination may show some clues.

High-density (97% of theoretical) pressed and sintered pellets of (0.75 U, 0.25 Pu)O_2 were obtained from Pacific Northwest Laboratories. These pellets were made to the Fast Flux Test Facility specifications except for a 0.127-cm-ID axial hole to contain a central thermocouple. From the very beginning of the irradiation, the fission gas release from these pellets (as observed during temperature variations) showed that the gas was diffusing from small cracks or interconnected porosity rather than diffusing from the fuel matrix. Since interconnected porosity is unlikely in high-density pellets, microscopic cracks caused by the heat treatment during fabrication were most probably the source of gas release.

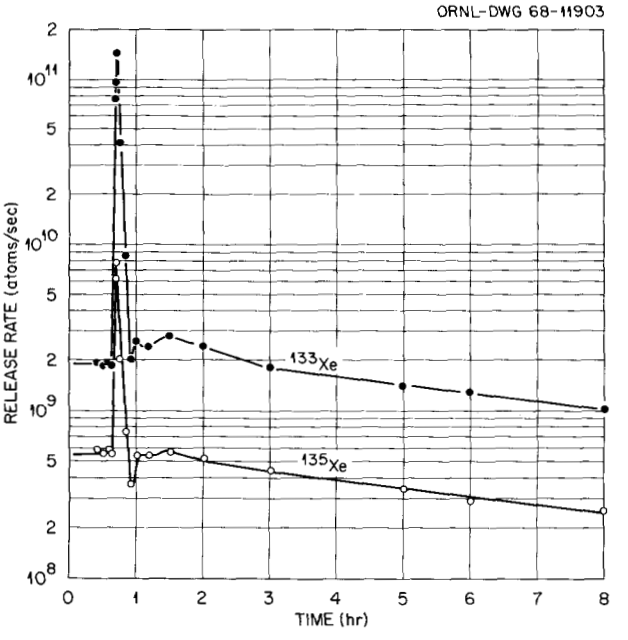

Fig. 8.7. Cooling Burst when UN Specimen (C1-23) was Cooled Quickly from 1340°C to 200°C.

We observed that some increase of cracking occurred as burnup progressed and that at 1300°C there was some evidence of crack healing. To attempt a higher rate of crack healing, we increased the fission rate by 75% and increased the temperature to 1450°C. This condition was only maintained for 20 min before extremely high fission gas releases forced the withdrawal of the specimen. Apparently the specimen was broken extensively by this treatment, because the subsequent gas release was more than an order of magnitude higher than for similar conditions just before the high-temperature run.

In-Pile Thermal Conductivity of Fuel Materials

R. M. Carroll R. B. Perez
J. G. Morgan

We have continued the feasibility studies on the thermal conductivity of fuel specimens during irradiation. Conventional thermal conductivity measurements cannot be applied to ceramic fuels during irradiation at realistic power levels because thermal stresses will break the specimen unless thin cross sections are used. For example, thick cylinders of fuel with thermocouples embedded at different locations cannot be used.

The thermal conductivity method which we have been pursuing uses a thin cylinder specimen with a thermocouple measuring the central temperature. The fission heat generation in the fuel specimen is changed in a stepwise fashion by moving it into a higher flux region in the reactor. The resulting temperature rise of the specimen and its surroundings is measured as a function of time (after the step change) by an automated data logger.

The initial results of computer processing of the data tapes showed that the values of thermal conductivity appeared too low to be realistic. This implied that the heat source was larger than calculated. Based on calculations, we had assumed that the heating by nonfission sources could be neglected in comparison with fission heating. The discovery that our heat source was very likely larger than calculated made it necessary that we measure the amount of the nonfission heating.

A copper slug suspended in a standard capsule was used to determine the amount of nonfission heating in our experiment. Two methods were used to produce a step change of temperature: a perturbation of position and a perturbation of heat removal. Since the thermal conductivity and specific heat of pure copper are well known, the amount of heat necessary to produce a given heating rate could be determined. A continual measurement of neutron flux was also made during these tests. This method allowed us to establish a relation between neutron flux and nonfission heating over a range never before attained.[29,30] The nonfission heating in copper varied from 0.2 to 9.5 w/g over the movement range of our experimental facility (ORR-C1).

We then included nonfission heating in our thermal conductivity calculations but found that the heat generation was still greater than could be accounted for. Moreover, the results were not consistent with time and did not vary smoothly with temperature, although each individual measurement appeared good.

We then noticed a pip of temperature on the heating curve of a UN specimen. This could only be explained as a release of stored energy. Reexamining the older data, we could see from the shape of the heating curve that, as the specimen power was step increased, the temperature rose in pulses. We believe, therefore, that energy stored by irradiation damage was producing the additional heat generation.

A small amount of stored energy has been found in UO_2 by postirradiation measurements.[31] However, from our dynamic defect-trap model it follows that a greater amount of energy is available for release during irradiation. In retrospect we can see that our explanation of the bursts of fission gas caused by increasing the temperature of a specimen during irradiation also implies a release of stored energy. Now that the problem is recognized, we may be able to step cool the specimen and thus measure thermal diffusivity without triggering stored energy. If so, the difference between step heating and step cooling will allow a measurement of the stored energy.

---

[29] R. M. Carroll and R. B. Perez, *Fuels and Materials Development Program Quart. Progr. Rept. Sept. 30, 1968*, ORNL-4330, pp. 54–58.

[30] R. M. Carroll, R. B. Perez and O. Sisman, "Non-Fission Heating in a High Neutron Flux Reactor," submitted to *Nucl. Sci. Eng.*

[31] G. H. Dienes (Ed.), *Studies in Radiation Effects on Solids*, vol. 2, p. 189, Gordon and Breach, New York, 1967.

Part IV. Nuclear Safety

9. Nuclear Safety Tests in Major Facilities

AGING BEHAVIOR OF FISSION PRODUCTS RELEASED BY IN-PILE MELTING OF UO_2

B. F. Roberts S. H. Freid O. W. Thomas[1]
W. H. Montgomery O. Sisman

The In-Pile Nuclear Safety Installation[2] at the Oak Ridge Research Reactor is being used to study the aging behavior of the realistic fission product aerosols released by molten UO_2 in simulated loss-of-coolant accidents. Four aging experiments have been performed. In the first two experiments an air atmosphere in the aging chamber was maintained at 35 and 103°C respectively. These experiments were described last year, and preliminary data were presented.[3] In the last two experiments an atmosphere consisting of a mixture of 50% steam and 50% air was maintained at 80°C. A pool of water on the bottom of the chamber was kept slightly above 80°C to maintain condensing steam on the chamber walls. As expected from the results of previous meltdown experiments, about half of the iodine inventory, a third of the cesium, 5% of the tellurium, and less than 1% of the other fission products reached the aging chamber. Although they were heated, the transfer line from the UO_2 furnace to the aging chamber and other steel surfaces trapped about a third of the inventory of the volatile iodine, tellurium, and cesium.

Although the aging behavior of several fission products was studied, that of iodine is emphasized because it can exist as various species and can change species during the aging process. Iodine aerosols are generally divided into three species: particulate, molecular, and organic. Particulate iodine is generally defined as that which is associated with particles large enough to be trapped on a high-efficiency filter. Molecular iodine readily reacts with silver or copper surfaces. Organic iodine is a mixture of alkyl iodides which can be conveniently trapped only by charcoal.

Figure 9.1 shows the aging behavior of particulate iodine. The ordinate, C/C_0, is the concentration of particulate iodine at time t, normalized to the concentration of total iodine at time t_0. This latter concentration is the amount of iodine entering the chamber divided by the volume of the chamber. The reason that particle removal by condensing steam is not faster may be due to the fact that the chamber is so well insulated that only a small condensing steam flux can occur under the isothermal conditions of the experiment. Fission products other than iodine appear to be entirely associated with particulate material but are not removed quite as rapidly as particulate iodine. The enhanced removal of particulate iodine indicates that iodine desorbs from particles while still in the aerosol state.

Figure 9.2 shows that the aging behavior of molecular iodine depends on the conditions in the aging chamber. In the first experiment the concentration decreased because the molecular iodine diffuses to the cool chamber walls and is adsorbed. The lower rate of decrease of molecular iodine relative to that of particulate iodine is caused by iodine desorbing from particulate matter while still in the airborne state and forming molecular iodine. In the second experiment the adsorption appears to be approximately balanced by desorp-

[1] On loan from the General Engineering Division.

[2] C. E. Miller, Jr., *et al.*, *Reactor Chem. Div. Ann. Progr. Rept. Dec. 31, 1966*, ORNL-4076, p. 153.

[3] S. H. Freid *et al.*, *Reactor Chem. Div. Ann. Progr. Rept. Dec. 31, 1967*, ORNL-4229, p. 149.

tion from the hot dry surface or by conversion of particulate iodine. In the condensing steam atmosphere, the molecular iodine is gradually washed out of the aerosol and dissolves in the water on the bottom of the chamber.

The aging behavior of organic iodine again depends on the conditions of the aging chamber. Organic iodine apparently also diffuses to the walls and is adsorbed on cool dry surfaces. In the hot dry chamber a significant conversion to organic iodine apparently occurs. However, in a condensing steam atmosphere organic iodine does not appear to show an aging effect. In the first two experiments, bulk aerosol samples were collected during the aging process and significant amounts of methyl, ethyl, and butyl iodides were identified by gas chromatography.

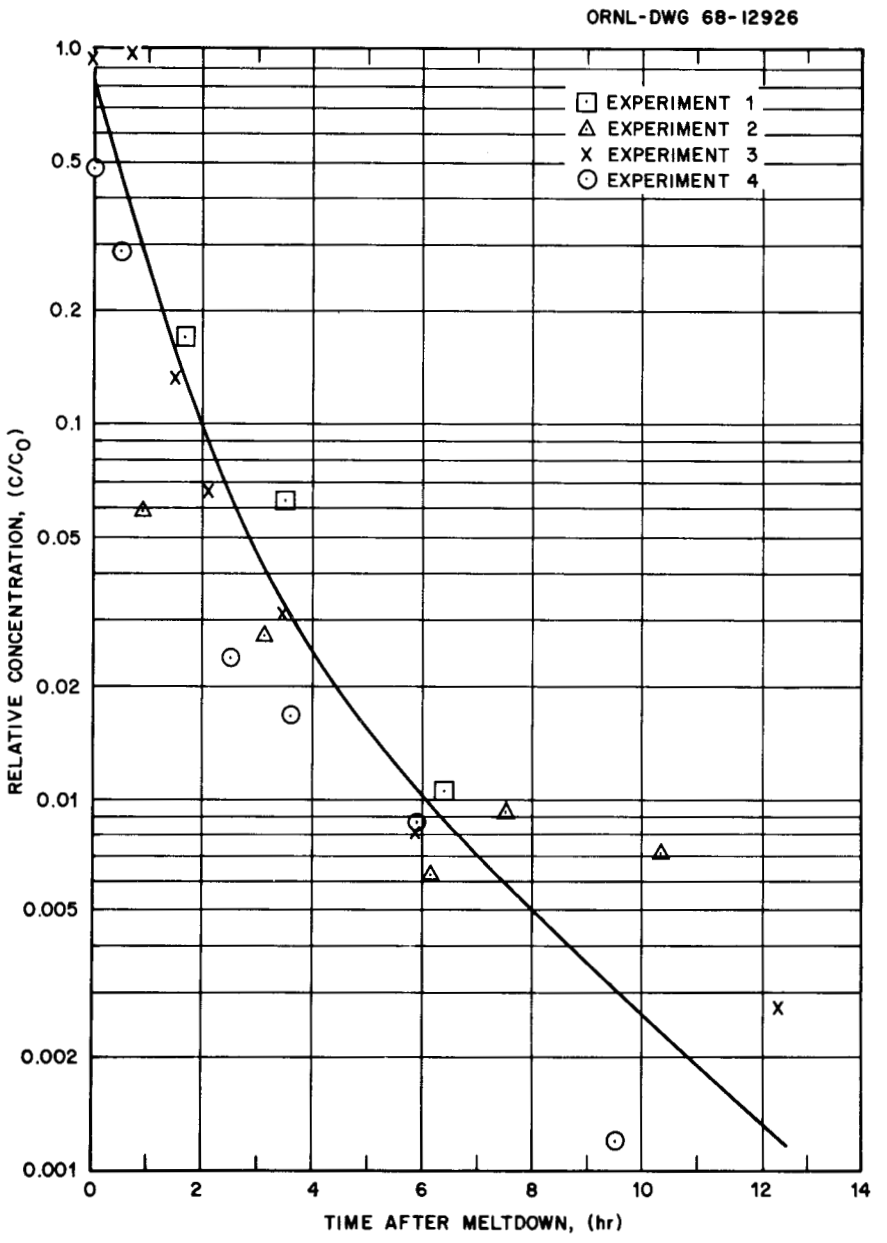

Fig. 9.1. Aging Behavior of Particulate Gas-Borne Iodine.

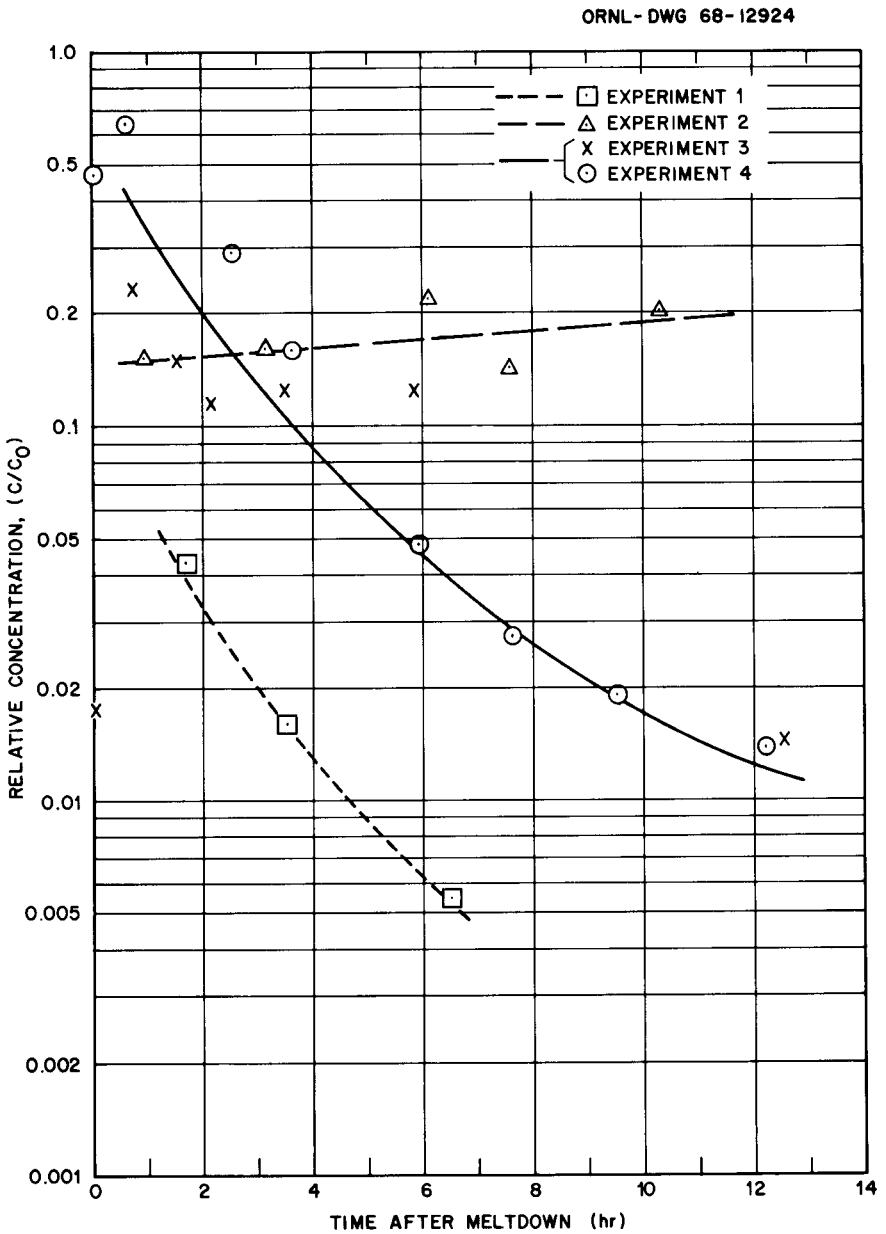

Fig. 9.2. Aging Behavior of Molecular Gas-Borne Iodine.

IN-PILE BEHAVIOR OF HTGR FUEL ELEMENTS IN MIXTURES OF STEAM AND HELIUM

S. H. Freid H. J. deNordwall B. F. Roberts
O. Sisman W. H. Montgomery

The objective of this program is to demonstrate that rate constants measured out-of-pile can be used to describe the way carbon is removed from an operating HTGR fuel element. Construction has begun of an experiment in which a model fuel element generating heat by fission can be exposed to helium containing controlled amounts of steam.

A sketch of the model fuel element is shown in Fig. 9.3. It differs from that used in the previous in-pile experiment,[4] which demonstrated the protection afforded to the fuel by surrounding graphite, in two respects. First, thermocouples can be placed in specially

[4]S. H. Freid *et al.*, *Nucl. Safety Program Ann. Progr. Rept. Dec. 31, 1967*, ORNL-4228, p. 257.

provided pockets to record a temperature close to the surface temperature. Second, both ends of the element are protected from steam by alumina caps, so that reaction geometry is more closely controlled. The model element contains carbon atoms arranged in three different structures: pyrocarbon, binder carbon, and what is loosely called graphite. In assessing the consequences of steam attack, one needs to know which carbon atoms are being removed. By making the simplifying assumption, justified by Overholser's[5] work, that pyrocarbon is very much less reactive than the other two carbons, one can make the necessary distinction between the oxidation products of the binder and graphite in a mixture by labeling the binder with ^{14}C.

The essential features of the experiment are: a source of dry helium free from extraneous oxidants, carbon compounds, and hydrogen; a source of water or steam; a reaction chamber situated in a movable capsule in the reactor (ORR); and an analysis train for stable and radioactive gases, so that carbon removal and fuel coating failure can be monitored almost continuously.

Necessary features of the reaction chamber are: well-defined simple geometry, a small volume so that it may be treated as a differential reactor, a controlled temperature, and a controlled fission rate. The number of fissions per cubic centimeter in the fuel stick determines the radial temperature gradient and is, in turn, determined by the neutron flux which is monitored with a self-powered flux monitor. The flux in the capsule may be changed by moving the capsule.

The fuel element's surface temperature is determined by the ease with which heat can be lost to the reactor cooling water that surrounds the capsule. The configuration of the insulation is therefore different for each experiment at a different temperature. The maximum surface temperature envisioned in this program is <1500°C.

The mixture of helium, reaction products, and possibly fission products leaving the reaction chamber is cooled rapidly to ~250°C, at which temperature it travels via filters to the analysis train. A completely new analysis train has been designed for this experiment. Water, carbon monoxide, carbon dioxide, hydrogen, and any hydrocarbons present are determined using a Monopole residual gas analyzer which doubles as a leak detector. A separate side stream is taken for ^{14}CO and $^{14}CO_2$ determination after drying.

[5]C. M. Blood and L. G. Overholser, *Compatibility of Pyrolytic-Carbon Coated Fuel Particles with Water Vapor*, ORNL-4014 (Nov. 29, 1966).

ORNL-DWG 69-189

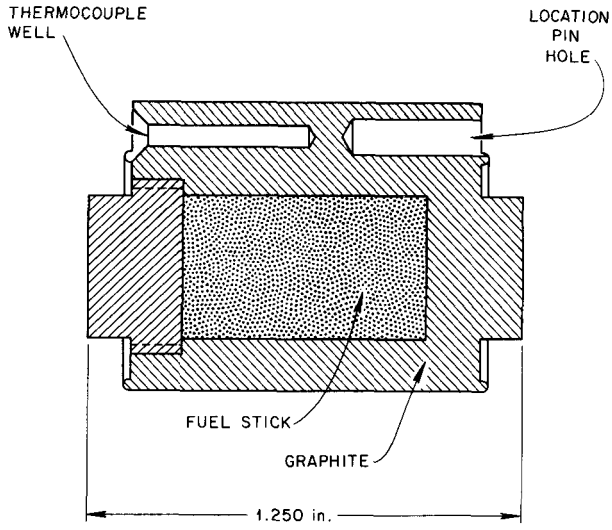

Fig. 9.3. HTGR Model Fuel Element.

A third stream, from which water is removed by a condenser followed by chemical driers, is used for continuous determinations of short-lived rare gases. Samples of gas may be withdrawn from lines containing water vapor and from points preceded by condensers and driers. A May pack is provided for iodine analysis. A degree of redundancy has been incorporated deliberately into the analytical instruments.

Work has begun on calculational models for reaction in a two-component system.

TREAT FUEL ROD FAILURE LOSS-OF-COOLANT EXPERIMENT

G. W. Parker R. A. Lorenz

The series of experiments to be performed in TREAT should provide answers to the following important questions about loss-of-coolant accidents. First, will dimensional changes in the fuel rods be large enough to impair the efficiency of emergency core cooling, and second, what amount and chemical form of fission products will be released from the ruptured fuel rods?

The planned TREAT experiments will simulate the post-blowdown portion of a loss-of-coolant accident and will use seven-rod clusters of 27-in.-long Zircaloy-2-clad UO_2 fuel rods. The center rod will contain fission products from a two-cycle 1800 Mwd/ton burnup irradiation in the MTR at a linear heat rating of 15 kw/ft. According to the D' (empirical) method of estimating fission product diffusion, we calculate that

10% of the iodine will be released from UO_2 to the fuel rod void spaces.[6] The center rod will be pressurized with 215 psia helium (25°C) to give a pressure equivalent to that of the fission gases released from UO_2 during an eight-month irradiation of 10,000 Mwd/ton.

In TREAT the loss-of-coolant simulation will be performed by operating TREAT at constant power for 17 sec. Fission heat in the 1.5%-enriched UO_2 pellets will raise the cladding temperature 70°C/sec in the first experiment. This high rate of heatup is typical of that which will occur immediately following the blowdown phase of a real accident when high heat content of the UO_2 is available to heat the cladding.

Flowing steam will provide a realistic atmosphere for the rod rupture and fission product release. A photograph of the experiment assembly is shown in Fig. 9.4. The entire steam system, including the primary vessel, will be preheated electrically to 130°C to prevent condensation. The flow system supplies 2 liters/min (STP) of helium and 11 liters/min (STP) of steam through the primary vessel. An additional 2 liters/min of helium is added to the fission product collection systems to provide a clean backflow through the second fission product collection system when the first collection system is in use. This flow rate of steam is realistic for pressurized and boiling-water reactors based on relative total cladding area.

The outer circle of six unirradiated rods will be pressurized with helium to 40, 65, 115, or 215 psia at 25°C. The pressure in two of these rods will be continuously monitored with pressure cells during the loss-of-coolant accident simulation. The predicted rupture temperatures, ranging from 730 to 1030°C, are based on the reported ultimate strength of Zircaloy 4.[7]

[6] G. W. Parker *et al.*, *Nucl. Safety Program Ann. Progr. Rept. Dec. 21, 1967*, ORNL-4228, pp. 11–17.

[7] H. C. Brassfield *et al.*, *Recommended Property and Reaction Kinetics for Use in Evaluating a Light-Water-Cooled Reactor Loss-of-Coolant Incident Involving Zircaloy-4 or 304-SS-Clad UO_2*, GEMP-482, p. 80 (April 1968).

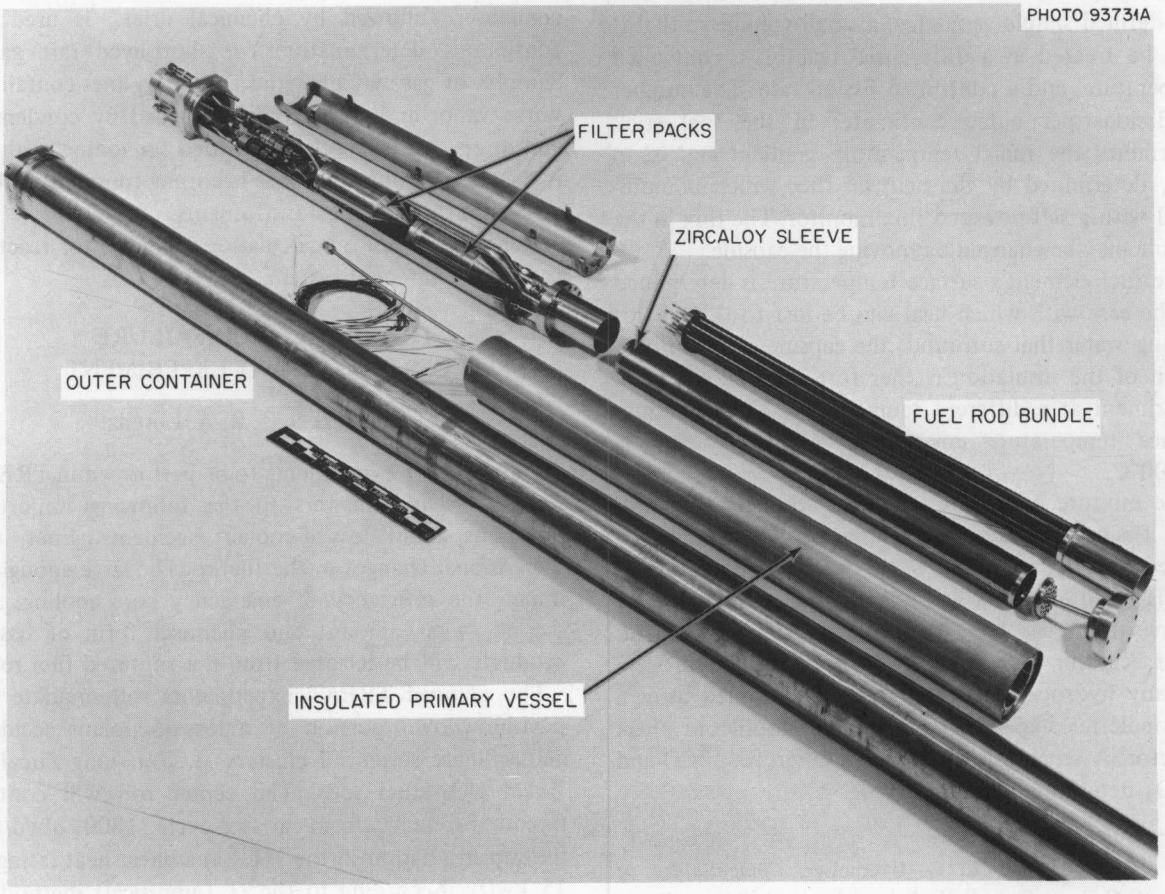

Fig. 9.4. Experiment Assembly for TREAT Loss-of-Coolant Test.

Correlation of rupture temperature with initial pressure will be made by using high-speed recordings of the four rod thermocouples and the two rod pressure cells. A high-sensitivity differential pressure cell on the primary vessel will be used to attempt to detect the bursts of gas released from ruptured rods.

The fission product collection system consists of two identical collection trains. The first one will be in use for the first 60 sec to collect the "prompt" fission product release. Flow will then be diverted to the second system to collect the delayed release. Each collection system has a filter pack located in the in-pile portion of the experiment to collect reactive forms of iodine and aerosol particles. Components outside the reactor are a steam condenser, water trap, methyl iodide trap, water freeze trap, and fission-gas traps. A rotometer and wet test meter will measure hydrogen formed by the metal-water reaction.

The center rod for the first experiment has been irradiated for one 18-day cycle in the MTR. The first TREAT assembly is nearly ready, but is being delayed until a rigid safety analysis is completed.

PROMPT CLAD FAILURE RELEASE OF FISSION PRODUCTS FROM REACTOR FUEL ELEMENTS (OUT OF PILE)

G. W. Parker M. F. Osborne

The biological hazards of a power reactor accident are dominated by the release of fission products from ruptured fuel elements coincident with or within a few minutes after a loss-of-coolant (LOC) accident. Therefore we are studying the release and behavior of those fission products which exist in the fuel-cladding void space under normal operating conditions and would be released in significant fraction under accident conditions. Irradiated fuel capsules of Zircaloy-clad UO_2 are heated to rupture in steam to simulate the accident, and the released fission products, principally I, Cs, Ru, and Te, are collected on filters and selective adsorbers for analysis.

GETR-Irradiated Capsules

Two of the twelve GETR-irradiated Zircaloy-2-clad UO_2 fuel capsules, which were described previously,[8] were heated to rupture in the capsule failure furnace, and the results were similar. Three of the capsules were examined destructively at Vallecitos Nuclear Center, and seven capsules remain to be tested. The prefix PR was added to capsule identification numbers to denote prompt release rupture tests. Each failure occurred after a few minutes at ~1300°C in a flowing helium-steam atmosphere. Cladding swelling was about 10% of the diameter or less, and extensive cladding oxidation was apparent. The cladding ruptures were small, and in both cases the embrittled cladding broke during posttest inspection despite careful handling. Typical fracture appearance is illustrated in Fig. 9.5, which shows that the oxide layer penetrated about 50% of the 0.035-in. wall thickness in the central region of the capsule.

Since these two capsules were irradiated at relatively low fuel temperature, very low fission product release was expected. The release data are summarized in Table 9.1, and compared with the estimated fuel-cladding gap activity, which is that fraction readily available for release. Data from Hoffman and Coplin[9] and from Parker *et al.*[10] were used to estimate the gap activities. The ^{85}Kr release data for two other capsules in this series, which were opened and analyzed at room temperature at Vallecitos Nuclear Center, are also shown in Table 9.1. No gas release data were obtained from the third capsule (042) opened at Vallecitos.

In an effort to obtain iodine release data, the fuel capsule in test PR-011 was reirradiated at low power in the ORR immediately prior to the test. However, the ^{130}I concentration, from activation of the fission product ^{129}I, was below the limit of reliable analysis. The principal released activity was ^{137}Cs, but trace amounts of ^{131}I, ^{135}Xe, ^{95}Zr-^{95}Nb, ^{113}Sn, and ^{125}Sb were collected also. Activation analysis was utilized to determine the amount of iodine collected.

In general, the observed release fractions correlate fairly well with the estimated gap activities, which are based on irradiation conditions, and with the results of iodine tracer experiments reported previously.[8] Subsequent tests of capsules irradiated at higher powers will extend the range for comparison to fuel temperatures of 2500°C (22.5 kw/ft); such conditions should result in gas release fractions of ~30% and correspondingly higher solid fission product release. Induction heating will be utilized to produce a rate of rise in test temperature as high as 100°C per second.

---

[8] M. F. Osborne and G. W. Parker, *Reactor Chem. Div. Ann. Progr. Rept. Dec. 31, 1967*, ORNL-4229, pp. 174–75.

[9] J. P. Hoffman and D. H. Coplin, *The Release of Fission Gases from Uranium Dioxide Pellet Fuel Operated at High Temperatures*, GEAP-4596 (September 1964).

[10] G. W. Parker *et al.*, *Out-of-Pile Studies of Fission Product Release from Overheated Reactor Fuels at ORNL, 1955–1965*, ORNL-3981.

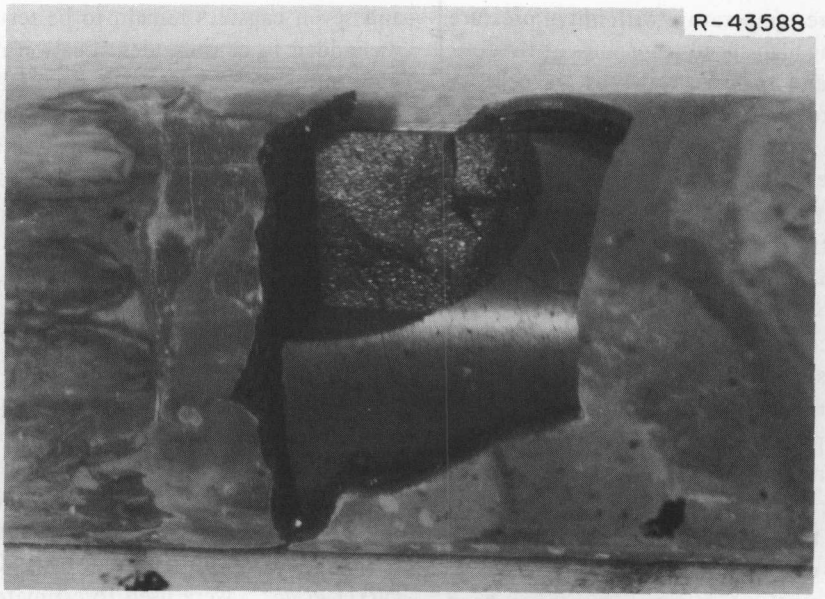

Fig. 9.5. Region of Posttest Fracture near Midlength in Capsule 041 (Test No. PR-041). Note the laminated appearance of the cladding, showing oxide penetration to 50% of the cladding thickness. 4.0X.

Table 9.1. Capsule Rupture Test Data

Test No.	Rupture Temperature (°C)	Irradiation Conditions: Maximum Fuel Temperature (°C)	Irradiation Conditions: Maximum Linear Power (kw/ft)	Nuclide	Total Inventory (atoms)	Percent in Gap (estimated)	Percent Released (measured)
PR-011	1300	1070	10.1	^{129}I	1.5×10^{18}	0.02	<0.001
				^{137}Cs	1.1×10^{19}	0.01	0.001
				^{85}Kr	5.6×10^{17}	0.01	<0.001
PR-041	1300	1370	11.9	^{129}I	1.4×10^{18}	0.8	0.22
				^{137}Cs	1.0×10^{19}	0.4	0.002
				^{85}Kr	4.9×10^{17}	0.4	0.7
Gas release data for unruptured capsules[a]							
031	30	1300	11.4	^{85}Kr	6.4×10^{17}	0.2	0.2
023	30	1960	17.8	^{85}Kr	1.1×10^{18}	20	18

[a]Opened and analyzed at room temperature at Vallecitos Nuclear Center.

Detailed examination of the three fuel capsules (023, 031, and 042) at Vallecitos Nuclear Center, under an ORNL subcontract, has been reported by Rowland.[11] Information on fission product behavior was obtained via gamma scans, gas collection, and radiochemical analysis of samples taken from the end of a fuel pellet. In addition, the fuel and cladding were examined metallographically.

The results of gamma scans at Vallecitos and at ORNL indicated that ^{131}I, ^{103}Ru, and ^{140}Ba had migrated to fuel pellet interfaces. Autoradiography showed distinct concentrations of beta and gamma radioactivity on the end of a fuel pellet. Five fuel samples were collected across the radius at the end of a pellet. Radiochemical analysis of these samples confirmed that both ruthenium and cesium had migrated from the hot interior (~1900°C) of the pellet to a much cooler region (~1000°C) near the outside surface. These observations are generally consistent with the work of Bates.[12]

[11]T. C. Rowland, *UO_2 Irradiation for ORNL – Final Report*, GEAP-5642 (June 1968).

[12]J. L. Bates, *Fission Product Distribution in Irradiated UO_2*, BNWL-58 (March 1965).

MTR-Irradiated Capsules

Specific knowledge of UO_2 fuel temperature during irradiation is necessary for reliable prediction of the inventory of fission products released from the fuel to the surrounding void space. An assembly of three fuel capsules, each 6 in. long and containing a central thermocouple, is being prepared for irradiation in the MTR. This assembly has a dual purpose: (1) to determine the fuel temperature in an uninstrumented 27-in.-long fuel rod, which will be irradiated in the same reactor position and will undergo rupture testing in TREAT (see the previous section), and (2) to provide well-characterized fuel specimens for rupture tests.

In addition, the three-capsule assembly and the long rod will be gamma scanned in a hot cell in Idaho one to two weeks after irradiation to investigate the migration of short-lived fission products in high-temperature UO_2. Previous studies[13] revealed concentrations of short-lived radioactivity, probably mostly iodine, at fuel pellet interfaces. If such concentrations are located on the Zircaloy cladding, zirconium-iodine chemical reactions could drastically influence the amount of radioiodine released on cladding rupture. Laboratory studies of Zircaloy reactions with iodine and cesium are being conducted also.

EFFECT OF EMERGENCY CORE COOLANT ON FISSION PRODUCT PROMPT FAILURE RELEASE AND CONTAINMENT BEHAVIOR

G. W. Parker R. A. Lorenz H. Feuerstein

The development of a theoretical model for estimating the fuel rod void-space accumulation of volatile fission products and the fractional release into the reactor coolant cavity under accident conditions has become an important area of discussion in the hazards analysis of water reactors protected by engineered safety systems.

In the current series of such reactors under construction, almost all have installed a redundant core coolant injection system designed to aid in removing the latent and decay heat in the event of a loss-of-coolant accident. The protection afforded by such a system tends to reduce the radiological burden of the containment system to that fraction of the fission product inventory which may be released mainly by clad failure or perforation upon rapid depressurization at elevated temperature. It is presently necessary to assume that the available gap inventory of free fission products (Kr, Xe, I, Cs) will be exhausted from the rod, without allowance for inherent retention qualities of the fuel rod especially by means of iodine-zirconium adsorption. That this is a conservative limit is probably well recognized, but the experimental verification of it is not adequately established. In addition, the various methods of calculating the gap inventory, besides having significant differences among them, have not considered the effect of ultrahigh burnup beyond the current level of 10,000 to 20,000 Mwd/ton.

An example of the range of calculated values for the gap inventory for the largest BWR (Browns Ferry) is given in Table 9.2 for three different procedures.[10,14,15] The expected result of additional burnup is presently assumed to follow the trend reported in the fast reactor literature,[16] for which the amount of diffused rare gases is doubled at 40,000 Mwd over that at 20,000 Mwd. There may be difficulty in applying the observation directly to thermal reactors, since it obviously is temperature dependent, and the extension of burnup to this region would imply a lower fission rate toward the end of the fuel cycle and therefore a lower fuel temperature than that in the fast reactors.

An investigation of the extent of iodine retention by the Zircaloy cladding is being conducted in the ORNL Fuel Rod Failure Program and in the LOFT Assistance Program.

The investigation is being conducted in two fuel failure experiments (capsule and long rod) and in a study of chemical reactions of iodine and cesium with tin and zirconium. The objectives of the fuel failure tests are to make direct observations of fractional release both with and without quenching (coolant addition) and of the chemical studies to characterize the reaction products and the volatility under realistic fuel rod environment conditions.

It has been shown in one capsule simulant test that only 15% of the iodine was released when the maximum temperature reached was 1200°C[17] and that most

[13] G. W. Parker *et al.*, *Nucl. Safety Program Ann. Progr. Rept. Dec. 31, 1967*, ORNL-4228, pp. 8,9.

[14] R. A. Lorenz *et al.*, *Nucl. Safety Program Ann. Progr. Rept. Dec. 31, 1967*, ORNL-4228, pp. 11–24.

[15] D. A. Morrison, *et al.*, *An Evaluation of the Applicability of Existing Data to the Analytical Description of a Nuclear Reactor Accident*, BMI-1810, p. 15 (July 1, 1967).

[16] H. Feuerstein *et al.*, *ORNL Nucl. Safety Res. Develop. Program Bimonthly Rept. March–April, 1968*, ORNL-TM-2230, p. 31.

[17] E. L. Zebroski, *Sodium Cooled Reactors, Fast Ceramic Reactor Development Program, Twenty-fourth Quarterly Report for August–October 1967*, GEAP-5541 (December 1967).

Table 9.2. Gap Inventory of ^{131}I at Equilibrium for 4000-Mwd/ton UO_2 in Browns Ferry Reactor

Gap Inventory (% of total)			Method
Peak Rod	Average Rod	Reactor Average	
15	2	~5.6	Battelle calculated[a]
13.6	0.4	1.55	ORNL diffusion calculated[b]
35	2.4	6.7	ORNL annealing data[c]

[a]Battelle computer code (REGAP) based on ORNL annealing data and parabolic temperature distribution.
[b]Canadian capsule data for xenon applied to iodine.
[c]Annealing data for short-period observation extrapolated linearly.

of the remaining iodine was retained on the Zircaloy surface.

In the observation of tin-iodine reactions, volatile products have consistently given nearly quantitative release of iodine (in a form approaching SnI_2) at 600°C in a short interval; however, the zirconium reaction has generally resulted in only 20% of the iodine transported promptly, which appears to require an equilibrium between ZrI_1[16] and ZrI_2 and ZrI_3.[18] The investigation by both experimental approaches is continuing, and more precision is expected in determining the composition of the volatile zirconium compounds by using some highly irradiated Zircaloy containing the tracers ^{95}Zr and ^{113}Sn.

The scope of the capsule and rod experiments is to be enhanced by measurement both of the adsorbed fraction of ^{129}I on the cladding and of the total diffused iodine in the fuel void.

[18]G. W. Parker *et al.*, *Nucl. Safety Res. Develop. Program Bimonthly Rept. May–June, 1968,* ORNL-TM-2283, pp. 12–14.

10. Aerosol Behavior

FISSION PRODUCT DEPOSITION CHARACTERISTICS IN THERMAL GRADIENT TUBES

C. M. Blood A. P. Malinauskas

Studies[1] conducted at Brookhaven National Laboratory suggested the possibility of utilizing the deposition characteristics of gas-borne species along thermal gradients as a tool for the identification of the chemical forms of these species. To explore this possibility as applied to fission product species of interest to high-temperature gas-cooled reactor safety considerations, a theoretical and experimental program of research has been initiated at this Laboratory.

The underlying physical principle upon which the operation of a thermal gradient tube is based can be stated in the following manner:

If a carrier gas is allowed to come into contact with some source of gas-borne species in such a fashion that saturation of the carrier by the components in question is prevented, then these species will remain in the gas phase as long as the temperature of this phase exceeds the equilibrium temperature corresponding to coexistence of the gas and condensed phases of the species. Hence, if the nonsaturated carrier gas is gradually cooled, as by passage through a tube along which is maintained a thermal gradient in the direction of flow, the gas-borne components will begin to deposit only when the surface temperature of the tube corresponds to the condensed-state–gaseous-state equilibrium temperature characteristic of the individual components. Similarly, separation of the various gas-borne components is achieved because of differences in the heats of condensation. Moreover, in first approximation the deposition profile of a given species in a particular thermal gradient will likewise be determined by the heat of condensation of this component. However, a considerable deviation from this first approximation should be observed experimentally, owing to the finite rate of transport of the condensing molecules to the tube surface. It thus becomes apparent that studies of the deposition characteristics of gas-borne species in thermal gradient tubes in principle yield two types of information: the heat of condensation (or sorption) of the component and its diffusion coefficient relative to the carrier gas. In turn, these data may be employed to identify the condensing species with respect to chemical form.

At least four types of mathematical models have been developed to describe the deposition profiles in thermal gradient tubes. The simplest, but most unrealistic, is a purely thermodynamic approach wherein diffusion of the condensing species to the wall of the deposition tube is considered to be infinitely rapid.[2] A more realistic approach was taken by Kress and Neill[3] and is claimed to be applicable to turbulent and laminar flow conditions. The treatment is somewhat empirical, however, owing to the introduction of the mass transfer coefficient. The remaining two models are more limited in application than the latter but are mathematically rigorous. The first of these is applicable under the assumption of "plug flow" of the carrier gas (very low flow rates),[1] whereas the second, which is an adaptation of a constant-temperature deposition model proposed by Gormley and Kennedy,[4] essentially extends the plug flow model to include laminar flow conditions.[5] All four types of model describe the general features exhibited by experimentally derived deposition profiles, but none have been adequately tested. With the exception of the thermodynamic treatment, each

[1] A. W. Castleman, Jr., I. N. Tang, and H. R. Munkelwitz, "Chemical Reactions and Transport Behavior of Fission-Product Iodine," pp. 325–43 in *Proceedings of the International Symposium on Fission Product Release and Transport Under Accident Conditions, Oak Ridge, Tennessee, April 5–7, 1965*, CONF-650407.

[2] A. P. Malinauskas, "Fission-Product Deposition Characteristics in Thermal Gradients," *Nucl. Safety Program Ann. Progr. Rept. Dec. 31, 1967*, ORNL-4228 (April 1968), pp. 281–83.

[3] T. S. Kress and F. H. Neill, *Calculating Convective Transport and Deposition of Fission Products*, ORNL-TM-2218 (September 1968).

[4] P. G. Gormley and M. Kennedy, *Proc. Roy. Irish Acad.* A52, 163 (1949).

[5] A. P. Malinauskas, private communication, November 1968.

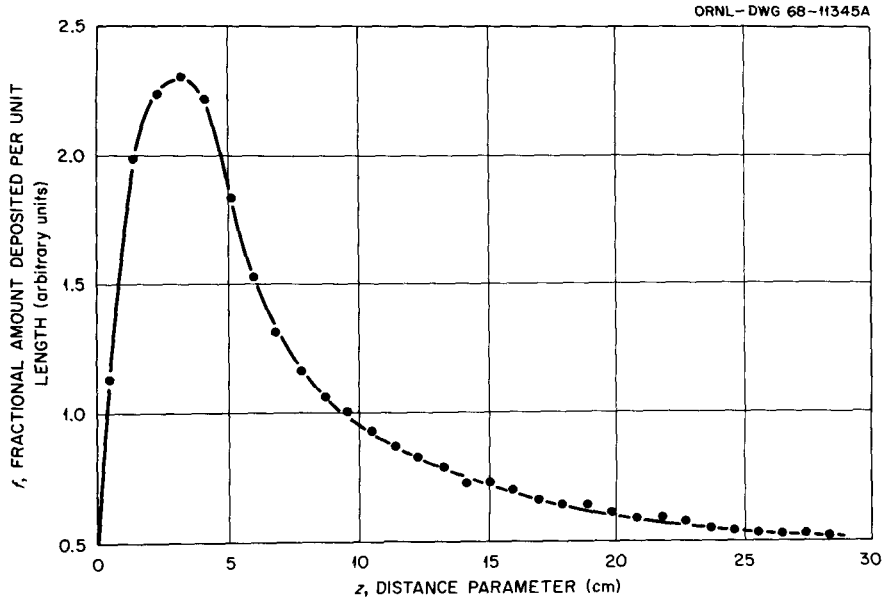

Fig. 10.1. Deposition of ^{110}Ag in a Linear Thermal Gradient Tube.

model leads to an expression which must be evaluated by numerical methods.

In an effort to test the applicability of these models, as well as to assess the feasibility of employing the technique to investigate various aspects associated with the migration and characterization of fission products, a thermal gradient device has been designed and constructed in this Laboratory. The main component of the apparatus was the thermal gradient tube itself, a 5-ft-long tube along which the thermal gradient was imposed. Preliminary studies demonstrated that it was possible to maintain a highly linear thermal gradient along some 40 in. of the tube over prolonged periods of time. In addition, the design permitted wide latitude in the steepness of the gradient.

Two experiments were performed using elemental ^{110}Ag before financial support for this work was curtailed. The first of these was actually a "shakedown" of all the many components of the apparatus, and the final results were of questionable value. The second run, however, was highly successful. With helium flowing at a rate of about 1 liter/min over a sample of silver spiked with ^{110}Ag and heated in a furnace, deposition of the silver was first observed at a temperature about 60° less than the source temperature of 1180°K, or approximately 10 cm from the point at which the linear decrease in temperature commenced.

The deposition profile of the ^{110}Ag, expressed in arbitrary units as the fraction deposited per unit length, is illustrated in Fig. 10.1. Initial deposition (extrapolated) of the silver had been chosen as the origin of the abscissa. The reasonably gradual rise to a maximum is inconsistent with the thermodynamic model but, as best we can tell at present, in accord with the remaining models, in which diffusion effects are taken into account. Our preliminary calculations lead us to believe that the thermal gradient technique can be made to yield reliable values of the pertinent thermodynamic and transport characteristics of the depositing species. Just after these calculations had been completed, however, financial support for the project was curtailed. This necessitated the discontinuance of both the experimental work and the computer programming which is required to make a detailed analysis of the data already obtained.

FILTRATION OF AEROSOLS

R. E. Adams R. J. Davis J. S. Gill
J. Truitt

High-efficiency particle filters are used in the containment systems of many power reactors. In order to estimate the rate of escape of radioactive aerosol particles from such a system, it is necessary to know the filtration efficiency of these filters for metal oxide particles under the environmental conditions produced during an accident. Quality control testing by the manufacturer commonly includes tests to ensure adequate mechanical strength under a variety of conditions and filter efficiency tests with an aerosol consisting of

0.3-μ liquid droplets of DOP (dioctyl phthalate). The nominal required efficiency of filtration of the DOP test aerosol in ambient (dry) air is 99.97%. The purpose of this program is to demonstrate the performance of commercially available filter media with aerosols similar to those expected in reactor accidents. Since the studies have been reported in detail elsewhere,[6] only a summary will be given here.

In the experiments performed, particles are generated in an electric arc, with the consumable electrode being a small irradiated stainless steel tube containing a cylindrical UO_2 insert. The aerosol-generation chamber is part of a recirculation loop that also includes a 100-liter tank. The experimental system and experimental techniques were described previously.[7,8] The 100-liter tank can be maintained at a temperature up to about 100°C. The filter packs, the arc generator, and the pump are contained in an insulated box which can also be maintained at about 100°C. The aerosol is normally generated for about 1 min and then passed through a pair of filter packs at a flow rate to give the desired velocity. The filter efficiencies are calculated as the ratio of radioactivity on the first filter to the total radioactivity on all three filters plus that on the assembly parts downstream from the first filter.

It has been shown[8] that the reproducibility is about ±0.01%; that is, filter efficiencies in the range near 99.97% were observed with an average deviation from the average (of 15 values) of ±0.01.

Filter efficiencies of eight commercial media to electric-arc-generated stainless-steel–UO_2 aerosol were measured as a function of aerosol velocity (3.5 to 10 fpm) at 25, 60, and 100°C and at low (less than 5%) humidity and at high (about 100%) humidity. The effects of velocity, temperature, and humidity (under conditions where condensation does not occur in the filter) are to increase the penetration of the filter from the nominal 0.03% to 0.06 or 0.08%. These effects are consistent with filtration theory. Condensation of moisture onto the filter media apparently results in somewhat larger increases in filter penetration. This effect is still being studied.

[6]R. E. Adams *et al.*, "Behavior of Radioactive Aerosols," *Nucl. Safety Program Ann. Progr. Rept. Dec. 31, 1968*, ORNL-4374, in press.

[7]R. E. Adams *et al.*, "Studies of Aerosol Behavior," *Nucl. Safety Program Ann. Progr. Rept. Dec. 31, 1966*, ORNL-4071, pp. 140–46.

[8]R. E. Adams *et al.*, "Filtration of Stainless Steel–UO_2 Aerosols," *Nucl. Safety Program Ann. Progr. Rept. Dec. 31, 1967*, ORNL-4228, pp. 133–48.

BEHAVIOR OF AEROSOLS IN A REACTOR CONTAINMENT VESSEL

R. E. Adams R. J. Davis J. S. Gill
J. Truitt

The most probable events in the life of an aerosol particle are mechanical in nature; these include motion due to thermal diffusion, collision and coagulation, acceleration due to the force of gravity or due to the Coulombic force (on charged particles), and others. These events can be described in terms of the particle size, charge, shape, and density. The particle shape is apparently not of predominant importance.[9] It is presumed that particles cannot remain charged in the radioactive environment of a reactor accident.[10] An important nonmechanical reaction of particles of interest is probably the reaction with water vapor.

It has been presumed therefore that behavior of aerosols in a reactor containment vessel will require a means of predicting the particle size (and size distribution), the particle density, and the effect of the reaction with water vapor on the particle size and density.

An experimental program has been started to measure particle size distribution as a function of environmental parameters such as initial particle concentration, turbulence, humidity, condensing steam, and age. Concurrently, a system of simple models has been organized to allow computer calculation, utilizing particle size distributions and other data, of aerosol concentration in a containment vessel as a function of time after an accident.

In regard to the experimental program, three experimental rigs have been assembled; the first will be used to measure particle size as a function of humidity and age for very young aerosols; the second will be used to measure particle size as a function of turbulence, humidity, and age; and the third will be used to measure particle size as a function of residence time in condensing steam.

In addition to these experimental rigs, a system of devices to measure particle sizes has been assembled. The system includes a General Electric condensation nuclei counter,[11] a Whitby electrostatic particle

[9]N. A. Fuchs, *The Mechanics of Aerosols*, p. 38, Macmillan, New York, 1964.

[10]B. Y. H. Liu, Department of Mechanical Engineering, University of Minnesota, Minneapolis, private communication, June 1967.

[11]G. F. Skala, "A New Instrument for the Continuous Measurement of Condensation Nuclei," *Anal. Chem.* 35, 702–6 (1963).

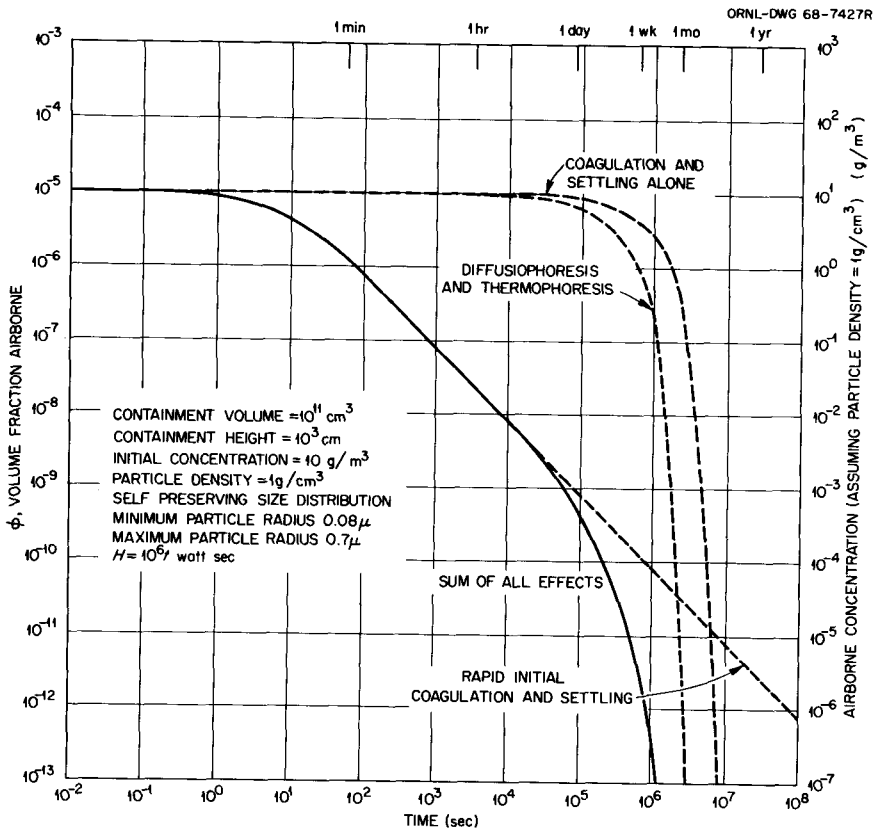

Fig. 10.2. Particle Removal by Mechanical Effects.

counter,[12] a Royco model 220 optical counter,[13] a low-pressure impactor,[14] an electrostatic precipitator[15] and a Cassela thermal precipitator[16] to provide samples for electron microscopic examination, and a filter sampler to provide a measurement of mass concentration of an aerosol.

The progress obtained thus far is mostly toward building and proving the performance of apparatus and procedures. Some preliminary data have been presented[6] to suggest the kind of results that can be obtained.

Regarding the effort to calculate aerosol concentration vs time, the following has been done. A study of the reactions of aerosol particles was made and reported[17] for the purpose of arriving at a short list of removal processes which would (hypothetically) account for actual removal rates within the accuracy required. The list includes: (1) settling of large particles which result from rapid coagulation in a concentrated aerosol, (2) stirred settling[18] of a less concentrated aerosol, and (3) removal by the sweeping action of diffusiophoresis and thermophoresis to the surfaces of cold drops of spray. A fourth process is the condensation of steam on the particles, which increases the particle sizes and affects the removal rate by stirred settling.

[12] K. T. Whitby and W. E. Clark, "Electric Aerosol Particle Counting and Size Distribution Measuring System for the 0.015 to 1 Micron Size Range," *Tellus* **XVIII**, 573–86 (1966).

[13] P. L. Magill, "An Automated Way to Count Fine Particles," *Air Eng.* 4(10), 31–34 (October 1962).

[14] G. W. Parker and H. Buchholz, *Size Classification of Submicron Particles by a Low-Pressure Cascade Impactor*, ORNL-4226 (June 1968).

[15] B. Y. H. Liu and A. C. Verma, "A Pulse-Charging, Pulse-Precipitating Electrostatic Aerosol Sampler," *Anal. Chem.* 40, 843–47 (1968).

[16] H. L. Green and W. R. Lane, *Particulate Clouds*, 2d ed., p. 264, E and F. N. Spon, London, 1964.

[17] R. J. Davis, *A Nuclear Safety Particle Primer*, ORNL-4337 (September 1968).

[18] D. Sinclair, "Stability of Aerosols and Behavior of Aerosol Particles," chap. V in *Handbook on Aerosols*, USAEC report (1950).

A system of equations was developed[17] and is being assembled into a computer code called SMOKLEAR.[19] The code provides for particle removal by a recirculation filter and for an aerosol source term. The calculations are based on the particle size distribution function: $dn/dr = K\phi r^{-x}$, where n is the particle number concentration, r is the particle radius, ϕ is the volume fraction of disperse phase (volume of particle phase per unit volume of aerosol), and K and x are adjustable parameters. The purpose of the above experimental program on particle size distribution is to supply values of K and x as functions of environmental parameters. The calculations make use of many simplifying assumptions with the hope that more complexity will be unnecessary for the accuracy required.

The kind of results which SMOKLEAR will provide is illustrated in Fig. 10.2, which is a plot of particle phase concentration vs time resulting from each of the three particle removal processes individually. The summation gives an estimate of particle phase concentration vs time resulting from all mechanisms simultaneously. The data used to make the calculation are listed on the figure. "Self-preserving size distribution" means that the presumed particle size distribution function was as noted above with $K = 0.05$ and $x = 4$. The term H refers to the total heat which has been transferred during the period of time zero to t seconds to cold drops of water spray. The results are reasonable and will be subsequently compared with observed experimental results.

EFFECT OF AEROSOL MASS CONCENTRATION ON THE NATURAL REMOVAL RATE IN A REACTOR CONTAINMENT VESSEL

G. W. Parker R. A. Lorenz
W. J. Martin G. E. Creek

In order to establish the correlation between fission product radioactivity and the solid disperse phase in a reactor-accident-generated aerosol, it has been necessary to classify particles and to determine concentrations and type of associated radioactivity. The ORNL low-pressure cascade impactor[14] has been successfully applied to the problem of unambiguously correlating airborne radioactivity (radioiodine, as well as solid fission products) with the mass and the removal rate of the vaporized fuel components.

In fuel-melting studies carried out in the Containment Research Installation (CRI), two cases were analyzed by means of the mark II impactor. In the first case (run 112) a low concentration of U_3O_8 (2 mg/m^3) was supplied, and in the second case (run 113) about 1 g/m^3 was provided. The initial tank temperature was about 112°C in each run. The initial tank atmosphere had an absolute pressure of 2.6 atm consisting of a mixture of steam and air. Smaller particle sizes were observed in the aerosol having the lower concentration of U_3O_8. As a measure of the effect of agglomeration processes, a total particle number count was made during the same time that the particle concentration and size analyses were made.

Analysis of the CRI Aerosol by the Effect of Stirred Settling

In both the U_3O_8 aerosols, an analysis of the settling behavior was applied to the gas-phase concentration data. Particle sizes (Stokes, d_8) calculated from the correlation for stirred settling are in fair agreement with particle sizes calculated from equations given in the *AEC Handbook on Aerosols* by Sinclair[20] and by Green and Lane.[21] The data comparisons are given in Table 10.1. Note that d_8 is the diameter calculated from stirred settling rates; d_6 (the mass median diameter) and d_g (the count median diameter) were then calculated from d_8 by assuming values of σ and using the equation

$$\log d_m = \log d_g + 2.303 \frac{m}{2} \log^2 \sigma ,$$

where m is the particle median weight, d_m is the geometric mean weight diameter, and σ is the geometric standard deviation in size distribution. The differences between d_8, d_6, and d_g depend on σ, and the equations are accurate only for spherical particles that have a log-normal size distribution. The table also shows the values of mass median diameter (d_6) and σ as measured by the low-pressure cascade impactor. A similarly useful analysis has been proposed by Adams and his associates[22] based on the concept that agglomeration and other natural processes tend to preserve the natural size distribution of the particles.

[19] R. J. Davis, *SMOKLEAR: A Computer Code to Calculate Particle Phase Concentration in a Containment vs Time*, ORNL-TM-2440, in press.

[20] D. Sinclair, "Stability of Aerosols and Behavior of Aerosol Particles," chap. 5, pp. 64–76 in *AEC Handbook on Aerosols*, H. F. Johnstone (ed.), STR-10-1 (1963).

[21] H. L. Green and W. R. Lane, *Particulate Clouds: Dusts, Smokes, and Mists*, Van Nostrand, Princeton, N.J. 1964.

[22] R. E. Adams *et al.*, "Characterization of Radioactive Particulate Aerosols," *Nucl. Safety Program Ann. Progr. Rept. Dec. 31, 1967*, ORNL-4228, pp. 148–63.

Table 10.1. Comparison of the Size of U_3O_8 Particles Calculated from Settling Velocity and Impactor Analysis

Time Interval (min)	Half-Time (min)	Settling Velocity (cm/sec)	Calculated Particle Diameter (μ)			Measured Values[a]	
			d_8, Mean	Mass Median if $\sigma = 2.0$	Mass Median if $\sigma = 2.5$	d_6	σ
		$\times 10^{-2}$					
0–120	140	1.65	0.74	0.46	0.32	0.40	1.8
180–430	85	2.72	0.96	0.60	0.42	0.30	2.3
1200–1550	200	1.15	0.61	0.38	0.265	0.20	2.2

[a]From impactor analysis.

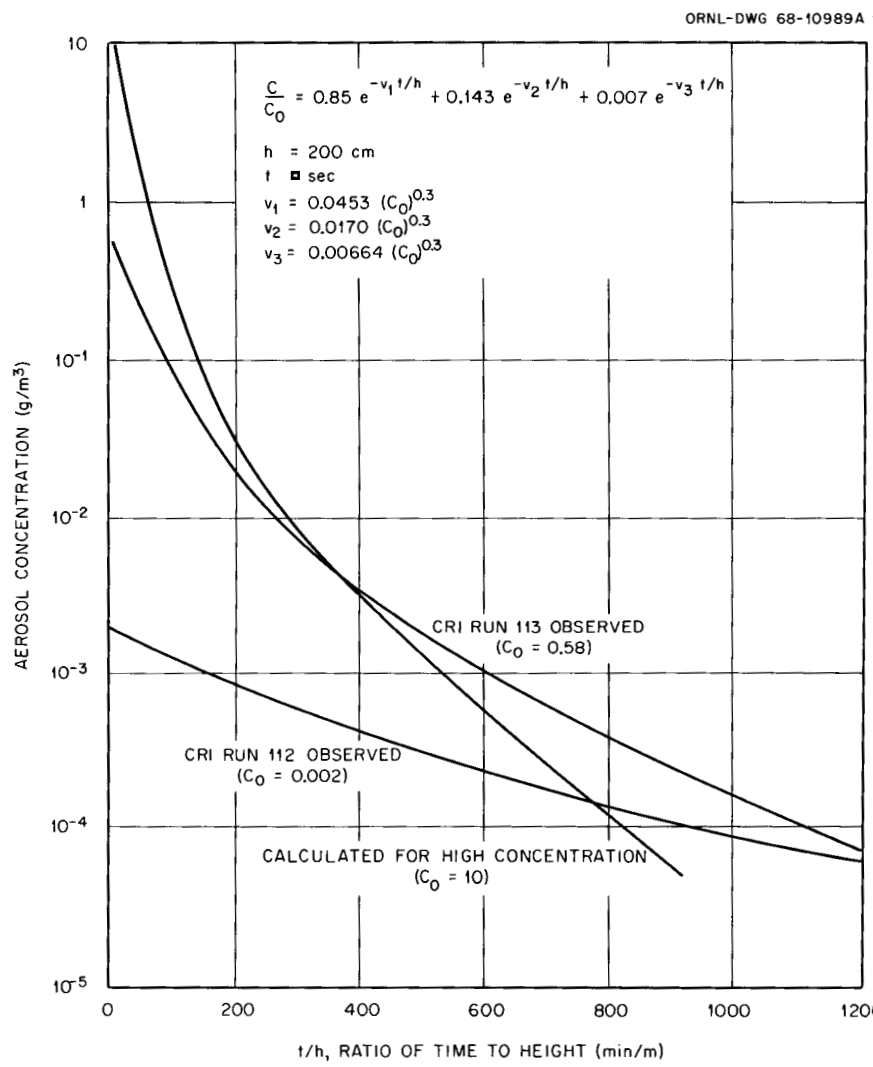

Fig. 10.3. Observed and Calculated Concentrations of U_3O_8 in CRI Aerosol.

Extrapolation of Results to Higher Aerosol Concentrations

Based on observed deposition behavior in two runs (112 and 113), a three-part rate equation was derived that most nearly fits the data. The correlating equation assumes that stirred settling is the predominant aerosol removal mechanism, that the aerosol may be described by three fractions each with its own constant settling rate, and that the settling rate of each fraction is proportional to the initial mass concentration raised to the same power. The data for runs 112 and 113 were used to evaluate the parameters. As an additional exercise, a higher concentration was assumed for a third case, and the corresponding behavior was calculated. Figure 10.3 shows the correlating equation and the decay curves calculated for CRI-112, CRI-113, and an extrapolation to C_0 = 10 g of U_3O_8 per cubic meter. The results are for a unit height of containment. The time scale should be multiplied by 2 for the CRI (2-m height). For a full-sized containment vessel, the factor is about 30 (30-m height).

11. Behavior of Elemental and Combined Iodine

SAMPLERS FOR CHARACTERIZATION OF IODINE

R. E. Adams R. L. Bennett W. H. Hinds

Because the behavior of iodine in containment and the effectiveness of engineered safety systems, such as adsorbers, filters, and sprays, depend on the form of the iodine, analytical samplers are needed which are capable of distinguishing and measuring particulate, elemental, and the less reactive iodine forms, such as methyl iodide, in experimental studies. Previously reported studies[1] have demonstrated that conventional May pack designs do not adequately separate elemental and particulate iodine. This led to the development of a new sampler which has a silver-plated honeycomb as the initial section. The honeycomb, which serves as an array of parallel diffusion tubes, removed the elemental iodine because the elemental form has greater diffusivity than particulate forms and has greater reactivity with silver than species such as methyl iodide. The sampler gave promising results in early tests, and its performance has been examined under an expanded range of conditions. The honeycomb iodine sampler consists of the following sequence: a 5-cm-long, $1\frac{3}{8}$-in.-diam silver-plated aluminum honeycomb with $\frac{1}{8}$-in. hexagonal diffusion channels, a filter section of three Gelman "A" glass fiber filters and one Flotronics silver membrane filter, and two $\frac{3}{4}$-in. iodine-impregnated charcoal beds. Two Gelman "A" filters are placed at the end of the second charcoal bed to remove any particles which might come off the charcoal. Details of the sampler construction, diffusion theory, and testing procedure have been reported.[2]

Although the sampler had shown satisfactory separation results at high humidity (90% relative humidity, 90°C), there was some concern about the performance under waterlogged conditions which might exist at times during actual sampling. Additional tests[3] have been made at 80°C in which small droplets of water condensed on the silver-plated honeycomb surfaces during the sampling period. Iodine removal efficiencies (based on the amount which reached the silver honeycomb) were as large (99.75 and 99.65%) as those obtained at 90% relative humidity (99.81 and 99.64%). Similar tests with methyl iodide indicated that slightly less was retained by the honeycomb in the waterlogged tests than at 90% relative humidity; in each case the amount was small, about 1% or less.

Additional testing of aging effects has been conducted with the honeycomb sampler. Surface contamination of the silver prior to use, with a resulting drop in iodine removal efficiency, was considered. One potential mode of contamination is reaction of the silver with sulfides in the air (tarnishing). An extreme case was simulated by passing hydrogen sulfide through a silver honeycomb to produce a coverage of silver sulfide. Three iodine samplers containing a fresh silver-plated honeycomb, a silver sulfide-coated honeycomb, and an unplated aluminum honeycomb, respectively, were exposed to a 90°C, 90% relative humidity air stream containing elemental iodine. The honeycomb with the sulfide surface was only very slightly less efficient (99.55%) for iodine removal than the fresh honeycomb (99.82%). The penetration of a large fraction (32.17%) of the iodine through the aluminum honeycombs showed that unplated aluminum is not satisfactory for this purpose.

A problem in testing the efficiency of elemental iodine removal by the silver honeycomb is maintaining the purity of the elemental iodine, especially at very low concentrations. Efficient retention has been observed with air streams ranging in iodine concentration from 10^2 down to 10^{-3} μg/liter (Table 11.1). Although there appears to be a reduction in removal efficiency at lower concentrations, this reduction is probably due to the presence of other iodine forms.

---

[1] R. E. Adams, R. L. Bennett, and W. H. Hinds, "Development of Iodine-Characterization Samplers," *Nucl. Safety Program Ann. Progr. Rept. Dec. 31, 1967,* ORNL-4228, pp. 124–33.

[2] R. L. Bennett, W. H. Hinds, and R. E. Adams, *Development of Iodine Characterization Sampler for Application in Humid Environments,* ORNL-TM-2071 (May 1, 1968).

[3] R. E. Adams, R. L. Bennett, and W. H. Hinds, "Development of Iodine-Characterization Samplers," *Nucl. Safety Program Ann. Progr. Rept. Dec. 31, 1968,* ORNL-4374 (to be published).

Table 11.1. Deposition on Silver Honeycombs from Elemental Iodine Streams

Test	Temperature (°C)	Relative Humidity (%)	Flow (liters/min)	Iodine Concentration (μg/liter)	Deposition (%)
X	80	100	1	107	99.7
U	90	90	1	32	99.7
LLP-1	25	96	1	6×10^{-2}	99.6
LLP-2	25	96	1	8×10^{-3}	99.9
LL5	25	98	1	4×10^{-3}	97.4
LL6	25	98	1	3×10^{-3}	98.4
AA	25	0	0.5	6×10^{-4}	95.2

REMOVAL OF MOLECULAR FORMS OF RADIOIODINE FROM MOIST-AIR SYSTEMS

R. E. Adams R. D. Ackley Zell Combs[4]

Elemental iodine and methyl iodide are regarded, from a nuclear safety standpoint, as being the most important of the possible forms of molecular radioiodine. Iodized charcoal is frequently employed for trapping ^{131}I that occurs as I_2 and/or CH_3I from air and steam-air streams; certain types of iodized charcoal extract the ^{131}I of $CH_3{}^{131}I$ by isotopic exchange (effecting so-called $CH_3{}^{131}I$ removal) even at rather high relative humidities. This capability for $CH_3{}^{131}I$ removal outweighs, in many applications, any slight reduction in the I_2 removal performance of the charcoal caused by the iodizing process. Investigation of ^{131}I removal from flowing humid air by iodized charcoal has been reported in detail elsewhere.[5]

The effect of high relative humidity (R.H.) on $CH_3{}^{131}I$ removal by iodized charcoal had previously been investigated extensively for steam-air systems at temperatures around 135°C but only minimally at ambient temperatures. Consequently, a series of measurements was conducted at 25°C and 90% R.H. The results obtained demonstrated that 90% R.H. is a considerably more severe condition than, say, 65% R.H. From the results of tests at 25°C for a group of six types of iodized charcoal, the $CH_3{}^{131}I$ removal efficiencies for a 2-in. depth of charcoal ranged from 99.0 to 99.99% when the prevailing R.H. was 65% and ranged from 16.3 to 99.3% when the prevailing R.H. was 90%. The effect of reducing the mass of CH_3I injected was also briefly investigated at 25°C and 90% R.H. With certain iodized charcoals the increase in removal efficiency observed for a given decrease in the amount of CH_3I injected was less than predicted; this finding suggests that solution of CH_3I in the water adsorbed by the charcoal is involved in the trapping process.

Additional data pertaining to the trapping of elemental radioiodine by iodized charcoal were obtained. Previous work demonstrated that the residual capacity of iodized charcoal for fission product iodine was adequate at least in exposures at 25°C. In the past various researchers have found, in studies with *noniodized* charcoal, that the apparent iodine removal efficiency tends to decrease as the iodine inlet concentration decreases. This behavior is presumably due to the presence of a species, such as CH_3I, which penetrates charcoal more readily than molecular iodine and whose proportion of the total airborne iodine inventory increases as the iodine concentration decreases. Accordingly, investigation of this phenomenon as it applies to *iodized* charcoal was undertaken, and the nature of the behavior observed is illustrated in Fig. 11.1 by the data for one of the types of iodized charcoal involved. Data points corresponding to the earlier experiments with high iodine loading are also included. At the higher inlet concentrations (which caused the iodine loadings to be large), there is a suggestion that the capacity of the charcoal for iodine was on the verge of having been exceeded. At the lower inlet concentrations, a lowering in iodine removal efficiency is clearly manifested, although the effect as shown here is less pronounced than that observed with noniodized charcoal. The available evidence suggests that methyl iodide is the species responsible for the lowering of iodine removal efficiency observed in this work.

After beds of charcoal are installed in air cleaning systems, the effects of aging, weathering (exposure to

[4] On loan from Analytical Chemistry Division.

[5] R. E. Adams, R. D. Ackley, and Zell Combs, "Trapping of Radioactive Iodine and Methyl Iodide by Impregnated Charcoals," *Nucl. Safety Program Ann. Progr. Rept. Dec. 31, 1968,* ORNL-4374 (to be published).

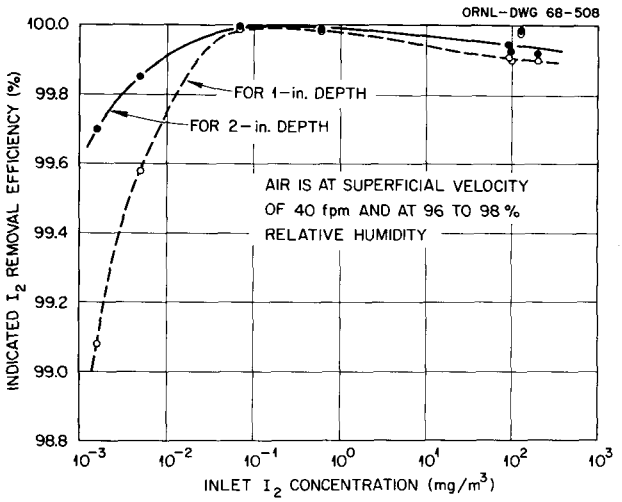

Fig. 11.1. Removal of Elemental Radioiodine from Flowing Air by MSA 85851 Iodized Charcoal at 25°C.

continued air flow), and poisoning by traces of organic matter become causes for concern. Conceivably, each of these three interrelated processes may deleteriously affect the performance of charcoal for trapping iodine and/or methyl iodide.

Therefore, two facilities for weathering charcoal were constructed and operated. In one facility, the degree of poisoning should have been a minimum; in the other, the degree of poisoning was probably typical of a reactor off-gas system. The effects were measured by determining $CH_3{}^{131}I$ removal efficiency as a function of exposure time or, alternatively, integrated air flow. Aging data were provided by similar tests on unexposed charcoal. The results accumulated over the past few years may be summarized as follows: aging, per se, has little effect; weathering has an appreciable effect; and poisoning may have a very serious effect. Fortunately, certain countermeasures can be incorporated into adsorber design and operation to offset the more adverse of these effects.

In related work, extensive experimental studies were performed on samples of unimpregnated charcoal removed from NS "Savannah" iodine trapping units. The results obtained were used in the elucidation of abnormal trapping behavior observed during in-place testing. The behavior noted was most probably related to the presence of organic material (hydraulic oil) adsorbed on the surfaces of the charcoal and to the presence of trace amounts of methyl iodide.

RADIOIODINE TRAPPING IN OFF-GAS SYSTEMS OF FUEL REPROCESSING PLANTS

R. E. Adams R. D. Ackley Zell Combs[4]

An investigation of factors relating to the behavior of radioiodine in off-gas systems of nuclear fuel reprocessing plants has been initiated. The ultimate objective of this project is to develop information which will aid in the design of an extremely efficient iodine removal system to treat gaseous effluent from an LMFBR fuel reprocessing plant. The work to date has been concerned primarily with radioiodine behavior in the off-gas system of the Transuranium Processing Plant (TRU) at ORNL. Operations at this plant provide an excellent opportunity for study of iodine trapping under conditions somewhat similar to those anticipated in future LMFBR fuel reprocessing plants.

During product recovery operations at TRU, the processing agents used are hydrochloric acid and the organic solvents diethylbenzene and Amsco 125-82 (kerosene). The TRU off-gas system is equipped with a bed of iodized charcoal, which is used to trap iodine and which, unless conditions are too unfavorable, is useful for trapping the radioiodine which occurs as CH_3I. However, this iodized charcoal has occasionally permitted the release of iodine (presumably as CH_3I). Accordingly, laboratory experiments were performed to ascertain the effect of the above chemicals on the $CH_3{}^{131}I$ removal capability of iodized charcoal.[6] The results demonstrated that exposing iodized charcoal to any one of these processing agents had a deleterious effect on $CH_3{}^{131}I$ removal efficiency. The effect of hydrochloric acid vapor on I_2 removal was also found harmful but to a considerably lesser degree than that for $CH_3{}^{131}I$ removal; the relative magnitudes of the reduction in removal efficiency for the two iodine forms are denoted by the data in Table 11.2. The air transporting the iodine in these studies was caused to bubble through either water or hydrochloric acid prior to entering the charcoal bed. Hydrochloric acid vapor seems not to be a difficult problem since it may be removed by a suitably designed caustic scrubber. (The primary TRU off-gas system was already so equipped, but the HCl effects were studied, in part, to determine if an additional scrubber would be helpful in a secondary system treating the off-gas from a dissolver vessel.)

[6]R. E. Adams, R. D. Ackley, and R. L. Bennett, *Brief Investigation of Radioiodine Behavior in Off-Gas System of TRU Facility (April–August 1968)*, ORNL-TM-2369 (Sept. 24, 1968).

Table 11.2. Effect of Hydrochloric Acid Vapor on the Radioiodine Trapping Capability of Iodized Charcoal

Iodine Form	Vapor Adsorbed on Charcoal	Removal Efficiency (%)
CH_3I	Water	95.7
	Hydrochloric acid	25.0
I_2	Water	99.98
	Hydrochloric acid	99.22

The effect of the organic solvents on $CH_3{}^{131}I$ removal has been and is to be studied in greater detail; available results indicate that the amount of organic loading which could be tolerated lies in the range of 5 to 15 wt % for either diethylbenzene or Amsco 125-82.

It seems clear, however, that a superior approach to the problem is to remove the organic materials, by catalytic oxidation to CO_2 and H_2O, before they contact the adsorber bed. Hopcalite, a proprietary mixture of metal oxides, has been chosen as the catalyst. We are using a type identified as MSA 21215 from Mine Safety Appliances Company in our studies. While the available literature suggests that it will be useful for this purpose, its efficiency for oxidizing the solvents used at TRU requires investigation. Data of a survey nature have been obtained for oxidation of diethylbenzene, Amsco 125-82, ethanol denatured with methanol, 2-ethyl-1-hexanol, and methyl iodide. Experimentally, air at a velocity of 40 fpm with one of the organics at a concentration in the range of interest is passed into a 2-in. bed of Hopcalite at 350°C. The upstream and downstream concentrations are monitored by gas chromatography with either flame ionization or electron capture detection. In each case, the observed extent of decomposition was nearly complete, indicating that the use of Hopcalite should greatly reduce the poisoning of iodized charcoal by adsorbed organics and greatly improve radioiodine removal performance.

REACTIONS OF IODINE VAPOR IN CONTAINMENT SYSTEMS

R. E. Adams R. L. Bennett Ruth Slusher

Organic iodides, as well as other iodine-containing species, can be present in the containment atmosphere following a reactor accident. The organic iodides are particularly important to the safety problem as they are more difficult to remove from the postaccident atmosphere by adsorbers or other trapping techniques than is elemental iodine. We are studying the modes of formation of organic iodides to help in predicting their concentration in atmospheres resulting from an accident. Both analytical and experimental programs have been conducted to gain insight into the processes leading to organic iodide formation.

Reaction of Iodine with Painted Surfaces

A potential source of volatile organic iodides is the reaction of radioiodine with organic paint coatings used on the inner surfaces of containment vessels. Investigation of the reaction between iodine and painted surfaces was conducted by coating the inner surface of stainless steel vessels (1.2-liter) with the paint formulation under study, adding the iodine contained in a glass tube, and then heating the sealed vessel at the desired temperature for an extended period of time. Gas samples were withdrawn periodically and analyzed using gas chromatography with dual detection (electron capture and hydrogen flame ionization). The electron capture detector is particularly sensitive to organic iodides which form, while the flame ionization detector responds to the numerous organic materials emanating from the surface of the paint. In previously reported tests,[7] the formation of methyl iodide and higher members of the homologous series was noted when Amercoat 66 and Phenoline 302 coatings were exposed to iodine vapor. The amount of CH_3I produced at 100°C with the six-coat Amercoat 66 surface (approximately 10^{-4} mg/liter after 4 hr) was essentially independent of the mass of iodine added at relatively high loadings (1 to 20 mg/liter). When the temperature was increased from 100 to 250°C, the amount of iodide formed was about 100 times larger. This previous study of the reactions between the Amercoat 66 paint system and iodine vapor was conducted under dry conditions. Similar studies have been made at 100% relative humidity;[8] sufficient water was added to the vessel to saturate the air at the exposure temperature (90°C). The amount of methyl iodide formed was nearly the

[7] R. E. Adams *et al.*, "Reactions of Iodine Vapor Under Accident Conditions," *Nucl. Safety Program Ann. Progr. Rept. Dec. 31, 1967*, ORNL-4228, pp. 115–19.

[8] R. E. Adams, R. L. Bennett, and Ruth Slusher, "Reaction of Iodine with Painted Surfaces," *Nucl. Safety Program Ann. Progr. Rept. Dec. 31, 1968*, ORNL-4374 (to be published).

same as that formed under dry conditions; however, the amount of ethyl iodide formed was about an order of magnitude larger than that amount obtained in the dry experiments.

The presence of considerable amounts of organic material in the gas contained in the reaction vessels was evident in all the tests. This organic material was baked out of the coating at the elevated exposure temperatures. In an effort to produce a simulated "aged" paint surface, a freshly painted vessel was maintained at 100°C for seven days while the gas space was continually purged with dry nitrogen. At the end of this period, analysis by gas chromatography indicated that the gas space was practically free of organic material. Iodine was then added and the vessel maintained at 100°C for 76 hr. The mass of methyl iodide formed was not greatly reduced, but the amount of ethyl iodide formed was barely detectable. This observation might suggest that ethyl iodide is formed by one of the more volatile constituents of the paint, while methyl iodide is formed on the paint surface by reaction with a less volatile constituent of the paint.

Simple equilibrium calculations[9] of the CH_4, I_2, CH_3I, H_2, and HI system indicate that increased H_2 concentration should decrease the equilibrium concentration of CH_3I. Although the gas composition of the paint-iodine system is far more complex, a test was made to determine if the addition of H_2 does inhibit organic iodide formation. The tests were identical with the previous ones except 0.5% H_2 (by volume) was added to the painted vessels prior to the addition of iodine. No reduction in iodide formation was evident; the amounts and variation with exposure time were not significantly different from those obtained in tests without H_2 addition.

Analytical Studies of Methyl Iodide Formation[10]

A study of calculated equilibrium and nonequilibrium concentrations of CH_3I for a range of conditions typical of reactor accidents was made to obtain a better understanding of the processes leading to its formation from CH_4. An earlier model of methyl iodide formation was expanded to include chemical-kinetic calculations for an additional CH_3I formation-dissociation path and the presence of inert species which aid iodine dissociation by energetic collision. The expanded model seems to reach equilibrium faster and apparently does so without the intermediate concentrations of CH_3I in excess of equilibrium which appeared in earlier calculations.[11]

The radiation-induced reaction of CH_4 with iodine has also been investigated in a ^{60}Co facility at temperatures from 100 to 500°C with and without steam or steam and air present. These radiation experiments indicate that (1) the rate of formation of methyl iodide by the radiation mechanism is somewhat enhanced by the presence of steam, (2) the reaction is independent of temperature over a wide range, and (3) the reaction between methane and iodine to form methyl iodide proceeds until a significant amount of iodine is converted. This implies that in the postulated reactor accident situation, conversions of several percent of iodine to methyl iodide could easily be achieved even at temperatures well below that at which the thermal mechanism is significant. The thermal reaction, which has a fairly high apparent activation energy, definitely predominates above 700 to 800°K. At intermediate temperatures there appears to be a synergistic effect leading to unexpectedly high methyl iodide concentrations.

REACTIONS OF METHYL IODIDE WITH CHEMICAL SPRAY SOLUTIONS

R. E. Adams R. L. Bennett Ruth Slusher

Unlike elemental iodine, methyl iodide reacts slowly with most cleanup spray solutions so that the overall removal process with sprays is slow. A significant increase in the removal efficiency will be obtained only if an additive which reacts rapidly with the CH_3I in solution is found. Accordingly, an examination of the reaction rate of methyl iodide with potential additives in the cleanup spray solution was started. The two solutions being considered for cleanup sprays, base-borate-thiosulfate and base-borate, were examined first.

The procedure used to measure the reaction rate of CH_3I with additives in aqueous spray solutions was that developed and used by Hasty[12] for determination of

[9] R. H. Barnes, J. F. Kircher, and C. W. Townley, *Chemical Equilibrium Studies of Organic-Iodide Formation Under Nuclear-Reactor-Accident Conditions*, BMI-1781 (Aug. 15, 1966).

[10] This phase of the study was conducted by Battelle Memorial Institute under contract to ORNL. This information was extracted from the following report: R. H. Barnes, *et al.*, *Studies of Methyl Iodide Formation Under Nuclear-Reactor-Accident Conditions*, BMI-1829 (Feb. 22, 1968).

[11] R. H. Barnes *et al.*, *Analytical Studies of Methyl Iodide Formation Under Nuclear-Reactor-Accident Conditions*, BMI-1816 (Sept. 15, 1967).

[12] R. A. Hasty, private communication.

the rate constants for the reaction of CH_3I with hydrazine solutions. It consists in adding a dilute aqueous solution of CH_3I to a thermostated reaction cell which is filled with the spray solution being studied. The reaction cell is sparged continuously with a constant nitrogen gas flow, and the concentration of CH_3I in the effluent nitrogen is determined periodically by gas chromatography (flame ionization detection). The observed CH_3I concentration above the solution is assumed to be proportional to that in the solution. The decrease in CH_3I concentration in the solution is dependent on two processes: the reaction rate of the CH_3I with the additive and the nitrogen sparging rate. If both processes are first order, then

$$C = C_0 e^{-k_{obs}t}, \qquad (1)$$

where C is the observed concentration at time t and C_0 is the initial CH_3I concentration. At a given sparging rate, the observed rate constant, k_{obs}, is the sum of the reaction rate constant k and the sparging rate constant k_s. By plotting the reciprocal of observed total rate constant, $1/k_{obs}$, vs the amount of CH_3I sparged and extrapolating to zero amount sparged, a value of the reciprocal of pseudo-first-order rate constant $1/k$ is obtained.

The base-borate-thiosulfate solution, which is one being considered for spray use, was prepared with the composition: 961.7 g H_2O, 5.93 g NaOH, 17.12 g H_3BO_3, and 15.8 g $Na_2S_2O_3 \cdot 5H_2O$. It contains 3000 ppm boron and 1 wt % thiosulfate and has a pH of 9.3 at 25°C. Pseudo-first-order rate constants for the reaction of CH_3I with thiosulfate in this cleanup solution measured at 30 to 70°C ranged from 0.157 to 1.85 min^{-1}. Extrapolation of the Arrhenius plot (log k vs $1/T$) to 130°C yields a reaction rate constant of about 96 min^{-1} (half-life of 0.4 sec) at this temperature (Fig. 11.2).

The base-borate solution being considered for spray application (978.2 g H_2O, 6.00 g NaOH, and 17.12 g H_3BO_3) has 3000 ppm boron and a pH of 9.35 at 25°C. The reaction with this solution was investigated at 50 and 70°C, but from these data it was apparent that the total amount of CH_3I sparged was essentially independent of the nitrogen sparging rate. A plot of $1/k_{obs}$ vs sparging rate yielded a nearly vertical line parallel to the ordinate. This indicates that the reaction rate is much slower than the sparging rate; therefore this procedure cannot be used to obtain the reaction rate constant k. This observed slow reaction rate is supported by the data of Moelwyn-Hughes,[13] which yield a pseudo-first-order rate constant of the order of 10^{-7} min^{-1} at 25°C for the reaction of CH_3I with OH^- ions at the hydroxyl concentration in this solution.

Distribution Coefficient of CH_3I Between Water and Air

The distribution coefficient of CH_3I between water and air is defined by the equation

$$K_d = \frac{\text{concentration of } CH_3I \text{ in the liquid phase}}{\text{concentration of } CH_3I \text{ in the vapor phase}}.$$

The large discrepancy in the values of K_d reported in the literature and its importance in cleanup spray

[13] E. A. Moelwyn-Hughes, *Proc. Roy. Soc. (London)* **A196**, 540 (1949).

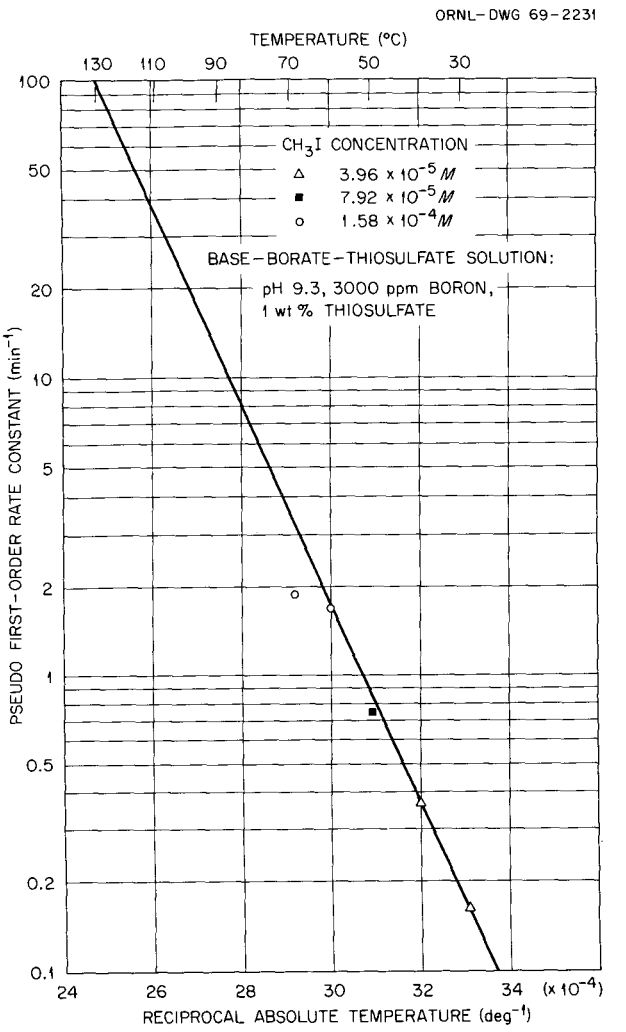

Fig. 11.2. Pseudo-First-Order Reaction Rate Constant of Methyl Iodide with Base-Borate-Thiosulfate Solution.

considerations prompted a further examination of this distribution. For nuclear safety spray applications the concentration range of CH_3I (10^{-8} mole/liter) examined by Hasty[14] is of most interest. Accordingly, the same technique was used for the K_d measurement. The concentration of CH_3I in glass bulbs was measured, water was added, and the concentration of CH_3I in the vapor was determined after the bulb was agitated sufficiently to attain equilibrium. Gas chromatography with an electron capture detector was used for CH_3I analysis. The K_d value obtained, 2.98 at 25°C with a 1.5×10^{-8} M solution, agrees with Hasty's measurements (2.75 at 29.90°C) in the same concentration range.

UPTAKE OF CH_3I BY WATER SOLUTIONS AND DROPS[15,16]

B. A. Soldano W. T. Ward

Single-drop wind-tunnel studies of the factors affecting the removal of CH_3I from gas streams suggest that the activated state for CH_3I removal involves a surface reaction whereby the iodide of an entrapped CH_3I reacts with water molecules and is oxidized to the I^0 state. This step is coupled to a subsequent removal of I^0 from the drop surface into the interior of the drop by means of the reduction of the I^0 to I^-. The latter step is aided by the addition of a reducing agent. Since surfactants can minimize the surface barrier to penetration and increase the CH_3I retention on the surface, as well as enhance the solubility of I^0, they should be useful in the first step.

Spray studies to date show that either of two basic spray additive solutions: (1) 0.3% by weight boron in the form of borate, pH 9.1, and (2) 1% by weight $Na_2S_2O_3$, 0.3% boron in form of borate, pH 9.1, is highly effective in the removal of I_2. The second solution has a definite advantage as far as the retention of CH_3I is concerned, since it alone (presumably because it is a reducing agent) has a demonstrable affinity for retaining CH_3I activity. From a rate standpoint, however, the $Na_2S_2O_3$ is not sufficiently effective for CH_3I removal. Therefore supplements to the $Na_2S_2O_3$ have been sought. They should be additives that can effectively remove both CH_3I and I_2 and yet meet requirements on rates, on radiation and thermal stability, corrosion, etc., and chemical compatibility in the basic pH range.

The performance of a particular group, that is, the iminic tetraethylenepentamine, suggested that the imino structure $(CH_2-CH_2-NH)_n$ built into surfactants not only is compatible with the basic solution but has a relatively high affinity for the methyl group of CH_3I (due to a tendency to form a quaternary ammonium salt). Thus the addition of a strong reducing agent to the iminic additive should help in the removal of CH_3I.

Results

In Fig. 11.3, we have plotted the efficiency of CH_3I pickup by solution 1 as a function of varying amounts of surfactant as well as in combination with reducing agents such as formaldehyde and $Na_2S_2O_3$.

The gain in the use of surfactant can be shown in two ways: First, if we add surfactant to a solution of composition 2 (one containing the reducing agent $Na_2S_2O_3$) the efficiency of the resultant system is increased. Second, a striking improvement in the efficiency of the surfactant's absorption of CH_3I is noted when the amount of the reducing agent, such as formaldehyde or $Na_2S_2O_3$, is increased (Fig. 11.3). That it is the combination of reducing agent and surfactant that gives significant improvement in the efficiency of CH_3I pickup is also suggested, in part, by the fact that formaldehyde alone has practically no affinity for CH_3I.

In view of the observation that the addition of a reducing agent to the iminic additive improves the

Table 11.3. Comparison of CH_3I Mass Transfer Coefficients and K_d Values for Representative Additive Systems at ~26°C

$$K_d = \frac{\text{steady-state concentration of } CH_3I \text{ inside the drop}}{\text{concentration of } CH_3I \text{ in tunnel gas}}$$

Solution Composition (wt %)	v_t (cm/sec)	K_d
4% tetraethylenepentamine	4.3×10^{-2}	4.25
1% $Na_2S_2O_3$ + 0.3% B; pH 9, 1.2×10^{-5} m PEI 1000	15.0×10^{-2}	55
1% $(NH_4)_2S$	4.22×10^{-2}	8.5
0.5% formaldehyde	2.95×10^{-2}	~3.0
1% $Na_2S_2O_3$ at pH 9	$\sim 2 \times 10^{-2}$	~3.5

[14] R. A. Hasty, *Can. J. Chem.* 46, 1643 (1968).

[15] B. A. Soldano and W. T. Ward, "A Wind Tunnel Study of the Mass Transport of CH_3I into a Drop of Water," paper presented at American Chemical Society meeting, San Francisco, Calif., Mar. 31–Apr. 5, 1968.

[16] B. A. Soldano and W. T. Ward, "Uptake of Methyl Iodide from Wind Tunnel Gases by a Suspended Drop of Water," paper presented at American Nuclear Society meeting, Toronto, Canada, June 11, 1968.

efficiency of CH_3I removal, it would appear that the $Na_2S_2O_3$ system would have a distinct advantage for the pickup of methyl iodide. Moreover, wind tunnel studies (Table 11.3) tend to substantiate the bubbler tests in suggesting that the addition of PEI to $Na_2S_2O_3$ should materially improve the latter's ability to remove CH_3I. One notes (Table 11.3) that the surfactant PEI 1000 combined with 1% $Na_2S_2O_3$, a reducing agent, clearly gives the highest K_d values as well as the largest mass transfer coefficients. These two quantities appear to be more indicative of the type of performance to be expected under actual spray conditions. Since a 1% $Na_2S_2O_3$ solution is at least a factor of 5 too slow for obtaining credit for the removal of CH_3I, the addition of an iminic additive to this reducing agent could improve the absorption rate of CH_3I. In this connection, preliminary pilot plant spray results appear to substantiate this idea.

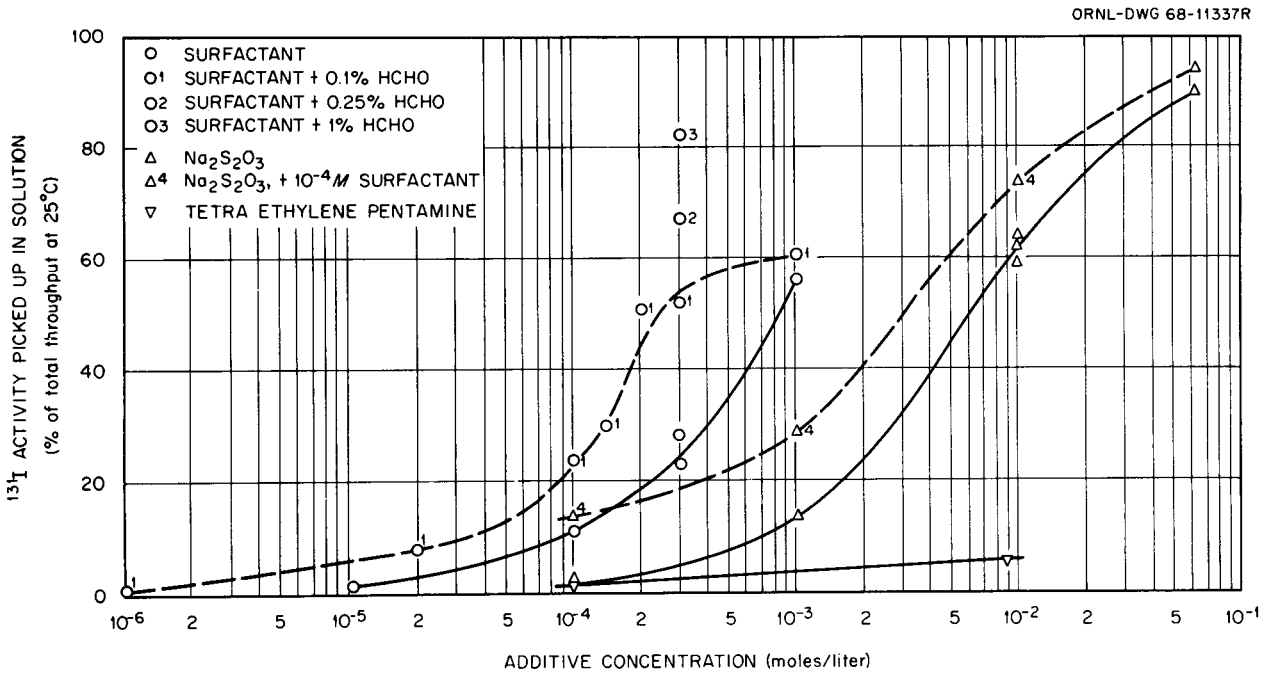

Fig. 11.3. The Effect of Additive Concentration and Type on the Efficiency of CH_3I Absorption.

12. Special Nuclear Safety Studies

IGNITION OF CHARCOAL ADSORBERS BY FISSION PRODUCT DECAY HEAT

R. E. Adams R. P. Shields

Charcoal iodine adsorbers are used in large reactor safety systems to help remove the large quantities of iodine and other fission products from the containment atmospheres following a major reactor accident. The heat generated in the adsorber is expected to be dissipated under normal air flows but will create a potential fire hazard if the air flow is interrupted. This hazard is being evaluated by studies including both in-pile experiments and laboratory testing of the effects of various parameters.

In-Pile Experiments

Four in-pile charcoal ignition experiments have been run in which the charcoal was exposed before ignition to air flow carrying fission products directly from fissioning uranium. The first two experiments involved unimpregnated charcoal (BC-KE)[1] and indicated no significant difference between charcoal ignition in the laboratory or in-pile. The third experiment[2] tested MSA 85851, an iodine-impregnated charcoal, which ignited 35°C lower in-pile than in the laboratory; this was most probably due to a loss of impregnant during irradiation. From the results of these in-pile experiments it may be assumed that the presence of fission products on charcoal will not cause an important change in ignition temperature.

The in-pile experiments contained auxiliary charcoal adsorbers which were exposed to the air carrying fission products to study the iodine distribution. In one experiment[2] an adsorber containing MSA 85851, an impregnated charcoal, showed a wide distribution with approximately 70% of the adsorbed iodine in the first ½ in. of the 2-in.-deep bed and that as much as 10% of the activity reaching the adsorber passed through to a backup trap. In another experiment three adsorbers exposed to moist and dry air containing fission products showed that more than 99% of the iodine was trapped. On the basis of the first experiment it must be assumed that, under certain conditions, some iodine may penetrate 2 in. of charcoal. This factor should be investigated further with charcoal adsorber efficiency tests made in very high radiation fields.

Laboratory Experiments

The development of the standard ignition apparatus was completed, and test results from this apparatus and procedure as set up by ORNL, Savannah River Laboratory, and Barnebey-Cheney showed good agreement. A sketch of this apparatus and details of the procedure as outlined in ref. 3 have been submitted to ASTM for consideration as a standard for charcoal ignition measurements.

The effect of large quantities of water vapor in the sweep gas on the ignition temperature of several charcoals has been studied to simulate postaccident environments.[4] The results of measuring the ignition temperature of three charcoals in sweep air (velocity 40 fpm) containing up to 70% (by volume) water vapor show that: (1) the ignition temperature of BC-416 is virtually unaffected by water vapor concentrations up to about 30%, and (2) at the higher water vapor concentrations the ignition temperature is increased, probably a consequence of the reduction in available oxygen. This same effect is noted for BC-592 and MSA 85851 after the initial reduction in ignition temperature noted between water vapor concentrations of 0 and

[1] R. P. Shields and C. E. Miller, Jr., *The Effect of Fission Products on Charcoal Ignition (In-Pile Experiment)*, ORNL-TM-1739 (Jan. 10, 1967).

[2] R. P. Shields and R. E. Adams, *The Effect of Fission Products on the Ignition of Iodized Charcoal (In-Pile Experiment IGR-3)*, ORNL-TM-2321 (August 1968).

[3] C. E. Miller, Jr., and R. P. Shields, "Ignition of Charcoal Adsorbers by Fission-Product Decay Heat," *Nucl. Safety Program Ann. Progr. Rept. Dec. 31, 1966*, ORNL-4071, pp. 151–53.

[4] *Nucl. Safety Program Ann. Progr. Rept. Dec. 31, 1968*, ORNL-4374, in press.

10%. In this interval indications are evident that the additives are being partially removed. In the case of MSA 85851, removal of some of the iodine results in an initial 10 to 15°C lowering of the ignition temperature, while a lowering of 35 to 40° for the BC-592 is very likely the result of the phosphates found in condensates from these experiments. A more serious effect demonstrated that under conditions of no air flow or very slow flows, water vapor resulting from the heating of the charcoal can free the surface of oxygen complexes. Laboratory experiments have shown that when air flow and oxygen supply are resumed after such treatment, the heat produced by readsorption of oxygen can cause a charcoal bed to ignite as much as 60°C below its nominal ignition temperature.

A modeling investigation[4] of the problems associated with the possible ignition of charcoal adsorbers containing quantities of radioiodine has been initiated. The purpose is to determine what information concerning decay heating is available, what the more important aspects of the problem are, and what calculational methods might best be used to evaluate the thermal conditions. A generalized ignition equation to describe the temperature profile resulting from decay heat in the charcoal adsorber is being developed. It is designed to take into account the time- and position-dependent parameters of the heat source.

KINETICS OF THE STEAM-GRAPHITE REACTION

C. M. Blood J. W. Gooch B. K. Annis
A. P. Malinauskas

The consequences of an accidental release of large quantities of steam into the coolant circuit of a high-temperature gas-cooled nuclear reactor are, of course, influenced in no small measure by the sequence of events which lead up to this accident as well as the condition of the system just prior to the actual injection of the steam. Quite naturally, this complicates the problem of safety analysis and broadens the necessary supporting research. It is nonetheless an important qualification which should be borne in mind in order that statements regarding possible effects of steam injection be put in proper perspective.

Of main concern in the postulate of steam inleakage in the present all-graphite designs is the chemical reaction between the steam and the graphite structure. With due regard for the considerations presented above, this reaction can conceivably result in serious attack of structure integrity and the generation of potentially explosive quantities of hydrogen and carbon monoxide. The accidental injection of steam into the coolant can also result in enhanced migration of fission products and in weakening or destruction of the primary fuel containment (i.e., the pyrolytic carbon coatings of the fuel).

In order to provide information which is required to adequately assess the severity of steam inleakage under a postulated set of plausible conditions or, conversely, to ascertain the conditions under which steam injection is a problem of concern, experimental and theoretical investigations of the kinetics associated with the steam-graphite reaction have been carried out during the period of this report.

One of the main aspects of this multifaceted problem which has yet to be satisfactorily resolved is the observed dependence of reaction rate on the extent of reaction ("burnoff"). Typical of this phenomenon are the data displayed in Fig. 12.1, where reaction rate is plotted as a function of the amount of carbon reacted relative to the original weight of the sample. The behavior which is depicted is believed to result from two factors: a transient effect, which accounts for the initially rapid increase in the experimentally determined reaction rate, and a dependence upon the internal geometry of the graphite specimen.

To test the hypothesis, a mathematical model had been developed which is reasonably realistic yet sufficiently uncomplicated that the physical processes do not become obscured by the mathematics. One of the more critical assumptions, however, restricts the application of the final results only to quasi-steady-state conditions, that is, to circumstances in which the time-dependent parameters are nearly constant.

Under conditions which are approximately satisfied by the experiment in which the data of Fig. 12.1 were

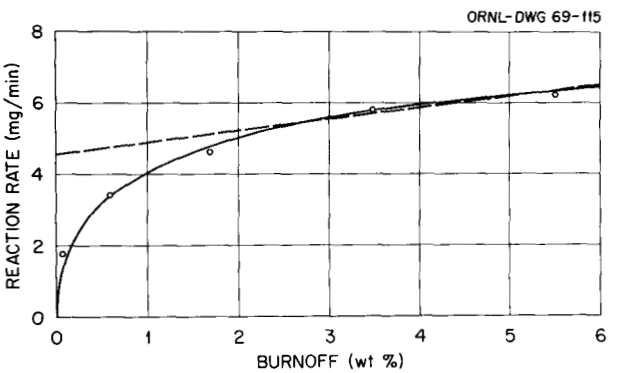

Fig. 12.1. Reaction Rate Data for a Needle-Coke Graphite Exposed to 0.033 Mole Fraction Steam at 1100°C. The dashed line represents the theoretical results based upon measurements of the internal geometry of the specimen.

obtained, the mathematical model relates changes in measured reaction rates to corresponding changes in internal geometry through the expression

$$\frac{R_1}{R_2} = \left[\frac{\epsilon_1(\epsilon'/q)_1}{\epsilon_2(\epsilon'/q)_2}\right]^{1/2}, \qquad (1)$$

where R_1 and R_2 represent the experimentally determined rates of reaction corresponding to two points on the rate vs burnoff curve and where ϵ and ϵ'/q are the total porosity and the porosity-tortuosity ratio characteristic of the graphite at the points in question. The dashed line in Fig. 12.1 is a linear extrapolation to zero burnoff employing the smoothed value of R at 5.6% burnoff and the geometric parameters which were determined from gas transport measurements on the graphite prior to and after reaction with steam.

The rather large deviations between theory and experiment up to about 2.5% burnoff are probably a manifestation of the transient effect; theoretical considerations of this contingency are currently in progress.

The factor ϵ'/q which appears in Eq. (1) arises from a consideration of in-pore diffusion of the steam through the graphite. Frequently this aspect of the problem has been ignored. In-pore diffusion effects can nonetheless be quite important, as has been demonstrated in a series of experiments conducted recently.[5] These experiments involved graphite oxidation studies of several fuel compacts at 1000, 1100, and 1200°C and at steam partial pressures of 20, 70, and 150 torrs. The compacts were constructed by injecting a mixture of charcoal and resin into a bed of pyrolytic-carbon-coated fuel particles contained in a graphite shell and then subjecting the agglomerate to appropriate heat treatments. The graphite container, which was later capped, was of needle-coke material similar to EGCR moderator graphite. The experimental results proved to be quite interesting; the graphite shell offered greater protection for the more reactive binder material at the higher temperatures than at 1000°C.

This observation is readily understood if one considers the temperature dependence of the in-pore diffusion coefficient D'_{12} and the "true" reaction rate constant k. As the term is generally applied, gaseous diffusion is not an activation process; this is evidenced by the observation that D'_{12} varies with temperature approximately as $T^{3/2}$. On the other hand, the variation of k with temperature is given by $e^{-a/T}$. Furthermore, even the most conservative estimates of the constant a indicate that the exponential dependence upon temperature is much greater than $T^{3/2}$. Hence, at the higher temperatures of the oxidation experiments, although the graphite shell allows greater transport of steam through it, less water vapor actually reaches the binder material because of reaction with the container.

The success of these experiments in demonstrating the effect of in-pore diffusion were of course largely due to a fortuitous choice of the graphite which was used as the container material. More porous materials, as well as less porous graphites, would not have demonstrated the paradox. In the former case, significant protection of the binder would probably not be observed at the temperatures at which the experiments were conducted, whereas in the latter case, significant reaction of the binder would probably not be detected.

EFFECT OF WATER VAPOR ON THE VOLATILITY OF FISSION PRODUCT OXIDES

J. W. Gooch J. D. Redman A. P. Malinauskas

There appears to be a rather broad class of oxides which display an enhanced volatility in the presence of water vapor. This enhancement is primarily believed to be the result of chemical reaction. For example, tellurium dioxide is suspected to interact with water vapor in accordance with the equation

$$TeO_2(s) + H_2O(g) = TeO(OH)_2(g)\,, \qquad (2)$$

wherein the product of the reaction appears to be stable only at elevated temperatures in the gaseous phase. A similar type of interaction is also suspected for oxides of ruthenium, iron, tungsten, and rhenium, to cite just a few by way of illustration.

In an effort to investigate those possibilities of pertinence to reactor safeguard assessments, while simultaneously obtaining data for use in quantitative evaluations, we constructed a mass transport apparatus for vapor pressure measurement. The experimental studies were initiated with TeO_2 because of its reasonably high vapor pressure even under normal conditions; this permitted some latitude from the standpoint of experimental accuracy.

The apparatus which was employed in the studies has been described elsewhere.[6] In brief, the technique

[5] C. M. Blood, G. M. Hebert, and L. G. Overholser, *Oxidation of Bonded Coated-Particle Fuel Compacts by Steam,* ORNL-4269 (July 1968).

[6] A. P. Malinauskas, *Nucl. Safety Program Ann. Progr. Rept. Dec. 31, 1967,* ORNL-4228, pp. 277–81.

involves saturating a suitable carrier gas with the species under investigation in one region of the apparatus and stripping it from the carrier in another region. Data which were obtained in this manner are displayed in Fig. 12.2. In this plot, the dependence of the apparent vapor pressure of TeO_2, which we designate as p^*, is shown as a function of partial pressure p_w of water vapor in an otherwise oxygen atmosphere at 925°K.

If Eq. (2) is correct, then we can form the thermodynamic relationship

$$K_p = \frac{p_{TeO(OH)_2}}{p_w} , \tag{3}$$

or

$$p_{TeO(OH)_2} = K_p p_w , \tag{4}$$

in which K_p represents the equilibrium constant characteristic of the reaction. But

$$p^* = p_{TeO_2} + p_{TeO(OH)_2} , \tag{5}$$

whence

$$p^* = K_p p_w + p_{TeO_2} . \tag{6}$$

Hence the observed linearity between p^* and p_w is a necessary (but not a sufficient) condition for the validity of the proposed mechanism.

Studies of the temperature dependence of K_p indicate that the heat of reaction corresponding to Eq. (2) is 30.4 ± 0.4 kcal/mole. The extent of vapor pressure enhancement is best realized when we compare this value with the heat of sublimation of TeO_2. A recent analysis[7] of TeO_2 vapor pressure data yields a heat of sublimation of 60.3 ± 0.3 kcal/mole.

As we have already indicated, the observed linearity between p^* and p_w is not conclusive evidence for the existence of $TeO(OH)_2$; the observation merely implies that Eq. (2) is a *plausible* mechanism for the vapor pressure enhancement. More convincing proof could be had, however, if it were possible to actually identify the species in question. (The material which was collected in the mass transport experiments always turned out to be TeO_2, as verified by x-ray diffraction.)

For this purpose a series of experiments was designed using a time-of-flight mass spectrometer to monitor the vapor species over solid TeO_2 under both dry and moist conditions. Studies of the vapor emanating from the orifice of a Knudsen cell under dry conditions indicated about 20% dimer formation among the TeO_2 vapor molecules. Since all the vaporization experiments which have been conducted to date on TeO_2 assume only monomer in the gas phase,[7] all the data reported are somewhat in error.

The Knudsen cell which was used in the mass spectrometer studies consisted of either a spun platinum or platinum-lined nickel crucible, as it was realized at an early stage of the research that nickel and TeO_2 were incompatible. When water was added to the cell, however, even the platinum proved to be incompatible. Nonetheless, several experiments were performed under this circumstance. In no case were fragments of $TeO(OH)_2$ observed, nor did the cracking pattern of the TeO_2 differ from that obtained under dry conditions. However, it must also be pointed out that TeO_2 vapor pressure enhancement under the moist conditions likewise could not unambiguously be determined up to the time financial support of the overall program was curtailed.

---

[7] A. P. Malinauskas, *Vapor Pressure of Tellurium Dioxide*, ORNL-4300 (September 1968). This work also describes the mass transport method and the Knudsen effusion technique for vapor pressure measurement.

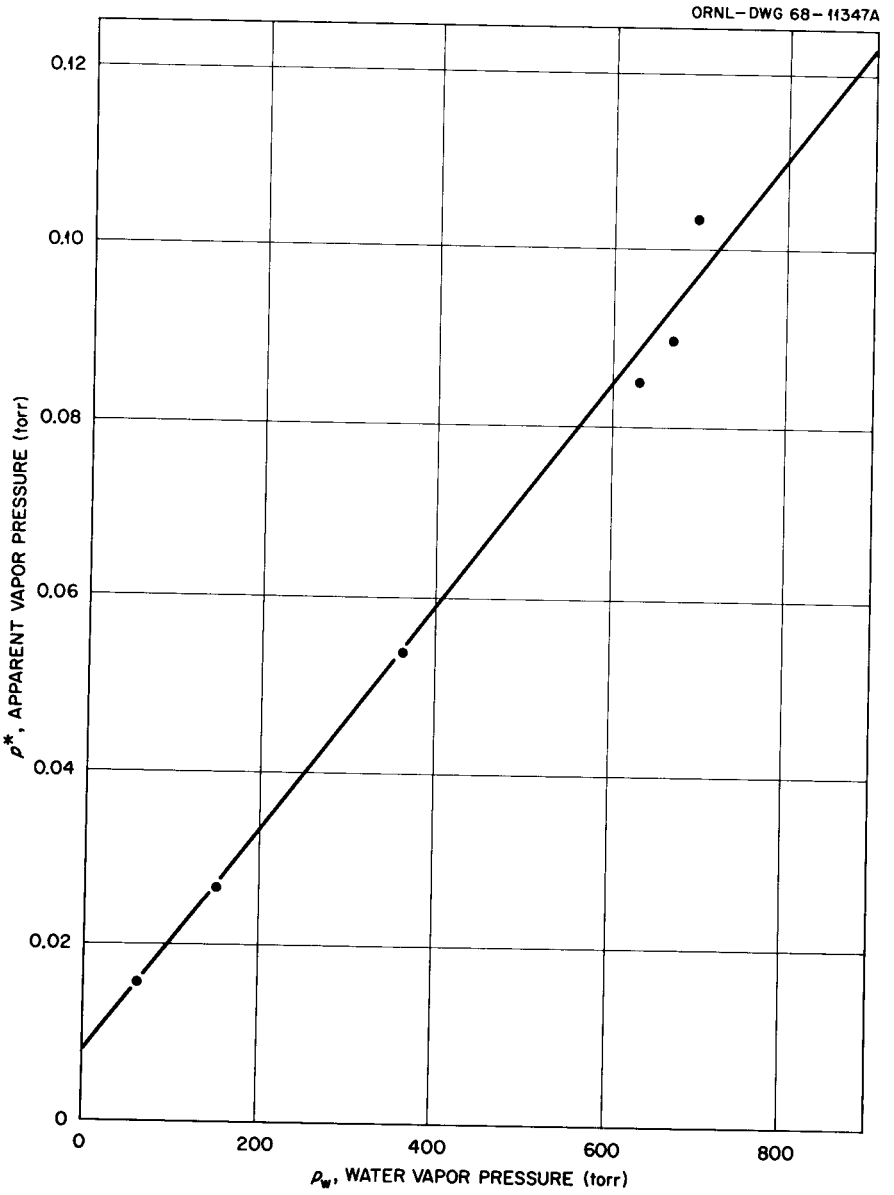

Fig. 12.2. Apparent Vapor Pressure of TeO_2 as a Function of Water Vapor Pressure at 925°K.

Part V. Special Researches

13. Effects of Neutron Irradiation on Refractory Materials

BEHAVIOR OF REFRACTORY METAL MONOCARBIDES

G. W. Keilholtz R. E. Moore H. E. Robertson

Carbides of refractory metals (i.e., Ti, Zr, Ta, Nb, and W) have very high melting points, and their technology is well developed. We are measuring the property changes of these carbides on irradiation because of their possible usage in high-temperature nuclear power plants or thermionic converters. Solid cylinders ($\frac{1}{2} \times \frac{1}{2}$ in.) made by (1) hot-pressing, (2) slip-casting and sintering, and (3) explosion-pressing and sintering were irradiated in the Engineering Test Reactor at temperatures in the range 300 to 1100°C.

Low-Temperature Irradiations

The data obtained from specimens irradiated in low-temperature (300–700°C) assemblies were reported previously.[1,2] We are now trying to explain the swelling-shrinkage phenomenon observed in these irradiations by a neutron annealing mechanism.[3] Theoretical curves

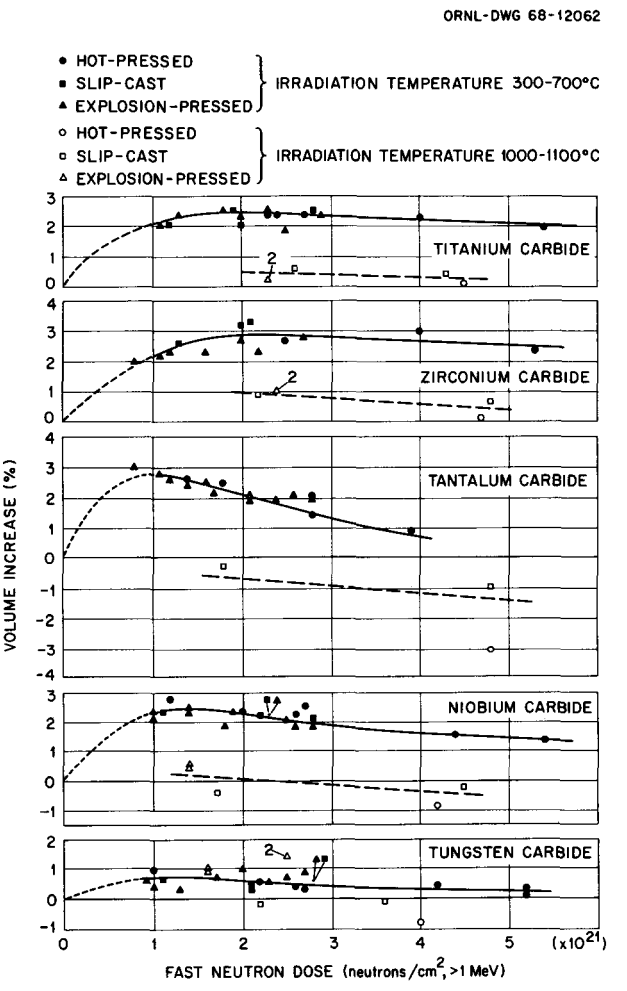

Fig. 13.1. Gross Volume Increase as a Function of the Fast-Neutron Dose for Monocarbides of Ti, Zr, Ta, Nb, and W at 300–700°C and 1000–1100°C.

[1] G. W. Keilholtz and R. E. Moore, "Effects of Large Doses of Fast Neutrons on the Monocarbides of Titanium, Zirconium, Tantalum, Niobium, and Tungsten," *Reactor Chem. Div. Ann. Progr. Rept. Dec. 31, 1967*, ORNL-4229, pp. 142–43.

[2] G. W. Keilholtz, R. E. Moore, and M. F. Osborne, "Fast-Neutron Effects on the Carbides of Titanium, Zirconium, Tantalum, Niobium, and Tungsten," *Nucl. Appl.* 4, 330 (1968).

[3] G. W. Keilholtz, R. E. Moore, and D. A. Dyslin, "Behavior of Refractory Materials Under Irradiation," *Fuels and Materials Development Program Quarterly Progress Report for Period Ending June 30, 1968*, ORNL-4330, pp. 151–58.

based on an equation derived from a theoretical model fit the volume expansion data for the five carbides with constants that appear to us not to be unreasonable. Very low neutron dose irradiations and a very high dose irradiation are now in progress to test the model and to obtain precise values for the constants in the derived equation. The low-temperature work is being pursued because of the general applicability of the proposed damage mechanism and to evaluate the significance of neutron annealing in nuclear reactors designed for very long-term operation.

High-Temperature Irradiations

In-reactor thermal annealing, in addition to neutron annealing discussed above, significantly reduces damage to carbides irradiated at 100 to 1100°C. Very little gross damage occurred to carbides irradiated at high temperatures, and their volume expansions were much less than those for corresponding carbides irradiated at 300 to 700°C. The gross volume increase of the five carbides irradiated at both high and low temperature is given in Fig. 13.1. The method of fabrication does not appear to affect the dimensional changes to a great extent. Metallographic examinations of the carbides made by all three processes revealed no grain boundary separation or transgranular fracture even at the highest doses of the irradiations (see Fig. 13.1). No changes in lattice parameters could be detected in x-ray diffraction examinations of carbides irradiated at high temperature; small lattice parameter increases were previously detected in specimens irradiated at 300 to 700°C. The results are very encouraging for the applicability of carbides in nuclear devices designed for long-term operation at high temperatures (>1000°C).

BEHAVIOR OF ALUMINA

G. W. Keilholtz H. E. Robertson
R. E. Moore D. A. Dyslin[4]

The use of alumina ceramics as electrical insulators in nuclear-powered thermionic converters is contingent upon their ability to withstand intense fast-neutron irradiation for long periods of time. The purpose of this program is to evaluate commercial products that are being considered for this application under realistic conditions of temperature and neutron dose. In addition, we are trying to gain an understanding of damage mechanisms so that recommendations can be made for making improved insulators and for specifying optimum operating conditions for thermionic converters.

Fast-Neutron Damage to Large-Grain (25 μm) Translucent Alumina

Low-temperature irradiation (300–600°C) results[5] and gross damage and dimensional changes at higher temperature (700–1000°C)[6] for large-grain (25 μm) alumina[7] were reported previously. We found that volume expansion was greater at temperatures between approximately 600 and 900°C than at 300 to 600°C. However, there was less expansion at 1000°C than at the "intermediate temperatures," that is, 600 to 900°C.

Present work shows that grain boundary separation contributes to the increase in volume expansion at temperatures above 600°C. There is an almost total absence of grain boundary separation in this material at temperatures below 600°C for doses less than 2 or 3×10^{21} neutrons/cm^2. Figure 13.2 shows severe grain boundary separation at 700°C as compared with virtually none at 300°C and a reduced amount of grain boundary separation at 1000°C. In-reactor thermal annealing probably accounts for the improved microstructure at 1000°C.

An explanation for the increased damage at intermediate temperatures can be found in the recent work of Wilks, Desport, and Smith.[8] These investigators discovered that the growth of the *a* and *c* axes of single crystals of Al_2O_3 during irradiation is almost equal at 150°C but is highly anisotropic and greater in magnitude at 650°C than at 150°C. This effect would cause an increased volume expansion at intermediate temperatures, and it would also cause grain boundary separation to occur in polycrystalline specimens at lower neutron doses than at low temperatures.

The intermediate-temperature effect seriously limits the usefulness of alumina in thermionic converters. The results suggest, however, that neutron damage can be minimized by operation at high temperatures (1000°C and higher). Use of alumina having small grain size should increase the neutron dose at which grain boundary separation begins.

---

[4] General Engineering Division.

[5] G. W. Keilholtz and R. E. Moore, *Nucl. Appl.* 3(11), 686–91 (1967).

[6] G. W. Keilholtz and R. E. Moore, *Reactor Chem. Div. Ann. Progr. Rept. Dec. 31, 1967,* ORNL-4229, pp. 144–45.

[7] Lucalox, a proprietary product of General Electric Co.

[8] R. S. Wilks, J. A. Desport, and J. A. G. Smith, *The Irradiation-Induced Macroscopic Growth of α-Al_2O_3 Single Crystals,* AERE-R-5460 (May 1967).

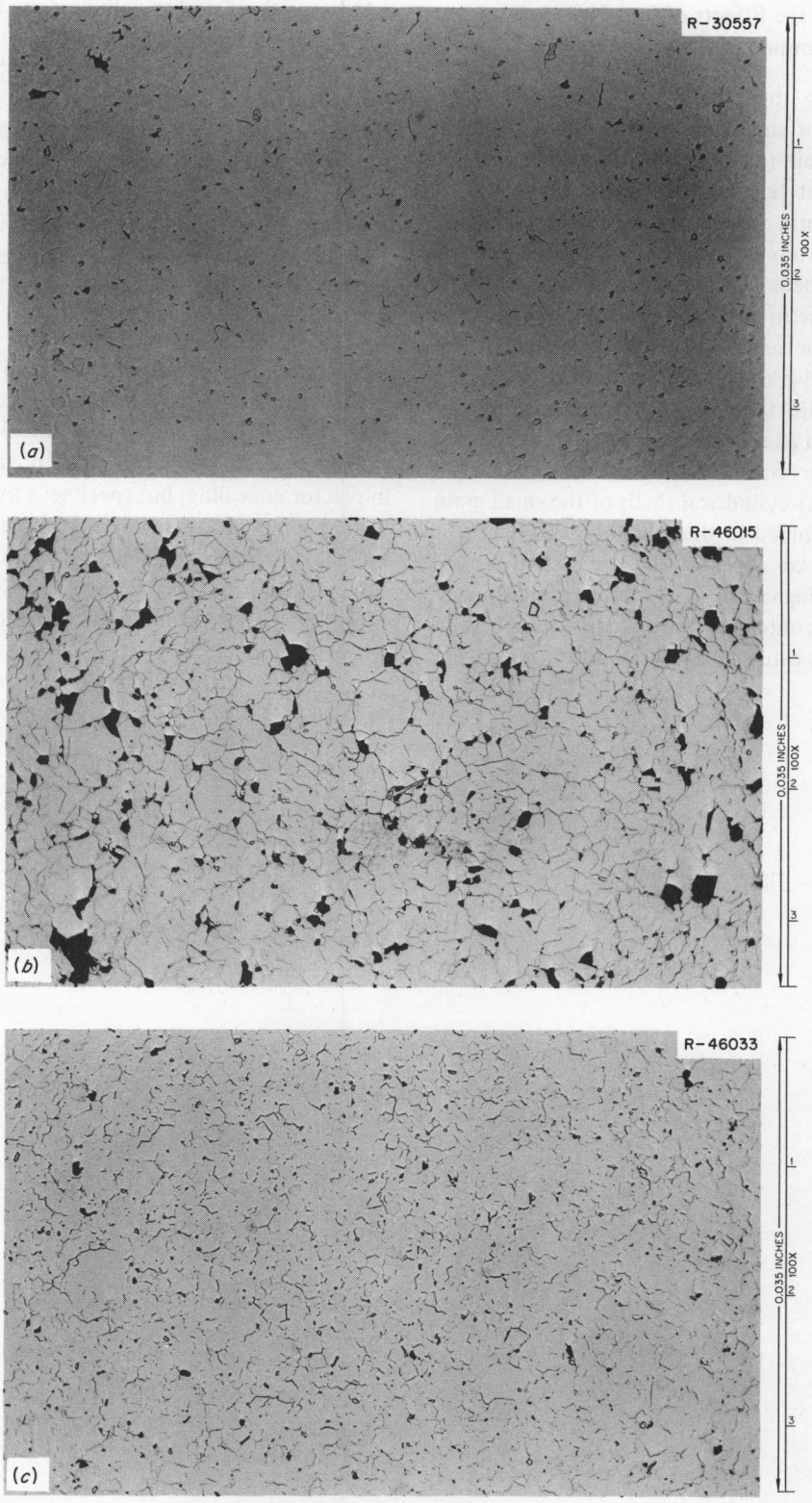

Fig. 13.2. The Effect of Irradiation Temperature on Grain-Boundary Separation in Large-Grain (25 μm) Translucent Alumina. (*a*) 300°C, 1.4×10^{21} neutrons/cm^2 (> 1 Mev); (*b*) 700°C, 1.1×10^{21} neutrons/cm^2; (*c*) 1000°C, 2.7×10^{21} neutrons/cm^2. As polished, 100X.

14. Effects of Radiation on Organic Materials

O. Sisman

TRAPPED ELECTRONS IN GAMMA-IRRADIATED POLYMERS

R. M. Keyser W. W. Parkinson
F. Williams[1]

Phenomena such as thermoluminescence and electrical conductivity in irradiated polymers have been attributed to trapped electrons, but direct evidence has so far been lacking. Trapped electrons have recently been identified in low-molecular-weight hydrocarbon glasses by means of optical[2] and electron spin resonance[3] (ESR) spectroscopy. This report summarizes the results of studies employing similar techniques which demonstrate the existence of physically trapped electrons in a number of antioxidant-free hydrocarbon polymers.[4]

In Fig. 14.1*a*, the first-derivative ESR spectrum of linear polyethylene after gamma irradiation at 77°K shows a very pronounced narrow singlet ($g = 2.0022 \pm 0.0002$, $\Delta H_{ms} = 3.3$ gauss)[5] situated in the center of an underlying six-line spectrum from the free radical $-CH_2-\dot{C}H-CH_2-$. Only the free radical spectrum (Fig. 14.1*b*) remains after photobleaching the sample with near-infrared light ($\lambda > 1000$ nm). Because of the marked sensitivity of the singlet toward light, all irradiations and measurements prior to photobleaching are of necessity carried out in the dark. Progressive microwave power saturation studies (Fig. 14.2) show that the singlet of Fig. 14.1*a* is readily saturated at the very low power level of 0.005 mw.

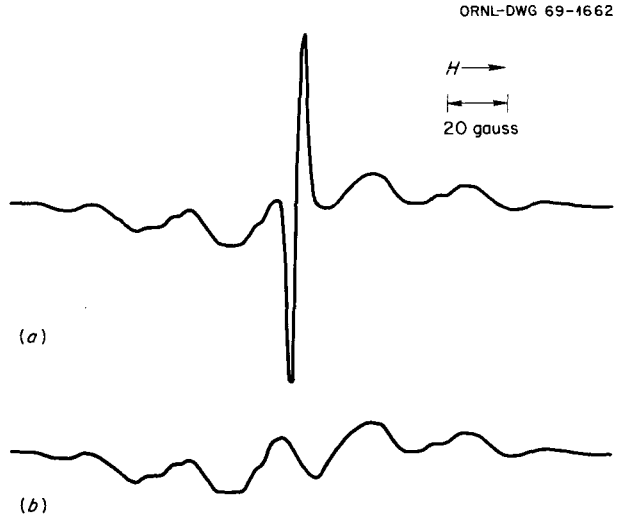

Fig. 14.1. Electron Spin Resonance First-Derivative Spectrum of Gamma-Irradiated Linear Polyethylene at 77°K (*a*) in the Dark and (*b*) After Photobleaching with Near-Infrared Light, $\lambda > 1000$ nm. Irradiation dose, 0.18 megarad; microwave power, 0.002 mw.

A narrow singlet in the ESR spectrum of low-molecular-weight hydrocarbon glasses is known to be due to physically trapped electrons.[3] This singlet is easily photobleached and readily saturated by increasing microwave power. Since the singlet of Fig. 14.1*a* displays these same characteristics, we conclude that it is due to electrons trapped in polyethylene.

By means of similar experiments we have also detected trapped electrons at 77°K in branched polyethylene, isotactic polypropylene, and isotactic poly-4-methylpentene-1, as well as in n-$C_{36}H_{74}$, N-$C_{32}H_{66}$, and n-C_{24}-H_{50}, a series of short-chain analogs for polyethylene. Variations in the line width of the ESR singlet were observed in these materials; ΔH_{ms} ranges from a high of 4.3 gauss in n-$C_{36}H_{74}$ to a low of 2.6 gauss in isotactic poly-4-methylpentene-1.

The yield of trapped electrons as a function of radiation dose is shown in Fig. 14.3 for both linear

---

[1] Department of Chemistry, University of Tennessee, Knoxville.

[2] J. B. Gallivan and W. H. Hamill, *J. Chem. Phys.* **44**, 1279 (1966).

[3] J. Lin, K. Tsuji, and F. Williams, *J. Am. Chem. Soc.* **90**, 2766 (1968).

[4] R. M. Keyser, K. Tsuji, and F. Williams, *Macromolecules* **1**, 289 (1968).

[5] Note: g = spectroscopic splitting factor; ΔH_{ms} = peak-to-peak line width.

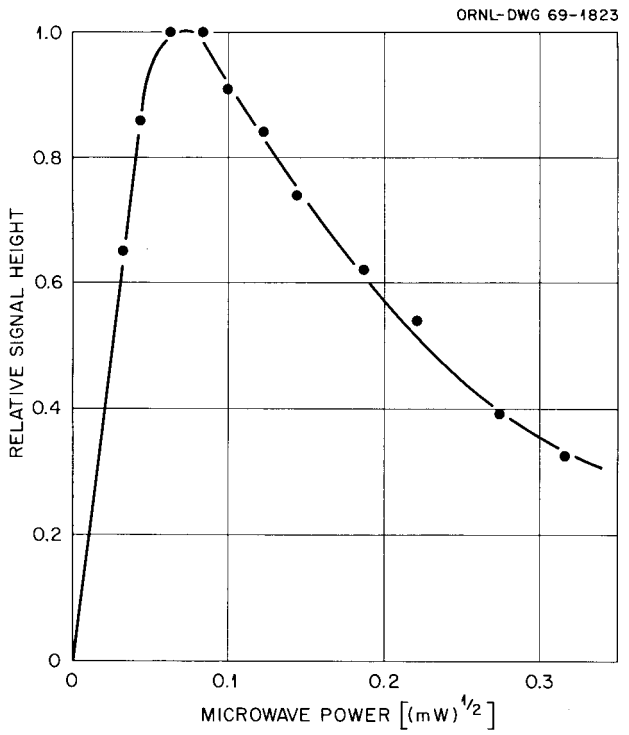

Fig. 14.2. Microwave Power Saturation Behavior of the Trapped Electron in Linear Polyethylene. Plot of relative ESR signal intensity vs square root of microwave power. Modulation frequency 400 Hz. $T = 77°K$.

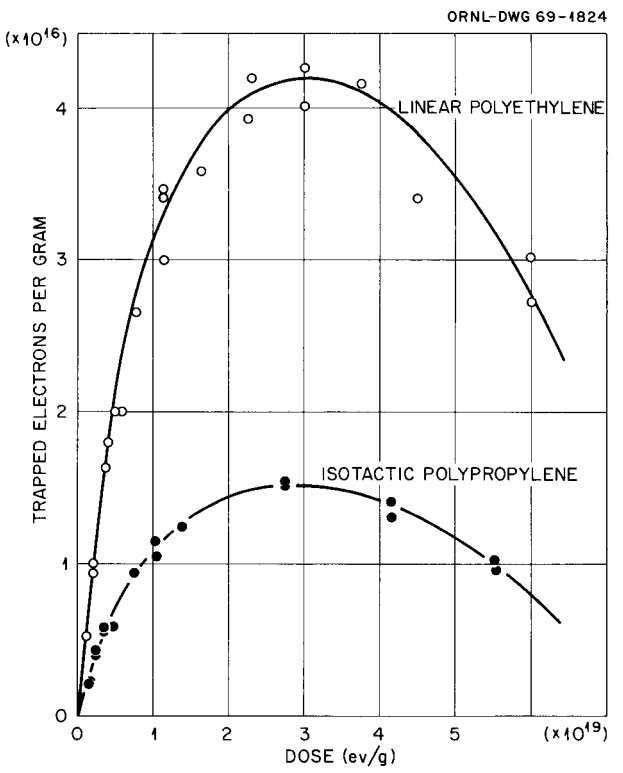

Fig. 14.3. Dose Dependence of the Yield of Trapped Electrons in Linear Polyethylene and Isotactic Polypropylene Measured at 77°K by ESR Spectroscopy.

polyethylene and isotactic polypropylene. The initial G value for trapped electrons in these materials is 0.46 and 0.17 electron/100 ev respectively. Both the G value and maximum concentration of trapped electrons decrease in the order linear polyethylene > isotactic polypropylene > isotactic poly-4-methylpentene-1 ~ branched polyethylene. It is noteworthy that the degree of crystallinity of these materials also follows precisely the same order. Moreover, in two samples of noncrystalline polymers, trapped electrons were either only barely detectable (atactic polypropylene) or not detectable (polyisobutylene). While the nature of the electron trap has not yet been established in these materials, the correlation of yield with crystallinity strongly suggests that electrons are trapped in crystalline regions of the polymers rather than in amorphous regions. This result was unexpected in view of previous findings[3] that in low-molecular-weight hydrocarbon glasses, any tendency toward increased crystallinity reduced the ability of the matrix to trap electrons.

In all materials studied there is a slow decay with time of the trapped electron ESR singlet at 77°K due to thermally stimulated recombination of the trapped electron with positive holes. In polyethylene, this decay amounts to about 30% over an 8-hr period. At higher temperatures the decay is more rapid, and at $T >$ 130°K the trapped electron can no longer be detected. The thermal decay does not correspond to any simple kinetic order, evidently reflecting a complex recombination mechanism.

RADIATION-INDUCED REACTIONS OF HYDROCARBONS

W. W. Parkinson W. K. Kirkland R. M. Keyser

An investigation of the radiation-induced addition of hydrogen and alkyl radicals from hexane onto naphthalene is being conducted to determine the feasibility of utilizing radiation in the alkylation and hydrogenation of coal. The naphthalene and hexane serve as convenient model compounds for coal and for petroleum hydrocarbon by-products. In previous reports[6] the

[6]R. M. Keyser *et al., Reactor Chem. Div. Ann. Progr. Rept. Dec. 31, 1967,* ORNL-4229, p. 184.

identification of the major volatile naphthalene addition products was described. These were: a dihydronaphthalene, an ethylnaphthalene, two propylnaphthalenes, a butylnaphthalene, and six hexylnaphthalenes. Earlier, six isomers, C_{12} addition products of hexane fragments, had been tentatively identified. On the other hand, molecular weight measurements on the unseparated products less volatile than naphthalene gave an average molecular weight in excess of 350 (hexylnaphthalene = 212).

Since a substantial portion of the radiation products would have to have more than one hexyl or naphthyl nucleus to account for such a high molecular weight, and since a very small quantity of radiation products less volatile than the hexylnaphthalenes was observed by gas chromatography, a careful vacuum distillation of the radiation products was carried out.

Infrared and gas chromatographic analyses of the distillation fractions indicated that the alkylnaphthalene fractions made up about 20 wt % of the products. The remainder of the radiation products consisted of compounds of the type: $(C_6H_{13})_n$–$(C_{10}H_x)_m$ in which either n or m, or both, were 2 or greater.

Mass spectral analysis[7] of this portion of the products revealed that about half was made up of mono- and dinaphthyl compounds having up to four alkyl branches. The balance consisted of compounds of even higher molecular weight, presumably composed of three, four, and perhaps more naphthalene nuclei. Significantly, the mass peaks for a substantial part of the products corresponded to dihydro or tetrahydro compounds which would arise from the combination of radicals formed by addition of an alkyl radical or hydrogen atom to an aromatic ring of naphthalene as shown below:

Apparently, addition products, as distinguished from completely aromatic products (e.g., the alkylnaphthalenes) resulting from radical disproportionation, occur in appreciable quantities.

The weights of the distillation fractions will permit a calculation of radiation yields if we make the reasonable assumption that equal numbers of hexane and naphthalene molecules are incorporated into the product molecules. On this basis, in the almost-saturated 10 mole % naphthalene-hexane solutions currently studied, the radiation yield is $G = 0.9$ original molecule per 100 ev incorporated into product of molecular weight greater than hexylnaphthalene. The yield of products of the alkylnaphthalene type is about 0.2, and the response of the chromatograph is being calibrated to determine the yields of specific compounds in this group. The dependence on total dose for the alkylnaphthalenes and the higher-molecular-weight products is being studied also, since the latter products must result from the combination of radical species which are themselves secondary addition products of radiation-generated radicals.

ADDITION REACTIONS OF FURAN DERIVATIVES

J. J. J. Myron W. W. Parkinson

The radiation-induced reactions of furan derivatives involving unsaturated groups have been explored as a possibility for utilizing radioisotopes in commercial production of chemicals.[8] The dimeric and trimeric

[7]W. T. Rainey, Jr., Analytical Chemistry Division.

[8]C. D. Bopp *et al.*, *Reactor Chem. Div. Ann. Progr. Rept. Dec. 31, 1967*, ORNL-4229, p. 185.

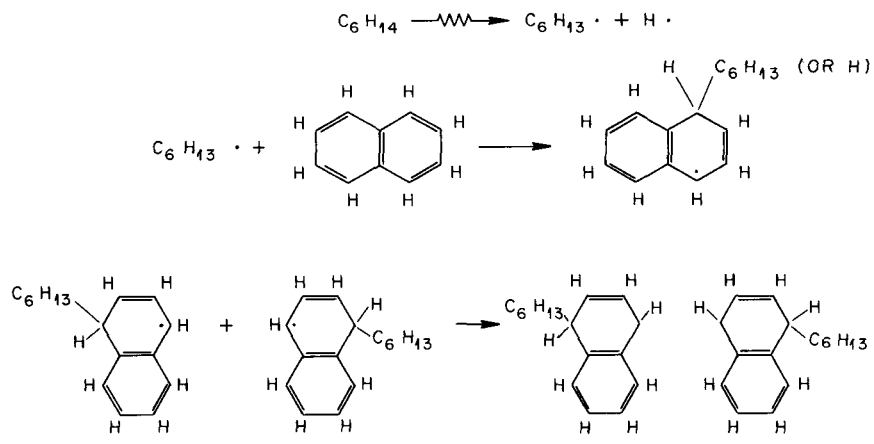

products of such reactions would be expected to have properties making them useful as nonvolatile solvents, plasticizers, chelating agents, humectants, and synthesis intermediates.

For the use of radiation from radioisotopes to be economically feasible, the yields must be very high. Previous work emphasized the dependence of the radiation yields from solutions of cyclohexene in tetrahydrofuran on reaction conditions such as concentration, temperature, and dose rate.[9] Since the high yields characteristic of chain reactions could not be attained in this system, a survey has been conducted of the reactions of more reactive furan compounds. This survey covered furfural, furfuryl alcohol, and tetrahydrofurfuryl alcohol along with an extension of the tetrahydrofuran solutions to include those containing dimethyl sulfoxide.[10]

[9]C. D. Bopp and J. J. J. Myron, *The Radiolysis of Tetrahydrofuran-Cyclohexene Mixtures,* ORNL-4320 (1968).

[10]J. J. J. Myron and W. W. Parkinson, *Radiation-Induced Reactions of Some Furan Chemicals,* ORNL-4373 (1969).

The sample materials used in the survey were reagent-grade chemicals (purity greater than 97% or boiling range less than 1°C) and were not further purified except for furfural. This reactive aldehyde was freshly distilled for some irradiations. The samples for irradiation were introduced into borosilicate glass tubes and degassed thoroughly by repeated freezing-pumping-thawing cycles, prior to sealing under vacuum.[10] The samples were irradiated in a ^{60}Co gamma source at a dose rate of about 10^5 rads/min for the room-temperature irradiations and at a lower dose rate, 3×10^3 rads/min, for the low-temperature irradiations. These irradiations were performed with the sample ampuls in liquid nitrogen (−196°C), and they were in a water cooling jacket at 25°C for the other irradiations.

Postirradiation examination of the samples chiefly consisted in a search for dimeric products by gas chromatographic analysis. Where appropriate, this procedure was supplemented by further analysis of nonvolatile residues by infrared spectrometry, thermogravimetric analysis, and nuclear magnetic resonance.

Table 14.1. Tabulation of Radiation-Induced Reactions of Furan Chemicals

Reactant[a]	Reaction Conditions			Nature of Major Product	Yield of Major Product (*G* value)	Yield of Dimeric Product (*G* value)
	Purity or Concentration (mole ratio)	Temperature (°C)	Dose (rads)			
			$\times 10^7$			
THF		25	1.2	Decomposition[b]	4–10	<5
DMSO		25	1.2	CH_3SH	4–10	<5
THF-DMSO	1:1	25	1.2	Decomposition + CH_3SH	4–10	<5
THF-DMSO	5:1	25	1.2	Decomposition + CH_3SH	4–10	<5
Furfural	As received	25	4.5	?	?	<0.2
Furfural	As received	25	74	Polymer[c]	4	<0.2
Furfural	Distilled	25	72	Polymer	~4	<0.2
Furfural	Air	25	74	Polymer	~4	<0.2
Furfural	As received	−196	2.2	Polymer	~4	<0.2
Furfural + DMSO	10:1	−196	3.0	Polymer	~4	<0.2
Furfural + DMSO	4:1	−196	6.6	Polymer	~4	<0.2
THFAlc	As received	25	4.5	Decomposition	?	<0.2
THFAlc	As received	25	9.5	Decomposition	?	<0.2
THFAlc-furfural	1:1	25	10	?	?	<0.2
THFAlc-furfural	1:100	25	10	?	?	<0.2
Pentadiene-FAlc	1:2	25	70	Polymer	~15	<0.2
Pentadiene-THFAlc	1:4	25	10	?	?	<0.2
Pentadiene-furfural	1:4	25	10	?	?	<0.2

[a]THF – tetrahydrofuran, DMSO – dimethyl sulfoxide, THFAlc – tetrahydrofurfuryl alcohol, FAlc – furfuryl alcohol.

[b]Products having chromatographic retention times shorter than the original reactants are considered "decomposition" products.

[c]Products of such high molecular weight and low volatility that they will not pass through the chromatograph are termed "polymer." Their yields are calculated as the number of molecules of original reactants incorporated in the polymer.

The results of this investigation are presented in Table 14.1 and are summarized for each system below. The investigation is discussed in greater detail in the report by Myron and Parkinson.[10]

Tetrahydrofuran and dimethyl sulfoxide: These reactants did not give high yields of dimeric products ($G < 5$) either as a solution of DMSO in THF or alone. The major products were decomposition products and appeared to be the same whether from the solution or the individual reagents; $G = 4$ to 10.

Furfural: The major product of furfural, both alone and containing dissolved DMSO, was a solid polymer, but only in moderate yield, $G = 4$. The yield was insensitive to temperature, purity, and the presence of O_2.

Tetrahydrofurfuryl alcohol: Upon irradiation, this reactant either alone or in solution in furfural showed only decomposition products in low or moderate yields.

1,3-Pentadiene with furan chemicals: A solution of 1,3-pentadiene in furfuryl alcohol gave little or no dimeric products but gave polymer in relatively high yield, $G \sim 15$. The nature of the polymer was not determined. The results of irradiating solutions of the diene in tetrahydrofurfuryl alcohol and in furfural appeared to be similar.

In conclusion, the radiation yields of products in the desired dimeric molecular weight range were less than five molecules per 100 ev for all the furan chemicals investigated. Furfural gave polymer in moderate yield ($G \sim 4$), and solutions of 1,3-pentadiene produced polymer in high yield ($G \sim 15$). However, both of these reagents are capable of polymerization under chemical initiation or catalysis. No products or processes having commercial potential are apparent in these studies.

DEVELOPMENT OF RADIATION-RESISTANT INSULATORS

M. J. Kelly W. W. Parkinson B. J. Sturm

As reported previously,[11] only polyphenylene oxide, polyethylene, polystyrene, and various copolymers, poly-*p*-xylylene and polymethylpentene, demonstrated desirable electrical properties before irradiation. Further electrical tests at elevated temperatures eliminated poly-*p*-xylylene and polymethylpentene from further consideration, as well as polyethylene terephthalate, which had been reported as marginal.

[11] M. J. Kelly *et al.*, *Reactor Chem. Div. Ann. Progr. Rept. Dec. 31, 1967*, ORNL-4229, p. 186.

None of the remaining materials had satisfactory postirradiation electrical properties in the "pure" state. The transient contribution after the 2000-r test dose from ^{60}Co resulted in an apparent conductivity about two orders of magnitude above the desired values in the case of polyethylene. For the other polymers the transient contribution decayed too slowly to make the materials usable for dosimeter dielectrics.

Many ultraviolet stabilizers and antioxidants were added to bulk polystyrene in efforts to find an additive which would allow rapid and consistent recombination of the charged species remaining after irradiation. Only organic phosphites were found effective, and of these only a few polymeric phosphites produced reasonably reproducible results.

The cooperation of the manufacturer of the original material used in OCD dosimeters enabled us to obtain small batches of material similar to the original styrene–α-methylstyrene copolymer produced by a persulfate-initiated emulsion polymerization scheme. This material retained the desirable properties characteristic of the original production material. Polymerization of styrene by the same recipe gave polystyrene which behaved post irradiation as well as the copolymer. Changing the emulsifying agent had no effect on the postirradiation recovery. Experiments are in process to determine if changing the persulfate cation will affect the postirradiation properties of the polymer. It is suspected that persulfate ends on the short-chain polymer units allow charge recombination to proceed rapidly post irradiation and that the chemically similar phosphite groups provide the same service.

Adjunct studies on sample preparation demonstrated that to achieve reproducible dielectric film with little or no electronic conductivity pre irradiation, the cast film must have the casting solvent carefully removed, and the surfaces of the film sample should be smooth. Casting from a 20% solution, drying with retarded evaporation, and curing the final product for 24 hr in a vacuum oven will achieve these requirements.

The magnitude and the total charge integral, post irradiation, do not appear to be significantly affected by dose rate. An increase in total dose increases the residual amplitude and charge integral, approaching a saturation value which remains the same with further dose increments.

Some cursory experiments have been performed with glasses. Their general postirradiation decay is similar to that observed with polymers. The initial amplitude and charge integral increase with dose, reaching a saturation value. Fused quartz is unsuitable for a dosimeter insulator. Of three glasses tested, Corning 1723, an

alkali-free aluminosilicate, had the best postirradiation performance.

The practical solution to this problem appears to be in hand, but the fundamental understanding of the observed phenomena remains in a confused state.

THE RADIATION CHEMISTRY OF THE REGISTRATION OF PARTICLE TRACKS IN PLASTICS

D. R. Sears C. D. Bopp
W. W. Parkinson

In recent years, plastics have been used in conjunction with suitable etching techniques to register the tracks of a variety of charged particles. Various plastics have different threshold values of the linear energy transfer rate (or ionization rate) below which they will not develop tracks. Gamma and x-ray photons neither produce tracks nor affect track production by charged particles. Consequently, suitable plastics have proved very useful in cosmic ray research, radiological dating, and particle dosimetry.[12,13]

Currently, the most widely used plastic track detectors are cellulose nitrate and acetate. The etching solutions are 5 to 30% aqueous sodium or potassium hydroxide. Both the etching reactions and the radiation chemistry of track formation are relatively unknown. To elucidate the radiation chemistry of the track detectors and to point the way toward development of materials with lower thresholds, this study[14] was conducted with the support of the Health Physics Division in its program of dosimetry development.[15]

Since it was known that the presence of air or oxygen is necessary for the formation of tracks in cellulose acetate but probably not in cellulose nitrate,[16] the gaseous products from these polymers and from the parent cellulose were measured after irradiation in vacuum, in air or O_2, and in gaseous scavengers. Sample materials were as-received commercial plastics ground to 20-mesh powder, except for regenerated cellulose, which was purified for some irradiations by repeated boiling in water and drying. The acetate and nitrate have two acetyl or nitrate groups per C_6 glucose unit, and the triacetate is almost completely acetylated, that is, three acetyl groups per glucose unit. Specimens irradiated in air were sealed without outgassing in air-filled (741 mm pressure) glass tubes prior to irradiation. All other specimens were outgassed by evacuation at 60 to 70°C to 5×10^{-5} mm prior to sealing in glass tubes either under vacuum or other irradiation atmosphere. The gaseous radiation products were measured by chromatography in the case of H_2, N_2, and O_2 and by infrared spectrometry for CH_4, CO, CO_2, and N_2O. In this exploratory work, the specimens were irradiated in a ^{60}Co source to 2.4×10^7 to 3.5×10^7 rads. The yields of gaseous products are recorded in Table 14.2.

The tabulated results show first that "air" irradiation gave considerably increased yields of nearly all products. But many of these are not oxidation products (e.g., H_2), and oxygen does not give increased yields. Therefore it appears that the high moisture content (5 to 10%) of the samples sealed in air enhanced the yields. Similarly, the high and unexpected methane yields from the nitrate can be explained as coming from a volatile additive, probably isopropyl alcohol. Of significance to track formation is the finding that moderate concentrations of low-molecular-weight additives can increase the yield of volatile products. It is also significant that the major products from both the acetates and nitrate are CO and CO_2, arising from chain cleavage, rather than CH_4 or oxides of nitrogen from pendant group decomposition. Chain cleavage yields lower-molecular-weight, more soluble polymer molecules with reactive end groups.

In a completely different approach, to develop track detectors with distinctly different chemical and threshold characteristics, the recrystallization of fluorocarbons was explored. These polymers are sensitive to radiation and undergo scission, which should accelerate crystal growth within a particle track. Various thermal treatments were tried both before and after particle bombardment of polytetrafluoroethylene and polychlorotrifluoroethylene. Nucleation proved to be dependent on uncontrollable surface irregularities and particulate inclusions. It was found that crystal growth and texture were not reproducible, and particle tracks could not be unequivocably demonstrated.

---

[12] R. L. Fleischer *et al.*, *Phys. Rev.* **156**, 353 (1967).

[13] R. L. Fleischer, P. B. Price, and R. M. Walker, *Ann. Rev. Nucl. Sci.* **15**, 1 (1965).

[14] D. R. Sears and C. D. Bopp, *Radiation Chemical Study of Plastics for Charged Particle Track Registration,* ORNL-4351 (1969).

[15] Advice and assistance of J. A. Auxier and Klaus Becker of the Dosimetry Research Section of the Health Physics Division is acknowledged and appreciated.

[16] K. Becker, private communication.

Table 14.2. The Yields of Gaseous Products

Sample	Atmosphere	Radiation Yield (G, molecules per 100 ev)						
		H_2	O_2	N_2	N_2O	CH_4	CO	CO_2
Cellulose (as received)	Vacuum	4.6	0.0			0.0	0.6	1.0
	Air[a]	16.0	−0.6			0.0	1.1	1.4
	N_2O	6.5	0.0	0.2		0.0	*b*	0.8
Cellulose (purified)	Vacuum	5.2	*b*			0.0	0.6	0.3
	O_2	5.2	1.4			0.0	1.0	0.8
	N_2O	3.6	0.2	0.9		0.0	0.9	0.5
Cellulose acetate	Vacuum	0.5	*b*			0.1	1.4	1.0
	Air[a]	0.9	−0.7			0.7	2.2	2.2
	O_2	0.6	−1.8			<0.1	1.5	1.2
	N_2O	1.0	*b*	3.5		0.6	1.6	1.6
Cellulose triacetate	Vacuum	0.8	*b*			0.6	1.2	1.1
	Air[a]	1.2	−0.3			0.9	1.3	2.1
	O_2	0.7	−0.9			0.6	1.6	1.2
	N_2O	0.9	*b*	2.2		0.6	1.2	1.1
	Propylene[c]	0.6	*b*	*b*		0.5	0.8	0.9
Cellulose nitrate	Vacuum	*d*			2.2	1.4	3.6	7.8
	Air[a]	*d*	*d*		2.9	3.9	3.6	7.5

[a]Samples irradiated in air were not outgassed and contained considerable absorbed moisture.

[b]Trace observed.

[c]Propylene initial pressure was 53 mm. It was completely consumed at a rate of $G > 1.7$.

[d]Not determined.

15. Surface Chemistry

HEATS OF IMMERSION IN THE ZIRCONIUM OXIDE–WATER SYSTEM

H. F. Holmes E. L. Fuller, Jr. R. B. Gammage

The calorimetric studies of the heats of immersion and adsorption in the thorium oxide–water system[1] are currently being expanded to include the zirconium oxide–water system. Although zirconium oxide is an important ceramic and, in addition, is a corrosion product in nuclear reactors, very little effort has been expended in the study of its surface properties. The calorimetric measurement of heats of immersion offers perhaps the least ambiguous method for studying the energetics of the interaction between water and a polar oxide surface.[2,3] Of basic importance in surface chemistry is the effect of substrate crystal habit on both the energy of adsorption and the quantity of water which is adsorbed in an irreversible manner. A comparison of the zirconium oxide–water and thorium oxide–water systems offers one convenient method for the study of this problem.

Fragmentary results obtained to date for the heat of immersion of zirconium oxide in water are given in Table 15.1. The calorimetric apparatus and techniques and the outgassing conditions have been described previously.[4] The results are estimated to be accurate to ±3%. Additional experimentation should permit a further refinement of the data.

Samples A and C were prepared by the thermal decomposition of zirconium hydroxide[5] at temperatures of 600 and 800°C respectively. This thermal treatment gave specific surface areas[6] of 87.4 and 52.7 m^2/g for samples A and C respectively. Sample G was purchased from A. D. McKay Company and had a specific surface area[6] of 23.0 m^2/g.

Table 15.1. Heat of Immersion of ZrO_2 in H_2O at 25°C

Outgassing Temperature (°C)	Heat of Immersion (ergs/cm^2)		
	Sample A	Sample C	Sample G
100	−755	−425	−567
150	−865	−498	−606
200	−1008	−540	−660
250			−680
500	−837		

Several interesting observations can be made even though the results are fragmentary at the present time. Obviously, zirconium oxide has the high energy surface which has come to be generally expected of insoluble oxides. Oxygen treatment after outgassing at 500°C had no effect on the subsequently measured heat of immersion. It can be safely concluded that surface reduction is not a complicating factor as it is in the case of, for example, TiO_2.[7] All three of the zirconium oxide samples gave a slow heat of immersion with a half-life of approximately 20 min. This is comparable with the results obtained for some of the thorium oxide samples, where the phenomenon was attributed to a slow diffusion of water into the pores of the particles.[1,8] The porosity of these zirconium oxide samples has not yet been investigated. It is obvious that the heat of immersion of sample A as a function of outgassing temperature will exhibit a pronounced maximum. This was never observed in the thorium oxide–water system.[1,7] Two possible reasons for this maximum immediately come to mind. One is that water (surface

[1] H. F. Holmes, E. L. Fuller, Jr., and C. H. Secoy, *J. Phys. Chem.* 72, 2095 (1968).

[2] H. F. Holmes, E. L. Fuller, Jr., and C. H. Secoy, *J. Phys. Chem.* 70, 436 (1966).

[3] J. J. Chessick and A. C. Zettlemoyer, *Advan. Catalysis* 11, 263 (1959).

[4] H. F. Holmes and C. H. Secoy, *J. Phys. Chem.* 69, 151 (1965).

[5] J. H. Shaffer *et al.*, *Reactor Chem. Div. Ann. Progr. Rept. Dec. 31, 1966*, ORNL-4076, p. 38.

[6] From application of BET method to nitrogen adsorption. Analytical Chemistry Division.

[7] C. M. Hollabaugh and J. J. Chessick, *J. Phys. Chem.* 65, 109 (1961).

[8] E. L. Fuller, Jr., *et al.*, *J. Phys. Chem.* 72, 573 (1968).

hydroxyl groups) is irreversibly lost during outgassing at the higher temperatures. This postulate has been used to explain the maximum observed in the silica-water system.[9] The second possible explanation is that sintering occurs at the higher outgassing temperatures. Although sample A was originally heated to 600°C, it is possible that additional sintering occurred during the prolonged (24 hr) outgassing at 500°C. This possibility will be checked experimentally.

One experimental result of –600 ergs/cm^2 for the heat of immersion of zirconium oxide in water has been reported.[10] In view of the results reported in Table 15.1 this can in no way be construed as a disagreement.

ADSORPTION OF WATER VAPOR ON THORIUM OXIDE BETWEEN 25 AND 500°C

R. B. Gammage E. L. Fuller, Jr. H. F. Holmes

Our previous studies of the adsorption of water vapor on thorium oxide were conducted at 25°C.[11] This gravimetric study represents our first attempt to extend the adsorption work to higher temperatures. The aim is to shed more light on the irreversible binding of water to the thorium oxide surface and to obtain isosteric heats of adsorption from equilibrium isotherms. Two samples have been investigated. Thorium oxide I was nonporous, having an area of 2.7 m^2/g. Thorium oxide B was more reactive toward water vapor,[2] having a finely porous nature and an area of 11.3 m^2/g.

Previous experience with adsorptions from the vapor phase at 25°C had shown that it was an extremely laborious process to completely satiate the thorium oxide surface with irreversibly bound water.[11] The hydrolysis process, however, was very rapid in the presence of the liquid phase.[2] With these behaviors in mind, two approaches were used in obtaining equilibrium isotherms at and above 25°C. The nonporous sample I was first soaked in liquid water at room temperature to produce the fully satiated surface. An adsorption of water vapor isotherm was measured first at 25°C and then at successively higher temperatures to 500°C. No particular difficulty was experienced in obtaining reversible isotherms, which are shown in Fig. 15.1. Each adsorption was characterized by an apparent monolayer uptake in the temperature range 60 to

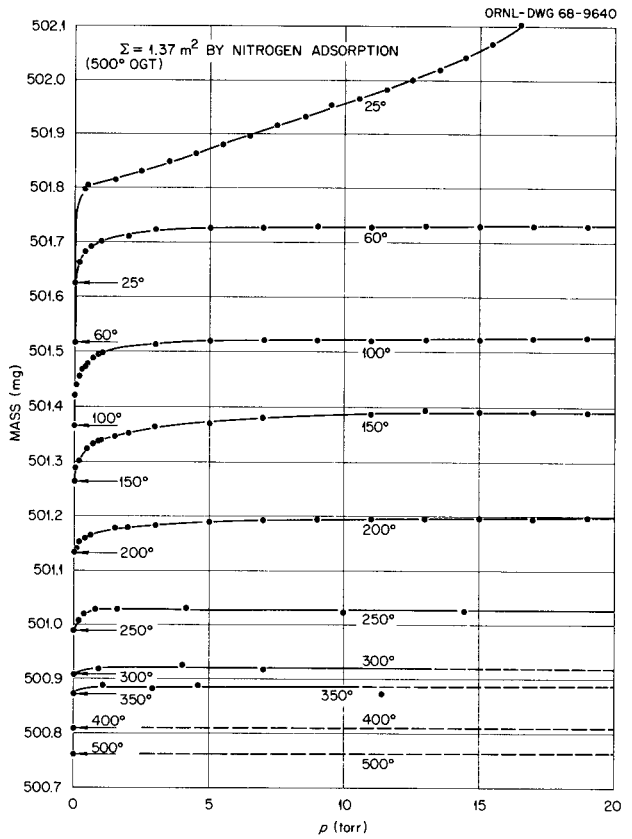

Fig. 15.1. Adsorption of Water Vapor on Thorium Oxide I.

300°C. No adsorption could be detected above the critical temperature of water, viz., 374°C. The more laborious approach for obtaining reversible isotherms was adopted when examining the porous sample B. A reversible isotherm was first constructed at 500°C, followed by other reversible isotherms for decrements of temperature to 25°C. The isotherms obtained are shown in Fig. 15.2 and yield information on slow irreversible binding processes at high temperatures. Unlike sample I, sample B adsorbs appreciably in the temperature range 300 to 500°C. The more heterogeneous and porous nature of the latter is the likely cause of the additional reactivity. On lowering the temperature to 200°C, there was a marked increase in the adsorptive capacity together with the onset of laboriously slow kinetics. Twenty sorption cycles were conducted over several months before the final reversible isotherm was obtained. Further slow reversible binding of water was seen on lowering the temperature to 100°C and then to 25°C. These observations support our previous contention[8] that irreversibly bound molecular water cannot be removed from the surface for

[9] A. C. Makrides and N. Hackerman, *J. Phys. Chem.* **63**, 594 (1959).

[10] W. D. Harkins and G. E. Boyd, *J. Am. Chem. Soc.* **64**, 1195 (1942).

[11] E. L. Fuller, Jr., H. F. Holmes, and C. H. Secoy, *J. Phys. Chem.* **70**, 1633 (1966).

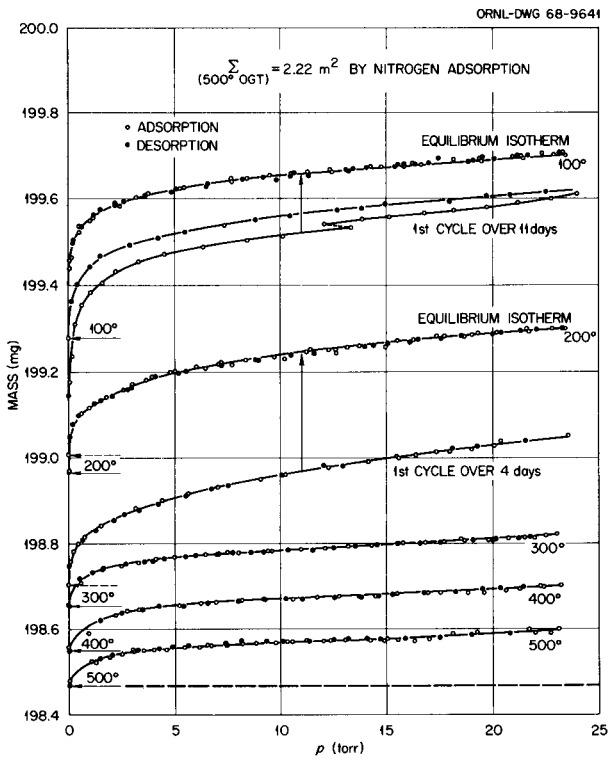

Fig. 15.2. Adsorption of Water Vapor on Thorium Oxide B.

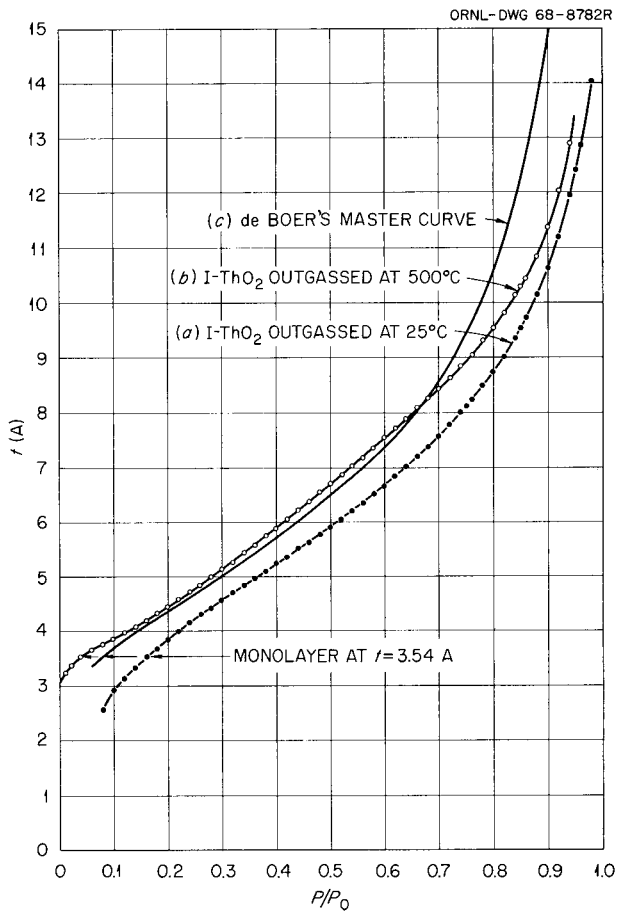

Fig. 15.3. *t* Values for Nitrogen Adsorbed on (*a*) Fully Hydrated and (*b*) Well-Outgassed Surface of Nonporous Thorium Oxide I and (*c*) the Master Curve of de Boer.

outgassing temperatures below 300°C. The way now seems to be clearer for making measurements of the isosteric heats of adsorption on different surfaces and in the temperature ranges corresponding to different states of hydration.

THORIUM OXIDE: THE INFLUENCE OF SURFACE WATER ON THE ADSORPTION OF NITROGEN AND THE *t* METHOD[12]

R. B. Gammage E. L. Fuller, Jr. H. F. Holmes

Nitrogen adsorptions were conducted at 77°K on two samples of thorium oxide, one porous (B) and the other nonporous (I). A range of outgassing temperature from 18 to 500°C was used, and the samples were carefully equilibrated with water vapor at each temperature. When the oxide surface contained irreversibly bound molecular water, the amount of nitrogen adsorbed in both monolayer and multilayer regions was basically different from the amount adsorbed on the surface containing only hydroxyl groups. An outgassing temperature of 300°C was required to rid the surface of all bound molecular water. These differences in nitrogen adsorption can clearly be seen in Fig. 15.3.

The *t*-plot technique employs the seemingly obvious device of comparing the adsorption of nitrogen on the oxide under investigation with the adsorption on a standard nonporous oxide. De Boer, Lippens, and Linsen[13] tout a universal *t* curve for open surfaces against which all adsorption behavior is to be gaged. Inherent to the universal *t* curve is the belief that once the monolayer is completed, the total amount adsorbed at a given pressure is invariant, being independent of the underlying surface. The results shown in Fig. 15.3 throw such an idea into dispute; surface water can affect the amount of adsorbed nitrogen even into the multilayer region.

[12] R. B. Gammage, E. L. Fuller, Jr., and H. F. Holmes, submitted for publication to the *Journal of Physical Chemistry*, 1968.

[13] B. C. Lippens, B. G. Linsen, and J. H. de Boer, *J. Catalysis* 3, 32 (1964).

Table 15.2. Specific Surface Area of Thorium Oxide B Using the BET and the t Methods

Outgassing Temperature (°C)	S_{BET} (m^2/g)	S_t [a] (m^2/g)	S_m [b] (m^2/g)	$(S_t + S_m)/S_{BET}$	Standard t vs P/P_0 Curve Used
300	11.14	10.16	0.91	0.99	Nitrogen adsorbed on thorium oxide I outgassed at 500°C
400	11.06	10.00	1.05	1.00	
500	11.25	10.13	1.24	1.01	

[a]Surface area obtained from the slope of the t plot.

[b]Equivalent surface area, obtained from a positive intercept on the t plot, which is contained in micropores.

The most satisfactory t plots for sample B were obtained when comparing the adsorption of nitrogen on surfaces which were outgassed at 300°C and above. These plots are shown in Fig. 15.4. From the slopes and intercepts, the area contributions from micropores and other surfaces can be calculated and then compared with the BET specific surface area as in Table 15.2. The results indicate that for sample B, about 10% of the apparent surface area is contained within micropores. The effect of capillary condensation in larger pores is also evident from Fig. 15.4: the adsorption is enhanced when the thickness of the adsorbed layer exceeds 7 A.

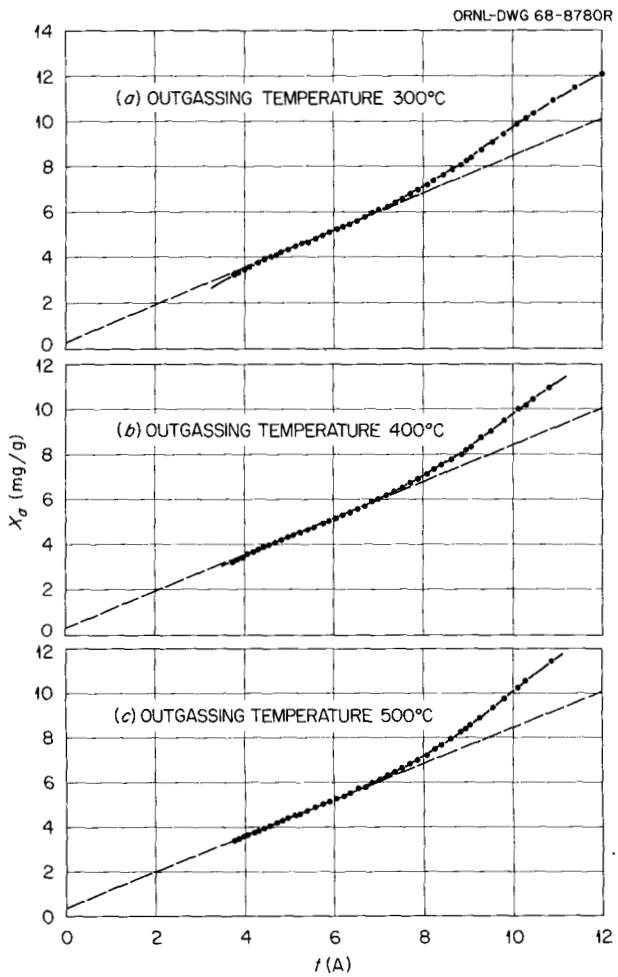

Fig. 15.4. t Plots of Nitrogen Adsorbed on Porous Thorium Oxide B Stripped of Molecular Water and Based on the Standard t vs P/P_0 Curve for Nitrogen Adsorbed on Thorium Oxide I Outgassed at 500°C.

Without delving further into the details of this study of t plots, the suggestions made[12] for investigating a porous oxide by the t method will be stated:

1. An outgassing temperature as high as the oxide can bear without losing pores or surface area should be employed. Not only will this provide for high net heats of adsorption, and hence better location of the completed monolayer, but it will also free very fine pores of adsorbed water which would otherwise exert a blocking effect. The standard nonporous oxide should be outgassed at the same temperature.
2. When the sample under investigation is outgassed so as to leave molecular water on the surface, so it should be with the standard nonporous material used for comparison.
3. Also, one must be careful to choose two oxide surfaces that have a comparable degree of heterogeneity such that each adsorbed water structure presents a like degree of polarity to the nitrogen molecules.

INFRARED SPECTRA OF THORIUM OXIDE SURFACES AND ADSORBED WATER

E. L. Fuller, Jr. H. F. Holmes R. B. Gammage

Sample cells have been constructed to allow the acquisition of infrared transmission data in controlled atmospheres from −196 to +1000°C (see Fig. 15.5). By use of two machine slides, the sample position can be precisely adjusted with respect to the incident light beam. The sample can be retracted horizontally to

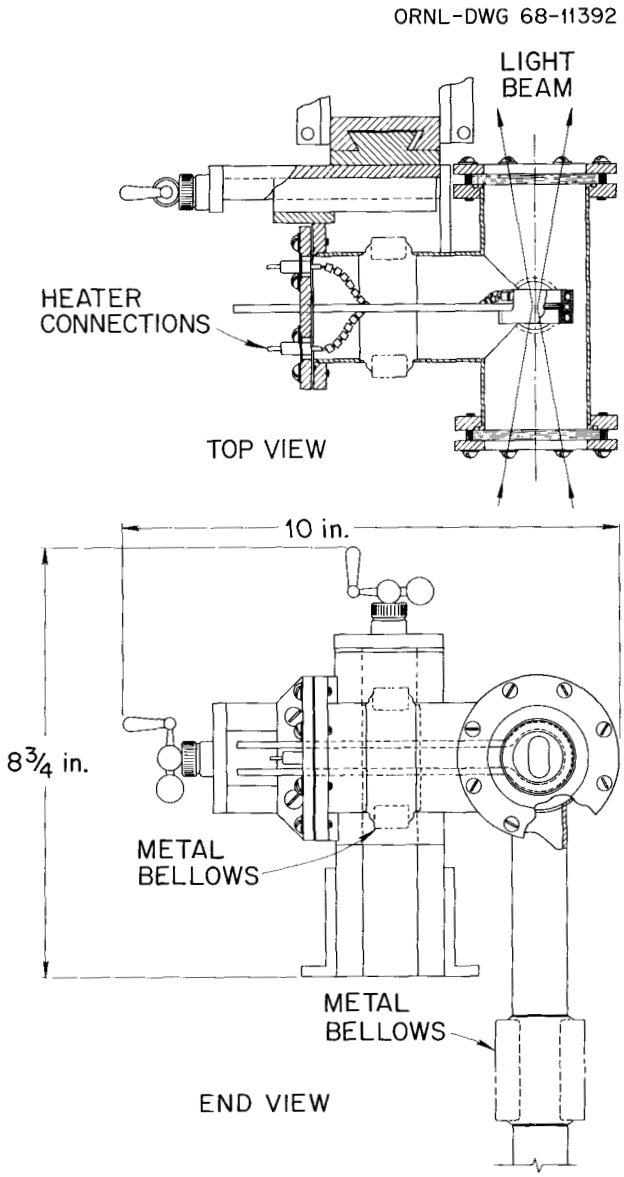

Fig. 15.5. Sample Chamber Assembly.

examine the spectra of the contained gas phase and/or the quality of the cell windows. An identical cell is placed in the reference beam for compensation and comparison purposes. The lower tube is connected to an environmental control system so that the effects of vacuum and/or various vapors can be analyzed. The sample temperature is controlled by proportional variance of the electrical energy to the heater surrounding the sample. The control temperature is measured by a Chromel-Alumel thermocouple inserted through the tubular supports. Cooling is effected by a flow of coolant through these supports, that is, water or liquid

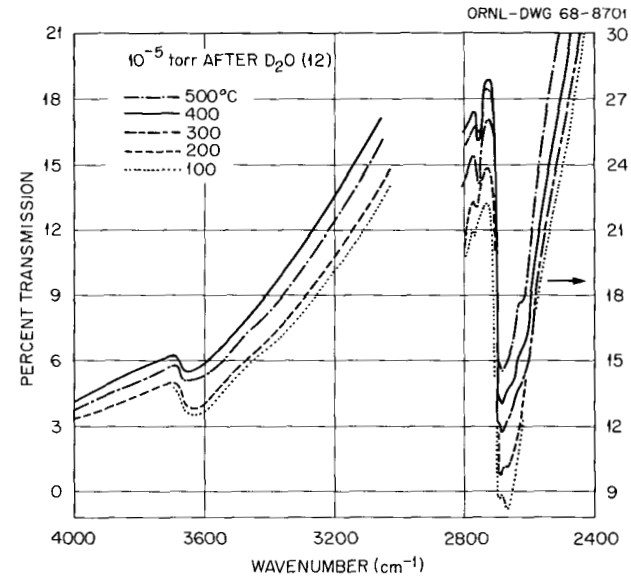

Fig. 15.6. Stepwise Cooling of Sample *F* in Vacuum After D_2O Exchange at 500°C.

nitrogen. The entire chamber can be lowered from the light beam, permitting the spectrophotometer[14] to be used in a conventional manner.

The merits of studying adsorbed species at elevated temperatures are revealed in Fig. 15.6. This sample of thoria was taken to 500°C in vacuo and subsequently subjected to D_2O vapor at 500°C. Reevacuation showed the total amount of exchange and the amount of retention. The tenacity of the water binding is noted in the nature of the exchange. The initial exposure to D_2O vapor brought about only a small fraction of the H_2O replacement. The process was complete in less than 15 min, with no progression noted in the prolonged exposure to D_2O vapor (96 hr). Each successive exposure after evacuation brought about a lesser increment of exchange (approximately the same fraction of the retained H_2O). The amount of D_2O in the vapor phase was not the limiting factor. It appears that there is a surface structural barrier to the exchange which is overcome only by a *cycling* from vapor to vacuum and back. Such a phenomenon has been noted gravimetrically for adsorption from the vapor phase.[15]

[14] E. L. Fuller, Jr., R. B. Gammage, and H. F. Holmes, *Reactor Chem. Div. Ann. Progr. Rept. Dec. 31, 1967*, ORNL-4229, p. 108.

[15] H. F. Holmes, E. L. Fuller, Jr., and C. H. Secoy, *J. Phys. Chem.* 72, 2293 (1968).

Table 15.3. Frequency Correlation for Thoria Surfaces

Series	1	2	3	3′
α	186 cm^{-1}	283 cm^{-1}	382 cm^{-1}	195 cm^{-1}
β	86	100	106	
γ	116	178	188	
δ		208		
ϵ		254		
Number of bands	11	16	15	

Bands occur at $\nu = n\alpha$ where $n = 2, 3, \ldots$ (up to 9 observed)
$= n\alpha + \beta$
$= n\alpha + \gamma$
etc.

The high affinity of water for the thoria surface is also demonstrated by the retention in vacuo (10^{-6} torr) at temperatures in excess of 600°C.

Cooling the sample in vacuo after the 500°C outgassing and D_2O exchange produced the spectral changes noted in Fig. 15.6. Here the pitfalls one encounters in the practice of observing room-temperature spectra as exemplifying the previous high-temperature state are obvious. With the imposed vacuum holding the amount of adsorbed species constant, we see that there is considerable rearrangement of the population of the various vibrational states. We have noted the free hydroxyl band (3742 cm^{-1}) and three predominating hydrogen-bonded species. Monitoring these bands and/or their deutero counterparts as a function of temperature and pressure has imposed several criteria that the structural interpretation must meet.

The reversible association of water with the surface, in excess of the vacuum retention, at the elevated temperatures is noted to persist to 500°C. This is counter to the concept of classical physical adsorption, with the adsorbed phase existing in a liquid-like state, since we are much in excess of the 374°C critical temperature of water. Thus we must conclude that the interaction of water with these surfaces involves forces much in excess of the molecule-molecule interactions involved in classical condensation.

A number of bands occur in the vibrational spectrum of thoria in the range 200 to 2000 cm^{-1} which seem to be inherent in the substrate.[14] These band frequencies are characteristic of the mode of preparation of the oxide and are relatively insensitive to temperature and pressure. Sintering of a given sample in air decreases the specific surface area and the band intensities without shifting their frequency. Thus they must be a result of a surface phenomenon. Their frequencies are correlated as multiples of a single redundant factor. There are also satellite bands associated with each of the prime multiples ($n\alpha$) and leading them by constant additive factors (β, γ, etc.). The values of these constants seem to be a function of the exposed crystalline face (dictated by the mode of oxide preparation). These correlation factors, given in Table 15.3, account for virtually every band found between 500 and 2000 cm^{-1}. Furthermore, these numerical values can be correlated well with the fundamental frequencies noted in other spectroscopic analyses of thoria. Each series represents a separate mode of oxide preparation.

Structural interpretations are incomplete for the surface and adsorbed water. However, the conclusions deduced from calorimetric[1] and gravimetric[15] analyses are in accord with the spectroscopic data.

Publications

JOURNAL ARTICLES

AUTHOR(S)	TITLE	PUBLICATION
Adams, R. E., and R. D. Ackley	Removal of Radioiodine from Gases	*Nucl. Safety* 9(5), 373 (1968)
Bamberger, C. E., J. P. Young, and C. F. Baes, Jr.	Containment of Molten Fluorides in Silica; Effect of Temperature on the Spectrum of U^{4+} in Molten $LiF\text{-}BeF_2$ Mixtures	*J. Inorg. Nucl. Chem.* **30**, 1979 (1968)
Brandon, C. A., D. R. Cuneo, G. B. Engle, and E. L. Long	The In-Pile Compatibility of Beryllium Oxide with Graphite at 1500°C	*Nucl. Appl.* **4**(1), 23 (1968)
Braunstein, J.	Non-Ideality and Association in Binary Mixtures of Molten Salts	*J. Chem. Phys.* **49**, 3508 (1968)
	Some Aspects of Solution Chemistry in Liquid Mixtures of Inorganic Salts with Water	*Inorg. Chim. Acta – Reviews* **2** (1968)
Burns, J. H., A. C. Tennissen, and G. D. Brunton	The Crystal Structure of Alpha Lithium Aluminum Fluoride, Li_3AlF_6	*Acta Cryst.* **B24**, Pt. 2, 225 (1968)
Carroll, R. M., R. B. Perez, and O. Sisman	The Mixing of a Trace Gas in Flowing Helium	*Nucl. Appl.* **4**, 268 (1968)
Carroll, R. M., O. Sisman, and R. B. Perez	The Effect of Fission Density on Fission-Gas Release	*Nucl. Sci. Eng.* **32**, 417 (1968)
Davis, R. J., J. Truitt, and J. S. Gill	Aerosol Studies in the Reactor Safety Program at Oak Ridge National Laboratory	*J. Air Pollution Control Assoc.* **18**, 675 (1968)
de Nordwall, H. J., V. H. Pierce, and L. R. Zumwalt	Experimental Test of the Frevap-8 Code for Calculating Metal Fission Product Release from HTGR Elements	*Trans. Am. Nucl. Soc.* **11**(2), 490 (1968)
Evans, R. B., III, J. L. Rutherford, and R. B. Perez	Recoil of Fission Products. II. In Heterogeneous Carbon Structures	*J. Appl. Phys.* **39**, 3253 (1968)
Fontana, M. H.	Core Melt-Through as a Consequence of Failure of Emergency Core Cooling	*Nucl. Safety* 9(1), 10 (1968)
Fontana, M. H., and R. E. Bailey	The Chemical Equilibria of Fission-Product Fuel Mixtures: The Gas-Phase Composition of the Uranium-Oxygen-Strontium System in the Presence of the Condensed Phase	*Trans. Am. Nucl. Soc.* **11**(1), 376 (1968)
Fuller, E. L., Jr., H. F. Holmes, C. H. Secoy, and J. E. Stuckey	Heats of Immersion in the Thorium Oxide–Water System. III. Variation with Specific Surface Area and Outgassing Temperature	*J. Phys. Chem.* **72**, 573 (1968)

AUTHOR(S)	TITLE	PUBLICATION
Griess, J. C., Jr.	Crevice Corrosion of Titanium in Aqueous Salt Solutions	*Corrosion* **24**, 96 (1968)
Holmes, H. F., E. L. Fuller, and C. H. Secoy	Gravimetric Adsorption Studies of Thorium Oxide. III. Adsorption of Water on Porous and Non-Porous Samples	*J. Phys. Chem.* **72**, 2293 (1968)
	Heats of Immersion in the Thorium Oxide–Water System. IV. Variation of the Net Differential Heat of Adsorption with Specific Surface Area	*J. Phys. Chem.* **72**, 2095 (1968)
Holmes, H. F., E. L. Fuller, R. B. Gammage, and C. H. Secoy	The Effect of Irreversibly Adsorbed Water on the Character of Thorium Oxide Surfaces	*J. Colloid Interfacial Sci.* **28**(3), 421 (1968)
Keilholtz, G. W., R. E. Moore, and M. F. Osborne	Fast Neutron Effects on the Carbides of Titanium, Zirconium, Tantalum, Niobium, and Tungsten	*Nucl. Appl.* **4**, 330 (1968)
Keilholtz, G. W., and G. C. Battle, Jr.	Fission Product Release and Transport in Liquid-Metal Fast Breeder Reactors	*Nucl. Safety* 9(6), 494 (1968)
Keyser, R. M., K. Tsuni, and F. Williams	Trapped Electrons in Gamma-Irradiated Polyethylene Identified by Electron Spin Resonance Spectroscopy	*Macromolecules* **1**, 289 (1968)
Macklin, R. L., J. H. Gibbons, E. Ricci, T. Handley, and D. R. Cuneo	Proton Reaction Determination of Lithium and Fluorine in Molten Salt Reactor Graphite	*Nucl. Appl.* **5**, 269 (1968)
Marshall, W. L.	Conductances and Equilibria of Aqueous Electrolytes over Extreme Ranges of Temperature and Pressure	*Rev. Pure Appl. Chem.* **18**, 167 (1968)
Marshall, W. L., and R. Slusher	Aqueous Systems at High Temperature. XIX. Solubility of Calcium Sulfate and Its Hydrates in Seawater and Saline Water Concentrates – Temperature-Concentration Limits	*J. Chem. Eng. Data* **13**, 83 (1968)
Mathews, A. L., and C. F. Baes, Jr.	Oxide Chemistry and Thermodynamics of Molten Lithium Fluoride–Beryllium Fluoride Solutions	*Inorg. Chem.* **7**, 373 (1968)
Mesmer, R. E.	Lanthanum Fluoride Electrode Response in Aqueous Chloride Media	*Anal. Chem.* **40**, 443 (1968)
Mesmer, R. E., and C. F. Baes, Jr.	Correlation of Change in Heat and Change in Entropy for the Association of the Rare Earth(III) Ions with Fluoride	*J. Phys. Chem.* **72**, 4720 (1968)
Miller, C. E., Jr.	A Boundary-Layer Diffusion Model of Fission Product Release from Reactor Fuels	*Nucl. Appl.* **5**, 198 (1968)
Moynihan, C. T., and S. Cantor	Viscosity and Its Temperature Dependence in Molten Beryllium Fluoride	*J. Chem. Phys.* **48**, 115 (1968)
Perez, R. B., G. M. Watson, P. Nelson, R. M. Carroll, and O. Sisman	A Dynamic Method to Study In-Pile Fission-Gas Release	*Trans. Am. Nucl. Soc.* **11**(1), 271 (1968)
Posey, F. A., and E. G. Bohlmann	Pitting of Titanium Alloys in Saline Waters	*Desalination* **3**, 269 (1968)
Quist, A. S., and W. L. Marshall	Electrical Conductances of Aqueous Sodium Chloride Solutions from 0 to 800° and at Pressures to 4000 Bars	*J. Phys. Chem.* **72**, 684 (1968)
	The Independence of Isothermal Equilibria in Electrolyte Solutions on Changes in Dielectric Constant	*J. Phys. Chem.* **72**, 1536 (1968)

AUTHOR(S)	TITLE	PUBLICATION
Quist, A. S., and W. L. Marshall	Electrical Conductances of Aqueous Hydrogen Bromide Solutions from 0 to 800° and at Pressures to 4000 Bars	*J. Phys. Chem.* **72**, 1545 (1968)
	Electrical Conductances of Aqueous Sodium Bromide Solutions from 0 to 800° and at Pressures to 4000 Bars	*J. Phys. Chem.* **72**, 2100 (1968)
	Ionization Equilibria in Ammonia–Water Solutions to 700° and to 4000 Bars of Pressure	*J. Phys. Chem.* **72**, 3122 (1968)
Roberts, B. F., S. H. Freid, and O. Sisman	Aging Behavior of Fission Products Released by In-Pile Melting of Uranium (IV) Oxide	*Trans. Am. Nucl. Soc.* **11**(2), 666 (1968)
Shor, A. J., K. A. Kraus, J. S. Johnson, and W. T. Smith	Hyperfiltration Studies. VII. Concentration Polarization in Tubular Systems with Dynamically Formed Membranes	*Ind. Eng. Chem. Fundamentals* **7**, 44 (1968)
Soldano, B. A., and W. T. Ward	Uptake of Methyl Iodide from Wind Tunnel Gases by a Suspended Drop of Water, Part II	*Trans. Am. Nucl. Soc.* **11**(1), 374 (1968)
Steinfink, H., and G. D. Brunton	The Crystal Structure of $CeBeF_3$	*Acta Cryst.* **B24**, 807 (1968)
Thoma, R. E., H. Insley, H. A. Friedman, and G. M. Hebert	Equilibrium Phase Diagram of the Lithium Fluoride–Beryllium Fluoride–Zirconium Fluoride System	*J. Nucl. Mater.* **27**, 166 (1968)
Tripp, T. B., and J. Braunstein	The Vapor Pressure of Lithium Nitrate–Potassium Nitrate–Water Mixtures Containing 5 to 75 Mole Percent Water	*Chem. Commun.* **1968**, p. 144
Watson, G. M., R. B. Perez, and M. H. Fontana	Effects of Containment-System Size on Fission-Product Behavior	*Nucl. Safety* 9(2), 128 (1968)

REPORTS ISSUED

AUTHOR(S)	TITLE	REPORT NUMBER
Adams, R. E., R. D. Ackley, and R. L. Bennett	Brief Investigation of Radioactive Behavior in Off-Gas System of TRU Facility (April–August 1968)	ORNL-TM-2369 (September 1968)
Baker, J. E., and L. G. Overholser	Oxidation of Pyrolytic-Carbon-Coated Fuel Particles by Low Concentrations of Water Vapor	ORNL-TM-2199 (April 1968)
Bennett, R. L., W. H. Hinds, and R. E. Adams	Development of Iodine Characterization Sampler for Application in Humid Environments	ORNL-TM-2071 (May 1968)
Blood, C. M., G. M. Hebert, and L. G. Overholser	Oxidation of Bonded Coated-Particle Fuel Compacts by Steam	ORNL-4269 (July 1968)
Bopp, C. D., and J. J. J. Myron	Radiolysis of Tetrahydrofuran-Cyclohexene Mixtures. Part A. Liquid Products. Part B. Gas Yields	ORNL-4320 (November 1968)
Cantor, S., J. W. Cooke, A. S. Dworkin, G. D. Robbins, R. E. Thoma, and G. M. Watson	Physical Properties of Molten Salt Reactor Fuel, Coolant, and Flush Salts	ORNL-TM-2316 (August 1968)
Davis, R. J.	A Nuclear Safety Particle Primer	ORNL-4337 (January 1969)
Evans, R. B., III, L. D. Love, and E. A. Mason	Graham's Laws. II. Simple Demonstrations of Gases in Motion – Experiments and Theory	ORNL-TM-2276 (November 1968)

AUTHOR(S)	TITLE	REPORT NUMBER
Fontana, M. H.	MONAT: A FORTRAN 63 Program for Computing Thermodynamic Properties of Monatomic Ideal Gases	ORNL-4305 (September 1968)
	TCDATA: A FORTRAN Program for Computing Thermodynamic Data of Compounds in Any Phase State	ORNL-4304 (September 1968)
	ONEPHASE: A Simplified FORTRAN 63 Program for Computing Tables of Thermodynamic Data for Compounds in One Phase	ORNL-4307 (September 1968)
Freid, S. H., H. J. de Nordwall, D. R. Cuneo, J. A. Conlin, C. L. Segaser, and E. L. Long	Fission Product Release from an Overheated HTGR Fuel (ORR Poolside Capsule 06-11)	ORNL-TM-2388 (November 1968)
Godfrey, T. G., J. L. Scott, R. L. Beatty, J. H. Coobs, J. W. Prados, L. G. Overholser, and L. M. Ferris	Coated Particle Fuels	ORNL-4324 (August 1968)
Keilholtz, G. W., C. E. Guthrie, and G. C. Battle, Jr.	Air Cleaning as an Engineered Safety Feature in Light-Water-Cooled Power Reactors	ORNL-NSIC-25 (September 1968)
Hitch, B. F., and C. F. Baes, Jr.	An EMF Study of LiF-BeF_2 Solutions	ORNL-4257 (July 1968)
Kelly, M. J., B. J. Sturm, and W. W. Parkinson	Annual Summary Report on the Development of Radiation Resistant Insulators	ORNL-TM-2077 (February 1968)
Kohn, H. W.	Bubbles, Drops, and Entrainment in Molten Salts	ORNL-TM-2373 (December 1968)
Longest, A. L., J. H. Conlin, D. R. Cuneo, E. L. Long, and M. F. Osborne	GCR-ORR Loop 1 Fuel Assembly 14 – an Irradiation Test of Large Loose Beds of Pyrolytic-Carbon-Coated Sol-Gel Oxide Particles	ORNL-TM-2278 (November 1968)
Malinauskas, A. P.	Vapor Pressure of Tellurium Dioxide	ORNL-4300 (September 1968)
Parker, G. W., G. E. Creek, and N. R. Horton	The Dissolution and Hydrolysis of Methyl Iodide in Mixing Spray Solutions	ORNL-TM-2053 (January 1968)
Parker, G. W., and H. Buchholz	Size Classification of Submicron Particles by a Low-Pressure Cascade Impactor	ORNL-4226 (June 1968)
Parker, G. W., G. B. Matheney, and R. E. Adams	LOFT Assistance Program in Engineering Development and Nuclear Safety Tests at the Oak Ridge National Laboratory	ORNL-4265 (June 1968)
Reagan, P. E., D. M. Hewett III, and J. G. Morgan	Comparison of Observed and Predicted Irradiation Performance of Pyrolytic-Carbon-Coated Uranium Dioxide Particles	ORNL-TM-2336 (December 1968)
Robbins, G. D.	Electrical Conductivity of Molten Fluorides. A Review	ORNL-TM-2180 (March 1968)
Shields, R. P., and R. E. Adams	The Effect of Fission Products on Ignition of Iodized Charcoal (In-Pile Experiment IGR-3)	ORNL-TM-2321 (December 1968)
Thoma, R. E.	Chemical Feasibility of Fueling Molten Salt Reactors with PuF_3	ORNL-TM-2256 (June 1968)
Weaver, C. F., D. N. Hess, H. F. McDuffie, W. T. Rainey, and B. A. Soldano	The Processing of ThO_2 and UO_2 Sol-Gel Materials	ORNL-TM-1809 (June 1968)
Yuille, W. D., and R. E. Adams	Behavior of Oxide Aerosols of Uranium and Stainless Steel in Humid Atmospheres	ORNL-4198 (January 1968)

THESES

AUTHOR	TITLE	
Fontana, M. H.	The Chemical Equilibria of Fission-Product Nuclear Fuel Mixtures – the Uranium-Oxygen and the Uranium-Oxygen-Strontium System	Thesis submitted in partial fulfillment of the requirements for the Ph.D. degree, Purdue University, Lafayette, Ind., January 1968
Shor, A. J.	Hyperfiltration Properties of Dynamically Formed Hydrous Zirconium(IV) Oxide Salt-Rejecting Membranes	Thesis submitted in partial fulfillment of the requirements for the Ph.D. degree, University of Tennessee, Knoxville, January 1968

PATENTS

AUTHOR(S)	TITLE	PATENT NUMBER
McDuffie, H. F.	Separation of Trivalent 4*f* Rare Earths from Molten Fluoride Compositions with UF_3	U.S. Pat. 3,379,648 (Apr. 23, 1968)
Shaffer, J. H., and W. R. Grimes	Recovery of Protactinium from Molten Fluoride Salts	U.S. Pat. 3,395,991 (Aug. 6, 1968)

Papers Presented at Scientific and Technical Meetings

AUTHOR(S)	TITLE	PLACE PRESENTED
Ackley, R. D., and R. E. Adams	Aging and Weathering of Impregnated Charcoals Used for Trapping Radioiodine	10th USAEC Air Cleaning Conference, New York, N.Y., Aug. 28, 1968
Adams, R. E., R. D. Ackley, and R. P. Shields	Application of Impregnated Charcoals for Removing Radioiodine from Flowing Air at High Relative Humidity	IAEA International Symposium, Air Cleaning Conference, New York, N.Y., Aug. 26–30, 1968
Baker, J. E., and L. G. Overholser	Oxidation of Pyrolytic Carbon Coated Fuel Particles by Low Concentrations of Water Vapor	Libby-Cockcroft Graphite Chemistry Meeting, Richland, Wash., May 20–22, 1968
Bamberger, C. E., and C. F. Baes, Jr.	Chemistry of Silicon Oxide in Molten $2LiF\text{-}BeF_2$	American Chemical Society, Atlantic City, N.J., Sept. 8–13, 1968
Barton, C. J., H. H. Stone, and J. C. Mailen	Recovery of Protactinium at the Parts per Million Concentration Level from Molten $LiF\text{-}ThF_4$	American Chemical Society, San Francisco, Calif., Mar. 31–Apr. 5, 1968
Barton, C. J., L. O. Gilpatrick, J. A. Bornmann, H. Insley, and T. N. McVay	Phase Relations in Fluoroborate Systems	American Chemical Society, San Francisco, Calif., Mar. 31–Apr. 5, 1968
Bennett, R. L., and R. E. Adams	A Sampling Device for Distinguishing the Forms of Iodine in a Humid Atmosphere	10th AEC Air Cleaning Conference, New York, N.Y., Aug. 26–30, 1968
Bien, P. B.	An Algebraic Analysis of the Behavior of Supercritical Water	American Chemical Society, Atlantic City, N.J., Sept. 8–13, 1968
Blood, C. M., G. M. Hebert, S. H. Freid, and L. G. Overholser	Oxidation of Bonded Coated-Particle Fuel Compacts by Steam	Libby-Cockcroft Graphite Chemistry Meeting, Richland, Wash., May 20–22, 1968
Braunstein, J.	Relations Between Coefficients in the Margules Expansion for Non-Ideal Binary Molten Salt Mixtures and Association Constants	American Chemical Society, San Francisco, Calif., Mar. 31–Apr. 5, 1968
	Non-Ideality and Association in Binary Mixtures of Molten Salts	EUCHEM Conference on Molten Salts, Salice Terme, Italy, May 6, 1968; Metallurgy Department Symposium, Imperial College, London, May 16, 1968
	Electrolyte Solutions with Water as a Solute	Department of Structural and Inorganic Chemistry, University of Leeds, England, May 20, 1968; Chemistry Seminar, University of Waterloo, Canada, Oct. 16, 1968
	Structural Aspects of Solution Chemistry in Molten Salts and Concentrated Aqueous Electrolytes	Southeastern Regional Meeting, American Chemical Society, Tallahassee, Fla., Dec. 4–7, 1968

AUTHOR(S)	TITLE	PLACE PRESENTED
Braunstein, J., and H. Braunstein	Hydration and Association Equilibria. III. The Association of Cadmium(II) Ion and Bromine(I) in the Solvent Potassium Nitrate–Calcium Nitrate–Water	American Chemical Society, Atlantic City, N.J., Sept. 8–13, 1968
Cantor, S., C. E. Roberts, and H. F. McDuffie	Vapor Pressures and Derived Thermodynamic Information for the System Sodium Fluoroborate–Sodium Fluoride	American Chemical Society, San Francisco, Calif., Mar. 31–Apr. 5, 1968
Coobs, J. H., and O. Sisman	Coated-Particle Fuels Development at Oak Ridge National Laboratory	14th AEC Coated-Particle Fuels Working Group Meeting, ORNL, Nov. 20–21, 1968
Cuneo, D. R.	High Burnup Coated Particle Experiment No. 3	14th AEC Coated Particle Fuels Working Group Meeting, ORNL, Nov. 20–21, 1968
Davis, R. J., J. Truitt, J. S. Gill, and W. D. Yuille	The Effects of Moisture on the Character and Filtration of Uranium(IV) Oxide–Stainless Steel Aerosols	IAEA International Symposium, Air Cleaning Conference, New York, N.Y., Aug. 25–30, 1968
Davis, R. J., J. Truitt, and J. S. Gill	Aerosol Studies in the Reactor Safety Program at Oak Ridge National Laboratory	Air Pollution Control Association, St. Paul, Minn., June 25, 1968
de Nordwall, H. J., V. H. Pierce, and L. R. Zumwalt	Experimental Test of the Frevap-8 Code for Calculating Metal Fission Product Release from HTGR Elements	American Nuclear Society, Washington, D.C., Nov. 10–15, 1968
Dunn, L. A.	Apparent Molar Volumes of Electrolytes	Chemistry Department, University of Louisville, Louisville, Ky., Mar. 11, 1968
Dunn, L. A., and W. L. Marshall	Electrical Conductance of Dilute Aqueous Sodium Iodide to 800°C and 4000 Bars	American Chemical Society, Atlantic City, N.J., Sept. 8–13, 1968
Fontana, M. H., and R. E. Bailey	The Chemical Equilibria of Fission-Product Fuel Mixtures: The Gas-Phase Composition of the Uranium-Oxygen-Strontium System in the Presence of the Condensed Phase	American Nuclear Society, Toronto, Canada, June 9–13, 1968
Fuller, E. L., Jr., R. B. Gammage, and H. F. Holmes	The Reversible Adsorption of Water Vapour on Thorium Oxide Between 25° and 500°C	American Chemical Society, Atlantic City, N.J., Sept. 8–13, 1968
Gilpatrick, L. O., and C. J. Barton	Differential Thermal Analysis Apparatus with Agitation and Sealed Specimens for Molten Salt Phase Studies	2d International Conference on Thermal Analysis, Worcester, Mass., Aug. 18–23, 1968
Griess, J. C., Jr.	The Corrosion of Titanium and Certain Copper Alloys in Aqueous Salt Solutions	Southeastern Regional Conference of National Association of Corrosion Engineers, Atlanta, Ga., Sept. 19, 1968
Grimes, W. R., D. M. Moulton, and J. H. Shaffer	The Removal of Uranium and Protactinium from Molten Fluorides by Reductive Extraction into Molten Bismuth	American Chemical Society, San Francisco, Calif., Mar. 31–Apr. 5, 1968
Grimes, W. R.	Chemistry of Molten Fluoride Fuels for Nuclear Reactors	Chemistry Seminar, Lawrence Radiation Laboratory, Berkeley, Calif., Dec. 9, 1968
Holmes, H. F., E. L. Fuller, R. B. Gammage, and C. H. Secoy	The Effect of Irreversibly Adsorbed Water on the Character of Thorium Oxide Surfaces	American Chemical Society, San Francisco, Calif., Mar. 31–Apr. 5, 1968
Keyser, R. M., J. Lin, K. Tsuji, and F. Williams	Trapped Electrons in Gamma-Irradiated Polyethylene and Hydrocarbon Glasses	American Chemical Society, San Francisco, Calif., Mar. 31–Apr. 5, 1968
Kirslis, S. S.	Aerosol Formation in the Cover Gas of the MSRE	American Chemical Society, Atlantic City, N.J., Sept. 8–13, 1968

AUTHOR(S)	TITLE	PLACE PRESENTED
Lorenz, R. A., and G. W. Parker	A Method for Calculating the Amount of Radioactive Volatiles in Fuel Rod Void Spaces	American Chemical Society, San Francisco, Calif., Mar. 31–Apr. 5, 1968
Malinauskas, A. P.	Intermolecular Forces and Gas Transport Properties	Chemistry Seminar, King's College, Wilkes-Barre, Pa., Feb. 14, 1968
	Thermal Transpiration	Susquehanna Valley Section of American Chemical Society, Feb. 14, 1968
Marshall, W. L.	Conductances and Equilibria of Aqueous Electrolytes over Extreme Ranges of Temperature and Pressure	University of California, Los Angeles, Calif., Feb. 9, 1968
		Plenary Lecture, 2d Australian Conference on Electrochemistry, Melbourne, Australia, Feb. 19–23, 1968
		Trichandra College, Kathmandu, Nepal, Mar. 4, 1968
		University of Karlsruhe, Institute for Physical Chemistry, Karlsruhe, Germany, Mar. 14, 1968
		Wayne University, Detroit, Mich., Apr. 29, 1968
Mesmer, R. E., and C. F. Baes	Beryllium Fluoride Complexes in 1 *M* Sodium Chloride and 1 *M* Sodium Perchlorate	American Chemical Society, Atlantic City, N.J., Sept. 8–13, 1968
Moulton, D. M., W. R. Grimes, and J. H. Shaffer	The Distribution of Metals Between Molten Fluorides and Liquid Metals	American Chemical Society, Atlantic City, N.J., Sept. 8–13, 1968
Parker, G. W., H. Buchholz, and W. J. Martin	Radioactive Aerosol Size Classification Experience with a Low Pressure Cascade Impactor	10th USAEC Air Cleaning Conference, New York, N.Y., Aug. 26–30, 1968
Perez, R. B., G. M. Watson, P. Nelson, R. M. Carroll, and O. Sisman	A Dynamic Method to Study In-Pile Fission-Gas Release	American Nuclear Society, Toronto, Canada, June 9–13, 1968
Quist, A.	Electrical Conductivity of Aqueous Electrolyte Solutions to 800°C and 4000 Bars	Second International Conference on High Pressure, Elmay, Germany, May 13–17, 1968; Imperial College, Southampton, England, Apr. 24, 1968; University of Paris, Mar. 20, 1968
Robbins, G. D., and J. Braunstein	Electrical Conductivity Measurements in Molten Fluoride Mixtures and Some General Considerations on Frequency Dispersion	American Chemical Society, Atlantic City, N.J., Sept. 8–13, 1968
Roberts, B. F., S. H. Freid, and O. Sisman	Aging Behavior of Fission Products Released by In-Pile Melting of Uranium(IV) Oxide	American Nuclear Society, Washington, D.C., Nov. 10–15, 1968
Shor, A. J., K. A. Kraus, J. S. Johnson, and W. T. Smith	Salt Rejection Properties of Dynamically Formed Hydrous Zirconium(IV) Oxide Membranes	American Chemical Society, San Francisco, Calif., Mar. 31–Apr. 5, 1968
Sisman, O.	A Review of the Work of ASTM Subcommittee II, D9-020, Effects of High Energy Radiation on Plastics and Electrical Insulation	American Chemical Society, Atlantic City, N.J., Sept. 8–10, 1968
Soldano, B. A., and W. T. Ward	A Windtunnel Study of the Mass Transport of Methyl Iodide into a Drop of Water	American Chemical Society, San Francisco, Calif., Mar. 31–Apr. 5, 1968
	Uptake of Methyl Iodide from Wind Tunnel Gases by a Suspended Drop of Water, Part II	American Nuclear Society, Toronto, Ontario, Canada, June 10–13, 1968

AUTHOR(S)	TITLE	PLACE PRESENTED
Strehlow, R. A., and D. M. Richardson	Water Chemisorption on Stainless Steel	4th International Vacuum Congress, London, England, Apr. 17–19, 1968
Thoma, R. E.	The Role of Phase Equilibria in Molten Salt Research	American Chemical Society, Atlantic City, N.J., Sept. 8–13, 1968
	Thermodynamic Properties of Rare Earth Halides	Gordon Research Conference on Fluorine Chemistry, Tilton, N.H., July 14–17, 1968
	Chemical Determination of Burnup in Uranium-235 Operations with the Molten Salt Reactor Experiment	American Chemical Society, Atlantic City, N.J., Sept. 8–13, 1968
	The ORNL Molten Salt Reactor Program	Gulf General Atomic Corporation, San Diego, Calif., Oct. 31, 1968
Thoma, R. E., S. S. Kirslis, F. F. Blankenship, and W. R. Grimes	Chemical Behavior in Molten Salt Reactor Experiment	American Chemical Society, San Francisco, Calif., Mar. 31–Apr. 5, 1968

ORNL-4400
UC-4 – Chemistry

INTERNAL DISTRIBUTION

1. Biology Library
2–4. Central Research Library
5. Laboratory Shift Supervisor
6. MIT Practice School
7–8. ORNL – Y-12 Technical Library Document Reference Section
9–49. Laboratory Records Department
50. Laboratory Records, ORNL R.C.
51. R. F. Hibbs
52. A. M. Weinberg
53. H. G. MacPherson
54–58. G. E. Boyd
59. F. R. Bruce
60. F. L. Culler
61. W. H. Jordan
62. A. H. Snell
63. G. Young
64. A. F. Rupp
65. M. Bender
66. A. L. Boch
67. R. B. Briggs
68. W. B. Cottrell
69. A. P. Fraas
70. K. A. Kraus
71. J. A. Lane
72. A. J. Miller
73. M. W. Rosenthal
74. D. B. Trauger
75. G. D. Whitman
76. S. E. Beall
77. D. S. Billington
78. D. E. Ferguson
79. J. H. Frye, Jr.
80. M. T. Kelley
81. E. H. Taylor
82. E. S. Bettis
83. M. A. Bredig
84. W. C. Colwell
85. L. T. Corbin
86. J. E. Cunningham
87. J. H. Crawford
88. P. N. Haubenreich
89. P. R. Kasten
90. M. A. Kastenbaum
91. E. M. King
92. R. N. Lyon
93. L. E. McNeese
94–95. R. B. Parker
96. W. P. Eatherly
97. M. J. Skinner
98. J. C. White
99–106. W. R. Grimes
107. E. G. Bohlmann
108. H. F. McDuffie
109. G. M. Watson
110. F. F. Blankenship
111. R. D. Ackley
112. R. E. Adams
113. B. K. Annis
114. A. L. Bacarella
115. C. F. Baes
116. C. E. Bamberger
117. C. J. Barton
118. C. D. Baumann
119. C. M. Blood
120. C. D. Bopp
121. Helen Braunstein
122. J. Braunstein
123. G. D. Brunton
124. S. Cantor
125. R. M. Carroll
126. Zell Combs
127. E. L. Compere
128. G. E. Creek
129. D. R. Cuneo
130. R. J. Davis
131. H. J. deNordwall
132. F. A. Doss
133. J. L. English
134. R. B. Evans III
135. L. L. Fairchild
136. H. F. Feuerstein
137. M. H. Fontana
138. S. H. Freid
139. H. A. Friedman
140. E. L. Fuller, Jr.
141. R. B. Gammage
142. J. S. Gill
143. L. O. Gilpatrick
144. J. C. Griess, Jr.
145. G. M. Hebert
146. B. F. Hitch
147. H. F. Holmes
148. G. H. Jenks
149. G. W. Keilholtz
150. M. J. Kelly
151. R. M. Keyser
152. S. S. Kirslis
153. H. W. Kohn
154. R. A. Lorenz
155. A. P. Malinauskas
156. W. L. Marshall, Jr.
157. W. J. Martin
158. T. H. Mauney
159. R. E. Mesmer
160. R. E. Moore
161. J. G. Morgan
162. M. T. Morgan
163. D. M. Moulton
164. P. D. Neumann
165. M. F. Osborne
166. L. G. Overholser
167. G. W. Parker
168. W. W. Parkinson, Jr.
169. A. S. Quist
170. J. D. Redman
171. S. A. Reed
172. D. M. Richardson
173. G. D. Robbins
174. H. E. Robertson
175. R. G. Ross
176. H. C. Savage
177. J. E. Savolainen
178. D. R. Sears (Y-12)
179. J. H. Shaffer
180. R. P. Shields

181. A. J. Shor
182. Oscar Sisman
183. Ruth Slusher
184. G. P. Smith
185. B. A. Soldano
186. H. H. Stone
187. R. A. Strehlow
188. B. J. Sturm
189. D. A. Sundberg
190. F. H. Sweeton
191. R. E. Thoma, Jr.
192. L. M. Toth
193. J. Truitt
194. W. T. Ward
195. G. C. Warlick
196. C. F. Weaver
197. J. F. Winesette
198. L. B. Yeatts
199. Leo Brewer (consultant)
200. J. W. Cobble (consultant)
201. Paul Cohen (consultant)
202. John Corbett (consultant)
203. P. H. Emmett (consultant)
204. H. S. Frank (consultant)
205. N. Hackerman (consultant)
206. H. Insley (consultant)
207. E. V. Jones (consultant)
208. G. Mamantov (consultant)
209. J. L. Margrave (consultant)
210. E. A. Mason (consultant)
211. R. F. Newton (consultant)
212. R. B. Perez (consultant)
213. J. E. Ricci (consultant)
214. Howard Reiss (consultant)
215. G. Scatchard (consultant)
216. D. A. Shirley (consultant)
217. H. Steinfink (consultant)
218. R. C. Vogel (consultant)
219. T. F. Young (consultant)
220. L. R. Zumwalt (consultant)

EXTERNAL DISTRIBUTION

221. G. Spaepen, Head, Chemical Technology, SCK-CEN, Mol, Belgium
222. Division of Isotopes Development, AEC, Washington
223. Reactor Development and Technology Division, AEC, Washington
224. Division of Research, AEC, Washington
225. Division of Space Nuclear Systems, AEC, Washington
226. Assistant General Manager for Reactors, AEC, Washington
227. Assistant General Manager, Research and Development, AEC, Washington
228. Laboratory and University Division, AEC, ORO
229. J. A. Swartout, 270 Park Ave., New York, N. Y.
230. W. W. Grigorieff, ORAU
231. John A. Bornmann, Lindenwood College, St. Charles, Mo.
232. Ralph E. Fuson, Tennessee Technological University, Cookeville, Tenn.
233. C. Sankey Sherer, Alabama College, Montevallo, Ala.

234–426. Given Distribution as shown in TID-4500 under Chemistry Category (25 copies – CFSTI)